Investigations of Stochastic Electromagnetic Fields

Untersuchungen zu Stochastischen Elektromagnetischen Feldern

Michael Haider
Lehrstuhl für Nanoelektronik
Fakultät für Elektrotechnik und Informationstechnik

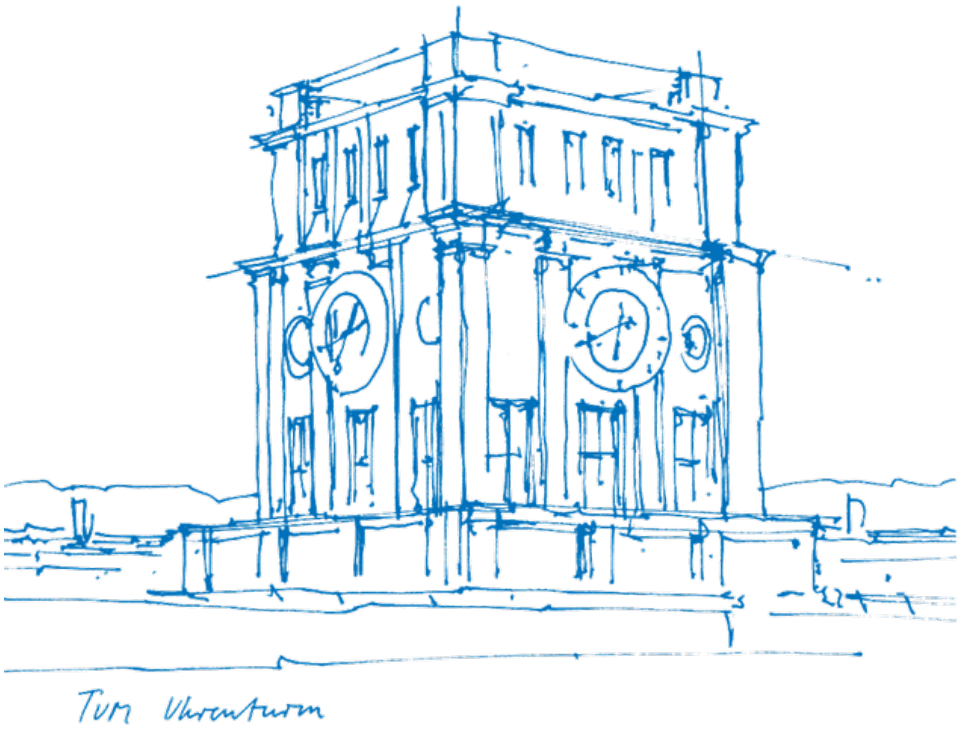

Technische Universität München
Fakultät für Elektrotechnik und Informationstechnik
Lehrstuhl für Nanoelektronik

Investigations of Stochastic Electromagnetic Fields

Michael Haider

Vollständiger Abdruck der von der Fakultät Elektrotechnik und Informationstechnik der Technischen Universität München zur Erlangung des akademischen Grades eines

Doktor-Ingenieurs (Dr.-Ing.)

genehmigten Dissertation.

Vorsitzender:	Prof. Dr. sc. techn. Andreas Herkersdorf
Prüfer der Dissertation:	
	1. Priv.-Doz. Dr. habil. Johannes A. Russer
	2. Prof. Dr.-Ing. habil. Erwin Biebl

Die Dissertation wurde am 18.06.2019 bei der Technischen Universität München eingereicht und durch die Fakultät Elektrotechnik und Informationstechnik am 02.11.2019 angenommen.

To my beloved wife Elisabeth.

Contents

List of Figures

List of Tables

Abstract

The performance of a communication channel is limited by the noise level present in the communication system. Quantifying the impact of noise on electric circuits and systems has been the subject of numerous experimental and theoretical studies. In network theory, noise in electric circuits can be easily modeled by equivalent noise sources at the terminals of abstract multiport representations of physical circuit elements. In this model, the propagation of noise through a linear network and how it is superimposed with the actual port voltages and port currents in the frequency-domain is governed by algebraic equations. For electromagnetic fields, where the governing equations are partial differential equations, the modeling of noise is less straightforward. From a network-oriented perspective, a method for describing noisy electromagnetic fields with Gaussian probability distribution has been proposed based on spatial auto-correlation and cross-correlation functions.

The intent of this work is to extend the mathematical framework for stochastic electromagnetic field modeling, such that stochastic electromagnetic fields with arbitrary statistics can be treated in a unified way. The description of stochastic electromagnetic fields in this thesis will be based on characteristic functionals, where propagation rules are devised, such that one can infer the statistics of an observed electromagnetic field in space and time, given a known random source field. In order to construct also this theoretical framework in a mathematically sound way, the required definitions, theorems, and proofs are presented in chapter 2 of the thesis. Based on the mathematical foundations, a theory for random fields is constructed by revisiting classical electromagnetism.

Inferring probability measures from realizations of stochastic processes with arbitrary statistics is in general not possible. Thus, for the experimental characterization of stochastic electromagnetic fields, we will restrict ourselves to the case of stationary ergodic Gaussian systems for which it is shown that the characteristic functional is uniquely determined by specifying a mean function and a correlation dyadic of the respective electromagnetic field quantity. The previous approach, where the propagation of Gaussian stochastic electromagnetic fields was described by correlation dyadics, is shown to be contained in our more general theory as a special case, by prescribing a characteristic functional corresponding to Gaussian statistics. In addition, a measurement-setup and a calibration procedure, capable of obtaining samples of random fields at pairs of distinct points in space are presented.

Furthermore, numerical methods for the propagation of correlation information are established in the frequency-domain and in the time-domain. Using these methods, it is shown that the spatial energy density distribution of a random electromagnetic field can be predicted. For this purpose, measured field-field correlation data, sampled on a plane directly above an aperture, is numerically propagated to another plane further apart from the initial measurement surface. Within this propagation example, a comparison between two selected methods is presented.

The theory presented in this work can be applied in modeling near-field communication channels, where the signals are perturbed by noise.

Finally, a method for data reduction for the description of stochastic electromagnetic field propagation will be presented. Data reduction is essential, since the measurement time as well as the amount of data that needs to be recorded for describing Gaussian random fields in terms of auto-correlation and cross-correlation functions, is very high in general. The amount of data depends on the measurement bandwidth and especially on the number of spatial sampling points. For a full characterization by auto-correlation and cross-correlation functions at all pairs of spatial sampling points, the amount of data scales quadratically with the number of spatial measurement positions. Thus, for a spatial resolution that is sufficiently fine, the size of the recorded data sets can become unmanageable.

Zusammenfassung

Die maximale Datenrate in einem Kommunikationskanal ist durch die im Kommunikationssystem vorhandene Rauschleistung begrenzt. Die Untersuchung der Auswirkungen von Rauschen auf elektronische Schaltungen und Systeme war bereits Gegenstand zahlreicher experimenteller und theoretischer Studien. In der Netzwerktheorie wird Störrauschen mittels äquivalenter Rauschquellen an den Ein- und Ausgängen von äquivalenten Mehrtoren modelliert, die ihrerseits vereinfachte Repräsentationen komplexer Schaltungen darstellen. In diesem Sinne wird die Ausbreitung durch ein lineares Netzwerk, sowie die Überlagerung der Torströme und -spannungen im Frequenzbereich, durch algebraische Gleichungen beschrieben. Die Verallgemeinerung dieses Konzeptes auf elektromagnetische Felder, wobei die beschreibenden Systemgleichungen durch partielle Differentialgleichungen gegeben sind, ist allerdings nicht so einfach. Aus einer netzwerkorientierten Perspektive wurde eine Methode zur Beschreibung von rauschenden elektromagnetischen Feldern mit Gaußscher Wahrscheinlichkeitsverteilung vorgeschlagen, die auf einer Charakterisierung der Felder bezüglich deren Auto- und Kreuzkorrelationen an verschiedenen Punkten im Raum basiert.

Mit dieser Arbeit wird angestrebt, diese Methoden dahingehend zu erweitern, dass sich stochastische elektromagnetische Felder mit beliebiger statistischer Verteilung in einer vereinheitlichten Theorie beschreiben lassen. Die Grundlage der theoretischen Behandlung von stochastischen elektromagnetischen Feldern in dieser Dissertation bilden charakteristische Funktionale. Dabei werden Regeln zur Feldausbreitung für charakteristische Funktionale ausgearbeitet, sodass sich von einem gegebenen Quellfeld auf die statistische Verteilung eines beobachteten Feldes in Raum und Zeit schließen lässt. Für die Ausarbeitung eines mathematisch einwandfreiem theoretischen Formalismus, werden die notwendigen Definitionen, Sätze und mathematischen Beweise in Kapitel 2 dieser Arbeit angegeben. Darauf aufbauend wird eine Theorie zur Behandlung von Zufallsfeldern konstruiert, indem aus dem klassischen Elektromagnetismus heraus, Ausbreitungsgleichungen hergeleitet werden, die im Rahmen der Wahrscheinlichkeitstheorie zur räumlichen und zeitlichen Entwicklung der statistischen Systemparameter Anwendung finden.

Wir beschränken uns für die experimentelle Charakterisierung von stochastischen Feldern auf den Fall stationärer ergodischer Gaußscher Zufallsprozesse. Es wird gezeigt, dass es in diesem Fall ausreichend ist, eine Mittelwertsfunktion, bzw. einen Korrelationstensor zu spezifizieren, um charakteristische Funktionale derartiger Zufallsprozesse eindeutig zu beschreiben. Darüber hinaus wird auch gezeigt, dass sich bestehende Methoden, bei denen die Ausbreitung stochastischer Felder mittels räumlicher Korrelation modelliert wird als Spezialfall der im Rahmen dieser Arbeit verallgemeinerten Theorie ergeben. Außerdem wird ein Messaufbau sowie eine Kalibrierungsmethode für die Aufnahme von Feldwerten an beliebigen Paaren von räumlich verteilten Messpunkten gezeigt.

Methoden zur numerischen Berechnung der Ausbreitung von Korrelationsinformationen im Zeit- sowie im Frequenzbereich werden erarbeitet. Mittels dieser Methoden wird die Möglichkeit der Vorhersage der räumlichen Energieverteilung eines stochastischen elektromagnetischen Feldes gezeigt. Dabei werden gemessene Feld-Feld Korrelationen, die auf einer Ebene direkt über einer Apertur aufgenommen wurden, numerisch auf eine andere Ebene, mit größerer Entfernung zur ursprünglichen Apertur weitergerechnet. Mittels dieses Beispiels zur Ausbreitung stochastischer elektromagnetischer Felder, wird ein quantitativer Vergleich zweier ausgesuchter numerischer Methoden gezogen.

Bezugnehmend auf Kommunikationssysteme werden theoretische Grundlagen sowie ein Messaufbau zur Multiple-Input-Multiple-Output Kommunikation im Nahfeld präsentiert. Dabei kann die in dieser Arbeit entwickelte Theorie zur Modellierung des störenden Systemrauschens im Kommunikationskanal eingesetzt werden.

Abschließend wird eine Methode zur Datenreduktion im gesamten Mess- und Charakterisierungsprozess für stochastische elektromagnetische Felder entwickelt. Ein derartiges Konzept zur Reduktion der Datenmenge scheint essentiell zu sein, da die benötigte Messzeit, sowie die bloße Menge an Messdaten für die Beschreibung Gaußscher Zufallsfelder mittels Auto- und Kreuzkorrelationen, im Allgemeinen sehr groß ist. Die zur Charakteri-

sierung von stochastischen Feldern aufgenommene Datenmenge hängt im Wesentlichen von der Messbandbreite sowie der Anzahl der räumlichen Messpunkte ab. Da zur Berechnung aller Auto- und Kreuzkorrelationsfuntionen jeweils eine Messung an jedem Paar von Punkten im Raum nötig ist, skaliert die Datenmenge annähernd quadratisch mit der Anzahl an Messpunkten. Daher kann die Datenmenge für eine Messung, mit ausreichender räumlicher Auflösung, schnell unhandhabbar werden.

1 Introduction

It has been a long journey from the first spoken words over a telephone line to today's wireless communication infrastructure. The foundations of wireless communications and electromagnetics in general have been developed by Maxwell and are summarized in his seminal work *A Treatise on Electricity and Magnetism* [1] from 1873. Contemporary wireless communication devices use electromagnetic waves in the radio frequency regime, which carry the information from a transmitter to a receiver. The electromagnetic radio frequency wave propagating from the transmitter to a receiver will be perturbed by noise. In digital communications, where the task of the receiver is to decide which symbol from a set of known possible symbols has been transmitted most probably, the ratio of the signal energy to the noise energy plays an important role. This detection should be reliable in a sense, that the probability of a wrong decision is very low. An increase in the noise energy or a decrease in the signal energy will increase the error rate in symbol estimation. A bound for the maximum rate at which information can be transferred from a receiver to a transmitter in a certain bandwidth with a fixed signal energy and under the presence of noise with a given power spectrum was derived in [2].

Already in the early days of radio communication, the impact of electromagnetic interference on the quality of wireless RF communication links was recognized [3]. Electromagnetic interference (EMI) results in an unintentional degradation in signal quality due to the superposition of the transmitted communication signal and noise. The noise itself may consist of radiation due to other communication links in the range of the receiver, or unintentional broadband noise radiated by electronic devices in close vicinity. Due to the advances in modern electronics and the ever-growing demands in bandwidth and data rates, where the signals need to cope with an ever-tighter power budget, design methods aware of signal integrity and electromagnetic interference effects become more and more important [4]–[6]. In an electromagnetic interference and signal integrity aware design process, one needs to model unintentional random radiations incident to the respective device under test, as well as radiation that is emitted by the device's own circuitry [7]. This even goes beyond the device level, as simultaneous switching noise and the resulting ground level fluctuations may perturb communication between distinct chips within a device or even communication within a single semiconductor chip [8].

Regardless of the source of the perturbing noisy electromagnetic field, one cannot predict deterministic amplitude and phase values for the interfering signals, and hence, one needs to treat radiated electromagnetic interference as a random process. This thesis is devoted to formulating a consistent approach in characterizing noisy electromagnetic fields and modeling their propagation through space and time. This work should be understood to build a bridge between the practical applications of EMI related problems to the abstract language of probability theory, which constitutes the mathematical framework for modeling stochastic electromagnetic fields.

The treatment of noise in active linear networks was pioneered by Hillbrand and Russer in [9], where they developed a concept for noise analysis in linear amplifier networks. The system noise there is modeled by equivalent noise sources, which are characterized by correlation matrices. The noise is characterized by energy and power spectra [10]. To describe the noise properties of a circuit completely, full correlation information of all noise sources is required. The concept of describing noise in terms of energy and power spectra has been applied to linear microwave circuits with general topology in [11]–[14]. The first generalization of the network concept for describing noisy electromagnetic fields has been given in [15], also from a network-oriented perspective. The modeling of random emissions by correlation dyadics has been treated in [16]–[19].

Previous work considers electromagnetic fields which are stationary, Gaussian, and ergodic. Stationary random processes exhibit time-independent averages while ergodic systems have the same averages over time and over the statistical ensemble [20]. Knowledge of the correlation dyadics completely describes Gaussian random fields, and one can formulate propagation rules for noise correlations by extending existing well known numerical techniques [21]–[24]. The description of signals with Gaussian probability distribution by auto-correlation functions and cross-correlation functions, completely determines the underlying random process.

Hence, as long as the propagation of the fields is governed by linear transformations, the resulting propagated fields will also exhibit Gaussian statistics. Thus, the theory developed in [16] provides a suitable framework for describing Gaussian stochastic electromagnetic fields. In the first chapter, the foundations of the theory of statistic processes are discussed. Our goal is to establish a general mathematical theory for describing stochastic electromagnetic fields, where we want to show that the characterization and propagation of Gaussian random fields by correlation dyadics is a special case of our general theory [25].

Within this thesis, we explicitly deal with random fields, i.e. the field is a stochastic process, and the environment the field is propagating in is fixed. Structural variations have been modeled in [26]–[29]. The mathematical framework, we will present in the following, is capable of also dealing with statistical variations in the device geometry, by treating the linear propagator in terms of a random operator. More investigations will be needed in order to combine those two approaches, where on the one hand, we have stochastic fields but deterministic propagation and on the other hand fields are deterministic but the propagation is perturbed by random parameter fluctuations.

Although we develop a more general concept for describing stochastic electromagnetic fields in chapters 2 and 3, we will restrict ourselves to the case of stationary ergodic Gaussian fields for implementations of numerical propagators as well as for the experimental characterization. If the underlying random processes were not stationary and ergodic, one could not, in general, infer statistical parameters from samples of the stochastic electromagnetic fields, which makes a practical assessment difficult. An extension to cyclostationary electromagnetic fields is given in [30]–[36], with preliminary work summarized in [37]. There are obstacles when considering an experimental characterization of Gaussian fields by determining auto-correlation functions and cross-correlation functions. As one needs to measure field samples at all possible pairs of points simultaneously, the measurement time and also the amount of recorded data can be very large. The sheer amount of data necessary for describing correlation functions and correlation spectra motivated researchers to find intelligent ways for reducing complexity in the recorded data while retaining as much information as possible. Preliminary work related to data reduction for stochastic electromagnetic fields is given in [38]–[41].

In chapter 2, we present the mathematical fundamentals this work is based upon. In chapter 3, we start with formulating a general model for random fields, where a random field could be any random function specified over a volume, which is varying with time. We investigate linear transformations of random fields and discuss the implications of stationarity and cyclostationarity. Then, classical electromagnetism based on Maxwell's equations is introduced. We also discuss concepts for solving Maxwell's equations and provide some fundamental theorems, which will be important for formulating propagation rules for stochastic electromagnetic fields. In section 3.6, the model for general random fields is refined to the case of stochastic electromagnetic fields. Chapter 4 deals with the characterization of stochastic electromagnetic fields. Here, we discuss concepts for measuring random electromagnetic radiation in the near-field and we present some first measurement and simulation results. In chapter 5, we discuss methods that have been developed for propagating stochastic electromagnetic fields from a source to an observed random field. A particularly interesting application for stochastic electromagnetic fields is given in terms of complex communication scenarios, which are perturbed by noise. In chapter 6, we introduce the concept of multiple-input-multiple-output communication in the near-field, where the theory of stochastic electromagnetic fields can deal with both, the modeling of noise in the system, as well as assessing the propagation of information in the wireless communication links themselves. Chapter 7 discusses a method for reducing the amount of data, which is necessary in order to describe stochastic electromagnetic fields. The method and the algorithm we present is based on principal component analysis and is capable of reducing the amount of data considerably. We conclude the work in chapter 8 and provide an outlook on yet unsolved problems related to the characterization and propagation of stochastic electromagnetic fields.

2 Mathematical Preliminaries

2.1 Introduction

In the following, we discuss the mathematical fundamentals for the theoretical framework of stochastic electromagnetic fields, to be developed in this work. We are going to follow a bottom-up approach, where we start with the mathematical foundations and preliminaries, on which we later construct a theory describing stochastic electromagnetic fields. The terms and theorems used later in this thesis, when constructing the theoretical framework, all further results are based upon are introduced here. We will first identify and define some important mathematical objects, discuss their properties, and prove some important theorems, that will be used in the remainder of this thesis. The definitions, theorems, and proofs presented in this chapter are directly taken from the literature, however, the results are presented in a notation that is consistent with the rest of the thesis, which should aid the reader in quickly referencing later results.

2.2 Linear Algebra, Topology and Functional Analysis

A fundamental concept in mathematics is given in terms of sets, which are collections of distinct elements. Different ideas and measures regarding sets have been developed over the years [42]. One important idea is the notion of distance between two elements of a specific set [43]. In order to introduce this notion of distance, one needs to extend the concept of a simple set to the concept of metric spaces. A metric on a set A is given in terms of a distance function d on two elements of the set A, which fulfills certain properties. These properties are summarized in the following definition [43].

Definition 2.1 (Metric Space)**.** *Let A be a set. The set A is called metric space, if there is a function $d : A \times A \to \mathbb{R}$ on A, such that for any $x, y, z \in A$ it holds*

$$\begin{aligned} &d(x,y) \geq 0\,, \\ &d(x,y) = 0 \Leftrightarrow x = y\,, \\ &d(x,y) = d(y,x)\ , \\ &d(x,z) \leq d(x,y) + d(y,z)\ . \end{aligned}$$

As soon as there is a notion of distance introduced on a set, one can define topological properties, such as open and closed subsets of a metric space A [43]. The distinction between open and closed sets will be used in several of the following definitions and theorems, hence, we want to introduce them rigorously here.

Definition 2.2 (Open and Closed Sets)**.** *Let A be a metric space with metric d. A subset $U \subset A$ is called open set, if for all $x \in U$, there exist $\varepsilon > 0$, such that the set of points $\{y \in A : d(x,y) < \varepsilon\}$ is a subset of U, i.e.*

$$\forall x \in U : \exists \varepsilon > 0 : \{y \in A : d(x,y) < \varepsilon\} \subseteq U\,.$$

A subset V is called closed, if the complement $A \setminus V$ is open, i.e.

$$\forall x \in A \setminus V : \exists \varepsilon > 0 : \{y \in A : d(x,y) < \varepsilon\} \subseteq A \setminus V\,.$$

The concept of open and closed sets is relevant for sequences in metric spaces. A sequence is an enumerated collection of members of a certain subset $U \subseteq A$ of a metric space A with metric d. In principle, a sequence is a mapping $I \subseteq \mathbb{N} \to U \subseteq A$, such that each element of the index set $n \in I$ is mapped to an element $x \in U \subseteq A$. The mapping does not need to be bijective, i.e. several indices might be mapped to the same element. There is a special class of sequences, called Cauchy sequences, which are defined by the following property [44].

Definition 2.3 (Cauchy Sequence)**.** *Let A be a metric space with metric d and let x_n with $n \in \mathbb{N}$ be a sequence of elements in A. The sequence $(x_n)_{n\in\mathbb{N}}$ is called Cauchy sequence if for all $\varepsilon > 0$ there exists an index $N \in \mathbb{N}$, such that $\forall n, m \geq N$ we have*

$$d(x_n, x_m) < \varepsilon .$$

Note that convergence of a sequence $(x_n)_{n\in\mathbb{N}}$ to an element $x \in A$ is defined with respect to Cauchy sequences according to Definition 2.3, in a sense that $(x_n)_{n\in\mathbb{N}} \to x$, if $\forall\varepsilon > 0$, $\exists N \in \mathbb{N}$, such that

$$d(x_n, x) < \varepsilon , \qquad \forall n \geq N . \tag{2.1}$$

With the notion of convergent sequences, we can introduce the notion of completeness of metric spaces by the following definition [43].

Definition 2.4 (Completeness)**.** *Let A be a metric space with metric d. We call A complete, with respect to the metric d if every Cauchy sequence $(x_n)_{n\in\mathbb{N}}$, $x_n \in A$ converges to an element $x \in A$.*

For any set, we can define mathematical operations, like e.g. addition, subtraction, multiplication, etc. For a general set, it is not granted that e.g. the sum of two elements still fulfills the defining property to be part of the set, i.e. it is not granted that the sum of two elements of a set belongs to the set. Hence, it is useful to introduce an algebraic structure, such that a set is closed under certain mathematical operations. Vector spaces are algebraic structures, which are closed under linear operations, i.e. summation and scalar multiplication [44].

Definition 2.5 (Vector Space)**.** *Let A be a set, and let $x, y \in A$. The set A is called vector space over a field $\mathbb{K}$, where $\mathbb{K}$ can be e.g. $\mathbb{R}$ or $\mathbb{C}$, if*

$$\lambda x \in A ,$$
$$x + y \in A ,$$

for all $\lambda \in \mathbb{K}$ and for all $x, y \in A$.

The vector addition operation and the scalar multiplication in Definition 2.5 are defined according to a number of requirements. Those axioms for vector addition and scalar multiplication are given as follows [44]. For all $x, y, z \in A$ and for all constants $\lambda, \mu \in \mathbb{K}$ it holds

$$x + (y + z) = (x + y) + z , \tag{2.2}$$
$$x + y = y + x , \tag{2.3}$$
$$\exists 0 \in A : x + 0 = x , \tag{2.4}$$
$$\exists (-x) \in A : x + (-x) = 0 , \tag{2.5}$$
$$\lambda(\mu x) = (\lambda\mu) x , \tag{2.6}$$
$$1x = x , \tag{2.7}$$
$$\lambda(x + y) = \lambda x + \lambda y , \tag{2.8}$$
$$(\lambda + \mu) x = \lambda x + \mu x . \tag{2.9}$$

In many situations, we want to assign a size or a length property to a vector. This is especially important when one is interested in whether one vector is smaller or larger than another. The assignment of a length property to a vector can be done in terms of a functional, which maps each vector of a vector space to a positive real number. In Definition 2.6, we define this mapping, called the norm of a vector [43].

Definition 2.6 (Normed Space)**.** *Let A be a vector space over a field $\mathbb{K}$. We call A a normed vector space, if there is a mapping $\|\cdot\| : A \to \mathbb{R}^+$ with the following properties. For all $x, y \in A$ and for all $\lambda \in \mathbb{K}$*

$$\|x\| = 0 \Rightarrow x = 0 ,$$
$$\|\lambda x\| = |\lambda| \, \|x\| ,$$
$$\|x + y\| \leq \|x\| + \|y\| .$$

Note here, that a norm defined on a vector space A implicitly defines a metric d on that vector space, given by $d(x, y) = \|x - y\|$. It can be easily verified that $\|x - y\|$ fulfills all requirements given in Definition 2.1.

In addition to the length of a vector and the distance between two vectors, the fraction of one vector that points in the same direction as another vector has proven to be an important property. Obtaining this fraction is done by generalizing the norm to a sesquilinear form, taking two vectors as an input. This generalization is called an inner product, which assigns a number to any two vectors it is applied to. With an inner product, one can define a basis for a vector space, where each element of a vector space can be given by scalar multiples of the basis elements, respectively. The scalar weights can be determined by applying the inner product to the vector with each basis element. Let us now define the inner product rigorously by its properties [43].

Definition 2.7 (Inner Product)**.** *Let A be a vector space over a field $\mathbb{K}$. We define an inner product as a sesquilinear form $\langle \cdot, \cdot \rangle : A \times A \to \mathbb{K}$, satisfying the following set of axioms. For all $x, y, z \in A$ and for all $\lambda \in \mathbb{K}$ it holds*

$$\begin{aligned} \langle y, x \rangle &= \langle x, y \rangle^* \,, \\ \langle y, \lambda x \rangle &= \lambda \langle y, x \rangle \,, \\ \langle z, x + y \rangle &= \langle z, x \rangle + \langle z, y \rangle \,, \\ \langle x, x \rangle &\geq 0 \,, \\ \langle x, x \rangle &= 0 \Leftrightarrow x = 0 \,. \end{aligned}$$

Note that our definition here differs from the standard definition as given in [43] such that the sesquilinear form in Definition 2.7 is linear in the second argument and antilinear in the first argument. In a natural way, the inner product induces a norm, and hence, a metric on a vector space, by $\|x\| = \sqrt{\langle x, x \rangle}$. It can be easily verified that this assignment of a norm to an inner product fulfills the requirements of Definition 2.6, and thus yields a valid norm.

Compiling what we have established so far, we can finally define a Hilbert space, which has a lot of desirable properties and thus serves as a mathematical framework for a lot of theories in physics and engineering. A Hilbert space can be defined as follows [43], [45]–[47].

Definition 2.8 (Hilbert Space)**.** *Let $\mathcal{H}$ be a vector space. The vector space $\mathcal{H}$ is called Hilbert space if there is an inner product $\langle \cdot, \cdot \rangle$ defined on $\mathcal{H}$, and $\mathcal{H}$ is complete with respect to the norm induced by the inner product.*

We will use Hilbert spaces when we discuss the numerical propagation of stochastic electromagnetic fields with the method of moments in chapter 5. Hilbert spaces are also important for us in the following when we will propose the use of characteristic functionals for describing random fields.

2.3 Probability Theory

In probability theory, the most basic term considered is a random experiment. In the literature, one finds examples like the flip of a coin or the roll of a die, all representing realizations of random experiments [48], [49]. Regardless of the actual realization of a random experiment, we are looking for a structured framework in which we are able to describe probabilistic experiments. We shall first define a sample space in terms of a simple set, which represents the most basic element of our probabilistic model [50], [51].

Definition 2.9 (Sample Space)**.** *A sample space Ω is the set of all possible outcomes of a random experiment.*

This definition is motivated by [52], where each possible outcome of a random experiment represents an element of a sample space Ω. In general, it is more convenient to consider events, rather than single outcomes of random experiments. This will be illustrated by a simple example. Take for instance the tossing of a coin twice. The possible outcomes of this basic random experiment are all possible 2-tuples containing heads (H) and tails (T) [50], [51]. Thus the sample space Ω is given by

$$\Omega = \{(\mathrm{H}, \mathrm{H}), (\mathrm{H}, \mathrm{T}), (\mathrm{T}, \mathrm{H}), (\mathrm{T}, \mathrm{T})\} \,. \tag{2.10}$$

The elements $\omega \in \Omega$ are referred to as elementary events [48]. It is obvious that the elementary events are not the only events one could be interested in assigning probabilities to. Take for example the event A, given by obtaining the same side of a coin twice after two tosses, regardless whether it is both heads or both tails. The event A is given by the set

$$A = \{(\mathrm{H}, \mathrm{H}), (\mathrm{T}, \mathrm{T})\} . \tag{2.11}$$

Such an event will be called a compound event, as it consists of several elementary events. Of course, it must be also possible to assign probabilities to the complementary event $\Omega \setminus A$, which is the event of tossing different sides of the coin for the first and the second toss, regardless whether the first toss yielded heads or tails. Probabilities may be assigned to all possible subsets $A \subseteq \Omega$ of interest to a certain probabilistic model. Therefore, we introduce a σ-algebra [52], [53], representing the set of all possible events, i.e. the set of subsets of the sample space Ω.

Definition 2.10 (σ-Algebra)**.** *Let Ω be a non-empty set and let $\mathcal{F}$ be a set of subsets $A_n \subseteq \Omega$. Then $\mathcal{F}$ is called σ-algebra if it satisfies the following criteria:*

1. *$\mathcal{F}$ contains the set Ω, i.e. $\Omega \in \mathcal{F}$,*
2. *$\mathcal{F}$ is closed under complements, i.e. let $A \in \mathcal{F}$, then the complement $\Omega \setminus A \in \mathcal{F}$,*
3. *$\mathcal{F}$ is closed under countable unions, i.e. $A_n \in \mathcal{F}$, $\forall n \in \mathbb{N}$, the countable union $\bigcup_{n=1}^{\infty} A_n \in \mathcal{F}$.*

For each event $A \in \mathcal{F}$ we say that A occurred if for the result $\omega \in \Omega$ of a random experiment it holds that $\omega \in A$ [50], [51]. Although the structure of a probabilistic model is now well defined, we are still lacking an essential ingredient for describing probabilities of elementary and compound events. This is the association of a probability P, such that the probability that an event $A \in \mathcal{F}$ occurs is assigned a so-called probability measure. A probability measure is a function mapping each event to the interval $[0, 1]$, i.e. it assigns a probability to each event in a σ-algebra $\mathcal{F}$ [50], [51]. A sample space, a corresponding σ-algebra and a probability measure together form a probability space, which forms the mathematical construct for modeling random experiments [52].

Definition 2.11 (Probability Space)**.** *A probability space is given by the triple $(\Omega, \mathcal{F}, P)$. Here, Ω is a sample space, $\mathcal{F}$ is a σ-algebra of all events of interest on Ω, i.e. all possible combinations of outcomes of interest of a random experiment performed on the probability space, and P are probability measures assigned to each event in $\mathcal{F}$. A probability measure is a function mapping $P : \mathcal{F} \to [0, 1]$. Furthermore the function P satisfies the following criteria*

1. *For all $A \in \mathcal{F}$, $P(A) \geq 0$,*
2. *$P(\Omega) = 1$,*
3. *For all $A_n \in \mathcal{F}$ with $A_m \cap A_n = \emptyset$, $\forall m, n \in \mathbb{N}$ it holds*

$$P\left(\bigcup_{n=1}^{\infty} A_n\right) = \sum_{n=1}^{\infty} P(A_n) .$$

From the definition of the probability space, especially from the definition of the probability measures P, it directly follows that for any event $A \in \mathcal{F}$, the probability $P(A)$ is bounded by

$$0 \leq P(A) \leq 1 . \tag{2.12}$$

The lower bound follows directly by Definition 2.11-1. The upper bound can be easily verified by considering the complementary event, $\Omega \setminus A \in \mathcal{F}$, which must exist by Definition 2.10-2. By Definition 2.11-2 and 2.11-3

$$P(A \cup (\Omega \setminus A)) = P(\Omega) = 1 = P(A) + P(\Omega \setminus A) , \tag{2.13}$$

since $A \cap \Omega \setminus A = \emptyset$. This shows that $P(A) \leq 1$ since $P(\Omega \setminus A) \geq 0$ by Definition 2.11-1. With the same argument, we can show that the probability $P(\emptyset)$ assigned to the empty set $\emptyset$ is zero, i.e.

$$P(\emptyset) = 0\,. \tag{2.14}$$

So far, we have constructed a mathematical framework in which we can model random experiments, like for example the tossing of a coin, as we have seen previously. Yet, the sets describing random events are rather general, like heads and tails for the coin-tossing example. In order to get a mathematical structure to the formalism developed so far, it would be beneficial to assign numeric values to uncertain events. Thus, let us introduce a random variable [50], [51], which is a function mapping outcomes of random experiments, like the tossing of a coin or the roll of a die, to numeric values.

Definition 2.12 (Random Variable)**.** *Let $(\Omega, \mathcal{F}, P)$ be a probability space and let (E, Σ) be a measurable space. Furthermore, let X be a function $X : \Omega \to E$. Then X maps each element $\omega \in \Omega$ to an element $X(\omega) \in E$, $\omega \mapsto X(\omega) \in \mathbb{R}$. The function X is called random variable if the inverse image of every subset $S \subset E$ that is measurable with respect to the σ-algebra Σ, $S \in \Sigma$, is an element of the σ-algebra of events $\mathcal{F}$, i.e.*

$$X^{-1}(S) \in \mathcal{F}\,, \qquad \forall S \in \Sigma\,.$$

In the case where the measurable space is the real line $\mathbb{R}$ equipped with the Borel σ-algebra of open sets, the definition of a random variable can be simplified to a function $X : \Omega \to \mathbb{R}$ [50], [51], such that the inverse image of each semi-closed interval $(-\infty, a]$ is an element of the σ-algebra of events $\mathcal{F}$, i.e.

$$X^{-1}((-\infty, a]) \in \mathcal{F}\,, \qquad \forall a \in \mathbb{R}\,.$$

The definition of a random variable in terms of semi-closed intervals directly leads to a description of the random variable itself. As for each $x \in \mathbb{R}$, the inverse image $X^{-1}((-\infty, x]) \in \mathcal{F}$, we can assign probabilities to each semi-closed interval $(-\infty, x]$. This is, the probability that a realization of the random variable *X* lies in the interval $(-\infty, x]$ exist, and is given by $P\left(X^{-1}((-\infty, x])\right) = P(\{X \leq x\})$. We call the collection of probabilities $P(\{X \leq x\})$ for all $x \in \mathbb{R}$ of a random variable *X* the probability distribution of *X*. This becomes clear with the following definition [50], [51].

Definition 2.13 (Probability Distribution)**.** *Let $(\Omega, \mathcal{F}, P)$ be a probability space and let X be a random variable. Then the function*

$$F(x) = P(\{X(\omega) \leq x\})$$

for $\omega \in \Omega$ and $x \in \mathbb{R}$ is called probability distribution of the random variable X.

A probability distribution is a function of a continuous variable $x \mapsto [0, 1]$, which yields the probability that the random variable is smaller or equal to x. From this definition, we can directly derive a list of important properties for probability distributions, which are given in the following [54].

Properties 2.1 (Probability Distribution)**.** *Let F be a probability distribution, then the following properties hold:*

1. *The limit of $F(x)$ for $x \to -\infty$ is 0, i.e.*

$$\lim_{x \to -\infty} F(x) = 0\,.$$

2. *The limit of $F(x)$ for $x \to \infty$ is 1, i.e.*

$$\lim_{x \to \infty} F(x) = 1\,.$$

3. *The probability distribution F is a non-decreasing function, i.e.*

$$F(x_1) \leq F(x_2)\,, \qquad \forall x_1 < x_2\,.$$

4. *The probability distribution F is a right-continuous function, i.e.*

$$\lim_{h \to 0^+} F(x+h) = F(x) \ .$$

Proof. We prove each of the properties 1-4 separately.

1. Let x_n with $n \in \mathbb{N}$ be a decreasing sequence with $x_n \to -\infty$. The sets of all $X \in \mathbb{R}$ with $X \leq x_n$, denoted by $\{X \leq x_n\}$, form a decreasing sequence of sets, i.e. $\{X \leq x_m\} \subset \{X \leq x_n\}$ for $m > n$. As $x_n \downarrow -\infty$, the countable intersection $\bigcap_{n=1}^{\infty} \{X \leq x_n\} = \emptyset$, thus the sets themselves converge to the empty set, $\{X \leq x_n\} \to \emptyset$. By Definition 2.13 the probability distribution $F(x_n) = P(\{X \leq x_n\}) \to P(\emptyset) = 0$, i.e. $F(x_n) \to 0$.

2. The proof of property 2 is similar to the proof of property 1 but with an increasing sequence x_n with $n \in \mathbb{N}$ and $x_n \to \infty$. The desired property then follows by noticing that the sets $\{X \leq x_n\} \to \mathbb{R}$ with $P(\mathbb{R}) = 1$ and $F(x_n) = P(\{X \leq x_n\}) \to P(\mathbb{R}) = 1$, i.e. $F(x_n) \to 1$.

3. Let $a, b \in \mathbb{R}$, with $a < b$. Furthermore, let us define the sets $A = \{X \leq a\}$ and $B = \{X \leq b\}$. Notice that $A \subset B$. Hence, we can construct

$$B = (B \setminus A) \cup A \, , \qquad (B \setminus A) \cap A = \emptyset \, .$$

   By Definition 2.11-3, we have

$$P(B) = P(B \setminus A) + P(A) \ ,$$

   with $P(A), P(B \setminus A) \geq 0$. Thus, it follows

$$\begin{gathered} P(A) \leq P(B) \ , \\ P(\{X \leq a\}) \leq P(\{X \leq b\}) \ , \\ F(a) \leq F(b) \ , \end{gathered}$$

   which is the desired property.

4. The concept involved in proving property 4 is also very similar to the proof of property 1. Let h_n with $n \in \mathbb{N}$ be a decreasing sequence with $h_n \to 0$. Furthermore, $\forall x \in \mathbb{R}$ it holds that $\{X \leq (x + h_m)\} \subset \{X \leq (x + h_n)\}$ for $m > n$. As $h_n \downarrow 0$, the countable intersection given by $\bigcap_{n=1}^{\infty} \{X \leq (x + h_n)\} = \{X \leq x\}$, thus the sets themselves converge to the set $\{X \leq (x + h_n)\} \to \{X \leq x\}$. From this it follows that $P(\{X \leq (x + h_n)\}) \to P(\{X \leq x\})$ and finally $F(x + h_n) \to F(x)$ from the right, which completes the proof.

□

The concept of random variables and probability distributions can easily be generalized to multivariate random variables and multivariate probability distributions [48]. This is done by extending the definition of a random variable as a function, such that the inverse image of any interval $(-\infty, a]$ for all $a \in \mathbb{R}$ is measurable with respect to the defining σ-algebra $\mathcal{F}$, to a multidimensional function such that the inverse image of all sets $B \subseteq \mathbb{R}^n$ with $n \geq 1$ is measurable. The multivariate probability distribution of a multivariate random variable X is then given by

$$F(x) = P(X \in B(x)) \ , \tag{2.15}$$

where for any given $x \in \mathbb{R}^n$ the set $B(x)$ is the Borel set $B(x) = \{b \in \mathbb{R}^n : b \leq x, \text{ componentwise}\}$ [48].

For a random variable X with continuous probability distribution $F(x)$, it can be beneficial to have a look at the derivative of the probability distribution, given by the probability density function [48].

Definition 2.14 (Probability Density Function)**.** *Let X be a random variable on the probability space* $(\Omega, \mathcal{F}, P)$ *with distribution function* $F(x)$*. As long as* $F(x)$ *is continuous the probability density function* $f(x)$ *exists and is defined by*

$$f(x) = \frac{\mathrm{d}F(x)}{\mathrm{d}x} = \frac{\mathrm{d}P(\{X \leq x\})}{\mathrm{d}x},$$

such that

$$F(x) = \int_{-\infty}^{x} f(\xi)\ \mathrm{d}\xi\,.$$

The conditions for the existence of a probability density are given in detail in [52]. There, a generalization to arbitrary measures is given in terms of the Radon-Nikodym theorem. Probability densities are extremely useful when calculating expected values of random variables, which are formally defined in the following [52].

Definition 2.15 (Expected Value)**.** *Let X be an random variable defined on a probability space* $(\Omega, \mathcal{F}, P)$*. The expected value of the random variable X, denoted by* $\langle\!\langle X \rangle\!\rangle$ *is defined by*

$$\langle\!\langle X \rangle\!\rangle = \int_{\mathbb{R}} x\ \mathrm{d}F(x)\,,$$

where $F(x)$ *is the probability distribution of X.*

If there exists a probability density function $f(x)$ according to Definition 2.14, the expected value can be evaluated in terms of the integral

$$\langle\!\langle X \rangle\!\rangle = \int_{-\infty}^{\infty} x f(x)\ \mathrm{d}x\,, \tag{2.16}$$

according to Theorem 16.11 of [52]. Probability distributions are given in terms of set functions, i.e. we assign a probability to a set $\{X \leq x\}$ for each $x \in \mathbb{R}$. Probability densities, however, describe probabilistic properties in terms of point functions, which are easier to handle using known mathematical tools [55]. The simplification from set functions to point functions, given in terms of probability densities comes with the price, that a probability density f determines a probability distribution F only up to an additive constant. This means that a probability density f corresponds to a whole set of probability distributions, given by $F + c$, since it is defined as a derivative. This ambiguity can be avoided by introducing characteristic functions [55].

Definition 2.16 (Characteristic Function)**.** *Let X be a random variable on a probability space* $(\Omega, \mathcal{F}, P)$*. The characteristic function* $\varphi : \mathbb{R} \to \mathbb{C}$ *is given by the expected value*

$$\varphi(u) = \left\langle\!\left\langle \mathrm{e}^{\mathrm{i}uX} \right\rangle\!\right\rangle = \int_{\mathbb{R}} \mathrm{e}^{\mathrm{i}ux}\ \mathrm{d}F(x)\,.$$

Note that the characteristic function is (almost) equal to the Fourier transform of the probability density function [56]. The characteristic function has some important properties [53], [54], [57], [58], which are listed and proved in the following.

Properties 2.2 (Characteristic Function)**.** *Let* φ *be a characteristic function, then the following properties hold:*

1. *The characteristic function* φ *is non-vanishing at zero, i.e.*

$$\varphi(0) = 1\,.$$

2. *The characteristic function* φ *is bounded by* 1*, i.e.*

$$|\varphi(u)| \leq 1\,.$$

3. *The characteristic function φ is uniformly continuous, i.e.*

$$\forall \varepsilon > 0, \exists \delta > 0 : \forall u, v \in \mathbb{R} : |u - v| < \delta \Rightarrow |\varphi(u) - \varphi(v)| < \varepsilon \,.$$

4. *The characteristic function φ is Hermitian (see Definition 2.34), i.e.*

$$\varphi(-u) = \varphi^*(u) \,.$$

5. *For any $N \in \mathbb{N}$, any $z_n \in \mathbb{C}$ and any $u_n \in \mathbb{R}$ with $n \leq N$ it holds that*

$$\sum_{m,n=1}^{N} \varphi(u_m - u_n) \, z_m z_n^* \geq 0 \,.$$

Proof. We prove each of the properties 1-5 separately.

1. This directly follows by inserting $u = 0$ into the definition of the characteristic function, given in Definition 2.16. We have

$$\varphi(0) = \left\langle\!\left\langle e^{i0X} \right\rangle\!\right\rangle = \int_{\mathbb{R}} e^{i0 \cdot x} \, \mathrm{d}F(x) = \int_{\mathbb{R}} \mathrm{d}F(x) = 1 \,.$$

2. The boundedness of the characteristic functional also directly follows from Definition 2.16 and the triangle inequality,

$$|\varphi(u)| = \left| \int_{\mathbb{R}} e^{iux} \, \mathrm{d}F(x) \right| \leq \int_{\mathbb{R}} \left| e^{iux} \right| \, \mathrm{d}F(x) = \int_{\mathbb{R}} \mathrm{d}F(x) = 1 \,,$$

since $\left| e^{iux} \right| = 1$ for all $u, x \in \mathbb{R}$.

3. For proving uniform continuity, we consider $u \in \mathbb{R}$ and $v = u + h \in \mathbb{R}$. Then we have

$$|\varphi(u+h) - \varphi(u)| = \left| \left\langle\!\left\langle e^{i(u+h)X} \right\rangle\!\right\rangle - \left\langle\!\left\langle e^{iuX} \right\rangle\!\right\rangle \right| = \left| \left\langle\!\left\langle e^{iuX} \left(e^{ihX} - 1 \right) \right\rangle\!\right\rangle \right| \,.$$

Using Property 2.2-2, we can then argue that

$$|\varphi(u+h) - \varphi(u)| = \left| \left\langle\!\left\langle e^{iuX} \left(e^{ihX} - 1 \right) \right\rangle\!\right\rangle \right| \leq \left\langle\!\left\langle \left| e^{ihX} - 1 \right| \right\rangle\!\right\rangle \,.$$

It can be easily verified that the last expression tends to 0 as $h \to 0$, which proves the property.

4. The Hermitian property is also easily shown as

$$\varphi^*(u) = \left(\left\langle\!\left\langle e^{iuX} \right\rangle\!\right\rangle \right)^* = \left\langle\!\left\langle \left(e^{iuX} \right)^* \right\rangle\!\right\rangle = \left\langle\!\left\langle e^{-iuX} \right\rangle\!\right\rangle = \varphi(-u)$$

5. Finally, we have for the fifth property

$$\begin{aligned}
\sum_{m,n=1}^{N} \varphi(u_m - u_n) \, z_m z_n^* &= \sum_{m,n=1}^{N} z_m z_n^* \int_{\mathbb{R}} e^{iu_m x} e^{-iu_n x} \, \mathrm{d}F(x) \\
&= \int_{\mathbb{R}} \left(\sum_{m=1}^{N} z_m e^{iu_m x} \right) \left(\sum_{n=1}^{N} z_n^* e^{-iu_n x} \right) \mathrm{d}F(x) \\
&= \int_{\mathbb{R}} \left(\sum_{m=1}^{N} z_m e^{iu_m x} \right) \left(\sum_{n=1}^{N} z_n e^{iu_n x} \right)^* \mathrm{d}F(x) \\
&= \int_{\mathbb{R}} \left| \sum_{m=1}^{N} z_m e^{iu_m x} \right|^2 \mathrm{d}F(x) \geq 0 \,.
\end{aligned}$$

Since all properties 1-5 have been shown to hold individually, this concludes the proof. □

It is also important to note that, conversely, by Bochner's theorem [58], any function satisfying Properties 2.2 is a characteristic function corresponding to some probability measure μ.

Another important concept in probability theory is given in terms of independence of two events $A, B \in \mathcal{F}$, where $\mathcal{F}$ is a σ-algebra on a probability space $(\Omega, \mathcal{F}, P)$. Intuitively, independence means that knowledge about the occurrence of an event B does not imply anything about the occurrence of an event A. Hence, the probability that both events occur simultaneously, i.e. $P(A \cap B)$, relative to the probability $P(B)$ is equal to the probability $P(A)$. Thus, the following definition [54] of independence makes sense.

Definition 2.17 (Independence)**.** *Let $(\Omega, \mathcal{F}, P)$ be a probability space. Two events $A, B \in \mathcal{F}$ are called independent if and only if their joint probability, i.e. the probability of the event $A \cap B \in \mathcal{F}$ is equal to the product of the probabilities of A and B, i.e.*

$$P(A \cap B) = P(A)\, P(B) \ .$$

For random variables *X* and *Y*, described by the probability distributions $F_X(x)$ and $F_Y(y)$, the notion of independence has direct consequences for their joint probability distribution $F_{XY}(x, y)$. According to Definition 2.13, the probability distributions $F_X(x)$ and $F_Y(y)$ are given by the probabilities of the events $\{X \leq x\}$ and $\{Y \leq y\}$. If for every $x, y \in \mathbb{R}$ the two events $\{X \leq x\}$ and $\{Y \leq y\}$ are independent, i.e.

$$P(\{X \leq x\} \cap \{Y \leq y\}) = P(\{X \leq x\})\, P(\{Y \leq y\}) \ , \tag{2.17}$$

the two random variables *X* and *Y* are called independent. Their joint probability distribution $F_{XY}(x, y)$ is given by

$$F_{XY}(x, y) = F_X(x)\, F_Y(y) \ . \tag{2.18}$$

In probability theory, one is typically concerned with identifying simple relationships between realizations of random variables, such that one is able to construct probabilistic models for the probability distributions governing random processes [59]. There is a huge set of different classes of probability distributions, characterizing a random variable, however, there is one that stands out. This outstanding class of random variables is given in terms of Gaussian probability distributions, as defined in the following [54].

Definition 2.18 (Gaussian Random Variable)**.** *Let X be a random variable over the probability space $(\Omega, \mathcal{F}, P)$. We call X a Gaussian random variable, if the characteristic function φ associated with the probability measure P on $\mathcal{F}$ has the form*

$$\varphi(u) = \mathrm{e}^{\mathrm{i}u\mu - \frac{1}{2}u^2\sigma^2} \ .$$

For a Gaussian random variable X, there exists a probability density function, given by

$$f(x) = \frac{1}{\sqrt{2\pi\sigma^2}} \mathrm{e}^{-\frac{(x-\mu)^2}{2\sigma^2}} \ .$$

By complex integration [60], it is easy to show that the two parameters μ and σ^2 are given by

$$\mu = \langle\!\langle X \rangle\!\rangle \ , \tag{2.19}$$

$$\sigma^2 = \langle\!\langle X^2 \rangle\!\rangle - \langle\!\langle X \rangle\!\rangle^2 \ . \tag{2.20}$$

As μ and σ^2 are the only parameters in the characteristic function and the probability density function of a Gaussian random variable, specifying those two parameters is sufficient for fully characterizing the random variable. Gaussian random variables are very important, as the Gaussian distribution is the limiting distribution of a combination of many independent and identically distributed random variables. Thus, we will give special emphasis on Gaussian statistics in the remainder of this thesis. Before we can formalize why Gaussian statistics are given as the limiting case for an ensemble of independent and identically distributed random variables, let us first define a notion of convergence in a probability theoretic sense [59].

Definition 2.19 (Convergence)**.** *Let $X(\omega)$ and $X_n(\omega)$ with $n \in \mathbb{N}$ be random variables on a probability space $(\Omega, \mathcal{F}, P)$.*

1. *The sequence $X_n(\omega)$ converges to $X(\omega)$ with probability 1, i.e. $\lim_{n\to\infty} X_n(\omega) = X(\omega)$, if*

$$\lim_{n\to\infty} P\left(\left\{\sup_{m\geq n} |X_m(\omega) - X_n(\omega)| \geq \epsilon\right\}\right) = 0\,, \qquad \forall \varepsilon > 0\,.$$

2. *The sequence $X_n(\omega)$ converges to $X(\omega)$ stochastically, i.e. $\operatorname{p\lim}_{n\to\infty} X_n(\omega) = X(\omega)$, if*

$$\lim_{n\to\infty} P\left(\{|X_n(\omega) - X(\omega)| \geq \epsilon\}\right) = 0\,, \qquad \forall \varepsilon > 0\,.$$

3. *The sequence $X_n(\omega)$ converges to $X(\omega)$ in distribution, i.e. it converges weakly, if*

$$\lim_{n\to\infty} P\left(\{X_n \leq x\}\right) = P\left(\{X \leq x\}\right)\,, \qquad \forall x \in \mathbb{R}$$

Equipped with the notion of convergence in distribution, we can now formally prove the central limit theorem [53], which states that the sum of a large collection of independent and identically distributed random variables will behave according to Gaussian statistics.

Theorem 2.1 (Central Limit Theorem)**.** *Let X_n with $n \in \mathbb{N}$ be independent and identically distributed random variables over the same probability space $(\Omega, \mathcal{F}, P)$ with finite mean and finite variance. Then the probability distribution of the sum of M random variables X_n converges to a Gaussian random variable in distribution, as $M \to \infty$.*

Proof. Let S_M be the sum of M independent and identically distributed random variables, i.e.

$$S_M = \sum_{m=1}^{M} X_m = X_1 + X_2 + \ldots + X_M\,.$$

The mean and variance of the random variable, generated by the sum over X_m are given by

$$\langle\!\langle S_M \rangle\!\rangle = \left\langle\!\!\left\langle \sum_{m=1}^{M} X_m \right\rangle\!\!\right\rangle = \sum_{m=1}^{M} \langle\!\langle X_m \rangle\!\rangle = M \langle\!\langle X_m \rangle\!\rangle\,,$$

$$\langle\!\langle S_M^2 \rangle\!\rangle - \langle\!\langle S_M \rangle\!\rangle^2 = \sum_{m=1}^{M}\sum_{n=1}^{M} \langle\!\langle X_m X_n \rangle\!\rangle - \sum_{m=1}^{M}\sum_{n=1}^{M} \langle\!\langle X_m \rangle\!\rangle \langle\!\langle X_n \rangle\!\rangle = M\left(\langle\!\langle X_m^2 \rangle\!\rangle - \langle\!\langle X_m \rangle\!\rangle^2\right)\,.$$

The last step holds because the random variables are independent and identically distributed. Let us now define an auxiliary random variable Z_M with zero mean and unit variance by standardization, given by

$$Z_M = \frac{S_M - M\langle\!\langle X_m \rangle\!\rangle}{\sqrt{M\left(\langle\!\langle X_m^2 \rangle\!\rangle - \langle\!\langle X_m \rangle\!\rangle^2\right)}}\,.$$

We can express Z_M in terms of the original independent random variables X_m by

$$Z_M = \sum_{m=1}^{M} \frac{X_m - \langle\!\langle X_m \rangle\!\rangle}{\sqrt{M\left(\langle\!\langle X_m^2 \rangle\!\rangle - \langle\!\langle X_m \rangle\!\rangle^2\right)}} = \frac{1}{\sqrt{M}} \sum_{m=1}^{M} Y_m\,,$$

where we introduced another set of auxiliary random variables Y_m with zero mean and unit variance, given by

$$Y_m = \frac{X_m - \langle\!\langle X_m \rangle\!\rangle}{\sqrt{\left(\langle\!\langle X_m^2 \rangle\!\rangle - \langle\!\langle X_m \rangle\!\rangle^2\right)}}\,.$$

Now let φ_{Z_M} be the characteristic function of the sum Z_M, which can, by Definition 2.16, be written as

$$\varphi_{Z_M}(u) = \left\langle\!\left\langle \mathrm{e}^{\mathrm{i}uZ_M} \right\rangle\!\right\rangle = \prod_{m=1}^{M} \left\langle\!\left\langle \mathrm{e}^{\mathrm{i}\frac{uY_m}{\sqrt{M}}} \right\rangle\!\right\rangle = \left\langle\!\left\langle \mathrm{e}^{\mathrm{i}\frac{uY_m}{\sqrt{M}}} \right\rangle\!\right\rangle^M .$$

Let us now perform a Taylor expansion of the exponential term

$$\left\langle\!\left\langle \mathrm{e}^{\mathrm{i}\frac{uY_m}{\sqrt{M}}} \right\rangle\!\right\rangle^M = \left(1 + \frac{\mathrm{i}u\langle\!\langle Y_m \rangle\!\rangle}{\sqrt{M}} + \frac{\left\langle\!\left\langle (\mathrm{i}uY_m)^2 \right\rangle\!\right\rangle}{2!M} + \frac{\left\langle\!\left\langle (\mathrm{i}u\langle\!\langle Y_m \rangle\!\rangle)^3 \right\rangle\!\right\rangle}{3!M^{\frac{3}{2}}} + \ldots\right)^M = \left(1 - \frac{u^2}{2M} + \mathcal{O}\left(\frac{u^2}{M}\right)\right)^M ,$$

where $\mathcal{O}\left(\frac{u^2}{M}\right)$ implies that the remaining error terms tend to zero faster than by quadratic order for $\frac{u^2}{M} \to 0$ [61]. Furthermore, we have used that the Y_m have all zero mean and unit variance. Hence, we have for the characteristic function φ_{Z_M} in the limiting case for a large number $M \to \infty$ of independent and identically distributed random variables Y_M

$$\lim_{M\to\infty} \varphi_{Z_M}(u) = \lim_{M\to\infty} \left(1 - \frac{u^2}{2M} + \mathcal{O}\left(\frac{u^2}{M}\right)\right)^M = \mathrm{e}^{-\frac{1}{2}u^2} .$$

By Definition 2.18, the last term is equal to the characteristic function of a Gaussian random variable, which by Bochner's theorem [58] and Levy's continuity theorem [61] implies convergence in distribution to a Gaussian random variable. □

This theorem emphasizes the importance of Gaussian random variables for modeling a whole variety of practically relevant physical processes. In nature, random processes often arise due to a lack of knowledge of the state of large ensembles of individual parameters. Hence, Gaussian statistics seems to be a suitable first-order assumption for modeling such processes by the central limit theorem.

A natural extension to the concept of a random variable is given in terms of a random process, which in turn is given by performing a random experiment repeatedly. Let us assume a random process with index set T, which is given in terms of a random variable X_{t_0} for each $t_0 \in T$. For different $t_0 \in T$, the random variable X_{t_0} might behave differently, i.e. it may be described by a different probability distribution. Therefore, it is useful to extend the definition of a random variable, which takes the outcome $\omega \in \Omega$ of a probabilistic experiment and maps it to a real number. This extension of a random variable is done by introducing a second variable, such that a random process is mapping the outcome of a random experiment to a real number, depending on an element of the index set T [25]. The index set T can be chosen to be an arbitrary set. For a general N-dimensional index set T, we introduce a random field in the following definition [25].

Definition 2.20 (Random Field)**.** *Let $(\Omega, \mathcal{F}, P)$ be a probability space and let X_t be a family of random variables indexed by some $t \in T$, where T is any arbitrary index set. For every $t_0 \in T$ and $\omega \in \Omega$, X_{t_0} is a random variable*

$$\begin{aligned} X_{t_0} : \Omega &\to \mathbb{R}^n , \\ \omega &\mapsto X_{t_0}(\omega) . \end{aligned}$$

Such a family $X_t = X(\omega, t)$ of random variables is called random field.

We distinguish between random fields and random processes, where a random process is a random field with index set $T \subseteq \mathbb{R}$ [25]. A random field may be indexed by any multidimensional index set $T \subseteq \mathbb{R}^n$ with $n \in \mathbb{N}$. Depending on the cardinality of the index set $T \subseteq \mathbb{R}$, one further distinguishes between random sequences and random processes [54]. For a finite or countable infinite index set T we call a process X_t with $t \in T$ a discrete parameter process or random sequence. If the index set T is an interval, i.e. an index set with more than countable infinitely many elements, then we call $X_t = X(\omega, t)$ with $t \in T$ a continuous parameter process [62].

The probability distribution for each random variable X_{t_0} with $t_0 \in T$ is given by

$$F_{t_0}(x) = P(\{X_{t_0}(\omega) \leq x\}) . \tag{2.21}$$

Thus, we can construct the finite dimensional joint probability distributions [59] for the process X_t by

$$F_{t_1,t_2,\ldots,t_n}(x_1,x_2,\ldots,x_n) = P\left(\{X_{t_1}(\omega) \leq x_1, X_{t_2}(\omega) \leq x_2, \ldots, X_{t_n}(\omega) \leq x_n\}\right). \tag{2.22}$$

Assuming continuity of $F_{t_1,t_2,\ldots,t_n}(x_1,x_2,\ldots,x_n)$ for all n, we can obtain the finite dimensional joint probability density functions [25]

$$f_{t_1,t_2,\ldots,t_n}(x_1,x_2,\ldots,x_n) = \frac{\partial^n F_{t_1,t_2,\ldots,t_n}(x_1,x_2,\ldots,x_n)}{\partial x_1 \partial x_2 \ldots \partial x_n}, \tag{2.23}$$

similar to Definition 2.14.

There are two different ways of interpreting a random field. The first way was illustrated above, where a stochastic process or a random field is seen as a collection of random variables, where for each element of the index set T, the random variable is described by a certain probability distribution. The probability distribution for each individual random variable can be extracted from the family of finite dimensional joint probability distributions by marginalization [48]. However, the finite dimensional joint probability distributions do not only contain information about the marginal probability distribution of each random variable but also how those random variables are interrelated. Obviously, the finite dimensional joint probability distributions, describing the random field, need to be mutually consistent [59]. The conditions for consistency are summarized in Definition 2.21.

Definition 2.21 (Compatibility Conditions)**.** *Let $F_{t_1,t_2,\ldots,t_n}(x_1,x_2,\ldots,x_n)$ for $n \geq 1$ be a family of finite dimensional joint probability distributions. The finite dimensional joint probability distributions are said to be consistent if*

$$F_{t_1,t_2,\ldots,t_m}(x_1,x_2,\ldots,x_m) = \lim_{x_j \to \infty, j \geq m+1} F_{t_1,t_2,\ldots,t_n}(x_1,x_2,\ldots,x_m,x_{m+1},\ldots,x_n),$$

and for each $m < n$,

$$F_{t_1,t_2,\ldots,t_n}(x_1,x_2,\ldots,x_n) = F_{t_{\pi(1)},t_{\pi(2)},\ldots,t_{\pi(n)}}\left(x_{\pi(1)},x_{\pi(2)},\ldots,x_{\pi(n)}\right),$$

where $\pi(\cdot)$ is an arbitrary permutation, i.e. a bijective mapping of indices.

It has been shown in [50], [51], that these conditions are sufficient in order to derive a measure in function space from a prescribed family of finite dimensional joint probability distributions. This fact is also given in terms of Kolmogorov's theorem in Theorem 2.2.

The second way of describing random fields is probably less intuitive. Previously, we introduced a random field as a two-parameter mapping of a random outcome $\omega \in \Omega$ and an element $t_0 \in T$ of an index set. The first approach corresponds to fixing the index t_0, and looking at each index position individually, where we have a random variable, mapping $\omega \mapsto X_{t_0}(\omega)$. In the second approach, also called sample-function or trajectory [63] of a random process, we fix a random outcome $\omega_0 \in \Omega$ and observe a function mapping $t \mapsto X(\omega_0, t)$. In this view, for each random outcome $\omega_0 \in \Omega$, there is a realization of a sample-function $X(\omega_0, t)$, where we can assign probabilities to each measurable set of sample-functions. A helpful construction of such a set of measurable functions is given in terms of cylindrical sets [50], [51].

Definition 2.22 (Cylindrical Set)**.** *Let $X_t = X(\omega,t)$, $\omega \in \Omega$ be a random field over the probability space $(\Omega, \mathcal{F}, P)$ mapping $t \in T$ into some measurable space $(Y, \mathcal{B})$. The set of functions $X(\omega,t)$ for which the point $[X(\omega,t_1), X(\omega,t_2), \ldots, X(\omega,t_n)] \in Y^n$ belongs to $B^n \in \mathcal{B}^n$, i.e. the set*

$$C_{t_1 \ldots t_n}(B^n) = \{X(\omega,\cdot) : [X(\omega,t_1), X(\omega,t_2), \ldots, X(\omega,t_n)] \in B^n\}$$

is called cylindrical set in Ω with basis B^n over the coordinates $t_1, t_2, \ldots, t_n$.

The concept of cylindrical sets was introduced in order to construct a σ-algebra, generated by cylindrical sets in function space. Such a σ-algebra, generated by cylindrical sets has interesting properties, which are shown in [64]. With this formal definition of a cylindrical set, we can give the statement of Kolmogorov's construction theorem, which is among the most fundamental theorems when considering probabilities in function spaces, as it ensures the existence of a probability measure, given a consistent family of finite dimensional joint probability distributions [65].

Theorem 2.2 (Kolmogorov). *Let X be the space of all fields X_t mapping an index set T to some measurable space $(Y, \mathcal{B})$, and let $\mathcal{H}$ be the minimum σ-algebra containing all the cylindrical sets of X. Any system of finite dimensional joint probability distributions satisfying the compatibility conditions from Definition 2.21 determines a probability measure μ on $\mathcal{H}$.*

Proof. The proof of this fundamental theorem is a bit lengthy and will not be presented here. It can be found in the original work by Kolmogorov [50], [51] and in a different form in [54]. □

Already in the original work from 1933, Kolmogorov noticed that difficulties arise if the index set has an uncountable number of entries [50], [51]. In [58], [66], it was pointed out that special care must be taken when discussing probabilities of random processes for a more than countable index set. In 1947, Doob proposed to impose a restriction on the class of random fields, depending on a continuous index set, called separability [59], [65]. This restriction is given in terms of separable random fields, which will be defined in the following.

Definition 2.23 (Separability). *Let $(\Omega, \mathcal{F}, P)$ be a probability space. A random field $X(\omega, t)$ on $(\Omega, \mathcal{F}, P)$ with index set T is called separable with respect to a class of sets $\mathcal{A}$ if there exists a countable subset $T_1 \subseteq T$ and there is a set $\Lambda \subset \mathcal{F}$ with $P(\Lambda) = 0$, such that for any $A \in \mathcal{A}$ and for any open set $I \subset T$ one has*

$$\{X(\omega, t) \in A, \forall t \in I \cap T_1\}\,, \qquad \{X(\omega, t) \in A, \forall t \in I \cap T\}\,,$$

differ at most on a subset of Λ. This is,

$$\bigcap_{t \in I \cap T_1} \{X(\omega, t) \in A\} \setminus \bigcap_{t \in I \cap T} \{X(\omega, t) \in A\} \subseteq \Lambda\,.$$

The smallest class $\mathcal{A}$ for which the concept of separability of a random process is useful is the class of all finite or infinite closed intervals [59]. For random fields, the class of closed sets is an important special case. In [59], Doob has not only shown that the problem of finding probabilities for sample functions to be e.g. continuous, or integrable can not be given consistently can be resolved for the class of separable processes, but also that separability does not pose a restriction on a random process at all. This is known in terms of Doob's theorem, which will be stated in the following [59].

Theorem 2.3 (Doob). *Let $X_t = X(\omega, t)$, $\omega \in \Omega$, $t \in T$ be a random field over the probability space $(\Omega, \mathcal{F}, P)$, with linear parameter set T. Then there is a random field $\tilde{X}_t = \tilde{X}(\omega, t)$, defined on the same probability space, which is separable relative to the class of closed sets, with the property*

$$P\left(X(\omega, t) = \tilde{X}(\omega, t)\right) = 1\,, \qquad t \in T\,.$$

Proof. We refrain from giving a proof for Doob's theorem here since we have not yet developed the complete setting necessary for proving the theorem, which is beyond the scope of this thesis. Nevertheless, the complete proof can be found in the original work by Doob from 1953 [59]. □

With the theorems by Kolmogorov (Theorem 2.2) and Doob (Theorem 2.3), the existence of a consistent measure μ on function space, given by the family of finite dimensional joint probability distributions is ensured. It has been shown in [54], that for an existing measure μ on a measurable function space X, there exists a characteristic functional, which is an extension of the definition of a characteristic function for random variables to the case of random fields in function space. The characteristic functional is a complete description of the underlying random field and will be formally defined in the following [54].

Definition 2.24 (Characteristic Functional). *Let $X_t = X(\omega, t)$ be a random field over $(\Omega, \mathcal{F}, P)$ in the space X of all fields mapping an index set T to a measurable space $(Y, \mathcal{B})$. We define the characteristic functional of the random field $X_t = X(\omega, t)$, $\chi : X \to \mathbb{C}$ for all fields $x \in X$ by*

$$\chi(l) = \int_X \mathrm{e}^{\mathrm{i}l(x)}\, \mu(\mathrm{d}x)\,,$$

where μ is the probability measure over the minimal σ-algebra $\mathcal{H}$ with respect to which all the functions in X are measurable.

Similar as for characteristic functions of random variables, the characteristic functional must be continuous in the sense that for a sequence of linear functionals $l_n \in L$, where L is the space of linear functionals on X, with $l_n(x) \to l(x)$ for all $x \in X$, $\chi(l_n) \to \chi(l)$ as $l_n \to l$. For a characteristic functional it must also hold that for arbitrary $N \in \mathbb{N}$, any linear functional $l_n \in L$ and any complex numbers $z_n \in \mathbb{C}$,

$$\sum_{m,n=1}^{N} \chi(l_m - l_n) z_m z_n^* \geq 0 \,. \tag{2.24}$$

This is true since by Definition 2.24 we have

$$\sum_{m,n=1}^{N} \chi(l_m - l_n) z_m z_n^* = \int_X \left| \sum_{m=1}^{N} z_m \mathrm{e}^{\mathrm{i} l_m(x)} \right|^2 \mu(\mathrm{d}x) \,. \tag{2.25}$$

It was shown in [54] that the probability measure μ is completely described by the characteristic functional $\chi(l)$. Thus, it is equivalent to describe a separable random field by a family of finite dimensional joint probability distributions or by a characteristic functional.

Now let X, i.e. the space of fields mapping the index set T to the measurable space Y be a Hilbert space. The following theorem [67] will be useful.

Theorem 2.4 (Riesz Representation Theorem)**.** *Let X be a Hilbert space and $L = X'$ the dual space. Then for each continuous linear functional $l \in L$, there exists a unique $z \in X$ such that*

$$l(x) = \langle z, x \rangle \,, \qquad \forall x \in X \,,$$

where $\langle \cdot, \cdot \rangle$ denotes an inner product on X.

We are going to prove this theorem in several steps. Let us first prove the following lemma [67].

Lemma 2.1. *Let X be a Hilbert space and let $T : X \to \mathbb{C}$ be a linear map (linear functional). Then T is continuous if and only if* $\ker T$ *is closed.*

Proof.
($\Rightarrow$) Suppose T is continuous. Then there exists a sequence $x_n \to x$ with $x_n, x \in X$, such that $T(x_n) \to T(x)$. Now let $x_n \in \ker T$ and $x_n \to x$. Then $T(x_n) = 0$, and by continuity

$$T(x) = \lim_{n \to \infty} T(x_n) = 0 \,.$$

Hence $x \in \ker T$ and thus $\ker T$ is closed.
($\Leftarrow$) Now suppose T is not continuous. Then there exists a bounded sequence $x_n \in X$ with $\|x_n\| \leq 1$ such that $|T(x_n)| \to \infty$ as $n \to \infty$. Let $a \notin \ker T$ and let us define a sequence x_n' by

$$x_n' = a - \frac{T(a)}{T(x_n)} x_n \,.$$

It is clear that $T(x_n') = 0$ and thus $x_n' \in \ker T$. Furthermore $x_n' \to a$ and $a \notin \ker T$. Thus $\ker T$ is not closed. □

For proving thr Riesz representation theorem, we will also make use of another lemma, which is directly contained in the proof of [67].

Lemma 2.2. *Let X be a Hilbert space and let $A \subseteq X$ be a closed subspace. Then the orthogonal complement of A, denoted by $A^\perp$, is closed and*

$$X = A \oplus A^\perp \,.$$

Proof. Let $x_n \to x_0$ with $x_n \in A^\perp$ be a sequence converging to an element $x_0 \in X$, then

$$\langle x_0, a\rangle = \left\langle \lim_{n\to\infty} x_n, a \right\rangle = \lim_{n\to\infty} \langle x_n, a\rangle = 0\,, \qquad \forall a \in A\,,$$

which implies that $x_0 \in A^\perp$ and thus $A^\perp$ is a closed subspace. Furthermore, $\forall x \in X$, there exists a best approximation of x in A, denoted by $a_0 \in A$, that satisfies $(x - a_0) \in A^\perp$. Thus, we can write x as

$$x = a_0 + (x - a_0)\ ,$$

which implies

$$X = A + A^\perp\,.$$

Additionally, if $y \in A \cap A^\perp$, then $\langle y, y\rangle = 0$, which means that $y = 0$ and thus,

$$A \cap A^\perp = \{0\}\ .$$

□

Equipped with Lemma 2.1 and Lemma 2.2, we are now ready for proving Riesz Representation Theorem 2.4 [67].

Proof of Riesz Representation Theorem 2.4.
Existence - If $l = 0$ we can take $z = 0$ and thereby have $l(x) = 0 = \langle 0, x\rangle$, $\forall x \in X$. Suppose now $l \neq 0$, i.e. $\ker l \neq X$. Recall that, since l is continuous $\ker l$ is a closed subspace of X by Lemma 2.1. It then follows from Lemma 2.2 that

$$X = \ker l \oplus (\ker l)^\perp\ ,$$

and as $\ker l \neq X$, we can find a $y \in (\ker l)^\perp$ such that $\|y\| = 1$. From the linearity of l we have

$$(l(x)\, y - l(y)\, x) \in \ker l\,, \qquad \forall x \in X\,.$$

Since $y \in (\ker l)^\perp$,

$$\begin{aligned} 0 &= \langle y, l(x)\, y - l(y)\, x\rangle \\ &= l(x)\,\langle y, y\rangle - l(y)\,\langle y, x\rangle \\ &= l(x)\,\|y\|^2 - \langle l^*(y)\, y, x\rangle \\ &= l(x) - \langle l^*(y)\, y, x\rangle\ , \end{aligned}$$

which implies

$$l(x) = \langle l^*(y)\, y, x\rangle\ .$$

The theorem follows by taking $z = l^*(y)\, y$.
Uniqueness - Suppose there were $z_1, z_2 \in X$ such that for all $x \in X$,

$$l(x) = \langle z_1, x\rangle = \langle z_2, x\rangle\ .$$

Then $\langle z_1 - z_2, x\rangle = 0$ for every $x \in X$. Taking $x = z_1 - z_2$ we obtain

$$\|z_1 - z_2\|^2 = 0\,,$$

which implies $z_1 = z_2$. □

As a result of this theorem, the characteristic functional of a random process $X_t = X(\omega, t)$ on a Hilbert space X of functions can be written in terms of an inner product by

$$\chi(z) = \int_X \mathrm{e}^{\mathrm{i}\langle z, x\rangle}\, \mu(\mathrm{d}x)\,. \tag{2.26}$$

This is a very important result, not only for characteristic functionals. When describing stochastic electromagnetic fields in the remainder of this thesis, we will exclusively assume the Hilbert space property (Definition 2.8) and hence describe random fields by characteristic functionals, given by inner products of field variables.

Similar to random variables, we can characterize a random process according to the probability distributions involved. The most important family of random fields is again governed by Gaussian statistics, with a similar argument as before, when considering random variables. A Gaussian random field is uniquely described by the form of the characteristic functional, which will be defined in the following [54].

Definition 2.25 (Gaussian Random Field)**.** *Let $X_t = X(\omega, t)$ be a separable random field with index set T over the probability space $(\Omega, \mathcal{F}, P)$ on the Hilbert space of fields X, taking on values in a measurable space $(Y, \mathcal{B})$. Let $\mathcal{H}$ denote the minimum σ-algebra to which all fields on the space X are measurable, and let μ define the probability measure on $\mathcal{H}$. The random field $X_t = X(\omega, t)$ is called a Gaussian field if the characteristic functional associated with the measure μ has the form*

$$\chi(z) = \exp\left(\mathrm{i}\,\langle z, m_X\rangle - \frac{1}{2}\left\langle z, \hat{\Gamma}_{\mathrm{X}} z\right\rangle\right),$$

for all $z \in X$. Here, m_X is called the mean value function and $\hat{\Gamma}_{\mathrm{X}}$ is referred to as correlation kernel operator.

For any finite set of elements $\{t_1, t_2 \ldots, t_n\}$, the finite dimensional joint probability density function $f_{t_1,t_2,\ldots,t_n}(x_1, x_2, \ldots, x_n)$ exists and has the form given in Definition 2.18, if $\hat{\Gamma}_{\mathrm{X}}$ is non-singular. Some authors even define Gaussian random fields by prescribing a multinormal Gaussian probability density, as it is the case in [25].

The first statistical moment of a random field is given in terms of a mean value function, that is described in terms of a so-called ensemble average. Ensemble averages shall be defined in the following [48].

Definition 2.26 (Ensemble Average)**.** *Let $X(\omega, t)$ be a random field over a probability space $(\Omega, \mathcal{F}, P)$ with $\omega \in \Omega$ and $t \in T$ with some index set T. Let us now keep the index parameter $t = t_n$ fixed. The integral*

$$\langle\!\langle X(\omega, t_n)\rangle\!\rangle = \int_{-\infty}^{\infty} x_n\, \mathrm{d}F_{t_n}(x_n)$$

over the random variable X_{t_n} with fixed $t_n \in T$ is called ensemble average of the random variable X_t at index t_n.

The second order moments of a random process, i.e. correlation functions or kernel operators, in turn, describe the interrelation of the realization of a random field at one index t_m with the realization at another index t_n. Correlation functions are also used as a measure of energy in random fields, which makes them an important concept when considering electromagnetic compatibility [16]. Let us define them according to sets of second order joint probability distributions [54].

Definition 2.27 (Correlation Function)**.** *Let $X(\omega, t)$ be a random field over a probability space $(\Omega, \mathcal{F}, P)$ with $\omega \in \Omega$ and $t \in T$ with some index set T. For any arbitrary pair of indices $t_m, t_n \in T$ the integral*

$$\langle\!\langle X(\omega, t_m)\, X^{\dagger}(\omega, t_n)\rangle\!\rangle = \int_{-\infty}^{\infty}\int_{-\infty}^{\infty} x_m x_n^{\dagger}\, \mathrm{d}F_{t_m,t_n}(x_m, x_n)$$

is called correlation function of the random field at indices t_m and t_n.

In general, the n-th order statistical moment of a random field can also be directly obtained from the characteristic functional, fully describing the random field, by the n-th order functional derivative of the characteristic functional, invoking an n-th order tensor product [68].

An important special case of a random field or a random process is if the statistics do not change over at least one dimension of the parameter space T, where typically time is considered. This means that for such a process, which is called a stationary process, the statistical properties remain constant over time. Stationarity also imposes shift-invariance for the moments of the random field, along the dimension which is considered stationary. Let us now formally define stationary according to [69].

Definition 2.28 (Stationarity)**.** *A stochastic process $X_t = X(\omega, t)$ with index set T is called stationary if for any arbitrary collection of indices $t_1, t_2, \ldots, t_n$ with $n \geq 1$, the associated finite dimensional joint probability distribution*

$$F_{t_1,t_2,\ldots,t_n}(x_1, x_2, \ldots, x_n) = F_{t_1+\tau,t_2+\tau,\ldots,t_n+\tau}(x_1, x_2, \ldots, x_n) \,,$$

for all τ such that $t_k + \tau \in T$ for any $t_k \in T$.

When considering stationary random fields, one is interested in the shift-invariance property for the first and second order statistical moments. Thus, a weaker definition of stationarity in terms of the following definition was proposed [69], [70].

Definition 2.29 (Wide-Sense Stationarity)**.** *A second order stochastic process $X_t = X(\omega, t) \in \mathcal{L}^2$ with index set T is called stationary in the wide sense if for the first and second moment*

$$\langle\!\langle X(\omega, t) \rangle\!\rangle = \langle\!\langle X(\omega, t + \tau) \rangle\!\rangle = \mu = \text{const.} \,,$$

and

$$\langle\!\langle X(\omega, s) X^{\dagger}(\omega, t) \rangle\!\rangle = \langle\!\langle X(\omega, s + \tau) X(\omega, t + \tau) \rangle\!\rangle \,,$$

for any $s, t, \tau \in T$.

If a random process is subjected to a repetitive operation, the resulting random process will usually exhibit statistical properties that vary periodically in time [70]. Such random processes are often encountered when considering digital signals which always operate using a certain clock. These periodically correlated or cyclostationary random processes will hence be useful for describing stochastic electromagnetic fields, emitted by digital signal sources [36]. However, let us first formally introduce cyclostationarity as a property of a random process [69].

Definition 2.30 (Cyclostationarity)**.** *A stochastic process $X_t = X(\omega, t)$ with index set T is called cyclostationary with periodicity T_0 if for any arbitrary collection of indices $t_1, t_2, \ldots, t_n$ with $n \geq 1$, the associated finite dimensional joint probability distribution*

$$F_{t_1,t_2,\ldots,t_n}(x_1, x_2, \ldots, x_n) = F_{t_1+T_0,t_2+T_0,\ldots,t_n+T_0}(x_1, x_2, \ldots, x_n) \,,$$

such that every $t_k + T_0 \in T$ for any $t_k \in T$.

Similar as for stationary random fields, one is interested in the periodic shift-invariance, introduced by cyclostationarity. Thus, we will introduce a weaker definition of cyclostationarity for second order processes in terms of wide-sense cyclostationarity [69].

Definition 2.31 (Wide-Sense Cyclostationarity)**.** *A second order stochastic process $X_t = X(\omega, t) \in L^2$ with index set T is called cyclostationary in the wide sense with periodicity T_0 if for the first- and second moment*

$$\langle\!\langle X(\omega, t) \rangle\!\rangle = \langle\!\langle X(\omega, t + T_0) \rangle\!\rangle \,,$$

and

$$\langle\!\langle X(\omega, s) X(\omega, t) \rangle\!\rangle = \langle\!\langle X(\omega, s + T) X(\omega, t + T) \rangle\!\rangle \,,$$

for any $s, t \in T$.

In general, it is easy to show that strict stationarity implies wide-sense stationarity. The same holds for cyclostationarity, as strict cyclostationarity implies wide-sense cyclostaitonarity. The converse is in general not true, i.e. wide-sense stationarity or cyclostationarity does not necessarily imply strict stationarity or cyclostationarity, respectively [69]. However, note that for Gaussian random fields, the converse holds, as Gaussian random fields are fully described by specifying the first and second order moments.

For a strictly stationary random field $X_t = X(\omega, t)$ over a probability space $(\Omega, \mathcal{F}, P)$, according to Definition 2.28, the family of finite dimensional joint probability distributions does not depend on the absolute indices t_1 and t_2, but rather on the index difference $\tau = t_1 - t_2$. One way of constructing a strictly stationary random field is by considering a transformation $S : \Omega \to \Omega$ [54]. Let $X_{t_0} = X(\omega, t_0)$ be a random variable. Then the transformation S transforms the random variable X_{t_0} into another random variable $S X_{t_0}$ with

$$SX(\omega, t_0) = X\left(S^{-1}\omega, t_0\right) = X(\omega, t_1) \ . \tag{2.27}$$

Let S now be a measure preserving map, i.e. $P\left(S^{-1}A\right) = P(A), \forall A \in \mathcal{F}$. From this property it follows that $P\left(S^{-1}\omega\right) = P(\omega)$, such that the random variables X_{t_0} and $S X_{t_0}$ have the same probability distributions. The same holds for arbitrary powers $S^n X_{t_0}$. Thus, with the group S_t of measure preserving transformations S, one can construct a strictly stationary random field by [54]

$$X_t = X(\omega, t) = S_t X(\omega, t_0) = X(S_{-t}\omega, t_0) = X(\omega, t_0 + t) \ . \tag{2.28}$$

In terms of the group S_t of measure preserving transformations S, we can define the concept of ergodicity for stationary random fields [54].

Definition 2.32 (Ergodicity)**.** *Let $X_t = X(\omega, t)$ be a random field over a probability space $(\Omega, \mathcal{F}, P)$ with $\omega \in \Omega$ and $t \in T$ with some index set T. Furthermore, let $S : \Omega \to \Omega$ be a measure preserving map, i.e. $P\left(S^{-1}(A)\right) = P(A)$, $\forall A \in \mathcal{F}$. The random field X_t is called ergodic with respect to the transformation S, if for every random variable $X_{t_0} : \Omega \to \mathbb{R}$ with $S X_{t_0} = X\left(S^{-1}\omega, t_0\right) = X_{t_0}$, X_{t_0} converges to a constant with probability* 1.

By Birkhoff's ergodicity theorem [59], [71], if X_n is ergodic with respect to S, we have for the ensemble average

$$\langle\!\langle X(\omega, t_n) \rangle\!\rangle = \int_{-\infty}^{\infty} x_n \ \mathrm{d}F_{t_n}(x_n) = \lim_{N\to\infty} \frac{1}{N} \sum_{k=1}^{N} S^{k-1} x(t_0) \ , \tag{2.29}$$

where $x(t_k)$ is a realization of the field X_t at $t = t_k$. For continuous parameter random fields with a group S_t of measure preserving transformations S we have

$$\langle\!\langle X(\omega, t_n) \rangle\!\rangle = \int_{-\infty}^{\infty} x_n \ \mathrm{d}F_{t_n}(x_n) = \lim_{T\to\infty} \frac{1}{2T} \int_{-T}^{T} S_t x(t_0) \ \mathrm{d}t \, , \tag{2.30}$$

thus, ensemble averages can be replaced with time-averages for ergodic random fields. This makes it possible to infer statistical parameters of a random field from field samples. For characterizing random fields by field measurements, as we will discuss in chapter 4, ergodicity is an essential property.

2.4 Vector Calculus

Maxwell's equations have been formulated in a whole variety of different notations. Among those, exterior differential forms [72], quaternions and Clifford algebras [73] are probably the most advanced concepts. In a recent work, electromagnetics has also been formulated using Dirac matrices by exploiting an isomorphism between Clifford algebra and Pauli algebra in three-dimensional space [74]. In relativistic electrodynamics, the typical mathematical framework is given in terms of tensor analysis in four-dimensional space-time [75]. For stochastic electromagnetic fields in particular, we have derived a representation in the framework of differential

forms [76]. Besides all these advanced formulations of electrodynamics, the by far most common formalism for writing down Maxwell's equations in physics and engineering is given in terms of vector calculus, which was developed by Gibbs [77] and Heaviside [78] in the late 19th century. In this section, we will prove some important results from vector calculus, which are necessary in order to formulate electromagnetism within an axiomatic setting.

Let us start with the definition of a radially convex set, which is an important construction for proving Poincaré's lemma later on. A radially convex set, or star domain, can be thought of as a set, where there exists a point x_0 from which all other points in the set are directly visible, i.e. there is a straight line connecting any point of the set with x_0 where all points on the straight line belong to the set itself. Formally, this is given by the following definition [79].

Definition 2.33 (Radially Convex Set)**.** *A set $U \subseteq \mathbb{R}^n$ is called radially convex set, if $\exists x_0 \in U$, such that $\forall x \in U$,*

$$\{x_0 + t\,(x - x_0) : t \in [0,1]\} \subseteq U\,.$$

The set of points $x_0 \in U$ is referred to as star center of the radially convex set U.

As mentioned before, Definition 2.33 can be seen as a starting point for proving the lemma of Poincaré, which will turn out to be fundamental in an axiomatic approach to electromagnetism [75], which we will develop in section 3.5 in the following chapter. The general version of Poincaré's lemma applies to exterior differential forms and states that on a radially convex set, each closed differential form is exact [80]. We do not give any detailed definitions on closed and exact differential forms here, as differential forms are beyond the scope of this thesis. Nevertheless, the interested reader is referred to [80] for further details. Lindell annotated the correspondence of the implications of Poincaré's lemma in differential form to the vector calculus analogies in [81]. In the following, we will state the lemma and prove it using vector calculus notation [79].

Lemma 2.3 (Poincaré's Lemma)**.** *Let $U \subseteq \mathbb{R}^3$ be a radially convex set and let $\boldsymbol{v} : U \to \mathbb{R}^3$ be a smooth vector field and $f : U \to \mathbb{R}$ be a smooth scalar field defined on U. Then the following relations hold.*

1. *If $\nabla \times \boldsymbol{v} = 0$ then there exists a scalar field g, such that*

$$\boldsymbol{v}\,(\boldsymbol{r}) = \nabla\, g\,(\boldsymbol{r})\,.$$

2. *If $\nabla \cdot \boldsymbol{v} = 0$ then there exists a vector field $\boldsymbol{u}$, such that*

$$\boldsymbol{v}\,(\boldsymbol{r}) = \nabla \times \boldsymbol{u}\,(\boldsymbol{r})\,.$$

3. *For any scalar field f on U there exists a vector field $\boldsymbol{u}$ such that*

$$f\,(\boldsymbol{r}) = \nabla \cdot \boldsymbol{u}\,(\boldsymbol{r})\,.$$

Proof. We proof each statement separately.

1. Let us parametrize a line segment from a star center point $\boldsymbol{r}_0 \in U$ to any point $\boldsymbol{r} \in U$ of the radially convex set U and consider the scalar field in terms of the integral

$$g\,(\boldsymbol{r}) = \int_0^1 \boldsymbol{v}\,(\boldsymbol{r}_0 + t\,(\boldsymbol{r} - \boldsymbol{r}_0)) \cdot (\boldsymbol{r} - \boldsymbol{r}_0)\;\mathrm{d}t\,.$$

The x-component of the gradient of above integral is given by

$$\begin{aligned}\frac{\partial}{\partial x}g(\boldsymbol{r}) &= \frac{\partial}{\partial x}\int_0^1 \left(v_x\left(\boldsymbol{r}_0+t\left(\boldsymbol{r}-\boldsymbol{r}_0\right)\right)\left(x-x_0\right)+v_y\left(\boldsymbol{r}_0+t\left(\boldsymbol{r}-\boldsymbol{r}_0\right)\right)\left(y-y_0\right)\right.\\ &\qquad \left.+v_z\left(\boldsymbol{r}_0+t\left(\boldsymbol{r}-\boldsymbol{r}_0\right)\right)\left(z-z_0\right)\right)\,\mathrm{d}t\\ &= \int_0^1 \left(\frac{\partial v_x\left(\boldsymbol{r}_0+t\left(\boldsymbol{r}-\boldsymbol{r}_0\right)\right)}{\partial x}t\left(x-x_0\right)+v_x\left(\boldsymbol{r}_0+t\left(\boldsymbol{r}-\boldsymbol{r}_0\right)\right)\right.\\ &\qquad \left.+\frac{\partial v_y\left(\boldsymbol{r}_0+t\left(\boldsymbol{r}-\boldsymbol{r}_0\right)\right)}{\partial x}t\left(y-y_0\right)+\frac{\partial v_z\left(\boldsymbol{r}_0+t\left(\boldsymbol{r}-\boldsymbol{r}_0\right)\right)}{\partial x}t\left(z-z_0\right)\right)\,\mathrm{d}t\,,\end{aligned}$$

which is by the fundamental theorem of calculus given by

$$\begin{aligned}\frac{\partial}{\partial x}g(\boldsymbol{r}) = v_x(\boldsymbol{r}) + \int_0^1 &\left[\left(\frac{\partial v_y\left(\boldsymbol{r}_0+t\left(\boldsymbol{r}-\boldsymbol{r}_0\right)\right)}{\partial x}-\frac{\partial v_x\left(\boldsymbol{r}_0+t\left(\boldsymbol{r}-\boldsymbol{r}_0\right)\right)}{\partial y}\right)t\left(y-y_0\right)\right.\\ &\left.+\left(\frac{\partial v_z\left(\boldsymbol{r}_0+t\left(\boldsymbol{r}-\boldsymbol{r}_0\right)\right)}{\partial x}-\frac{\partial v_x\left(\boldsymbol{r}_0+t\left(\boldsymbol{r}-\boldsymbol{r}_0\right)\right)}{\partial z}\right)t\left(z-z_0\right)\right]\,\mathrm{d}t\,,\end{aligned}$$

The two other components follow equally. Thus, we have

$$\nabla\, g(\boldsymbol{r}) = \boldsymbol{v}(\boldsymbol{r}) + \int_0^1 t\left(\boldsymbol{r}-\boldsymbol{r}_0\right)\times\nabla\times\boldsymbol{v}\left(\boldsymbol{r}_0+t\left(\boldsymbol{r}-\boldsymbol{r}_0\right)\right)\,\mathrm{d}t\,.$$

This proves the first relation since

$$\boldsymbol{v}(\boldsymbol{r}) = \nabla\, g(\boldsymbol{r}) + \int_0^1 \nabla\times\boldsymbol{v}\left(\boldsymbol{r}_0+t\left(\boldsymbol{r}-\boldsymbol{r}_0\right)\right)\times t\left(\boldsymbol{r}-\boldsymbol{r}_0\right)\,\mathrm{d}t\,,$$

and as $\nabla\times\boldsymbol{v}(\boldsymbol{r}) = 0$ the statement follows.

2. Let us again parametrize a line segment from a star center point $\boldsymbol{r}_0 \in U$ to any point $\boldsymbol{r} \in U$ of the radially convex set U and consider now the vector field in terms of the integral

$$\boldsymbol{u}(\boldsymbol{x}) = -\int_0^1 t\left(\boldsymbol{r}_0+\left(\boldsymbol{r}-\boldsymbol{r}_0\right)\right)\times\boldsymbol{v}\left(\boldsymbol{r}_0+t\left(\boldsymbol{r}-\boldsymbol{r}_0\right)\right)\,\mathrm{d}t\,.$$

The x-component of the curl of the vector field $\boldsymbol{u}$ is given by

$$\begin{aligned}&-\int_0^1 \left[\frac{\partial}{\partial y}\left(t\left(x-x_0\right)v_y\left(\boldsymbol{r}_0+t\left(\boldsymbol{r}-\boldsymbol{r}_0\right)\right)-t\left(y-y_0\right)v_x\left(\boldsymbol{r}_0+t\left(\boldsymbol{r}-\boldsymbol{r}_0\right)\right)\right)\right.\\ &\qquad \left.-\frac{\partial}{\partial z}\left(t\left(z-z_0\right)v_x\left(\boldsymbol{r}_0+t\left(\boldsymbol{r}-\boldsymbol{r}_0\right)\right)-t\left(x-x_0\right)v_z\left(\boldsymbol{r}_0+t\left(\boldsymbol{r}-\boldsymbol{r}_0\right)\right)\right)\right]\,\mathrm{d}t\\ &= -\int_0^1 \left[t^2\left(\frac{\partial v_y\left(\boldsymbol{r}_0+t\left(\boldsymbol{r}-\boldsymbol{r}_0\right)\right)}{\partial y}+\frac{\partial v_z\left(\boldsymbol{r}_0+t\left(\boldsymbol{r}-\boldsymbol{r}_0\right)\right)}{\partial z}\right)\left(x-x_0\right)-2v_x\left(\boldsymbol{r}_0+t\left(\boldsymbol{r}-\boldsymbol{r}_0\right)\right)\right.\\ &\qquad \left.-t^2\frac{\partial v_x\left(\boldsymbol{r}_0+t\left(\boldsymbol{r}-\boldsymbol{r}_0\right)\right)}{\partial y}\left(y-y_0\right)-t^2\frac{\partial v_x\left(\boldsymbol{r}_0+t\left(\boldsymbol{r}-\boldsymbol{r}_0\right)\right)}{\partial z}\left(z-z_0\right)\right]\,\mathrm{d}t\,.\end{aligned}$$

Adding and subtracting $t^2 \frac{\partial v_x(\boldsymbol{r}_0+t(\boldsymbol{r}-\boldsymbol{r}_0))}{\partial x}(x-x_0)$, where the remaining components follow analogously, yields for the whole expression

$$\begin{aligned}\nabla\times\boldsymbol{u}(\boldsymbol{r}) = -\int_0^1 \Big(& t^2(\boldsymbol{r}-\boldsymbol{r}_0)\nabla\cdot\boldsymbol{v}(\boldsymbol{r}_0+t(\boldsymbol{r}-\boldsymbol{r}_0)) - 2t\boldsymbol{v}(\boldsymbol{r}_0+t(\boldsymbol{r}-\boldsymbol{r}_0)) \\ & -t^2\frac{\mathrm{d}}{\mathrm{d}t}\boldsymbol{v}(\boldsymbol{r}_0+t(\boldsymbol{r}-\boldsymbol{r}_0))\Big)\,\mathrm{d}t \\ & -\int_0^1 t^2(\boldsymbol{r}-\boldsymbol{r}_0)\nabla\cdot\boldsymbol{v}(\boldsymbol{r}_0+t(\boldsymbol{r}-\boldsymbol{r}_0))\,\mathrm{d}t + \int_0^1 \frac{\mathrm{d}}{\mathrm{d}t}\left(t^2\boldsymbol{v}(\boldsymbol{r}_0+t(\boldsymbol{r}-\boldsymbol{r}_0))\right)\mathrm{d}t\,.\end{aligned}$$

Finally we have by the fundamental theorem of calculus

$$\nabla\times\boldsymbol{u}(\boldsymbol{r}) = \boldsymbol{v}(\boldsymbol{r}) - \int_0^1 t^2(\boldsymbol{r}-\boldsymbol{r}_0)\nabla\cdot\boldsymbol{v}(\boldsymbol{r}_0+t(\boldsymbol{r}-\boldsymbol{r}_0))\,\mathrm{d}t\,.$$

This proves the second part of the theorem since

$$\boldsymbol{v}(\boldsymbol{r}) = \nabla\times\boldsymbol{u}(\boldsymbol{r}) + \int_0^1 t^2(\boldsymbol{r}-\boldsymbol{r}_0)\nabla\cdot\boldsymbol{v}(\boldsymbol{r}_0+t(\boldsymbol{r}-\boldsymbol{r}_0))\,\mathrm{d}t\,.$$

and as $\nabla\cdot\boldsymbol{v}(\boldsymbol{r}) = 0$ the statement follows.

3. For the third relation, let us again parametrize a line segment from a star center point $\boldsymbol{r}_0 \in U$ to any point $\boldsymbol{r} \in U$ of the radially convex set U and consider now the vector field $\boldsymbol{u}$ in terms of the integral

$$\boldsymbol{u}(\boldsymbol{r}) = \int_0^1 t^2(\boldsymbol{r}-\boldsymbol{r}_0)f(\boldsymbol{r}_0+t(\boldsymbol{r}-\boldsymbol{r}_0))\,\mathrm{d}t\,.$$

The divergence of $\boldsymbol{u}$ is given by

$$\begin{aligned}\nabla\cdot\boldsymbol{u}(\boldsymbol{r}) &= \int_0^1 t^2\left[\frac{\partial}{\partial x}\left((\boldsymbol{r}-\boldsymbol{r}_0)f(\boldsymbol{r}_0+t(\boldsymbol{r}-\boldsymbol{r}_0))\right) + \frac{\partial}{\partial y}\left((\boldsymbol{r}-\boldsymbol{r}_0)f(\boldsymbol{r}_0+t(\boldsymbol{r}-\boldsymbol{r}_0))\right)\right. \\ &\qquad \left. + \frac{\partial}{\partial z}\left((\boldsymbol{r}-\boldsymbol{r}_0)f(\boldsymbol{r}_0+t(\boldsymbol{r}-\boldsymbol{r}_0))\right)\right]\mathrm{d}t \\ &= \int_0^1 \left[3t^2 f(\boldsymbol{r}_0+t(\boldsymbol{r}-\boldsymbol{r}_0)) + t^3(\boldsymbol{r}-\boldsymbol{r}_0)\cdot\nabla f(\boldsymbol{r}_0+t(\boldsymbol{r}-\boldsymbol{r}_0))\right]\mathrm{d}t \\ &= \int_0^1 \frac{\mathrm{d}}{\mathrm{d}t}\left(t^3 f(\boldsymbol{r}_0+t(\boldsymbol{r}-\boldsymbol{r}_0))\right)\mathrm{d}t \\ &= f(\boldsymbol{r})\,,\end{aligned}$$

which proves the statement and thereby concludes the proof.

□

In vector calculus notation, electrodynamics is formulated in such a way, that we describe electric and magnetic fields and their corresponding source densities in terms of vector fields. In the classical three-dimensional case,

a vector field is a mapping $\mathbb{R}^3 \times \mathbb{R} \to \mathbb{R}^3$, where we assign a three-dimensional field vector to each point in space at a certain time or frequency, respectively. Especially the source and flux terms in electromagnetic theory are described by surface or volume densities, i.e. they are quantities that might be integrated over some volume or some area. Even the fields themselves may be integrated over curves in space. Hence, it is useful to develop some important statements regarding integrals over scalar and vector fields within the framework of vector calculus. In the following, we will state and prove Green's theorem [79], [82], which will serve as a lemma for proving Gauss's divergence theorem and Stoke's theorem, which are fundamental in an axiomatic development of the theory of electromagnetism [75].

Theorem 2.5 (Green's Theorem)**.** *Let $\boldsymbol{u} : \mathbb{R}^2 \to \mathbb{R}^2$ be a vector field and let $S \subset \mathbb{R}^2$ be a region with positively oriented, piecewise smooth, closed boundary curve ∂S. Then it holds that*

$$\int_{\partial S} \boldsymbol{u}\left(\boldsymbol{r}\right) \cdot \mathrm{d}\boldsymbol{r} = \iint_S \left(\frac{\partial u_y\left(x,y\right)}{\partial x} - \frac{\partial u_x\left(x,y\right)}{\partial y} \right) \mathrm{d}x\,\mathrm{d}y\,.$$

Proof. Let us rewrite the expression for the line integral over ∂S of the vector field $\boldsymbol{u}$ in component notation,

$$\int_{\partial S} \boldsymbol{u}\left(\boldsymbol{r}\right) \cdot \mathrm{d}\boldsymbol{r} = \int_{\partial S} u_x\left(x,y\right)\,\mathrm{d}x + \int_{\partial S} u_y\left(x,y\right)\,\mathrm{d}y\,.$$

It suffice to prove Green's theorem for convex regions $S \subset \mathbb{R}^2$ since every non-convex region can be decomposed into a sum of convex regions and due to linearity, the integrals of the regions will sum up. For a convex region S, we can find parameterizations $S = \left\{ [x,y]^{\mathrm{T}} : a \le x \le b, f_1\left(x\right) \le y \le f_2\left(x\right) \right\}$ and similarly $S = \left\{ [x,y]^{\mathrm{T}} : g_1\left(y\right) \le x \le g_2\left(y\right), c \le y \le d \right\}$. Thus, we can write for the line integral

$$\begin{aligned}\int_{\partial S} u_x\left(x,y\right)\,\mathrm{d}x + \int_{\partial S} u_y\left(x,y\right)\,\mathrm{d}y = &\int_a^b \left[u_x\left(x,f_1\left(x\right)\right) - u_x\left(x,f_2\left(x\right)\right)\right]\,\mathrm{d}x \\ &+ \int_c^d \left[u_y\left(g_2\left(y\right),y\right) - u_y\left(g_1\left(y\right),y\right)\right]\,\mathrm{d}y\,.\end{aligned}$$

Using the fundamental theorem of calculus, it turns out that

$$\begin{aligned}&\int_a^b \left[u_x\left(x,f_1\left(x\right)\right) - u_x\left(x,f_2\left(x\right)\right)\right]\,\mathrm{d}x + \int_c^d \left[u_y\left(g_2\left(y\right),y\right) - u_y\left(g_1\left(y\right),y\right)\right]\,\mathrm{d}y \\ &\qquad = \int_c^d \int_{g_1(y)}^{g_2(y)} \frac{\partial u_y\left(x,y\right)}{\partial x}\,\mathrm{d}x\,\mathrm{d}y - \int_a^b \int_{f_1(x)}^{f_2(x)} \frac{\partial u_x\left(x,y\right)}{\partial y}\,\mathrm{d}y\,\mathrm{d}x\,,\end{aligned}$$

and since both integral boundaries are different parameterizations of the same region S,

$$\int_{\partial S} \boldsymbol{u}\left(\boldsymbol{r}\right) \cdot \mathrm{d}\boldsymbol{r} = \iint_S \left(\frac{\partial u_y\left(x,y\right)}{\partial x} - \frac{\partial u_x\left(x,y\right)}{\partial y} \right) \mathrm{d}x\,\mathrm{d}y\,,$$

which proves the theorem. □

Equipped with Green's theorem, we are ready to prove Stoke's theorem, which relates the surface integral of the curl of a vector field to a line integral along the surface's oriented closed boundary curve of the vector field itself. In section 3.5, we will make use of Stoke's theorem for deriving Faraday's law from implications of the experimental observation of the induction principle. The theorem is stated as follows [82].

Theorem 2.6 (Stokes' Theorem)**.** *Let $\boldsymbol{u} : \mathbb{R}^3 \to \mathbb{R}^3$ be a vector field and let $S \subset \mathbb{R}^3$ be a two dimensional surface with positively oriented, piecewise smooth, closed boundary curve ∂S. Then it holds that*

$$\iint_S \nabla \times \boldsymbol{u}(\boldsymbol{r}) \cdot \mathrm{d}\boldsymbol{A} = \int_{\partial S} \boldsymbol{u}(\boldsymbol{r}) \cdot \mathrm{d}\boldsymbol{r}\,.$$

Proof. Again, we show the theorem for convex surfaces $S \subset \mathbb{R}^3$, since every non-convex set can be decomposed into convex subsets and by linearity, the integrals will sum up to the integral of the total surface. Expressing the line integral in terms of the x-, y-, and z-components of the vector field, we have

$$\int_{\partial S} \boldsymbol{u}(\boldsymbol{r}) \cdot \mathrm{d}\boldsymbol{r} = \int_{\partial S} u_x(x,y,z)\ \mathrm{d}x + \int_{\partial S} u_y(x,y,z)\ \mathrm{d}y + \int_{\partial S} u_z(x,y,z)\ \mathrm{d}z\,.$$

Since we consider convex surfaces $S \subset \mathbb{R}^3$ we can find parameterizations

$$\begin{aligned}
S &= \left\{ [x,y,z]^{\mathrm{T}} : f_1(y(t),z(t)), y(t), z(t), t_0 \le t \le t_1 \right\}, \\
S &= \left\{ [x,y,z]^{\mathrm{T}} : x(t), f_2(x(t),z(t)), y(t), t_0 \le t \le t_1 \right\}, \\
S &= \left\{ [x,y,z]^{\mathrm{T}} : x(t), y(t), f_3(x(t),y(t)), t_0 \le t \le t_1 \right\}.
\end{aligned}$$

Thus we have for the integrals respectively

$$\begin{aligned}
\int_{\partial S} \boldsymbol{u}(\boldsymbol{r}) \cdot \mathrm{d}\boldsymbol{r} = &\int_{t_0}^{t_1} u_x(f_1(y(t),z(t)), y(t), z(t)) \frac{\mathrm{d}x}{\mathrm{d}t}\ \mathrm{d}t \\
&+ \int_{t_0}^{t_1} u_y(x(t), f_2(x(t),z(t)), y(t)) \frac{\mathrm{d}y}{\mathrm{d}t}\ \mathrm{d}t \\
&+ \int_{t_0}^{t_1} u_z(x(t), y(t), f_3(x(t),y(t))) \frac{\mathrm{d}z}{\mathrm{d}t}\ \mathrm{d}t\,,
\end{aligned}$$

which is equal to

$$\begin{aligned}
\int_{\partial S} \boldsymbol{u}(\boldsymbol{r}) \cdot \mathrm{d}\boldsymbol{r} = &\int_{\partial S} u_x(f_1(y,z),y,z) \frac{\partial f_1(y,z)}{\partial y}\,\mathrm{d}y + \int_{\partial S} u_x(f_1(y,z),y,z) \frac{\partial f_1(y,z)}{\partial z}\,\mathrm{d}z \\
&+ \int_{\partial S} u_y(x, f_2(x,z), z) \frac{\partial f_2(x,z)}{\partial z}\,\mathrm{d}z + \int_{\partial S} u_y(x, f_2(x,z), z) \frac{\partial f_2(x,z)}{\partial x}\,\mathrm{d}x \\
&+ \int_{\partial S} u_z(x,y,f_3(x,y)) \frac{\partial f_3(x,y)}{\partial x}\,\mathrm{d}x + \int_{\partial S} u_z(x,y,f_3(x,y)) \frac{\partial f_3(x,y)}{\partial y}\,\mathrm{d}y\,.
\end{aligned}$$

By Green's theorem (see Theorem 2.5) we can now argue that the line integrals can be converted to surface integrals with

$$\begin{aligned}
\int_{\partial S} \boldsymbol{u}(\boldsymbol{r}) \cdot \mathrm{d}\boldsymbol{r} = &\iint_S \left(\frac{\partial u_x(f_1(y,z),y,z)}{\partial y} \cdot \frac{\partial f_1(y,z)}{\partial z} - \frac{\partial u_x(f_1(y,z),y,z)}{\partial z} \cdot \frac{\partial f_1(y,z)}{\partial y} \right) \mathrm{d}y\,\mathrm{d}z \\
&+ \iint_S \left(\frac{\partial u_y(x,f_2(x,z),z)}{\partial z} \cdot \frac{\partial f_2(x,z)}{\partial x} - \frac{\partial u_y(x,f_2(x,z),z)}{\partial x} \cdot \frac{\partial f_2(x,z)}{\partial z} \right) \mathrm{d}z\,\mathrm{d}x \\
&+ \iint_S \left(\frac{\partial u_z(x,y,f_3(x,y))}{\partial x} \cdot \frac{\partial f_3(x,y)}{\partial y} - \frac{\partial u_z(x,y,f_3(x,y))}{\partial y} \cdot \frac{\partial f_3(x,y)}{\partial x} \right) \mathrm{d}x\,\mathrm{d}y\,.
\end{aligned}$$

The surface normal $\boldsymbol{n}$ for each surface integral is different. It can be calculated for each parameterization separately by means of the partial derivatives of the parameter functions f_i for $i \in \{1,2,3\}$. Since each

parameterization parameterizes the same surface $S \subset \mathbb{R}^3$ the surface elements can be combined into a single element $\mathrm{d}\boldsymbol{A}$. With the appropriate surface normal for each integral, we can identify an integral over a vector field

$$\int_{\partial S} \boldsymbol{u}\left(\boldsymbol{r}\right) \cdot \mathrm{d}\boldsymbol{r} = \iint_S \begin{bmatrix} \frac{\partial u_z(x,y,z)}{\partial y} - \frac{\partial u_y(x,y,z)}{\partial z} \\ \frac{\partial u_x(x,y,z)}{\partial z} - \frac{\partial u_z(x,y,z)}{\partial x} \\ \frac{\partial u_y(x,y,z)}{\partial x} - \frac{\partial u_x(x,y,z)}{\partial y} \end{bmatrix} \cdot \mathrm{d}\boldsymbol{A} = \iint_S \nabla \times \boldsymbol{u}\left(\boldsymbol{r}\right) \cdot \mathrm{d}\boldsymbol{A}\,,$$

which proves the theorem. □

The next important result from vector calculus we want to prove here is given in terms of Gauss's divergence theorem [82]. The divergence theorem relates the volume integral over the divergence of a vector field to the surface integral of the vector field along the closed boundary surface, enclosing the volume. Gauss's theorem will be later used for deriving Ampére-Maxwell's law from the continuity equation, i.e. from the conservation of charges [75].

Theorem 2.7 (Gauss's Divergence Theorem)**.** *Let $V \subset \mathbb{R}^3$ be a volume bounded by a surface ∂V, and let $\boldsymbol{u} : \mathbb{R}^3 \to \mathbb{R}^3$ be a vector field. Then it holds that*

$$\iiint_V \nabla \cdot \boldsymbol{u}\left(\boldsymbol{r}\right) \,\mathrm{d}V = \iint_{\partial V} \boldsymbol{u}\left(\boldsymbol{r}\right) \cdot \mathrm{d}\boldsymbol{A}\,.$$

Proof. Let us rewrite the expression of the volume integral over V of the vector field $\boldsymbol{u}$ in terms of the components of $\boldsymbol{u}$ by

$$\iiint_V \nabla \cdot \boldsymbol{u}\left(\boldsymbol{r}\right) \,\mathrm{d}V = \iiint_V \left(\frac{\partial u_x\left(x,y,z\right)}{\partial x} + \frac{\partial u_y\left(x,y,z\right)}{\partial y} + \frac{\partial u_z\left(x,y,z\right)}{\partial z} \right) \mathrm{d}x\,\mathrm{d}y\,\mathrm{d}z\,.$$

Again, it suffice to show the theorem for convex volumes $V \subset \mathbb{R}^3$, since a non-convex volume can always be decomposed in a set of convex volumes and the integrals will sum up by linearity. Since we are dealing with a convex volume V, consider three different parameterizations, given by

$$\begin{aligned} V &= \left\{ \left[x,y,z\right]^{\mathrm{T}} : f_1\left(y,z\right) \leq x \leq f_2\left(y,z\right), \left[y,z\right]^{\mathrm{T}} \in D_x \right\}, \\ V &= \left\{ \left[x,y,z\right]^{\mathrm{T}} : g_1\left(x,z\right) \leq y \leq g_2\left(x,z\right), \left[x,z\right]^{\mathrm{T}} \in D_y \right\}, \\ V &= \left\{ \left[x,y,z\right]^{\mathrm{T}} : h_1\left(x,y\right) \leq x \leq h_2\left(x,y\right), \left[x,y\right]^{\mathrm{T}} \in D_z \right\}. \end{aligned}$$

Using these parameterizations, we can write for the volume integral

$$\begin{aligned} \iiint_V \nabla \cdot \boldsymbol{u}\left(\boldsymbol{r}\right) \,\mathrm{d}V = \iint_{\partial V} \int_{f_1(y,z)}^{f_2(y,z)} \frac{\partial u_x\left(x,y,z\right)}{\partial x} \,\mathrm{d}x\,\mathrm{d}y\,\mathrm{d}z + \iint_{\partial V} \int_{g_1(x,z)}^{g_2(x,z)} \frac{\partial u_y\left(x,y,z\right)}{\partial y} \,\mathrm{d}y\,\mathrm{d}z\,\mathrm{d}x \\ + \iint_{\partial V} \int_{h_1(x,y)}^{h_2(x,y)} \frac{\partial u_z\left(x,y,z\right)}{\partial z} \,\mathrm{d}z\,\mathrm{d}x\,\mathrm{d}y\,. \end{aligned}$$

By the fundamental theorem of calculus we then have

$$\begin{aligned} \iiint_V \nabla \cdot \boldsymbol{u}\left(\boldsymbol{r}\right) \,\mathrm{d}V = \iint_{D_x} u_x\left(f_2\left(y,z\right),y,z\right) \,\mathrm{d}y\,\mathrm{d}z - \iint_{D_x} u_x\left(f_1\left(y,z\right),y,z\right) \,\mathrm{d}y\,\mathrm{d}z \\ + \iint_{D_y} u_y\left(x,g_2\left(x,z\right),z\right) \,\mathrm{d}z\,\mathrm{d}x - \iint_{D_y} u_y\left(x,g_1\left(x,z\right),z\right) \,\mathrm{d}z\,\mathrm{d}x \\ + \iint_{D_z} u_z\left(x,y,h_2\left(x,y\right)\right) \,\mathrm{d}x\,\mathrm{d}y - \iint_{D_z} u_z\left(x,y,h_1\left(x,y\right)\right) \,\mathrm{d}x\,\mathrm{d}y\,. \end{aligned}$$

Note that the surface normals at f_1, g_1, and h_1 point in the opposite direction as the surface normals at f_2, g_2, and h_2. Hence, the minus sign can be absorbed into the surface normal $\mathrm{d}\boldsymbol{A}$ since all parameterizations parameterize the same volume $V \subset \mathbb{R}^3$, and we have

$$\iiint_V \nabla \cdot \boldsymbol{u}(\boldsymbol{r}) \, \mathrm{d}V = \iint_{\partial V} \boldsymbol{u}(\boldsymbol{r}) \cdot \mathrm{d}\boldsymbol{A} \,,$$

which proves the theorem. □

2.5 Fourier Analysis

Fourier analysis has found widespread application within science and engineering. Physical processes are typically time-dependent, i.e. a process evolves as time goes on. More generally, time can be replaced by any parameter of an abstract function. The dependency on this parameter can be arbitrarily complex. In terms of Fourier analysis, one is concerned with a special kind of time-dependence, given by an oscillatory harmonic time variation. Fourier analysis deals with the decomposition of functions into a harmonic time basis, where one is interested in the contributions of sinusoidal functions with certain harmonic frequencies to a time-varying signal. In the case of electromagnetic theory, the governing equations, i.e. Maxwell's equations are linear, which, as we will see later, leads to the simplification that field solutions can be constructed by superposition of harmonic contributions [83]. In the following, we want to prove an interesting property related to Fourier analysis, which is, that the Fourier transform of a real function is Hermitian [84]. This fact has particular implications on the structure of the spectral components we need to consider when dealing with stochastic electromagnetic fields. Furthermore, this property also gives implications on the structure of frequency-domain correlation matrices, which we will be dealing with numerically when considering the propagation of stationary Gaussian random fields. For proving the statement that the Fourier transform of a real function is Hermitian, let us first introduce the notion of Hermitian functions [84].

Definition 2.34 (Hermitian Function)**.** *Let $f : \mathbb{R} \to \mathbb{C}$ be a complex function. The function f is called Hermitian, if*

$$f(-t) = f^*(t) \,,$$

where the asterisk * indicates complex conjugation.

For the proof, we also need to distinguish between even and odd functions. Let us now rigorously define the terms even and odd function [85].

Definition 2.35 (Even and Odd Functions)**.** *A function $f : \mathbb{R} \to \mathbb{C}$ is called even, if*

$$f(t) = f(-t) \,.$$

Furthermore, the function f is called odd, if

$$f(t) = -f(-t) \,.$$

As we have defined what is understood when talking about an even and an odd function, we prove a short lemma on how to decompose an arbitrary function f into an even part f_e and an odd part f_o [85].

Lemma 2.4. *Let $f : \mathbb{R} \to \mathbb{R}$ be an arbitrary real-valued function. Then f can be written as a sum of even and odd functions,*

$$f(t) = f_\mathrm{e}(t) + f_\mathrm{o}(t) \,,$$

where f_e denotes the even part and f_o denotes the odd part.

Proof. The proof is based on adding an artificial zero, given by $f(-t) - f(-t)$, to the following equation,

$$f(t) = \frac{1}{2}\left[f(t) + f(t)\right] = \frac{1}{2}\left[f(t) + f(-t) - f(-t) + f(t)\right] \,.$$

By regrouping the terms in above equation, one obtains

$$f(t) = \frac{1}{2}\left[f(t) + f(-t)\right] + \frac{1}{2}\left[f(t) - f(-t)\right] .$$

The first term is identified as f_{e} and the second term as f_{o}, so

$$f_{\mathrm{e}}(t) = \frac{1}{2}\left[f(t) + f(-t)\right]$$
$$f_{\mathrm{o}}(t) = \frac{1}{2}\left[f(t) - f(-t)\right] .$$

Now it remains to be shown that f_{e} is even and f_{o} is odd, which can immediately be seen, since

$$f_{\mathrm{e}}(t) = \frac{1}{2}\left[f(t) + f(-t)\right] = \frac{1}{2}\left[f(-t) + f(t)\right] = f_{\mathrm{e}}(-t)$$

and

$$f_{\mathrm{o}}(t) = \frac{1}{2}\left[f(t) - f(-t)\right] = -\frac{1}{2}\left[f(-t) - f(t)\right] = -f_{\mathrm{o}}(-t) .$$

This completes the proof, as we have shown that $f(t) = f_{\mathrm{e}}(t) + f_{\mathrm{o}}(t)$. □

An interesting observation is now given in the following lemma. This is, that the integral of the product of an even and an odd function over the definition space where both functions are non-vanishing is always equal to zero. This result can greatly simplify calculations in certain situations. We will now state and prove the lemma [84].

Lemma 2.5. *Let $f_{\mathrm{e}} \in L^1$ be an even absolutely integrable function and let $f_{\mathrm{o}} \in L^1$ be an odd absolutely integrable function. Then*

$$\int_{-\infty}^{\infty} f_{\mathrm{e}}(t)\, f_{\mathrm{o}}(t)\, \mathrm{d}t = 0 .$$

Proof. The integral can be split into two parts, one from $-\infty$ to 0, and the other from 0 to ∞. This yields

$$\int_{-\infty}^{\infty} f_{\mathrm{e}}(t)\, f_{\mathrm{o}}(t)\, \mathrm{d}t = \int_{-\infty}^{0} f_{\mathrm{e}}(t)\, f_{\mathrm{o}}(t)\, \mathrm{d}t + \int_{0}^{\infty} f_{\mathrm{e}}(t)\, f_{\mathrm{o}}(t)\, \mathrm{d}t .$$

In the first integral above, we substitute, t by $-t$, and consequently the differential $\mathrm{d}t$ is replaced by $-\,\mathrm{d}t$ and the limits are adjusted accordingly. Thus, we obtain

$$\begin{aligned}\int_{-\infty}^{\infty} f_{\mathrm{e}}(t)\, f_{\mathrm{o}}(t)\, \mathrm{d}t &= -\int_{\infty}^{0} f_{\mathrm{e}}(-t)\, f_{\mathrm{o}}(-t)\, \mathrm{d}t + \int_{0}^{\infty} f_{\mathrm{e}}(t)\, f_{\mathrm{o}}(t)\, \mathrm{d}t \\ &= \int_{0}^{\infty} \left[f_{\mathrm{e}}(-t)\, f_{\mathrm{o}}(-t) + f_{\mathrm{e}}(t)\, f_{\mathrm{o}}(t)\right] \mathrm{d}t .\end{aligned}$$

Using the defining properties of even and odd functions, given in Definition 2.35, we can substitute $f_{\mathrm{e}}(-t)$ for $f_{\mathrm{e}}(t)$ and $-f_{\mathrm{o}}(-t)$ for $f_{\mathrm{o}}(t)$, which yields

$$\int_{-\infty}^{\infty} f_{\mathrm{e}}(t)\, f_{\mathrm{o}}(t)\, \mathrm{d}t = \int_{0}^{\infty} \left[f_{\mathrm{e}}(-t)\, f_{\mathrm{o}}(-t) - f_{\mathrm{e}}(-t)\, f_{\mathrm{o}}(-t)\right] \mathrm{d}t = 0 .$$

The whole integral is equal to zero, since we have shown that the term under the integral vanishes, which completes the proof. □

Finally, we have all the necessary tools to show that the Fourier transform of a real function is Hermitian [84]. The proof makes use of the definitions of even and odd functions, where both, the real function f, as well as the complex exponential in the Fourier transform are decomposed into their even and odd components.

Theorem 2.8. *Let $f \in L^1$ be a real-valued absolutely integrable function, and let $\underline{F}$ be its Fourier transform. Then the Fourier transform $\underline{F}$ of the real-valued function f is Hermitian, i.e.*

$$f(t) = f^*(t) \Leftrightarrow \underline{F}(-\omega) = \underline{F}^*(\omega) \ .$$

Proof. The Fourier transform $\underline{F}$ of f is given by

$$\underline{F}(\omega) = \int_{-\infty}^{\infty} f(t)\, \mathrm{e}^{-\mathrm{i}\omega t}\ \mathrm{d}t = \int_{-\infty}^{\infty} f(t) \cos(\omega t)\ \mathrm{d}t - \mathrm{i} \int_{-\infty}^{\infty} f(t) \sin(\omega t)\ \mathrm{d}t \, .$$

The second equality follows for real-valued functions f from Euler's formula. By Lemma 2.4, the real-valued function f can be decomposed into even and odd components. Hence, we obtain

$$\begin{aligned} \underline{F}(\omega) = &\int_{-\infty}^{\infty} f_{\mathrm{e}}(t) \cos(\omega t)\ \mathrm{d}t + \int_{-\infty}^{\infty} f_{\mathrm{o}}(t) \cos(\omega t)\ \mathrm{d}t \\ &- \mathrm{i} \int_{-\infty}^{\infty} f_{\mathrm{e}}(t) \sin(\omega t)\ \mathrm{d}t - \mathrm{i} \int_{-\infty}^{\infty} f_{\mathrm{o}}(t) \sin(\omega t)\ \mathrm{d}t \, . \end{aligned}$$

Since $\cos(\omega t)$ is an even function and $\sin(\omega t)$ is clearly an odd function, the second and third integral vanish due to Lemma 2.5. It follows that

$$\underline{F}(\omega) = \int_{-\infty}^{\infty} f_{\mathrm{e}}(t) \cos(\omega t)\ \mathrm{d}t - \mathrm{i} \int_{-\infty}^{\infty} f_{\mathrm{o}}(t) \sin(\omega t)\ \mathrm{d}t \, .$$

It is now clear that, since f is real-valued, the even component f_{e} of f gives rise to the real part of the Fourier transform $\underline{F}$ and the odd component f_{o} is responsible for the imaginary part. Changing the sign for the angular frequency variable ω then yields

$$\underline{F}(-\omega) = \int_{-\infty}^{\infty} f_{\mathrm{e}}(t) \cos(\omega t)\ \mathrm{d}t + \mathrm{i} \int_{-\infty}^{\infty} f_{\mathrm{o}}(t) \sin(\omega t)\ \mathrm{d}t = F^*(\omega) \ ,$$

due to Definition 2.35. □

3 Stochastic Electromagnetic Fields

3.1 General Stochastic Field Model

The overall objective of this chapter is to introduce and establish a mathematical framework for modeling noisy electromagnetic fields. Thus, after introducing the necessary mathematical preliminaries in chapter 2, the general model for describing stochastic fields will be introduced in the following. At first, a general framework will be introduced, without making any assumptions on the probability measures involved. As for many situations, the generality of the model needs to be traded for applicability in particular situations. In this sense, it is desirable to be as general as possible but still as applicable as needed. After the general model is established, it will be applied to several different scenarios that one encounters in a broad range of applications.

3.1.1 Mathematical Framework

The general scenario is as follows. A random field according to Definition 2.20, specified on a volume $V' \subseteq \mathbb{R}^3$, varying with time $t \in \mathbb{R}$ is prescribed. Note that the random field may model any physical quantity, scalar or vector valued, defined over a volume V' in space and varying with time. This general description is independent of the physical quantity to be described. Depending on whether the underlying quantity is scalar or vector valued, we define a measurable image space Y, which is either a subset of the real line $\mathbb{R}$ for scalar fields or a subset of the Euclidean space $\mathbb{R}^3$ for vector fields. Random fields $X_s = X(\omega, s) : \Omega \times T' \to Y$ with index set $T' \subseteq \mathbb{R}^4$, defined on a probability space $(\Omega, \mathcal{F}, P)$ are considered. For the elements s of the index set T', we write $s = \left[\boldsymbol{r}^{\mathrm{T}}, t\right]^{\mathrm{T}}$, where $\boldsymbol{r} = [x, y, z]^{\mathrm{T}} \in V' \subseteq \mathbb{R}^3$ represents spatial coordinates in Euclidean space, and t represents time. For a fixed $\omega_0 \in \Omega$, the realization $X(\omega_0, s)$ is a function mapping $T' \to Y$. Thus, for all random parameters $\omega_0 \in \Omega$, we have a random variable X_s mapping the random event ω_0 to a function $X(\omega_0, s) : T' \to Y$. We will describe the random field by means of finite dimensional joint probability distributions. Let $B_n \subset Y$ with $n \geq 1$ be measurable Borel sets and $F_{s_1,s_2,\ldots,s_n}(x_1, x_2, \ldots, x_n)$ be a family of finite dimensional joint probability distributions, given by

$$F_{s_1,s_2,\ldots,s_n}(x_1, x_2, \ldots, x_n) = P\left(\{X_{s_1} \in B(x_1), X_2 \in B(x_2), \ldots, X_{s_n} \in B(x_n)\}\right), \tag{3.1}$$

where each x_j gives rise to an $\mathcal{F}$-measurable [52] set $B(x_j)$, which is in the general vector valued case given by

$$B(x_j) = \left\{b \in \mathbb{R}^3 : b_x \leq x_j, b_y \leq y_j, b_z \leq z_j\right\}. \tag{3.2}$$

According to Kolmogorov's existence theorem [50], [51] (see Theorem 2.2), there is a measure $\tilde{P}$ on the measurable space $(X, \mathcal{H})$ of fields $X_s : T' \to Y$, with the σ-algebra $\mathcal{H}$ containing all cylindrical sets $C \subset X$, defined over the probability space $(\Omega, \mathcal{F}, P)$. The measure $\tilde{P}$ is completely determined by the family of finite dimensional joint probability distributions (3.1) of the random field $X_s = X(\omega, s)$. For any $C \in \mathcal{H}$, the probability that a certain function $X(\omega, \cdot)$ belongs to the cylindrical set C is given by

$$P\left(\{X(\omega, \cdot) \in C\}\right) = P\left(\{\omega \in \Omega : X(\omega, s_0) \in C, \forall s_0 \in T\}\right), \tag{3.3}$$

which determines the distribution function $F(C) = P\left(\{X(\omega, \cdot) \in C\}\right)$. If the family of finite dimensional joint probability distributions $F_{s_1,s_2,\ldots,s_n}(x_1, x_2, \ldots, x_n)$ is prescribed, all properties of the resulting random process can be deduced from those finite dimensional distributions [54], [59].

The set of functions $X : T' \to Y$ can be any set of functions [54]. One could, for example, restrict oneself to everywhere continuous functions or functions with finite L_2-norm, or to band-limited functions.

We consider the expectation value of the random field $X_s = X(\omega, s)$ given for any index $s_j \in T'$ by the ensemble average (see Definition 2.26) as

$$\boldsymbol{\mu}_{\mathrm{X}}(s_j) = \left\langle\!\left\langle X(\omega, s_j) \right\rangle\!\right\rangle = \int_Y x_j \, \mathrm{d}F_{s_j}(x_j) \,. \tag{3.4}$$

For the correlations of the fields at different locations and times s_i and s_j, as introduced in Definition 2.27, we have

$$\boldsymbol{\Gamma}_{\mathrm{X}}(s_i, s_j) = \left\langle\!\left\langle X(\omega, s_i) X^{\mathrm{T}}(\omega, s_j) \right\rangle\!\right\rangle = \int_Y \int_Y x_i x_j^{\mathrm{T}} \, \mathrm{d}F_{s_i, s_j}(x_i, x_j) \,. \tag{3.5}$$

Typically, we will consider random processes which have finite second-order moments, i.e. processes with finite energy, which are a very realistic "down-to-earth class" of random processes [62]. By assuming that the finite dimensional joint probability distributions $F_{s_1,s_2,\ldots,s_n}(x_1, x_2, \ldots, x_n)$ of the process $X_s = X(\omega, s)$ are absolutely continuous, there is a family of finite dimensional joint probability density functions $f_{s_1,s_2,\ldots,s_n}(x_1, x_2, \ldots, x_n)$, given by

$$f_{s_1,s_2,\ldots,s_n}(x_1, x_2, \ldots, x_n) = \frac{\partial^n F_{s_1,s_2,\ldots,s_n}(x_1, x_2, \ldots, x_n)}{\partial x_1 \partial x_2 \ldots \partial x_n} \,. \tag{3.6}$$

Specifying a family of finite dimensional joint probability density functions is equivalent up to a constant to specifying the finite dimensional joint probability distribution as [25]

$$F_{s_1,s_2,\ldots,s_n}(x_1, x_2, \ldots, x_n) = \int_{B(x_1)} \int_{B(x_2)} \cdots \int_{B(x_n)} f_{s_1,s_2,\ldots,s_n}(x_1, x_2, \ldots, x_n) \, \mathrm{d}x_1 \, \mathrm{d}x_2 \ldots \mathrm{d}x_n \,, \tag{3.7}$$

with the sets $B(x_j)$ as defined above. Thus, an absolutely continuous random process is completely defined by the family of finite dimensional joint probability density functions.

The expectation and the correlation function of the stochastic process $X_s = X(\omega, s)$ with respect to the finite dimensional joint probability density functions $f_{s_1,s_2,\ldots,s_n}(x_1, x_2, \ldots, x_n)$ are given by

$$\boldsymbol{\mu}_{\mathrm{X}}(s_j) = \left\langle\!\left\langle X(\omega, s_j) \right\rangle\!\right\rangle = \int_Y x_j f_{s_j}(x_{s_j}) \, \mathrm{d}x_j \,. \tag{3.8}$$

$$\boldsymbol{\Gamma}_{\mathrm{X}}(s_i, s_j) = \left\langle\!\left\langle X(\omega, s_i) X^{\mathrm{T}}(\omega, s_j) \right\rangle\!\right\rangle = \int_Y \int_Y x_i x_j^{\mathrm{T}} f_{s_i,s_j}(x_i, x_j) \, \mathrm{d}x_i \, \mathrm{d}x_j \,. \tag{3.9}$$

3.1.2 Linear Transformation of Random Fields

The random field $X_s = X(\omega, s)$ assigns a random vector in the measurable space Y to each coordinate s. Now suppose that the random vectors in Y, determined by the field $X_s = X(\omega, s)$ give rise to a new transformed random field $Y_r = Y(\omega, r)$ with indices $r \in T$, defined in a volume $V \subset \mathbb{R}^3$, also varying with time. Hence, $Y_r = Y(\omega, r)$ with index set $T \subseteq \mathbb{R}^4$ is a mapping $Y_r = Y(\omega, r) : \Omega \times T \to Z$ where $Z \subseteq \mathbb{R}^3$ is a measurable space of outcomes of the random field $Y_r = Y(\omega, r)$. The fields $X_s = X(\omega, s)$, giving rise to the transformed fields $Y_r = Y(\omega, r)$ are referred to as source fields, while the transformed fields $Y_r = Y(\omega, r)$ will be called observed fields. The transformation itself may be modeled as a linear transformation operator $\hat{\boldsymbol{M}}_{r,s} : Y \to Z$, taking a random source field $X_s = X(\omega, s)$ defined over an index $s \in T'$ to a transformed random observed field $Y_r = Y(\omega, r)$, defined over an index $r \in T$, such that

$$Y(\omega, r) = \hat{\boldsymbol{M}}_{r,s} X(\omega, s) \,. \tag{3.10}$$

Here, $\hat{\boldsymbol{M}}_{r,s}$ can be an integral transformation operator or any other linear mapping. Note that the linear transformation operator $\hat{\boldsymbol{M}}_{r,s}$ may also be a random operator in the most general case. The randomness in the operator is governed by random fluctuations in the linear transformation, which means that there is a certain probability that $\hat{\boldsymbol{M}}_{r,s}$ maps a function X_r to a function Y_r. This general problem with stochastic linear transformation operators is beyond the scope of this thesis. Instead of source fields and observed fields, one can also consider the source field as an input to a distributed linear system, giving rise to an output field, i.e. the observed field after the linear transformation. The linear transformation depends on the system itself,

while the randomness in the transformation operator arises from uncertainties in the structures comprising the linear system. In the case of electromagnetic fields, the linear system is the propagation environment for electromagnetic waves. Uncertainties in the environment or deliberate perturbations to the geometric structures give rise to a random linear transformation operator $\hat{\boldsymbol{M}}_{r,s}$. A random operator $\hat{\boldsymbol{M}}_{r,s}$ in the electromagnetic case is used in particular for modeling reverberation chambers, where a deterministic source field is transformed into a stochastic observed field through a random linear transformation [86]. Throughout this work, only deterministic transformations will be considered, although, interesting work has been done in the areas of random matrix theory [86], [87]. For investigating the influence of random parameters on electromagnetic systems, polynomial chaos expansion and stochastic collocation techniques [88]–[90] have been successfully applied. Electromagnetic wave propagation through randomly varying wave-guides has been modeled in [91] using stochastic differential equations, which are a generalization to the Telegrapher's equations.

Let a family of finite dimensional joint probability distributions $F_{s_1,s_2,\ldots,s_n}(x_1, x_2, \ldots, x_n)$ of a random source field $X_s = X(\omega, s)$ be prescribed. It would now be interesting to ask the question of how the finite dimensional joint probability distributions $F_{r_1,r_2,\ldots,r_n}(y_1, y_2, \ldots, y_n)$ of the observed field $Y_r = Y(\omega, r)$ look like, depending on the prescribed distributions of the source field. In general, the finite dimensional joint probability distributions of the observed random field $Y_r = Y(\omega, r)$ are given by

$$F_{r_1,r_2,\ldots,r_n}(y_1, y_2, \ldots, y_n) = P\left(\left\{Y_{r_1} \in B(y_1), Y_{r_2} \in B(y_2), \ldots, Y_{r_n} \in B(y_n)\right\}\right), \tag{3.11}$$

where the sets $B(x_j)$ for $j \geq 1$ are defined as above. As long as the linear transformation operator $\hat{\boldsymbol{M}}_{r,s}$ is deterministic and suffice certain regularity conditions, the probability distribution of the observed field is completely determined by the probability distribution of the source field. The finite dimensional joint probability distributions of the random field $Y_r = Y(\omega, r)$ can be obtained from the finite dimensional joint probability distributions of the source field $X_s = X(\omega, s)$ by

$$\begin{aligned} F_{r_1,\ldots,r_n}(y_1, \ldots, y_n) = & P\left(\left\{\omega \in \Omega : X(\omega, \cdot) \in \left\{x(s) \in X : \left(\hat{\boldsymbol{M}}_{r,s} x(s)\right)\Big|_{r=r_1} \in B(y_1)\right\} \cap \ldots\right.\right. \\ & \left.\left. \ldots \cap \left\{x(s) \in X : \left(\hat{\boldsymbol{M}}_{r,s} x(s)\right)\Big|_{r=r_n} \in B(y_n)\right\}\right\}\right), \end{aligned} \tag{3.12}$$

for any $n \geq 1$, where X is the $\tilde{P}$-measurable set of source fields. The resulting family of finite dimensional joint probability distributions also needs to satisfy the compatibility conditions from Definition 2.21. This is the most general description for the probability distributions of the observed field, using the probability measure induced by the known family of finite dimensional joint probability distributions of the source field. This method is, however, very impractical, as it involves for each index $j \in \mathbb{N} : 1 \leq j \leq n$ to evaluate the set of functions $x(s) \in X$ for which the linear transformation $\hat{\boldsymbol{M}}_{r,s} x(s)$ at a certain index r_j is an element of the set $B(y_j)$ and finding the measure of the n-fold intersection of those sets. The first and second order statistical moments, i.e. the expectation value and the correlation function of the resulting field $Y_r = Y(\omega, r)$ need to be taken as ensemble averages over the resulting probability distributions, i.e.

$$\boldsymbol{\mu}_{\mathrm{Y}}(r_j) = \left\langle\!\left\langle Y(\omega, r_j) \right\rangle\!\right\rangle = \int_Z y_j \, \mathrm{d}F_{r_j}(y_j). \tag{3.13}$$

$$\boldsymbol{\Gamma}_{\mathrm{Y}}(r_i, r_j) = \left\langle\!\left\langle Y(\omega, r_i) Y^{\mathrm{T}}(\omega, r_j) \right\rangle\!\right\rangle = \int_Z \int_Z y_i y_j^{\mathrm{T}} \, \mathrm{d}F_{r_i,r_j}(y_i, y_j). \tag{3.14}$$

If the finite dimensional joint probability distributions of the resulting process are absolutely continuous, finite dimensional joint probability density functions of the random field $Y_r = Y(\omega, r)$ can be obtained by the derivative

$$f_{r_1,r_2,\ldots,r_n}(y_1, y_2, \ldots, y_n) = \frac{\partial^n F_{r_1,r_2,\ldots,r_n}(y_1, y_2, \ldots, y_n)}{\partial y_1 \partial y_2 \ldots \partial y_n}. \tag{3.15}$$

As discussed in chapter 2, it is equivalent to describe a random field by means of characteristic functionals [54]. Suppose that instead of a family of finite dimensional joint probability distributions, a certain characteristic functional $\chi_{\mathrm{X}}(z)$ with $z \in X$ is prescribed. Let the characteristic functional

$$\chi_{\mathrm{X}}(z) = \int_X \mathrm{e}^{\mathrm{i}\langle z, x\rangle} \mu(\mathrm{d}x), \tag{3.16}$$

for a given measure μ on the Hilbert space of random fields mapping $\Omega \times T'$, defined over some volume V' to a measurable Hilbert space X be given. As previously, when we discussed finite dimensional joint probability distributions, we are interested in a random field Y_r, resulting from a linear operation $\hat{\boldsymbol{M}}_{r,s}$ on the source field X_s. Again, the linear operation is assumed to be deterministic. As the observed random field is given by $Y_r = \hat{\boldsymbol{M}}_{r,s} X_s$, we have for the characteristic functional

$$\chi_{\mathrm{Y}}(z) = \int_X \mathrm{e}^{\mathrm{i}\langle z,y\rangle} \mu(\mathrm{d}y) = \int_X \mathrm{e}^{\mathrm{i}\langle z,\hat{\boldsymbol{M}}_{r,s}x\rangle} \mu(\mathrm{d}x) = \int_X \mathrm{e}^{\mathrm{i}\left\langle \hat{\boldsymbol{M}}^{\dagger}_{r,s}z,x\right\rangle} \mu(\mathrm{d}x) \,, \tag{3.17}$$

with the adjoint operator $\hat{\boldsymbol{M}}^{\dagger}_{r,s}$. Thus, it follows [54]

$$\chi_{\mathrm{Y}}(z) = \chi_{\mathrm{X}}\left(\hat{\boldsymbol{M}}^{\dagger}_{r,s} z\right) . \tag{3.18}$$

This gives a simple mapping rule for characteristic functionals of random source fields to characteristic functionals of observed random fields. Characteristic functionals are, hence, a suitable candidate to be used as a fundamental description of random fields for the sake of propagation in space and time.

In the following, we will consider some special cases, i.e. what happens when we propagate a random field with Gaussian statistics, and also the implications of stationary and cyclostationary random fields on deriving second-order statistics.

3.2 Gaussian Random Fields

A Gaussian random field $X_s = X(\omega, s)$ on a Hilbert space of random fields X is characterized by the characteristic functional

$$\chi_{\mathrm{X}}(z) = \exp\left(\mathrm{i}\langle z, m_{\mathrm{X}}\rangle - \frac{1}{2}\left\langle z, \hat{\boldsymbol{\Gamma}}_{\mathrm{X}} z\right\rangle\right) , \tag{3.19}$$

according to Definition 2.25. From (3.18) it follows that the characteristic functional of a linear transformed Gaussian random field $Y_r = \hat{\boldsymbol{M}}_{r,s} X_s$ is given by

$$\begin{aligned}\chi_{\mathrm{Y}}(z) &= \exp\left(\mathrm{i}\left\langle \hat{\boldsymbol{M}}^{\dagger}_{r,s} z, m_{\mathrm{X}}\right\rangle - \frac{1}{2}\left\langle \hat{\boldsymbol{M}}^{\dagger}_{r,s} z, \hat{\boldsymbol{\Gamma}}_{\mathrm{X}} \hat{\boldsymbol{M}}^{\dagger}_{r,s} z\right\rangle\right) \\ &= \exp\left(\mathrm{i}\left\langle z, \hat{\boldsymbol{M}}_{r,s} m_{\mathrm{X}}\right\rangle - \frac{1}{2}\left\langle z, \hat{\boldsymbol{M}}_{r,s} \hat{\boldsymbol{\Gamma}}_{\mathrm{X}} \hat{\boldsymbol{M}}^{\dagger}_{r,s} z\right\rangle\right) .\end{aligned} \tag{3.20}$$

This shows that a linear transformation of a Gaussian random field X_s yields a Gaussian random field Y_r with transformed parameters $\hat{\boldsymbol{\Gamma}}_{\mathrm{Y}} = \hat{\boldsymbol{M}}_{r,s} \hat{\boldsymbol{\Gamma}}_{\mathrm{X}} \hat{\boldsymbol{M}}^{\dagger}_{r,s}$ and $m_{\mathrm{Y}} = \hat{\boldsymbol{M}}_{r,s} m_{\mathrm{X}}$. Hence it suffice to consider only those parameters for Gaussian fields, as they completely determine the assigned probability measures.

The parameters m_{X}, m_{Y}, $\hat{\boldsymbol{\Gamma}}_{\mathrm{X}}$, and $\hat{\boldsymbol{\Gamma}}_{\mathrm{Y}}$ are given as the expectation value functions and the correlation operators of the processes X and Y, respectively. For the continuous case, where the index sets T' and T have more than countably many elements, the correlations need to be treated as integral kernels, where the operator multiplication $\hat{\boldsymbol{\Gamma}}_{\mathrm{X}} z$ is given by the integral

$$\hat{\boldsymbol{\Gamma}}_{\mathrm{X}} z = \int_{T'} \boldsymbol{\Gamma}_{\mathrm{X}}(s_1, s_2)\, z(s_2)\, \mathrm{d}s_2 \,. \tag{3.21}$$

Assume that for every $s \in T'$ and for every $s_1, s_2 \in T'$ the ensemble average $m_{\mathrm{X}}(s)$ and the correlation dyadic $\boldsymbol{\Gamma}_{\mathrm{X}}(s_1, s_2)$ of the Gaussian random field $X_s = X(\omega, s)$ are known. Then the resulting random field $Y_r = Y(\omega, r)$, after the linear transformation $\hat{\boldsymbol{M}}_{r,s}$, is again Gaussian with transformed parameters

$$m_{\mathrm{Y}}(r) = \hat{\boldsymbol{M}}_{r,s} m_{\mathrm{X}}(s) \,, \tag{3.22}$$

$$\boldsymbol{\Gamma}_{\mathrm{Y}}(r_1, r_2) = \hat{\boldsymbol{M}}_{r_1,s_1} \boldsymbol{\Gamma}_{\mathrm{X}}(s_1, s_2)\, \hat{\boldsymbol{M}}^{\dagger}_{r_2,s_2} \,. \tag{3.23}$$

The characteristic functional of the random field Y is then completely determined by the new parameters. We have hence devised a simple propagation scheme for Gaussian random fields, where it is sufficient to calculate the linear transformation of the first and second order statistical moment in order to have a full characterization of the random measure on function space. For a general Gaussian random source field, it is very difficult to infer the statistical parameters of the underlying Gaussian process without any a-priori knowledge of the mean value function and the correlation kernel. Thus it is also difficult to propagate these parameters if they are not well known. For practical reasons, one often assumes that the random fields are stationary, in order to be able to calculate the statistical parameters of the source fields more easily. Stationarity has direct implications on the probability measures involved, and hence also simplifies the evaluation of the statistical moments, as we will see in the following section.

3.3 Stationary Random Fields

Dealing with the most general description of random fields in terms of finite dimensional joint probability distributions is practically not applicable as even for Gaussian statistics, it is hard to infer the mean and correlation of the source field.

Let us now consider strictly stationary random fields. The notion of stationarity was introduced in Definition 2.28, such that the family of finite dimensional joint probability distributions does not depend on an absolute index t, but only on the relative difference of two indices $\tau = t_1 - t_2$.

For a stationary random field $X_s = X(\omega, s)$ depending on a four-dimensional index $s = \left[\boldsymbol{r}^{\mathrm{T}}, t\right]^{\mathrm{T}} \in T'$, we consider temporal stationarity only. This means, we write the random process $X_s = X(\omega, s)$ as $X_{\boldsymbol{r},t} = X(\omega, \boldsymbol{r}, t)$, where the finite dimensional joint probability distributions are given by

$$F_{(\boldsymbol{r}_1,t_1),(\boldsymbol{r}_2,t_2),\ldots,(\boldsymbol{r}_n,t_n)}(x_1, x_2, \ldots, x_n) = F_{(\boldsymbol{r}_1,t_1+\tau),(\boldsymbol{r}_2,t_2+\tau),\ldots,(\boldsymbol{r}_n,t_n+\tau)}(x_1, x_2, \ldots, x_n) \;, \tag{3.24}$$

for all τ such that $t_j + \tau \in T'$. From here it follows for the expectation value

$$\boldsymbol{m}_{\mathrm{X}}(\boldsymbol{r}_j, t_j) = \left\langle\!\left\langle X(\omega, \boldsymbol{r}_j, t_j) \right\rangle\!\right\rangle = \int_Y x_j \; \mathrm{d}F_{(\boldsymbol{r}_j,t_j)}(x_j) = \int_Y x_j \; \mathrm{d}F_{(\boldsymbol{r}_j,t_j+\tau)}(x_j) \,. \tag{3.25}$$

Since (3.25) needs to be true for any τ such that $t_j + \tau \in T'$, the probability distribution $F_{(\boldsymbol{r}_j,t_j)}(x_j)$ does not explicitly depend on time. Therefore, we have for the expectation value

$$\boldsymbol{m}_{\mathrm{X}}(\boldsymbol{r}_j, t_j) = \left\langle\!\left\langle X(\omega, \boldsymbol{r}_j, t_j) \right\rangle\!\right\rangle = \int_Y x_j \; \mathrm{d}F_{\boldsymbol{r}_j}(x_j) = \boldsymbol{m}_{\mathrm{X}}(\boldsymbol{r}_j) \;. \tag{3.26}$$

For the correlation functions, we have accordingly

$$\begin{aligned} \boldsymbol{\Gamma}_{\mathrm{X}}(\boldsymbol{r}_i, t_i, \boldsymbol{r}_j, t_j) &= \left\langle\!\left\langle X(\omega, \boldsymbol{r}_i, t_i) X^{\mathrm{T}}(\omega, \boldsymbol{r}_j, t_j) \right\rangle\!\right\rangle = \int_Y \int_Y x_i x_j^{\mathrm{T}} \; \mathrm{d}F_{(\boldsymbol{r}_i,t_i),(\boldsymbol{r}_j,t_j)}(x_i, x_j) \\ &= \int_Y \int_Y x_i x_j^{\mathrm{T}} \; \mathrm{d}F_{(\boldsymbol{r}_i,t_i+\tau),(\boldsymbol{r}_j,t_j+\tau)}(x_i, x_j) \,. \end{aligned} \tag{3.27}$$

Again, since (3.27) needs to be satisfied for all τ such that $t_j + \tau \in T'$, we can set one time-argument to zero, without loss of generality. The resulting correlation function is only dependent on the time difference τ, such that

$$\begin{aligned} \boldsymbol{\Gamma}_{\mathrm{X}}(\boldsymbol{r}_i, t_i, \boldsymbol{r}_j, t_i + \tau) &= \left\langle\!\left\langle X(\omega, \boldsymbol{r}_i, t_i) X^{\mathrm{T}}(\omega, \boldsymbol{r}_j, t_i + \tau) \right\rangle\!\right\rangle \\ &= \int_Y \int_Y x_i x_j^{\mathrm{T}} \; \mathrm{d}F_{(\boldsymbol{r}_i,t_i),(\boldsymbol{r}_j,t_i+\tau)}(x_i, x_j) = \boldsymbol{\Gamma}_{\mathrm{X}}(\boldsymbol{r}_i, \boldsymbol{r}_j, \tau) \;. \end{aligned} \tag{3.28}$$

Stationarity in the wide sense, as given by Definition 2.29 has similar implications for the mean value function and for the correlation kernel. Therefore, wide-sense stationarity and stationarity in the strict sense are equivalent in the case of Gaussian statistics, as the second order statistics completely describe the Gaussian measure. The importance of these results must not be underestimated, as stationarity combined with ergodicity will enable the characterization of stochastic electromagnetic fields by measurement, as we will see in chapter 4.

3.4 Cyclostationary Random Fields

The concept of cyclostationarity and cyclostationarity in the wide sense was mathematically introduced in Definitions 2.30 and 2.31. An extensive review of cyclostationary processes in general is given in [37]. Early definitions and properties of cyclostationary processes have been given in the PhD thesis of Gardner [70] and in [69]. For a strictly cyclostationary random process $X_s = X(\omega, s) = X(\omega, \boldsymbol{r}, t)$ we have for the finite dimensional joint probability distributions

$$F_{(\boldsymbol{r}_1,t_1),(\boldsymbol{r}_2,t_2),\ldots,(\boldsymbol{r}_n,t_n)}(x_1, x_2, \ldots, x_n) = F_{(\boldsymbol{r}_1,t_1+T_0),(\boldsymbol{r}_2,t_2+T_0),\ldots,(\boldsymbol{r}_n,t_n+T_0)}(x_1, x_2, \ldots, x_n) \;, \tag{3.29}$$

for a certain periodicity T_0. Consequently, it follows for the expectation value function that

$$\boldsymbol{m}_{\mathrm{X}}(\boldsymbol{r}_j, t_j) = \langle\!\langle X(\omega, \boldsymbol{r}_j, t_j) \rangle\!\rangle = \int_Y x_j \; \mathrm{d}F_{(\boldsymbol{r}_j,t_j)}(x_j) = \int_Y x_j \; \mathrm{d}F_{(\boldsymbol{r}_j,t_j+T_0)}(x_j) = \boldsymbol{m}_{\mathrm{X}}(\boldsymbol{r}_j, t_j + T_0) \;. \tag{3.30}$$

This means that the mean value function is periodic with the cyclic period T_0. Something similar holds for the correlation kernel function, as

$$\begin{aligned} \boldsymbol{\Gamma}_{\mathrm{X}}(\boldsymbol{r}_i, t_i, \boldsymbol{r}_j, t_j) &= \left\langle\!\!\left\langle X(\omega, \boldsymbol{r}_i, t_i) X^{\mathrm{T}}(\omega, \boldsymbol{r}_j, t_j) \right\rangle\!\!\right\rangle = \int_Y \int_Y x_i x_j^{\mathrm{T}} \; \mathrm{d}F_{(\boldsymbol{r}_i,t_i),(\boldsymbol{r}_j,t_j)}(x_i, x_j) \\ &= \int_Y \int_Y x_i x_j^{\mathrm{T}} \; \mathrm{d}F_{(\boldsymbol{r}_i,t_i+T_0),(\boldsymbol{r}_j,t_j+T_0)}(x_i, x_j) = \boldsymbol{\Gamma}_{\mathrm{X}}(\boldsymbol{r}_i, t_i + T_0, \boldsymbol{r}_j, t_j + T_0) \;. \end{aligned} \tag{3.31}$$

We define the time difference $\tau = t_i - t_j$. Since the time difference is not affected by a periodic shift with T_0 and (3.31) must be valid for arbitrary t_i and t_j, we can furthermore write

$$\boldsymbol{\Gamma}_{\mathrm{X}}(\boldsymbol{r}_i, \boldsymbol{r}_j, t, t - \tau) = \boldsymbol{\Gamma}_{\mathrm{X}}(\boldsymbol{r}_i, \boldsymbol{r}_j, t + T_0, t + T_0 - \tau) \;. \tag{3.32}$$

This implies that the correlation kernel function depends on the time shift and depends on the absolute time periodically. Due to this fact, one can now think of expanding the correlation kernel function into a Fourier series in the direction of the absolute time t [31]. The Fourier series expansion is given by

$$\boldsymbol{\Gamma}_{\mathrm{X}}(\boldsymbol{r}_i, \boldsymbol{r}_j, t, t - \tau) = \sum_{n=-\infty}^{\infty} \boldsymbol{\Gamma}_{\mathrm{X},n}(\boldsymbol{r}_i, \boldsymbol{r}_j, \tau) \, \mathrm{e}^{\mathrm{i}2\pi \frac{n}{T_0} t} \;. \tag{3.33}$$

The Fourier coefficients are then given by

$$\boldsymbol{\Gamma}_{\mathrm{X},n}(\boldsymbol{r}_i, \boldsymbol{r}_j, \tau) = \frac{1}{T_0} \int_{-\frac{T_0}{2}}^{\frac{T_0}{2}} \boldsymbol{\Gamma}_{\mathrm{X}}(\boldsymbol{r}_i, \boldsymbol{r}_j, t, t - \tau) \, \mathrm{e}^{\mathrm{i}2\pi \frac{n}{T_0} t} \;. \tag{3.34}$$

For all $n \in \mathbb{Z}$, the Fourier coefficients $\boldsymbol{\Gamma}_{\mathrm{X},n}(\boldsymbol{r}_i, \boldsymbol{r}_j, \tau)$ are referred to as cyclic auto-correlation functions and the frequencies $\frac{n}{T_0}$ are called cyclic frequencies [37]. Wide-sense cyclostationary random fields have the same implications for their mean and correlation functions, but do not require all sets of the finite dimensional joint probability distributions to be periodic.

In real-world applications, cyclostationary random signals play an important role when considering random fields originating from digital data signals on contemporary electronic devices. As with digital data transmission and manipulation, there is typically a strict, repetitive clock timing involved, the EMI radiated from these devices needs to be treated as a cyclostationary random process [92].

For stochastic electromagnetic fields, the notion of stationary Gaussian random fields has been extended to the cyclostationary case theoretically in [31], [32]. Correlation measurements on cyclostationary electromagnetic fields have been performed in [34], [36] and deeper experimental characterization of the underlying signals and processes was described in [33], where cyclic auto-correlation cumulant functions have been proposed for describing spatially resolved cyclostationary processes. Finally, cyclic cross-correlation cumulant functions have been used in [35] for separating signals from different sources out of a single field measurement by exploiting their cyclic behavior.

3.5 Electromagnetic Fields

In the theory of electromagnetic fields, one is concerned with states in space and time, that occur due to the presence of an electric charge [93]. Electric charge is a property of matter, such that the respective object carrying the property will experience a force when placed close to another object carrying the property of charge. The interaction between these two objects will be repelling if the value of the number assigned to the charge property of both objects has the same sign. If the signs of the numbers assigned to the charge property of two objects are unlike, there will be an attractive force between them. An electric field is now considered as the condition in space that results due to the presence of a charged object. Consider a single charged object in space. Due to the presence of the single charge, there will be a force acting on any other charged object that is brought close to the single charge, described by the Coulomb force [93]. In that way, there will be a certain force with a certain direction assigned to all points in space. By removing the actual charge but keeping the condition that we assign a certain force to all points in space, acting on other charges, the electric field is defined as exactly these forces in space. In an abstract mathematical way, the electric field is an assignment of a vector $\boldsymbol{E} \in \mathbb{R}^3$ to all points $\boldsymbol{r} = [x, y, z]^{\mathrm{T}} \in \mathbb{R}^3$. The electrical force vector $\boldsymbol{F} \in \mathbb{R}^3$ is then given by

$$\boldsymbol{F} = q\boldsymbol{E}\,. \tag{3.35}$$

The mathematical quantity assigned to the property of charge is just a number. There is no information on the spatial distribution of charges involved, as for now, charge is assumed as a simple property of matter. But since for the electric field, only the presence of charges and the dielectric properties of the space are important, charge as a property can be directly assigned to points in space without considering the actual objects that carry the charge property. This is done in terms of a volume charge density ρ. The total charge property of an object in space is then given by the volume integral of the charge density ρ over the volume occupied by the object. The total charge q in a volume $V \subseteq \mathbb{R}^3$ is given by

$$q\,(t) = \iiint_V \rho\,(\boldsymbol{r}, t)\,\mathrm{d}^3 r\,. \tag{3.36}$$

3.5.1 Maxwell's Equations

The complete fundamental set of equations describing electromagnetism has been formulated by Maxwell in 1873 [1]. We will postulate Maxwell's equation in an axiomatic setting [75], where we will make use of various results from vector calculus, as presented in section 2.4. Gauss's law will be derived purely by applying Lemma 2.3 and the way we describe charges in space. Maxwell's theory will be constructed in such a way, that the continuity equation, i.e. the conservation of charges and the phenomenological observation of induction are naturally contained as physical inputs.

The charge density ρ is a scalar field. If the space $U \subseteq \mathbb{R}^3$, where the charge ρ is defined on, fulfills certain topological conditions, i.e. U must be a radially convex set according to Definition 2.33, then ρ can be expressed in terms of a vector field $\boldsymbol{D}$ with

$$\nabla\cdot\,\boldsymbol{D}\,(\boldsymbol{r}, t) = \rho\,(\boldsymbol{r}, t)\ , \tag{3.37}$$

by the lemma of Poincaré (see Lemma 2.3-3) [75]. The vector field $\boldsymbol{D}$ is called electric displacement field and equation (3.37) is known as Gauss's law in differential form. The electric displacement field $\boldsymbol{D}$ describes the distribution of the electric field passing through an area ∂V surrounding a volume V where a charge density ρ is defined. Equation (3.37) solely follows by the fact that the charge density is modeled by a scalar field on $\mathbb{R}^3$.

Charge is an inherent property of matter and is thus conserved, i.e. it cannot be created or destroyed. The total charge q inside a volume V can only change if there is a flux of charge, i.e. an electrical current through the surface ∂V enclosing V. The rate of change of the total charge is given by

$$\frac{\mathrm{d}q\,(t)}{\mathrm{d}t} + \iint_{\partial V} \boldsymbol{J}\,(\boldsymbol{r}, t)\cdot\mathrm{d}\boldsymbol{A} = 0\,, \tag{3.38}$$

where $\boldsymbol{J}$ is a vector field describing the electric current density. By (3.36) and by Gauss's divergence theorem (Theorem 2.7), (3.38) can be brought to differential form

$$\frac{\partial \rho\left(\boldsymbol{r}, t\right)}{\partial t}+\nabla \cdot \boldsymbol{J}\left(\boldsymbol{r}, t\right)=0\,. \tag{3.39}$$

Using Gauss's law from equation (3.37) and the linearity of the derivative, the continuity equation (3.39) can be rewritten as

$$\nabla \cdot\left(\frac{\partial \boldsymbol{D}\left(\boldsymbol{r}, t\right)}{\partial t}+\boldsymbol{J}\left(\boldsymbol{r}, t\right)\right)=0\,. \tag{3.40}$$

This means that the resulting vector field from the sum $\frac{\partial \boldsymbol{D}}{\partial t}+\boldsymbol{J}$ is free of divergence. Consequently, again by Lemma 2.3-2, there exists a vector field $\boldsymbol{H}$ such that

$$\nabla \times \boldsymbol{H}\left(\boldsymbol{r}, t\right)=\frac{\partial \boldsymbol{D}\left(\boldsymbol{r}, t\right)}{\partial t}+\boldsymbol{J}\left(\boldsymbol{r}, t\right)\,. \tag{3.41}$$

The vector field $\boldsymbol{H}$ is the magnetic field and (3.41) is known as Ampére-Maxwell's law. According to this law, there is a magnetic field specified in space, originating from electric current densities and temporal changes of the electric displacement field. The only axiomatic input used here for deriving Ampére-Maxwell's law was the conservation of charges. The existence of the magnetic field follows by the lemma of Poincaré.

Consider a charge q moving with velocity $\boldsymbol{v}$. It is known from experiment that the total force exerted on the charge q is given by

$$\boldsymbol{F}=q\left(\boldsymbol{E}+\boldsymbol{v} \times \boldsymbol{B}\right)\,, \tag{3.42}$$

where $\boldsymbol{B}$ is known as the magnetic field or magnetic flux density. Also by experiment, it is known that a time-varying magnetic field through a surface S gives rise to an electric field along the boundary path ∂S. This fact is reflected by

$$\int_{\partial S} \boldsymbol{E}\left(\boldsymbol{r}, t\right) \cdot \mathrm{d} \boldsymbol{r}=-\iint_{S} \frac{\partial}{\partial t} \boldsymbol{B}\left(\boldsymbol{r}, t\right) \cdot \mathrm{d} \boldsymbol{A}\,. \tag{3.43}$$

By Stokes' theorem (Theorem 2.6), (3.43) can be brought to differential form [75], given by

$$\nabla \times \boldsymbol{E}\left(\boldsymbol{r}, t\right)=-\frac{\partial \boldsymbol{B}\left(\boldsymbol{r}, t\right)}{\partial t}\,, \tag{3.44}$$

which is known as Faraday's law of induction. By applying the divergence operator to (3.44) we obtain

$$\nabla \cdot \nabla \times \boldsymbol{E}\left(\boldsymbol{r}, t\right)+\frac{\partial}{\partial t} \nabla \cdot \boldsymbol{B}\left(\boldsymbol{r}, t\right)=0\,. \tag{3.45}$$

It can be easily verified that $\nabla \cdot \nabla \times \boldsymbol{E}=0$ for every vector field $\boldsymbol{E}$, and hence, $\nabla \cdot \boldsymbol{B}$ does not vary with time. This implies that $\nabla \cdot \boldsymbol{B}$ is only a function of spatial coordinates $\nabla \cdot \boldsymbol{B}=f\left(x, y, z\right)$. On the other hand, the divergence $\nabla \cdot \boldsymbol{B}$ does not depend on the coordinates and thus

$$\nabla \cdot \boldsymbol{B}\left(\boldsymbol{r}, t\right)=0\,. \tag{3.46}$$

The electric field and the electric displacement field are interrelated by the constitutive relation

$$\boldsymbol{D}\left(\boldsymbol{r}, t\right)=\boldsymbol{\varepsilon}\left(\boldsymbol{r}, t\right) \boldsymbol{E}\left(\boldsymbol{r}, t\right)\,, \tag{3.47}$$

where $\boldsymbol{\varepsilon}$ is the permittivity tensor, which in general depends on space and time and is non-diagonal for anisotropic media. In a similar manner, the magnetic field $\boldsymbol{H}$ and the magnetic flux density $\boldsymbol{B}$ are related by the constitutive relation

$$\boldsymbol{B}\left(\boldsymbol{r}, t\right)=\boldsymbol{\mu}\left(\boldsymbol{r}, t\right) \boldsymbol{H}\left(\boldsymbol{r}, t\right)\,, \tag{3.48}$$

with the permeability tensor $\boldsymbol{\mu}$.

3.5.2 Potential Theory

Equation (3.46) poses a condition on the magnetic field, i.e. the magnetic field is free of divergence. Comparing (3.46) to Gauss's law in (3.37) yields the conclusion, that there are no magnetic charges or magnetic monopoles. Exploiting the fact that the magnetic field is free of divergence, we can use Poincaré's lemma (Lemma 2.3-2) to express the magnetic field in terms of a vector potential $\boldsymbol{A}$ by

$$\boldsymbol{B}(\boldsymbol{r},t) = \nabla\times \boldsymbol{A}(\boldsymbol{r},t)\,. \tag{3.49}$$

Inserting (3.49) into Faraday's law of induction (3.44), we have

$$\nabla\times\left(\boldsymbol{E}(\boldsymbol{r},t) + \frac{\partial \boldsymbol{A}(\boldsymbol{r},t)}{\partial t}\right) = 0\,, \tag{3.50}$$

and again by Poincaré's lemma (Lemma 2.3-1), there exists a scalar function Φ such that

$$\boldsymbol{E}(\boldsymbol{r},t) = -\nabla\,\Phi(\boldsymbol{r},t) - \frac{\partial \boldsymbol{A}(\boldsymbol{r},t)}{\partial t}\,, \tag{3.51}$$

where the negative sign of Φ was chosen due to the physical convention in the definition of potentials [83]. In the following, we assume vacuum, i.e. the permittivity tensor $\boldsymbol{\varepsilon}$ and the permeability tensor $\boldsymbol{\mu}$ become scalars, $\boldsymbol{\varepsilon}(\boldsymbol{r},t) = \varepsilon_0$ and $\boldsymbol{\mu}(\boldsymbol{r},t) = \mu_0$, that are neither space nor time dependent. Inserting (3.49) and (3.51) into Ampére-Maxwell's law (3.41) and using the Lorenz gauge condition

$$\nabla\cdot \boldsymbol{A}(\boldsymbol{r},t) + \varepsilon_0\mu_0\frac{\partial\Phi(\boldsymbol{r},t)}{\partial t} = 0\,, \tag{3.52}$$

results in the wave equation for the vector potential

$$\Delta\,\boldsymbol{A}(\boldsymbol{r},t) - \frac{1}{c_0^2}\cdot\frac{\partial^2\boldsymbol{A}(\boldsymbol{r},t)}{\partial t^2} = -\mu_0\boldsymbol{J}(\boldsymbol{r},t)\,, \tag{3.53}$$

where we have defined the vector Laplace operator $\Delta\,\boldsymbol{A} = \nabla(\nabla\cdot\boldsymbol{A}) - \nabla\times(\nabla\times\boldsymbol{A})$ and $c_0 = \frac{1}{\sqrt{\varepsilon_0\mu_0}}$ is the speed of light. A similar equation can be derived for the scalar potential Φ by inserting (3.51) into Gauss's law (3.37) and using the Lorenz gauge (3.52), yielding

$$\Delta\,\Phi(\boldsymbol{r},t) - \frac{1}{c_0^2}\cdot\frac{\partial^2\Phi(\boldsymbol{r},t)}{\partial t^2} = -\frac{\rho(\boldsymbol{r},t)}{\varepsilon_0}\,, \tag{3.54}$$

with the scalar Laplace operator $\Delta\,\Phi = \nabla\cdot\nabla\,\Phi$. General solutions to the wave equations for the vector potential (3.53) and the scalar potential (3.54) are known [94] for free space, and given in terms of

$$\boldsymbol{A}(\boldsymbol{r},t) = \frac{\mu_0}{4\pi}\iiint_{V'}\int_{-\infty}^{\infty}\frac{\boldsymbol{J}(\boldsymbol{r}',t')}{\|\boldsymbol{r}-\boldsymbol{r}'\|}\delta\left(t-t'-\frac{\|\boldsymbol{r}-\boldsymbol{r}'\|}{c_0}\right)\mathrm{d}t'\,\mathrm{d}^3r'\,, \tag{3.55}$$

$$\Phi(\boldsymbol{r},t) = \frac{1}{4\pi\varepsilon_0}\iiint_{V'}\int_{-\infty}^{\infty}\frac{\rho(\boldsymbol{r}',t')}{\|\boldsymbol{r}-\boldsymbol{r}'\|}\delta\left(t-t'-\frac{\|\boldsymbol{r}-\boldsymbol{r}'\|}{c_0}\right)\mathrm{d}t'\,\mathrm{d}^3r'\,. \tag{3.56}$$

The magnetic field $\boldsymbol{H}$ can be obtained from the magnetic vector potential by

$$\boldsymbol{H}(\boldsymbol{r},t) = \frac{1}{\mu_0}\nabla\times\boldsymbol{A}(\boldsymbol{r},t) = \iiint_{V'}\int_{-\infty}^{\infty}\boldsymbol{G}_{\mathrm{HJ}}\left(\boldsymbol{r}-\boldsymbol{r}',t-t'\right)\boldsymbol{J}\left(\boldsymbol{r}',t'\right)\,\mathrm{d}t'\,\mathrm{d}^3r'\,, \tag{3.57}$$

with the free space dyadic Green's function $\boldsymbol{G}_{\mathrm{HJ}}$ given by

$$\boldsymbol{G}_{\mathrm{HJ}}(\boldsymbol{r},t) = \frac{1}{4\pi}\boldsymbol{r}\times\mathbf{1}\left[\frac{1}{c_0\|\boldsymbol{r}\|^2}\delta'\left(t-\frac{\|\boldsymbol{r}\|}{c_0}\right) - \frac{1}{\|\boldsymbol{r}\|^3}\delta\left(t-\frac{\|\boldsymbol{r}\|}{c_0}\right)\right]\,, \tag{3.58}$$

with the identity matrix $\mathbf{1}$, the Dirac delta distribution $\delta(\cdot)$, $\|\boldsymbol{r}\| = \sqrt{x^2+y^2+z^2}$, the free space velocity of light c_0, and

$$\boldsymbol{r} \times \mathbf{1} = \begin{bmatrix} 0 & -z & y \\ z & 0 & -x \\ -y & x & 0 \end{bmatrix} . \tag{3.59}$$

A similar result can be obtained in terms of Jefimenko's equations [95]–[97]. The solution for the corresponding electric field can be given in terms of

$$\boldsymbol{E}(\boldsymbol{r},t) = \frac{1}{\varepsilon_0} \nabla \times \int_{-\infty}^{t} \boldsymbol{H}\left(\boldsymbol{r},t'\right) \mathrm{d}t' , \tag{3.60}$$

The solution for the electric field in free space can be reformulated in terms of a Green's dyadic $\boldsymbol{G}_{\mathrm{EJ}}$ by the integral

$$\boldsymbol{E}(\boldsymbol{r},t) = \iiint_{V'} \int_{-\infty}^{\infty} \boldsymbol{G}_{\mathrm{EJ}}\left(\boldsymbol{r}-\boldsymbol{r}',t-t'\right) \boldsymbol{J}\left(\boldsymbol{r}',t'\right) \mathrm{d}t' \, \mathrm{d}^3 r' . \tag{3.61}$$

According to [98] a solution for the free space Green's dyadic $\boldsymbol{G}_{\mathrm{EJ}}$ of the electric field can be found to be

$$\begin{aligned} \boldsymbol{G}_{\mathrm{EJ}}(\boldsymbol{r},t) = \frac{1}{4\pi}\sqrt{\frac{\mu_0}{\varepsilon_0}} \Bigg[\left(\mathbf{1} - 3\frac{\boldsymbol{r}\boldsymbol{r}^{\mathrm{T}}}{\|\boldsymbol{r}\|^2}\right) \left(\frac{\delta\left(t-\frac{\|\boldsymbol{r}\|}{c_0}\right) - c_0\delta(\|\boldsymbol{r}\|)}{\|\boldsymbol{r}\|^2} + \frac{c_0 U(c_0 t - \|\boldsymbol{r}\|) - c_0 U(-\|\boldsymbol{r}\|)}{\|\boldsymbol{r}\|^3} \right) \\ - \frac{\boldsymbol{r}\boldsymbol{r}^{\mathrm{T}}}{\|\boldsymbol{r}\|^2} \left(\frac{\delta'\left(t-\frac{\|\boldsymbol{r}\|}{c_0}\right) + c_0\delta'(\|\boldsymbol{r}\|)}{\|\boldsymbol{r}\|} \right) + \mathbf{1} \left(\frac{\delta'\left(t-\frac{\|\boldsymbol{r}\|}{c_0}\right)}{\|\boldsymbol{r}\|} \right) \Bigg] , \end{aligned} \tag{3.62}$$

with the step function $U(\cdot)$ and with

$$\boldsymbol{r}\boldsymbol{r}^{\mathrm{T}} = \begin{bmatrix} xx & xy & xz \\ yx & yy & yz \\ zx & zy & zz \end{bmatrix} . \tag{3.63}$$

3.5.3 Hertz Potentials

Now suppose that an electric field is applied to a dielectric medium. The atoms in the lattice of the dielectric material respond to the applied fields by forming microscopic electric dipoles [83]. The positively charged nuclei move a tiny bit in the direction of the field while the associated electrons move in the opposite direction. This tiny movement of charges produces a macroscopic bound charge in the material. This macroscopic bound charge within a material can be described by the polarization density $\boldsymbol{P}_{\mathrm{e}}$. A similar effect takes place with microscopic currents, associated with the angular momentum of the electrons within a certain material. By applying a magnetic field, eddy currents are created around the surface of the material. These eddy currents can be described analogously to the polarization densities for the electric field by a magnetic polarization $\boldsymbol{P}_{\mathrm{m}}$. The electric and magnetic polarization densities $\boldsymbol{P}_{\mathrm{e}}$ and $\boldsymbol{P}_{\mathrm{m}}$ are related to the electric and magnetic fields by

$$\boldsymbol{D}(\boldsymbol{r},t) = \boldsymbol{\varepsilon}(\boldsymbol{r},t)\,\boldsymbol{E}(\boldsymbol{r},t) + \boldsymbol{P}_{\mathrm{e}}(\boldsymbol{r},t) , \tag{3.64}$$

$$\boldsymbol{B}(\boldsymbol{r},t) = \boldsymbol{\mu}(\boldsymbol{r},t)\,\boldsymbol{H}(\boldsymbol{r},t) + \boldsymbol{P}_{\mathrm{m}}(\boldsymbol{r},t) . \tag{3.65}$$

Let us now consider a source-free region of space, i.e. $\boldsymbol{J} = 0$ and $\rho = 0$, in an isotropic dielectric medium with permittivity ε, and let us express the electric displacement field $\boldsymbol{D}$ in terms of equation (3.64) and the magnetic flux density by $\boldsymbol{B} = \mu_0 \boldsymbol{H}$. Then we have the following system of equations to solve [99]

$$\nabla \cdot \boldsymbol{E}(\boldsymbol{r},t) = -\frac{1}{\varepsilon} \nabla \cdot \boldsymbol{P}_{\mathrm{e}}(\boldsymbol{r},t) , \qquad \nabla \times \boldsymbol{E}(\boldsymbol{r},t) = -\mu_0 \frac{\partial \boldsymbol{H}(\boldsymbol{r},t)}{\partial t} ,$$

$$\mu_0 \nabla \cdot \boldsymbol{H}(\boldsymbol{r},t) = 0 , \qquad \nabla \times \boldsymbol{H}(\boldsymbol{r},t) = \varepsilon \frac{\partial \boldsymbol{E}(\boldsymbol{r},t)}{\partial t} + \frac{\partial \boldsymbol{P}_{\mathrm{e}}(\boldsymbol{r},t)}{\partial t} .$$

By the lemma of Poincaré (Lemma 2.3-2), there is a magnetic vector potential $\boldsymbol{A}$ with $\nabla\times\boldsymbol{A}=\mu_0\boldsymbol{H}$ and analogous to (3.50) and (3.51) there is a scalar potential Φ such that with (3.52) we have

$$\Delta\,\boldsymbol{A}\left(\boldsymbol{r},t\right)-\frac{1}{c^2}\cdot\frac{\partial^2\boldsymbol{A}\left(\boldsymbol{r},t\right)}{\partial t^2}=-\mu_0\frac{\partial\boldsymbol{P}_{\mathrm{e}}\left(\boldsymbol{r},t\right)}{\partial t}\,, \tag{3.66}$$

$$\Delta\,\Phi\left(\boldsymbol{r},t\right)-\frac{1}{c^2}\cdot\frac{\partial^2\Phi\left(\boldsymbol{r},t\right)}{\partial t^2}=\frac{1}{\varepsilon}\,\nabla\cdot\boldsymbol{P}_{\mathrm{e}}\left(\boldsymbol{r},t\right). \tag{3.67}$$

The Lorenz gauge condition (3.52) is fulfilled if $\boldsymbol{A}$ and Φ are derived from a single vector field $\boldsymbol{\Pi}_{\mathrm{e}}$ [83], such that

$$\boldsymbol{A}\left(\boldsymbol{r},t\right)=\varepsilon\mu_0\frac{\partial\boldsymbol{\Pi}_{\mathrm{e}}\left(\boldsymbol{r},t\right)}{\partial t}\,, \tag{3.68}$$

$$\Phi\left(\boldsymbol{r},t\right)=-\,\nabla\cdot\boldsymbol{\Pi}_{\mathrm{e}}\left(\boldsymbol{r},t\right). \tag{3.69}$$

By inserting (3.68) into (3.66) or (3.69) into equation (3.67), we arrive at a wave equation for the so called electric Hertz potential $\boldsymbol{\Pi}_{\mathrm{e}}$ [83], given by

$$\Delta\,\boldsymbol{\Pi}_{\mathrm{e}}\left(\boldsymbol{r},t\right)-\frac{1}{c^2}\cdot\frac{\partial^2\boldsymbol{\Pi}_{\mathrm{e}}\left(\boldsymbol{r},t\right)}{\partial t^2}=-\frac{1}{\varepsilon}\boldsymbol{P}_{\mathrm{e}}\left(\boldsymbol{r},t\right)\,, \tag{3.70}$$

where the sources of the electric Hertz vector are given in terms of electric polarizations. The solution to (3.70) in a free space region V' can be given in terms of [83], [99]

$$\boldsymbol{\Pi}_{\mathrm{e}}\left(\boldsymbol{r},t\right)=\frac{1}{4\pi\varepsilon}\iiint_{V'}\int_{-\infty}^{\infty}\frac{\boldsymbol{P}_{\mathrm{e}}\left(\boldsymbol{r}',t'\right)}{\left\|\boldsymbol{r}-\boldsymbol{r}'\right\|}\delta\left(t-t'-\frac{\left\|\boldsymbol{r}-\boldsymbol{r}'\right\|}{c_0}\right)\,\mathrm{d}t'\,\mathrm{d}^3r'\,. \tag{3.71}$$

The magnetic field $\boldsymbol{H}$ can be recovered from the electric Hertz vector $\boldsymbol{\Pi}_{\mathrm{e}}$ by

$$\boldsymbol{H}\left(\boldsymbol{r},t\right)=\varepsilon\,\nabla\times\frac{\partial\boldsymbol{\Pi}_{\mathrm{e}}\left(\boldsymbol{r},t\right)}{\partial t}\,. \tag{3.72}$$

Hence, we can interrelate the magnetic field $\boldsymbol{H}$ to an exciting electric polarization $\boldsymbol{P}_{\mathrm{e}}$ by means of the dyadic Green's function $\boldsymbol{G}_{\mathrm{HP_e}}$ by [7]

$$\boldsymbol{H}\left(\boldsymbol{r},t\right)=\iiint_{V'}\int_{-\infty}^{\infty}\boldsymbol{G}_{\mathrm{HP_e}}\left(\boldsymbol{r}-\boldsymbol{r}',t-t'\right)\boldsymbol{P}_{\mathrm{e}}\left(\boldsymbol{r}',t'\right)\,\mathrm{d}t'\,\mathrm{d}^3r'\,, \tag{3.73}$$

where $\boldsymbol{G}_{\mathrm{HP_e}}$ is given in free space by [94], [100]

$$\boldsymbol{G}_{\mathrm{HP_e}}\left(\boldsymbol{r},t\right)=\frac{1}{4\pi}\boldsymbol{r}\times\mathbf{1}\left[\frac{1}{\left\|\boldsymbol{r}\right\|^3}\delta'\left(t-\frac{\left\|\boldsymbol{r}\right\|}{c_0}\right)-\frac{1}{c_0\left\|\boldsymbol{r}\right\|^2}\delta''\left(t-\frac{\left\|\boldsymbol{r}\right\|}{c_0}\right)\right]\,. \tag{3.74}$$

The solution for the corresponding electric field can be given in terms of

$$\boldsymbol{E}\left(\boldsymbol{r},t\right)=\frac{1}{\varepsilon_0}\,\nabla\times\int_{-\infty}^{t}\boldsymbol{H}\left(\boldsymbol{r},t'\right)\mathrm{d}t'\,. \tag{3.75}$$

A solution to the integral equation

$$\boldsymbol{E}\left(\boldsymbol{r},t\right)=\iiint_{V'}\int_{-\infty}^{\infty}\boldsymbol{G}_{\mathrm{EP_e}}\left(\boldsymbol{r}-\boldsymbol{r}',t-t'\right)\boldsymbol{P}_{\mathrm{e}}\left(\boldsymbol{r}',t'\right)\,\mathrm{d}t'\,\mathrm{d}^3r'\,, \tag{3.76}$$

is given for free space by the Green's dyadic [7]

$$\boldsymbol{G}_{\mathrm{EP_e}}(\boldsymbol{r},t) = \frac{\mu_0}{4\pi}\sqrt{\frac{\mu_0}{\varepsilon_0}}\left[\left(\mathbf{1}-3\frac{\boldsymbol{r}\boldsymbol{r}^{\mathrm{T}}}{\|\boldsymbol{r}\|^2}\right)\left(\frac{c_0\delta'\left(t-\frac{\|\boldsymbol{r}\|}{c_0}\right)}{\|\boldsymbol{r}\|^2}+\frac{c_0^2\delta\left(c_0t-\|\boldsymbol{r}\|\right)}{\|\boldsymbol{r}\|^3}\right)\right.$$
$$\left.+\left(\mathbf{1}-\frac{\boldsymbol{r}\boldsymbol{r}^{\mathrm{T}}}{\|\boldsymbol{r}\|^2}\right)\left(\frac{\delta''\left(t-\frac{\|\boldsymbol{r}\|}{c_0}\right)}{\|\boldsymbol{r}\|}\right)\right]. \tag{3.77}$$

In case of a magnetically polarizable isotropic medium with permeability μ in a source-free region, where the magnetic flux density is expressed in terms of (3.65), and $\boldsymbol{D}=\varepsilon_0\boldsymbol{E}$, Maxwell's equations are given by

$$\nabla\cdot\boldsymbol{H}(\boldsymbol{r},t) = -\frac{1}{\mu}\nabla\cdot\boldsymbol{P}_{\mathrm{m}}(\boldsymbol{r},t), \qquad \nabla\times\boldsymbol{H}(\boldsymbol{r},t) = \varepsilon_0\frac{\partial\boldsymbol{E}(\boldsymbol{r},t)}{\partial t},$$
$$\varepsilon_0\nabla\cdot\boldsymbol{E}(\boldsymbol{r},t) = 0, \qquad \nabla\times\boldsymbol{E}(\boldsymbol{r},t) = -\mu\frac{\partial\boldsymbol{H}(\boldsymbol{r},t)}{\partial t}-\frac{\partial\boldsymbol{P}_{\mathrm{m}}(\boldsymbol{r},t)}{\partial t}.$$

With $\nabla\cdot(\varepsilon_0\boldsymbol{E})$ and Poincaré's lemma (Lemma 2.3-2), there exists an electric vector potential $\boldsymbol{F}$, and similar to (3.50) and (3.51), there is a scalar magnetic potential Ψ, given by $\nabla\times\boldsymbol{F}=-\varepsilon_0\boldsymbol{E}$ and $\boldsymbol{H}=-\nabla\Psi-\frac{\partial\boldsymbol{F}}{\partial t}$. With a modified Lorenz gauge condition $\nabla\cdot\boldsymbol{F}+\mu\varepsilon_0\frac{\partial\Psi}{\partial t}=0$, one can derive wave equations for the electric vector potential $\boldsymbol{F}$ and the scalar potential Ψ resulting in

$$\Delta\boldsymbol{F}(\boldsymbol{r},t)-\frac{1}{c^2}\cdot\frac{\partial^2\boldsymbol{F}(\boldsymbol{r},t)}{\partial t^2} = -\varepsilon_0\frac{\partial\boldsymbol{P}_{\mathrm{m}}(\boldsymbol{r},t)}{\partial t}, \tag{3.78}$$
$$\Delta\Psi(\boldsymbol{r},t)-\frac{1}{c^2}\cdot\frac{\partial^2\Psi(\boldsymbol{r},t)}{\partial t^2} = \frac{1}{\mu}\nabla\cdot\boldsymbol{P}_{\mathrm{m}}(\boldsymbol{r},t). \tag{3.79}$$

The modified Lorenz gauge condition $\nabla\cdot\boldsymbol{F}+\mu\varepsilon_0\frac{\partial\Psi}{\partial t}=0$ is satisfied by choosing $\boldsymbol{F}$ and Ψ, such that

$$\boldsymbol{F}(\boldsymbol{r},t) = \mu\varepsilon_0\frac{\partial\boldsymbol{\Pi}_{\mathrm{m}}(\boldsymbol{r},t)}{\partial t}, \tag{3.80}$$
$$\Psi(\boldsymbol{r},t) = -\nabla\cdot\boldsymbol{\Pi}_{\mathrm{m}}(\boldsymbol{r},t). \tag{3.81}$$

Inserting (3.80) into (3.78) or (3.81) into (3.79), yields a wave equation for the magnetic Hertz potential $\boldsymbol{\Pi}_{\mathrm{m}}$, given by

$$\Delta\boldsymbol{\Pi}_{\mathrm{m}}(\boldsymbol{r},t)-\frac{1}{c^2}\cdot\frac{\partial^2\boldsymbol{\Pi}_{\mathrm{m}}(\boldsymbol{r},t)}{\partial t^2} = -\frac{1}{\mu}\boldsymbol{P}_{\mathrm{m}}(\boldsymbol{r},t), \tag{3.82}$$

A solution to the wave equation in (3.82) in a free space region V' is given in terms of

$$\boldsymbol{\Pi}_{\mathrm{m}}(\boldsymbol{r},t) = \frac{1}{4\pi\mu}\iiint_{V'}\int_{-\infty}^{\infty}\frac{\boldsymbol{P}_{\mathrm{m}}(\boldsymbol{r}',t')}{\|\boldsymbol{r}-\boldsymbol{r}'\|}\delta\left(t-t'-\frac{\|\boldsymbol{r}-\boldsymbol{r}'\|}{c_0}\right)\mathrm{d}t'\,\mathrm{d}^3r', \tag{3.83}$$

with the magnetic polarization $\boldsymbol{P}_{\mathrm{m}}$ as source term of the magnetic Hertz vector $\boldsymbol{\Pi}_{\mathrm{m}}$. The electric field $\boldsymbol{E}$ can be recovered from the magnetic Hertz vector $\boldsymbol{\Pi}_{\mathrm{m}}$ by

$$\boldsymbol{E}(\boldsymbol{r},t) = -\mu\nabla\times\frac{\partial\boldsymbol{\Pi}_{\mathrm{m}}(\boldsymbol{r},t)}{\partial t}. \tag{3.84}$$

The electric field $\boldsymbol{E}$ can be related to an exciting magnetic polarization $\boldsymbol{P}_{\mathrm{m}}$ by means of the dyadic Green's function $\boldsymbol{G}_{\mathrm{EP_m}}$ by [7]

$$\boldsymbol{E}(\boldsymbol{r},t) = \iiint_{V'}\int_{-\infty}^{\infty}\boldsymbol{G}_{\mathrm{EP_m}}\left(\boldsymbol{r}-\boldsymbol{r}',t-t'\right)\boldsymbol{P}_{\mathrm{m}}\left(\boldsymbol{r}',t'\right)\,\mathrm{d}t'\,\mathrm{d}^3r', \tag{3.85}$$

where $\boldsymbol{G}_{\mathrm{EP_m}}$ is given by [94], [100]

$$\boldsymbol{G}_{\mathrm{EP_m}}(\boldsymbol{r},t) = \frac{1}{4\pi}\boldsymbol{r}\times\mathbf{1}\left[\frac{1}{c_0\left\|\boldsymbol{r}\right\|^2}\delta''\left(t-\frac{\left\|\boldsymbol{r}\right\|}{c_0}\right)-\frac{1}{\left\|\boldsymbol{r}\right\|^3}\delta'\left(t-\frac{\left\|\boldsymbol{r}\right\|}{c_0}\right)\right]. \tag{3.86}$$

The solution for the corresponding magnetic field can be given in terms of

$$\boldsymbol{H}(\boldsymbol{r},t) = -\frac{1}{\mu_0}\nabla\times\int_{-\infty}^{t}\boldsymbol{E}\left(\boldsymbol{r},t'\right)\mathrm{d}t'. \tag{3.87}$$

A solution to the integral equation

$$\boldsymbol{H}(\boldsymbol{r},t) = \iiint_{V'}\int_{-\infty}^{\infty}\boldsymbol{G}_{\mathrm{HP_m}}\left(\boldsymbol{r},\boldsymbol{r}',t,t'\right)\boldsymbol{P}_{\mathrm{m}}\left(\boldsymbol{r}',t'\right)\,\mathrm{d}t'\,\mathrm{d}^3r', \tag{3.88}$$

is given for free space by the Green's dyadic [7]

$$\begin{aligned}\boldsymbol{G}_{\mathrm{HP_m}}(\boldsymbol{r},t) = \frac{1}{4\pi}\sqrt{\frac{\varepsilon_0}{\mu_0}}\Bigg[&\left(\mathbf{1}-3\frac{\boldsymbol{r}\boldsymbol{r}^{\mathrm{T}}}{\left\|\boldsymbol{r}\right\|^2}\right)\left(\frac{\delta'\left(t-\frac{\left\|\boldsymbol{r}\right\|}{c_0}\right)}{\left\|\boldsymbol{r}\right\|^2}+\frac{\delta\left(c_0t-\left\|\boldsymbol{r}\right\|\right)}{\mu_0\left\|\boldsymbol{r}\right\|^3}\right)\\&+\left(\mathbf{1}-\frac{\boldsymbol{r}\boldsymbol{r}^{\mathrm{T}}}{\left\|\boldsymbol{r}\right\|^2}\right)\left(\frac{\delta''\left(t-\frac{\left\|\boldsymbol{r}\right\|}{c_0}\right)}{c_0\left\|\boldsymbol{r}\right\|}\right)\Bigg].\end{aligned} \tag{3.89}$$

3.5.4 Time-Harmonic Fields

Consider a field quantity $\boldsymbol{F}$ that is space depended but has a harmonic time-dependence, e.g. with frequency f_0. This means it can be written as

$$\boldsymbol{F}(\boldsymbol{r},t) = \begin{bmatrix}F_x(\boldsymbol{r})\cos\left(2\pi f_0t+\varphi_x(\boldsymbol{r})\right)\\F_y(\boldsymbol{r})\cos\left(2\pi f_0t+\varphi_y(\boldsymbol{r})\right)\\F_z(\boldsymbol{r})\cos\left(2\pi f_0t+\varphi_z(\boldsymbol{r})\right)\end{bmatrix}. \tag{3.90}$$

Using complex phasors [83], [101], the time-harmonic field vector can be represented by

$$\boldsymbol{F}(\boldsymbol{r},t) = \mathrm{Re}\left\{\underline{\boldsymbol{F}}(\boldsymbol{r})\,\mathrm{e}^{\mathrm{i}2\pi f_0t}\right\}, \tag{3.91}$$

with the complex vector phasor

$$\underline{\boldsymbol{F}}(\boldsymbol{r}) = \begin{bmatrix}F_x(\boldsymbol{r})\,\mathrm{e}^{\mathrm{i}\varphi_x(\boldsymbol{r})}\\F_y(\boldsymbol{r})\,\mathrm{e}^{\mathrm{i}\varphi_y(\boldsymbol{r})}\\F_z(\boldsymbol{r})\,\mathrm{e}^{\mathrm{i}\varphi_z(\boldsymbol{r})}\end{bmatrix}. \tag{3.92}$$

Note that the time derivative of a time-harmonic field $\boldsymbol{F}$ is given by

$$\frac{\partial\boldsymbol{F}(\boldsymbol{r},t)}{\partial t} = \frac{\partial}{\partial t}\mathrm{Re}\left\{\underline{\boldsymbol{F}}(\boldsymbol{r})\,\mathrm{e}^{\mathrm{i}2\pi f_0t}\right\} = \mathrm{Re}\left\{\mathrm{i}2\pi f_0\underline{\boldsymbol{F}}(\boldsymbol{r})\,\mathrm{e}^{\mathrm{i}2\pi f_0t}\right\}. \tag{3.93}$$

Since all the information about the field distribution is contained within the space dependent vector phasor $\underline{\boldsymbol{F}}$, it suffices to consider only complex phasors for time-harmonic fields. In that sense, we can rewrite Maxwell's equations for the vector phasors $\underline{\boldsymbol{E}}$, $\underline{\boldsymbol{H}}$, $\underline{\boldsymbol{D}}$, and $\underline{\boldsymbol{B}}$ of a time-harmonic field to

$$\nabla\cdot\underline{\boldsymbol{D}}(\boldsymbol{r}) = \underline{\rho}(\boldsymbol{r}), \tag{3.94}$$

$$\nabla\times\underline{\boldsymbol{H}}(\boldsymbol{r}) = \mathrm{i}2\pi f_0\underline{\boldsymbol{D}}(\boldsymbol{r})+\underline{\boldsymbol{J}}(\boldsymbol{r}), \tag{3.95}$$

$$\nabla\times\underline{\boldsymbol{E}}(\boldsymbol{r}) = -\mathrm{i}2\pi f_0\underline{\boldsymbol{B}}(\boldsymbol{r}), \tag{3.96}$$

$$\nabla\cdot\underline{\boldsymbol{B}}(\boldsymbol{r}) = 0, \tag{3.97}$$

where the actual field quantities can be retained by means of equation (3.91).

In terms of the Fourier transformation, any integrable complex function $s : \mathbb{R} \to \mathbb{C}$ can be represented by a superposition of complex exponential functions, where the amplitude and phase relations are determined by a frequency-dependent complex phasor $\underline{S}_\mathrm{f}$. The superposition is given by

$$s(t) = \int_{-\infty}^{\infty} \underline{S}_\mathrm{f}(f)\, \mathrm{e}^{\mathrm{i}2\pi f t}\, \mathrm{d}f\,. \tag{3.98}$$

The complex phasor $\underline{S}_\mathrm{f}$ is obtained by means of the Fourier transformation. In this context, the real function s is projected onto the complex exponentials with a suitable inner product by

$$\underline{S}_\mathrm{f}(f) = \int_{-\infty}^{\infty} s(t)\, \mathrm{e}^{-\mathrm{i}2\pi f t}\, \mathrm{d}t\,. \tag{3.99}$$

As time-domain field quantities are real, it is easy to show that for any real function $g : \mathbb{R} \to \mathbb{R}$ we can write

$$g(t) = g^*(t) = \mathrm{Re}\{g(t)\} = \mathrm{Re}\left\{\int_{-\infty}^{\infty} \underline{G}(f)\, \mathrm{e}^{\mathrm{i}2\pi f t}\, \mathrm{d}f\right\} = \int_{-\infty}^{\infty} |\underline{G}(f)| \cos\left(2\pi f t + \varphi_g(f)\right)\, \mathrm{d}f\,, \tag{3.100}$$

where $|\underline{G}|$ is the magnitude of the complex phasor $\underline{G}$, and φ_g is the associated phase. An important property of the Fourier transform of a real-valued function has been shown in section 2.5 by Theorem 2.8. Thus, for any arbitrary real field $\boldsymbol{F}$, a complex vector phasor $\underline{\boldsymbol{F}}$ can be associated by means of the Fourier transformation

$$\underline{\boldsymbol{F}}(\boldsymbol{r}, f) = \int_{-\infty}^{\infty} \boldsymbol{F}(\boldsymbol{r}, t)\, \mathrm{e}^{-\mathrm{i}2\pi f t}\, \mathrm{d}t\,, \tag{3.101}$$

where the original field can be reconstructed by the inverse Fourier transformation

$$\boldsymbol{F}(\boldsymbol{r}, t) = \int_{-\infty}^{\infty} \underline{\boldsymbol{F}}(\boldsymbol{r}, f)\, \mathrm{e}^{\mathrm{i}2\pi f t}\, \mathrm{d}f = \int_{-\infty}^{\infty} \begin{bmatrix} F_x(\boldsymbol{r}, f) \cos\left(2\pi f t + \varphi_x(\boldsymbol{r}, f)\right) \\ F_y(\boldsymbol{r}, f) \cos\left(2\pi f t + \varphi_y(\boldsymbol{r}, f)\right) \\ F_z(\boldsymbol{r}, f) \cos\left(2\pi f t + \varphi_z(\boldsymbol{r}, f)\right) \end{bmatrix} \mathrm{d}f\,. \tag{3.102}$$

We introduce a change of variables $\omega = 2\pi f$, i.e. we switch from frequency f to angular frequency ω. This will introduce an additional scaling factor of $\frac{1}{2\pi}$ in the inverse Fourier transformation. Thus we have

$$\underline{S}(\omega) = \int_{-\infty}^{\infty} s(t)\, \mathrm{e}^{-\mathrm{i}\omega t}\, \mathrm{d}t\,, \tag{3.103}$$

for the Fourier transformation, and

$$s(t) = \frac{1}{2\pi} \int_{-\infty}^{\infty} \underline{S}(\omega)\, \mathrm{e}^{\mathrm{i}\omega t}\, \mathrm{d}\omega\,, \tag{3.104}$$

for the inverse Fourier transformation. Note that the two complex functions $\underline{S}_\mathrm{f}$ and $\underline{S}$ are not equal. It holds that $\underline{S}(\omega) = \underline{S}_\mathrm{f}\left(\frac{\omega}{2\pi}\right)$. In the following, we will not explicitly distinguish between complex phasors obtained in terms of $\underline{S}_\mathrm{f}$ or $\underline{S}$, but it will be clear which transformation to use whether the phasors depend on f or on ω.

Since Maxwell's equations are linear, and so is the Fourier transformation, we can consider each frequency component independently in terms of the associated complex phasors. Later, we can inverse Fourier transform the resulting complex phasors in order to obtain the time-domain field solutions. Thus, Maxwell's equations for each angular frequency component ω can be written as

$$\nabla\cdot \underline{\boldsymbol{D}}(\boldsymbol{r}, \omega) = \underline{\rho}(\boldsymbol{r}, \omega)\,, \tag{3.105}$$

$$\nabla\times \underline{\boldsymbol{H}}(\boldsymbol{r}, \omega) = \mathrm{i}\omega \underline{\boldsymbol{D}}(\boldsymbol{r}, \omega) + \underline{\boldsymbol{J}}(\boldsymbol{r}, \omega)\,, \tag{3.106}$$

$$\nabla\times \underline{\boldsymbol{E}}(\boldsymbol{r}, \omega) = -\mathrm{i}\omega \underline{\boldsymbol{B}}(\boldsymbol{r}, \omega)\,, \tag{3.107}$$

$$\nabla\cdot \underline{\boldsymbol{B}}(\boldsymbol{r}, \omega) = 0\,. \tag{3.108}$$

Similar to the time-domain, one can define vector and scalar potentials $\underline{\boldsymbol{A}}$ and $\underline{\Phi}$ such that $\underline{\boldsymbol{B}} = \nabla \times \underline{\boldsymbol{A}}$ and $\underline{\boldsymbol{E}} = -\nabla \underline{\Phi} - \mathrm{i}\omega \underline{\boldsymbol{A}}$, respectively. By enforcing the frequency-domain version of the Lorenz gauge condition, one obtains the so called Helmholtz equations for the vector and scalar potentials

$$\Delta \underline{\boldsymbol{A}}(\boldsymbol{r},\omega) + \omega^2 \underline{\boldsymbol{A}}(\boldsymbol{r},\omega) = -\mu_0 \underline{\boldsymbol{J}}(\boldsymbol{r},\omega) \,, \tag{3.109}$$

$$\Delta \underline{\Phi}(\boldsymbol{r},\omega) + \omega^2 \underline{\Phi}(\boldsymbol{r},\omega) = -\frac{\underline{\rho}(\boldsymbol{r},\omega)}{\varepsilon_0} \,. \tag{3.110}$$

Let us now consider a current density vector $\underline{\boldsymbol{J}}$, describing the source of the electromagnetic field. The magnetic vector potential $\underline{\boldsymbol{A}}$, originating from $\underline{\boldsymbol{J}}$ in free space, as a solution to equation (3.109), can be given by

$$\underline{\boldsymbol{A}}(\boldsymbol{r},\omega) = \frac{\mu_0}{4\pi} \int_{V'} \frac{\underline{\boldsymbol{J}}(\boldsymbol{r}',\omega)}{\|\boldsymbol{r}-\boldsymbol{r}'\|} \mathrm{e}^{-\mathrm{i}\omega \frac{\|\boldsymbol{r}-\boldsymbol{r}'\|}{c_0}} \, \mathrm{d}^3 r \,. \tag{3.111}$$

The magnetic field $\underline{\boldsymbol{H}}$ from $\underline{\boldsymbol{A}}$ can be obtained by

$$\underline{\boldsymbol{H}}(\boldsymbol{r},\omega) = \frac{1}{\mu_0} \nabla \times \underline{\boldsymbol{A}}(\boldsymbol{r},\omega) \,, \tag{3.112}$$

and thus directly from $\underline{\boldsymbol{J}}$ by

$$\underline{\boldsymbol{H}}(\boldsymbol{r},\omega) = \int_{V'} \underline{\boldsymbol{G}}_{\mathrm{HJ}}(\boldsymbol{r}-\boldsymbol{r}',\omega) \, \underline{\boldsymbol{J}}(\boldsymbol{r}',\omega) \, \mathrm{d}^3 r' \,, \tag{3.113}$$

where $\underline{\boldsymbol{G}}_{\mathrm{HJ}}$ is the Green's dyadic of the system under consideration, relating the excited magnetic field $\underline{\boldsymbol{H}}$ to the source current density $\underline{\boldsymbol{J}}$. The total Green's dyadic for free space, also accounting for the near-field contributions is given by [16], [102]

$$\underline{\boldsymbol{G}}_{\mathrm{HJ}}(\boldsymbol{r},\omega) = \frac{1}{4\pi} \boldsymbol{r} \times \mathbf{1} \frac{c_0 + \mathrm{i}\omega \|\boldsymbol{r}\|}{c_0 \|\boldsymbol{r}\|^3} \mathrm{e}^{-\mathrm{i}\omega \frac{\|\boldsymbol{r}\|}{c_0}} \,. \tag{3.114}$$

The corresponding electric field $\underline{\boldsymbol{E}}$ can be obtained by

$$\underline{\boldsymbol{E}}(\boldsymbol{r},\omega) = \frac{1}{\mathrm{i}\omega\varepsilon_0} \nabla \times \underline{\boldsymbol{H}}(\boldsymbol{r},\omega) \,, \tag{3.115}$$

and directly from $\underline{\boldsymbol{J}}$ by

$$\underline{\boldsymbol{E}}(\boldsymbol{r},\omega) = \int_{V'} \underline{\boldsymbol{G}}_{\mathrm{EJ}}(\boldsymbol{r}-\boldsymbol{r}',\omega) \, \underline{\boldsymbol{J}}(\boldsymbol{r}',\omega) \, \mathrm{d}^3 r' \,, \tag{3.116}$$

where $\underline{\boldsymbol{G}}_{\mathrm{EJ}}$ is the Green's dyadic of the system under consideration, relating the excited electric field $\underline{\boldsymbol{E}}$ to the source current density $\underline{\boldsymbol{J}}$. The free space Green's dyadic for the electric field, excited by an electric current density is given by [16], [102]

$$\underline{\boldsymbol{G}}_{\mathrm{EJ}}(\boldsymbol{r},\omega) = -\frac{\mathrm{i}}{4\pi} \sqrt{\frac{\varepsilon_0}{\mu_0}} \left[\left(\frac{\omega}{c_0 \|\boldsymbol{r}\|} + \frac{\mathrm{i}}{\|\boldsymbol{r}\|^2} - \frac{c_0}{\omega \|\boldsymbol{r}\|^3} \right) \mathbf{1} - \left(\frac{\omega}{c_0 \|\boldsymbol{r}\|^3} + \frac{3\mathrm{i}}{\|\boldsymbol{r}\|^4} - \frac{3c_0}{\omega \|\boldsymbol{r}\|^5} \right) \boldsymbol{r}\boldsymbol{r}^{\mathrm{T}} \right] \mathrm{e}^{-\mathrm{i}\omega \frac{\|\boldsymbol{r}\|}{c_0}} \,. \tag{3.117}$$

Using the Green's dyadics (3.114) and (3.117), one can solve electromagnetic field propagation problems directly in the frequency-domain.

3.5.5 Uniqueness Theorem and Equivalence Principle

Let us assume we have electric and magnetic sources $\boldsymbol{J}$ and $\boldsymbol{M}$, respectively. Furthermore, we assume that $\boldsymbol{J}$ and $\boldsymbol{M}$ are non-vanishing only in a closed volume V', bounded by the surface $\partial V'$. A very elegant way for denoting this property [103] is by introducing the indicator function $\mathbf{1}_V : \mathbb{R}^3 \to \{0,1\}$. The indicator function is given by

$$\mathbf{1}_V(\boldsymbol{r}) = \begin{cases} 1 & \text{for } \boldsymbol{r} \in V, \\ 0 & \text{for } \boldsymbol{r} \notin V. \end{cases} \tag{3.118}$$

With this definition, we can write

$$\boldsymbol{J}(\boldsymbol{r},t) = \mathbf{1}_{V'}(\boldsymbol{r})\,\boldsymbol{J}(\boldsymbol{r},t)\ , \tag{3.119}$$

$$\boldsymbol{M}(\boldsymbol{r},t) = \mathbf{1}_{V'}(\boldsymbol{r})\,\boldsymbol{M}(\boldsymbol{r},t)\ . \tag{3.120}$$

The electromagnetic field in the volume $V = \mathbb{R}^3 \setminus V'$ is then given by multiplying Maxwell's equations with the indicator function $\mathbf{1}_V$ for the volume V. Thus, we have

$$\mathbf{1}_V(\boldsymbol{r})\,\nabla\times\boldsymbol{E}(\boldsymbol{r},t) = -\mathbf{1}_V(\boldsymbol{r})\,\frac{\partial\boldsymbol{B}(\boldsymbol{r},t)}{\partial t}\,, \tag{3.121}$$

$$\mathbf{1}_V(\boldsymbol{r})\,\nabla\times\boldsymbol{H}(\boldsymbol{r},t) = \mathbf{1}_V(\boldsymbol{r})\,\frac{\partial\boldsymbol{D}(\boldsymbol{r},t)}{\partial t}\,. \tag{3.122}$$

where $\mathbf{1}_V\boldsymbol{J} = 0$ and $\mathbf{1}_V\boldsymbol{M} = 0$, since $\mathbf{1}_{V'}(\boldsymbol{r})\,\mathbf{1}_V(\boldsymbol{r}) = 0$ for $V \cap V' = \emptyset$. By the product rule for partial derivatives, we have

$$\nabla\times\boldsymbol{E}_V(\boldsymbol{r},t) = -\frac{\partial\boldsymbol{B}_V(\boldsymbol{r},t)}{\partial t} + \nabla\,\mathbf{1}_V(\boldsymbol{r})\times\boldsymbol{E}(\boldsymbol{r},t)\ , \tag{3.123}$$

$$\nabla\times\boldsymbol{H}_V(\boldsymbol{r},t) = \frac{\partial\boldsymbol{D}_V(\boldsymbol{r},t)}{\partial t} + \nabla\,\mathbf{1}_V(\boldsymbol{r})\times\boldsymbol{H}(\boldsymbol{r},t)\ , \tag{3.124}$$

where the subscript $_V$ denotes multiplication of the quantity with the indicator function $\mathbf{1}_V$, i.e. only the part of the quantity that lies in the region V. Consider an arbitrary integrable vector field $\boldsymbol{F}$. Then we have

$$\begin{aligned}\iiint_{\mathbb{R}^3} \nabla\,\mathbf{1}_V\cdot\boldsymbol{F}(\boldsymbol{r},t)\ \mathrm{d}^3r &= \iiint_{\mathbb{R}^3}\nabla\cdot[\mathbf{1}_V\boldsymbol{F}(\boldsymbol{r},t)]\ \mathrm{d}^3r - \iiint_{\mathbb{R}^3}\mathbf{1}_V\,\nabla\cdot\boldsymbol{F}(\boldsymbol{r},t)\ \mathrm{d}^3r\\ &= -\iiint_V \nabla\cdot\boldsymbol{F}(\boldsymbol{r},t)\ \mathrm{d}^3r = \iint_{\partial V'}\boldsymbol{F}(\boldsymbol{r},t)\cdot\mathrm{d}\boldsymbol{A}'\,,\end{aligned} \tag{3.125}$$

where the first integral vanishes as by Gauss's theorem (Theorem 2.7) it corresponds to a surface integral at infinity, where the vector field $\boldsymbol{F}$ must vanish. The last step follows by applying Gauss's theorem again for the second integral. The surface normal vector $\mathrm{d}\boldsymbol{A}$ points outwards of V, and thus into V'. Therefore, the sign was changed accordingly when switching from $\mathrm{d}\boldsymbol{A}$ to $\mathrm{d}\boldsymbol{A}'$. Let now $\boldsymbol{n}$ denote the normal vector, perpendicular to $\partial V'$ pointing outwards of V' into V. Then, $\nabla\,\mathbf{1}_V$ can be interpreted as [103]

$$\nabla\,\mathbf{1}_V = \boldsymbol{n}(\boldsymbol{r})\,\delta_{\partial V'}(\boldsymbol{r})\ , \tag{3.126}$$

where $\delta_{\partial V'}(\boldsymbol{r})$ is the Dirac delta distribution, defined on the surface $\partial V'$, given by

$$\delta_{\partial V'}(\boldsymbol{r}) = \delta(\boldsymbol{r}-\boldsymbol{a})\ , \qquad \forall\boldsymbol{a}\in\partial V'\,. \tag{3.127}$$

For the fields in the source-free region V, equations (3.123) and (3.124) resemble Maxwell's equations when considering electric and magnetic sources by replacing

$$\boldsymbol{J}(\boldsymbol{r},t) = \boldsymbol{n}(\boldsymbol{r})\times\boldsymbol{H}(\boldsymbol{r},t)\,\delta_{\partial V'}(\boldsymbol{r})\ , \tag{3.128}$$

$$\boldsymbol{M}(\boldsymbol{r},t) = -\boldsymbol{n}(\boldsymbol{r})\times\boldsymbol{E}(\boldsymbol{r},t)\,\delta_{\partial V'}(\boldsymbol{r})\ . \tag{3.129}$$

This is well known as equivalence principle [83], [104] or Huygens' principle [103]. The uniqueness theorem now assures that the solution in a source free region V is uniquely determined by specifying the tangential field components of either $\boldsymbol{n}\times\boldsymbol{H}$ or $-\boldsymbol{n}\times\boldsymbol{E}$.

Theorem 3.1 (Uniqueness Theorem)**.** *The electromagnetic field in a source-free region V is determined in a unique way, if the tangential components of either the electric field or the magnetic field are known on the boundary $\partial V'$.*

Proof. We refrain here from a rigorous proof of the uniqueness theorem, as it involves the concept of losses, which was not introduced so far. Proofs for the uniqueness theorem can be found in the literature, e.g. in [83], [101], [102].

The converse of the theorem is, however, not true. There is an infinite number of possible source distributions in V' that yield the same field distribution in V. Reconstruction of the actual sources in V' is in general not possible in an exact manner. The problem of finding equivalent sources on $\partial V'$ can, however, still be formulated in terms of an estimation problem, as we will see in section 4.4. The uniqueness theorem and the equivalence principle are fundamental for propagating and characterizing stochastic electromagnetic fields in chapters 4 an 5.

3.6 Stochastic Model for Electromagnetic Fields

The aim of this section is to adopt the general stochastic field model, which is valid for any field quantity, e.g. sound waves, etc., to the specific field concept of electromagnetism. In that sense, this section should provide a bridge between the general model, developed and outlined in section 3.1, and the fundamental concepts of electromagnetic fields from section 3.5. Special emphasis is given to the identification of the corresponding quantities and transformations involved.

3.6.1 Propagation of Statistical Parameters for Electromagnetic Fields

We consider a source current density field $\boldsymbol{J}$, where the spatial and temporal distribution of the field is subjected to random fluctuations. It is assumed, that $\boldsymbol{J}$ is vanishing outside a certain volume $V' \subset \mathbb{R}^3$, that is, the source field is confined within a certain region of space. According to the general stochastic field model from section 3.1, the source field can be described as a random field $\boldsymbol{J} : \Omega \times (V' \times \mathbb{R}) \to \mathbb{R}^3$ over a probability space $(\Omega, \mathcal{F}, P)$. Now let X be the space of all possible fields $\boldsymbol{j} : V' \times \mathbb{R} \to \mathbb{R}^3$ and let $\mathcal{H}$ be the minimal σ-algebra containing all cylindrical sets $C \subset X$. According to Theorem 2.2, there is a probability measure $\tilde{P}$ defined on the measurable space $(X, \mathcal{H})$ that is completely determined by the family of finite dimensional joint probability distributions of the random field $\boldsymbol{J}$. Thus, the random process for the source field is completely determined by specifying the distributions

$$F^{\mathrm{J}}_{(\boldsymbol{r}_1,t_1),\ldots,(\boldsymbol{r}_n,t_n)}\left(\boldsymbol{j}_1,\ldots,\boldsymbol{j}_n\right) = P\left(\left\{\boldsymbol{J}\left(\boldsymbol{r}_1,t_1\right) \in B\left(\boldsymbol{j}_1\right),\ldots,\boldsymbol{J}\left(\boldsymbol{r}_n,t_n\right) \in B\left(\boldsymbol{j}_n\right)\right\}\right) , \tag{3.130}$$

where each $\boldsymbol{j}_k$ gives rise to a set $B\left(\boldsymbol{j}_k\right)$, given by

$$B\left(\boldsymbol{j}_k\right) = \left\{\left[b_x, b_y, b_z\right]^{\mathrm{T}} \in \mathbb{R}^3 : b_x \leq j_{x,k}, b_y \leq j_{y,k}, b_z \leq j_{z,k}, \boldsymbol{j}_k = \left[j_{x,k}, j_{y,k}, j_{z,k}\right]^{\mathrm{T}}\right\} . \tag{3.131}$$

Because it is known that for the finite dimensional probability distributions $F^{\mathrm{J}}_{(\boldsymbol{r}_1,t_1),\cdots,(\boldsymbol{r}_n,t_n)}\left(\boldsymbol{j}_1,\cdots,\boldsymbol{j}_n\right)$, there exists a probability measure $\tilde{P}$ on the function space X by Theorem 2.2, it is more convenient to consider characteristic functionals χ_{J}, associated with the measure $\tilde{P}$, instead of finite dimensional distributions. The characteristic functional χ_{J} for $\boldsymbol{z} \in X$ is given by

$$\chi_{\mathrm{J}}\left(\boldsymbol{z}\right) = \int_X \mathrm{e}^{\mathrm{i}\langle \boldsymbol{z},\boldsymbol{j}\rangle}\, \tilde{P}\left(\mathrm{d}\boldsymbol{j}\right) . \tag{3.132}$$

For general random processes with arbitrary finite dimensional distributions, it is hard to make any predictions, as an infinite amount of distributions needs to be specified. In studying the propagation of stochastic electromagnetic fields, it is of great interest to determine the random electric and magnetic fields $\boldsymbol{E}$ and $\boldsymbol{H}$ in some volume $V \subset \mathbb{R}$, generated by the random source field $\boldsymbol{J}$. Since the exciting field is totally random, it does not make sense to determine explicit values for the emerging electric and magnetic fields. We are rather interested in how to infer the statistics of the propagated fields from the statistics of the source field. We assume for now, that the statistics of the source field $\boldsymbol{J}$ are known, i.e. there is a known characteristic functional χ_{J}, completely describing the random field. From section 3.5, we know that the magnetic field $\boldsymbol{H}$ due to a current density $\boldsymbol{J}$ is given by

$$\boldsymbol{H}\left(\boldsymbol{r},t\right) = \iiint_{V'} \int_{-\infty}^{\infty} \boldsymbol{G}_{\mathrm{HJ}}\left(\boldsymbol{r}-\boldsymbol{r}',t-t'\right) \boldsymbol{J}\left(\boldsymbol{r}',t'\right)\, \mathrm{d}t'\, \mathrm{d}^3 r' . \tag{3.133}$$

For our stochastic model, this means that every possible realization $\boldsymbol{j} \in X$ of the random field $\boldsymbol{J}$ gets mapped to a certain realization $\boldsymbol{h}$ of the random field $\boldsymbol{H}$, by the linear integral transformation with kernel $\boldsymbol{G}_{\mathrm{HJ}}$. Let Y denote the space of all possible propagated magnetic fields $\boldsymbol{h} : V \times \mathbb{R} \to \mathbb{R}^3$. Thus, we can identify the linear transformation operator $\hat{\boldsymbol{M}} : X \to Y$ to be the integral transformation with kernel $\boldsymbol{G}_{\mathrm{HJ}}$. The characteristic functional χ_{H} of the propagated field $\boldsymbol{H}$ can be obtained according to section 3.1.2 by

$$\chi_{\mathrm{H}}(\boldsymbol{z}) = \chi_{\mathrm{J}}\left(\hat{\boldsymbol{M}}^{\dagger}\boldsymbol{z}\right) . \tag{3.134}$$

Since the time-domain Green's dyadics are real, the adjoint of the integral operator $\hat{\boldsymbol{M}}^{\dagger}$ is obtained by exchanging the role of the primed and unprimed arguments of the integral kernel, given by the dyadic Green's function [105]. Obtaining the adjoint operator $\hat{\boldsymbol{M}}^{\dagger}$ in the time-domain poses some difficulties for the retarded time-domain Green's dyadics, as given for free space in section 3.5. It is obvious that for exchanging the spatial arguments $\boldsymbol{r}$ and $\boldsymbol{r}'$ we have $\boldsymbol{G}_{\mathrm{HJ}}(\boldsymbol{r}' - \boldsymbol{r}, t - t') = \boldsymbol{G}_{\mathrm{HJ}}^{\dagger}(\boldsymbol{r} - \boldsymbol{r}', t - t')$ since $(\boldsymbol{r} \times \mathbf{1})^{\dagger} = -\boldsymbol{r} \times \mathbf{1}$. For exchanging the time arguments t and t', however, the direction of propagation would be reversed, leading to non-causal solutions. In [98], the time-domain dyadic Green's function was derived using the so called propagator method [106]. There, the Green's function was defined as

$$\boldsymbol{G}_{\mathrm{HJ}}(\boldsymbol{r}, t, \boldsymbol{r}', t') = U(t - t')\, \boldsymbol{K}_{\mathrm{HJ}}(\boldsymbol{r}, t, \boldsymbol{r}', t') , \tag{3.135}$$

with the propagator $\boldsymbol{K}_{\mathrm{HJ}}$ and the Heaviside step function U. Using this definition, and then exchanging the role of t and t', it is obvious that the dyadic Green's function is self-adjoint in the time argument, i.e. $\boldsymbol{G}_{\mathrm{HJ}}(\boldsymbol{r} - \boldsymbol{r}', t - t') = \boldsymbol{G}_{\mathrm{HJ}}^{\mathrm{T}}(\boldsymbol{r} - \boldsymbol{r}', t' - t)$. In case of the definition from [98], the sign of the propagation direction gets reversed for both, the retarded, as well as the advanced components of the propagator $\boldsymbol{K}_{\mathrm{HJ}}$. But since the sign of the argument of the Heaviside function U is also changed, the former retarded components are rejected and only the advanced components remain, with a reversed propagation direction. As $\boldsymbol{K}_{\mathrm{HJ}}$ is symmetric for both, retarded and advanced components, the adjoint solution is equivalent to the original dyadic Green's function. A similar argument can be made, as for obtaining the retarded solution in [94], the advanced components have been suppressed in order to obtain a causal solution. By reversing the time coordinate, the condition on causality also changes accordingly, yielding a similar result.

Thus, one can infer the statistics of the excited random field $\boldsymbol{H}$ from the characteristic functional χ_{J} of the random source field $\boldsymbol{J}$ by means of the characteristic functional χ_{H}, given by

$$\begin{aligned}
\chi_{\mathrm{H}}(\boldsymbol{z}) &= \int_{Y} \exp\left(\mathrm{i} \iiint_{V} \int_{-\infty}^{\infty} \boldsymbol{z}^{\mathrm{T}}(\boldsymbol{r}, t)\, \boldsymbol{h}(\boldsymbol{r}, t)\, \mathrm{d}t\, \mathrm{d}^3 r \right) \tilde{P}(\mathrm{d}\boldsymbol{h}) , \\
&= \int_{Y} \exp\left(\mathrm{i} \iiint_{V} \int_{-\infty}^{\infty} \iiint_{V'} \int_{-\infty}^{\infty} \boldsymbol{z}^{\mathrm{T}}(\boldsymbol{r}, t)\, \boldsymbol{G}_{\mathrm{HJ}}(\boldsymbol{r} - \boldsymbol{r}', t - t')\, \boldsymbol{j}(\boldsymbol{r}', t')\, \mathrm{d}t'\, \mathrm{d}^3 r'\, \mathrm{d}t\, \mathrm{d}^3 r \right) \tilde{P}(\mathrm{d}\boldsymbol{j}) .
\end{aligned} \tag{3.136}$$

3.6.2 Gaussian Stochastic Electromagnetic Fields

Let us now assume that the statistics of the random source field $\boldsymbol{J}$ are essentially governed by a Gaussian probability distribution, as described in section 3.2. This assumption is widely justified in practice by the central limit theorem (Theorem 2.1), which states that as long as the number of independent, identically distributed source fields is large enough, the superimposed source field will converge to a Gaussian distributed field, regardless of the individual, identical source distributions. As the number of statistical sources in practical electronic circuits is typically very large, a Gaussian probability distribution of a random field, emitted by

such circuits seems to be a legit assumption. The characteristic functional of the source field $\boldsymbol{J}$ is completely determined by the field's expectation value function $\boldsymbol{m}_\mathrm{J}$ and by the correlation dyadic $\boldsymbol{\Gamma}_\mathrm{J}$. It is given by

$$\chi_\mathrm{J}(\boldsymbol{z}) = \exp\left(\mathrm{i}\iiint_{V'}\int_{-\infty}^{\infty}\boldsymbol{z}^\mathrm{T}(\boldsymbol{r}',t')\,\boldsymbol{m}_\mathrm{J}(\boldsymbol{r}',t')\;\mathrm{d}t'\,\mathrm{d}^3r'\right)\times$$
$$\times\exp\left(-\frac{1}{2}\iiint_{V'}\int_{-\infty}^{\infty}\iiint_{V'}\int_{-\infty}^{\infty}\boldsymbol{z}^\mathrm{T}(\boldsymbol{r}_1',t_1')\,\boldsymbol{\Gamma}_\mathrm{J}(\boldsymbol{r}_1',\boldsymbol{r}_2',t_1',t_2')\,\boldsymbol{z}(\boldsymbol{r}_2',t_2')\;\mathrm{d}t_2'\,\mathrm{d}^3r_2'\,\mathrm{d}t_1'\,\mathrm{d}^3r_1'\right), \tag{3.137}$$

for all $\boldsymbol{z}\in X$. By applying (3.134) where the propagation operator is given by the integral transformation with kernel $\boldsymbol{G}_\mathrm{HJ}$, we have found a propagation rule for the characteristic functional of the source field χ_J to the characteristic functional of the observed field χ_H. This relation is given by

$$\chi_\mathrm{H}(\boldsymbol{z}) = \exp\left(\mathrm{i}\iiint_{V}\int_{-\infty}^{\infty}\iiint_{V'}\int_{-\infty}^{\infty}\boldsymbol{z}^\mathrm{T}(\boldsymbol{r},t)\,\boldsymbol{G}_\mathrm{HJ}(\boldsymbol{r}-\boldsymbol{r}',t-t')\,\boldsymbol{m}_\mathrm{J}(\boldsymbol{r}',t')\;\mathrm{d}t'\,\mathrm{d}^3r'\,\mathrm{d}t\,\mathrm{d}^3r\right)\times$$
$$\times\exp\left(-\frac{1}{2}\iiint_{V}\int_{-\infty}^{\infty}\iiint_{V}\int_{-\infty}^{\infty}\iiint_{V'}\int_{-\infty}^{\infty}\iiint_{V'}\int_{-\infty}^{\infty}\boldsymbol{z}^\mathrm{T}(\boldsymbol{r}_1,t_1)\,\boldsymbol{G}_\mathrm{HJ}(\boldsymbol{r}_1-\boldsymbol{r}_1',t_1-t_1')\right.$$
$$\left.\times\,\boldsymbol{\Gamma}_\mathrm{J}(\boldsymbol{r}_1',\boldsymbol{r}_2',t_1',t_2')\,\boldsymbol{G}_\mathrm{HJ}^\mathrm{T}(\boldsymbol{r}_2-\boldsymbol{r}_2',t_2-t_2')\,\boldsymbol{z}(\boldsymbol{r}_2,t_2)\;\mathrm{d}t_2'\,\mathrm{d}^3r_2'\,\mathrm{d}t_1'\,\mathrm{d}^3r_1'\,\mathrm{d}t_2\,\mathrm{d}^3r_2\,\mathrm{d}t_1\,\mathrm{d}^3r_1\right), \tag{3.138}$$

for all $\boldsymbol{z}\in Y$. Hence, as the characteristic functional χ_J transforms to χ_H by (3.134), the statistical parameters $\boldsymbol{m}_\mathrm{J}$ and $\boldsymbol{\Gamma}_\mathrm{J}$ of the Gaussian source field transform like

$$\boldsymbol{m}_\mathrm{H}(\boldsymbol{r},t) = \iiint_{V'}\int_{-\infty}^{\infty}\boldsymbol{G}_\mathrm{HJ}(\boldsymbol{r}-\boldsymbol{r}',t-t')\,\boldsymbol{m}_\mathrm{J}(\boldsymbol{r}',t')\;\mathrm{d}t'\,\mathrm{d}^3r', \tag{3.139}$$

$$\boldsymbol{\Gamma}_\mathrm{H}(\boldsymbol{r}_1,\boldsymbol{r}_2,t_1,t_2) = \iiint_{V'}\int_{-\infty}^{\infty}\iiint_{V'}\int_{-\infty}^{\infty}\boldsymbol{G}_\mathrm{HJ}(\boldsymbol{r}_1-\boldsymbol{r}_1',t_1-t_1')\,\boldsymbol{\Gamma}_\mathrm{J}(\boldsymbol{r}_1',\boldsymbol{r}_2',t_1',t_2')\times$$
$$\times\,\boldsymbol{G}_\mathrm{HJ}^\mathrm{T}(\boldsymbol{r}_2-\boldsymbol{r}_2',t_2-t_2')\;\mathrm{d}t_2'\,\mathrm{d}^3r_2'\,\mathrm{d}t_1'\,\mathrm{d}^3r_1'. \tag{3.140}$$

In order to have a complete description of the observed random field, it is thus sufficient to propagate the expectation value function and the correlation dyadic of the Gaussian random source field using electromagnetic dyadic Green's functions. The resulting observed random field will again exhibit a Gaussian distribution with the transformed parameters given in (3.139) and (3.140).

The use of characteristic functionals thus generalizes the treatment of stochastic electromagnetic fields, and it was shown that the theoretical concept that was developed earlier for stationary ergodic Gaussian random fields in [7], [15], [16] is actually contained as a special case in the general framework introduced here.

3.6.3 Stochastic Electromagnetic Fields in the Frequency-Domain

Assigning probability measures to stochastic electromagnetic fields in the frequency-domain is indeed not a trivial task, as it involves Fourier transforms of randomly fluctuating fields, which do not exist in general, especially if one considers stationary random fields, where the field amplitudes do not sufficiently decay as $t\to\infty$. Let us, for now, assume that the space of all random source fields $X\subseteq L^2$, such that all realizations of the random field $\boldsymbol{J}$ are square integrable and form a Hilbert space. Furthermore, let us denote the space of

Fourier transformed realizations $\underline{\boldsymbol{j}}$ by $\underline{X}$. Then we can define measures on the Fourier transformed random field in terms of characteristic functionals in the same way as for other linear transformations. Let us consider the temporal Fourier transformation $\mathcal{F}$ of a realization $\boldsymbol{j} \in X$ of the random field $\boldsymbol{J}$, given by

$$\underline{\boldsymbol{j}}\left(\boldsymbol{r},\omega\right) = \mathcal{F}\left(\boldsymbol{j}\left(\boldsymbol{r},t\right)\right) = \int\limits_{-\infty}^{\infty} \boldsymbol{j}\left(\boldsymbol{r},t\right) \mathrm{e}^{-\mathrm{i}\omega t}\ \mathrm{d}t\,. \tag{3.141}$$

Now suppose that every realization $\boldsymbol{j}$ is assigned a differential probability measure $\tilde{P}\left(\mathrm{d}\boldsymbol{j}\right)$. The same probability measure should be assigned to the Fourier transform $\underline{\boldsymbol{j}}$ of the realization $\boldsymbol{j}$. In terms of characteristic functionals, this is expressed by

$$\chi_{\underline{\mathrm{J}}}\left(\underline{\boldsymbol{z}}\right) = \chi_{\mathrm{J}}\left(\mathcal{F}^{-1}\underline{\boldsymbol{z}}\right)\,, \tag{3.142}$$

for all $\underline{\boldsymbol{z}} \in \underline{X}$. Thus we have

$$\chi_{\underline{\mathrm{J}}}\left(\underline{\boldsymbol{z}}\right) = \int_{\underline{X}} \mathrm{e}^{\mathrm{i}\left\langle \underline{\boldsymbol{z}},\underline{\boldsymbol{j}}\right\rangle} \tilde{P}\left(\mathrm{d}\underline{\boldsymbol{j}}\right) = \int_{X} \mathrm{e}^{\mathrm{i}\left\langle \mathcal{F}^{-1}\underline{\boldsymbol{z}},\boldsymbol{j}\right\rangle} \tilde{P}\left(\mathrm{d}\boldsymbol{j}\right) = \int_{X} \mathrm{e}^{\mathrm{i}\left\langle \underline{\boldsymbol{z}},\mathcal{F}\boldsymbol{j}\right\rangle} \tilde{P}\left(\mathrm{d}\boldsymbol{j}\right)\,, \tag{3.143}$$

For Gaussian random source fields, as given in section 3.2, where the space of all realizations of the source field $X \subseteq L^2$, the characteristic functional of the Fourier transformed source field is given by

$$\begin{aligned}\chi_{\underline{\mathrm{J}}}\left(\underline{\boldsymbol{z}}\right) = \exp\Bigg(\mathrm{i}\iiint_{V'} \int\limits_{-\infty}^{\infty}\int\limits_{-\infty}^{\infty} \underline{\boldsymbol{z}}^{\dagger}\left(\boldsymbol{r}',\omega\right)\boldsymbol{m}_{\mathrm{J}}\left(\boldsymbol{r}',t'\right)\mathrm{e}^{-\mathrm{i}\omega' t'}\ \mathrm{d}t'\,\mathrm{d}\omega'\,\mathrm{d}^3 r'\Bigg) \times \\ \times \exp\Bigg(-\frac{1}{2}\iiint_{V'} \int\limits_{-\infty}^{\infty} \iiint_{V'} \int\limits_{-\infty}^{\infty}\int\limits_{-\infty}^{\infty}\int\limits_{-\infty}^{\infty} \underline{\boldsymbol{z}}^{\dagger}\left(\boldsymbol{r}_1',\omega_1'\right)\mathrm{e}^{-\mathrm{i}\omega_1' t_1'}\boldsymbol{\Gamma}_{\mathrm{J}}\left(\boldsymbol{r}_1',\boldsymbol{r}_2',t_1',t_2'\right)\mathrm{e}^{\mathrm{i}\omega_2' t_2'} \times \\ \times\ \underline{\boldsymbol{z}}\left(\boldsymbol{r}_2',\omega_2'\right)\ \mathrm{d}t_2'\,\mathrm{d}t_1'\,\mathrm{d}\omega_2'\,\mathrm{d}^3 r_2'\,\mathrm{d}\omega_1'\,\mathrm{d}^3 r_1'\Bigg)\,.\end{aligned} \tag{3.144}$$

For convenience, we define the frequency-domain expectation value and the frequency-domain correlation dyadic

$$\underline{\boldsymbol{m}}_{\mathrm{J}}\left(\boldsymbol{r}',\omega'\right) = \int\limits_{-\infty}^{\infty} \boldsymbol{m}_{\mathrm{J}}\left(\boldsymbol{r}',t'\right)\mathrm{e}^{-\mathrm{i}\omega' t'}\ \mathrm{d}t'\,, \tag{3.145}$$

$$\underline{\boldsymbol{\Gamma}}_{\mathrm{J}}\left(\boldsymbol{r}_1',\boldsymbol{r}_2',\omega_1',\omega_2'\right) = \int\limits_{-\infty}^{\infty}\int\limits_{-\infty}^{\infty} \boldsymbol{\Gamma}_{\mathrm{J}}\left(\boldsymbol{r}_1',\boldsymbol{r}_2',t_1',t_2'\right)\mathrm{e}^{-\mathrm{i}\omega_1' t_1'}\mathrm{e}^{\mathrm{i}\omega_2' t_2'}\ \mathrm{d}t_2'\,\mathrm{d}t_1'\,. \tag{3.146}$$

By the linearity of the expectation value, one can immediately see that $\underline{\boldsymbol{m}}_{\underline{\mathrm{J}}}$ is the expectation value of the Fourier transformed process, i.e.

$$\underline{\boldsymbol{m}}_{\mathrm{J}}\left(\boldsymbol{r}',\omega'\right) = \left\langle\!\left\langle \underline{\boldsymbol{J}}\left(\boldsymbol{r}',\omega'\right)\right\rangle\!\right\rangle\,. \tag{3.147}$$

The same holds for the correlation dyadics, i.e.

$$\underline{\boldsymbol{\Gamma}}_{\mathrm{J}}\left(\boldsymbol{r}_1',\boldsymbol{r}_2',\omega_1',\omega_2'\right) = \left\langle\!\!\left\langle \underline{\boldsymbol{J}}\left(\boldsymbol{r}_1',\omega_1'\right)\underline{\boldsymbol{J}}^{\dagger}\left(\boldsymbol{r}_1',\omega_1'\right)\right\rangle\!\!\right\rangle\,, \tag{3.148}$$

The rule for propagating means and correlation dyadics in the frequency-domain is similar to equations (3.139) and (3.140), using frequency-domain Green's dyadics, as given in (3.114). The propagation scheme is governed by

$$\underline{\boldsymbol{m}}_{\mathrm{H}}\left(\boldsymbol{r},\omega\right) = \iiint_{V'} \underline{\boldsymbol{G}}_{\mathrm{HJ}}\left(\boldsymbol{r}-\boldsymbol{r}',\omega\right)\underline{\boldsymbol{m}}_{\mathrm{J}}\left(\boldsymbol{r}',\omega\right)\ \mathrm{d}^3 r'\,, \tag{3.149}$$

$$\underline{\boldsymbol{\Gamma}}_{\mathrm{H}}\left(\boldsymbol{r}_1,\boldsymbol{r}_2,\omega_1,\omega_2\right) = \iiint_{V'}\iiint_{V'} \underline{\boldsymbol{G}}_{\mathrm{HJ}}\left(\boldsymbol{r}_1-\boldsymbol{r}_1',\omega_1\right)\underline{\boldsymbol{\Gamma}}_{\mathrm{J}}\left(\boldsymbol{r}_1',\boldsymbol{r}_2',\omega_1,\omega_2\right)\underline{\boldsymbol{G}}_{\mathrm{HJ}}^{\dagger}\left(\boldsymbol{r}_2-\boldsymbol{r}_2',\omega_2\right)\ \mathrm{d}^3 r_2'\,\mathrm{d}^3 r_1'\,. \tag{3.150}$$

For the case of stationary fields, which are clearly not contained in L^2, one can think of time-windowing the time-domain realizations, such that the Fourier integral converges for finite window lengths T and then taking the limit of $T \to \infty$ [107].

3.7 Ensemble Averages and Sample Averages

In real-life applications, we typically do not know the exact parameters of a random field. Thus, those parameters need to be reconstructed by recorded samples of the actual field in a data post-processing step. A required assumption for being able to recover the statistical parameters from samples of a random field is ergodicity (see Definition 2.32). Note that ergodicity implicitly requires the random field to be stationary, as otherwise, one cannot infer statistical parameters from sampled data. Let now $\boldsymbol{J}$ be a Gaussian random source field which is stationary and ergodic in the time argument. Motivated by the Birkhoff-Khinchin theorem [59], [71] for ergodic random fields, the ensemble averages for the parameters $\boldsymbol{m}_\mathrm{J}$ and $\boldsymbol{\Gamma}_\mathrm{J}$ can be replaced by time averages. Therefore, the parameters are given by

$$\boldsymbol{m}_\mathrm{J}\left(\boldsymbol{r}'\right) = \langle\!\langle \boldsymbol{J}\left(\boldsymbol{r}', t'\right)\rangle\!\rangle = \lim_{T\to\infty} \frac{1}{2T} \int_{-T}^{T} \boldsymbol{j}\left(\boldsymbol{r}', t'\right)\, \mathrm{d}t'\,, \tag{3.151}$$

$$\boldsymbol{\Gamma}_\mathrm{J}\left(\boldsymbol{r}_1', \boldsymbol{r}_2', \tau\right) = \langle\!\langle \boldsymbol{J}\left(\boldsymbol{r}_1', t'\right) \boldsymbol{J}^\dagger\left(\boldsymbol{r}_2', t'-\tau\right)\rangle\!\rangle = \lim_{T\to\infty} \frac{1}{2T} \int_{-T}^{T} \boldsymbol{j}\left(\boldsymbol{r}_1', t'\right) \boldsymbol{j}^\dagger\left(\boldsymbol{r}_2', t'-\tau\right)\, \mathrm{d}t'\,, \tag{3.152}$$

where $\boldsymbol{j}$ is a realization of the random field $\boldsymbol{J}$. The mean value function $\boldsymbol{m}_\mathrm{H}$ and the correlation dyadic $\boldsymbol{\Gamma}_\mathrm{H}$ of the observed Gaussian random field $\boldsymbol{H}$ are similarly given in terms of the realization $\boldsymbol{h}$ by

$$\boldsymbol{m}_\mathrm{H}\left(\boldsymbol{r}\right) = \langle\!\langle \boldsymbol{H}\left(\boldsymbol{r}, t\right)\rangle\!\rangle = \lim_{T\to\infty} \frac{1}{2T} \int_{-T}^{T} \boldsymbol{h}\left(\boldsymbol{r}, t\right)\, \mathrm{d}t\,, \tag{3.153}$$

$$\boldsymbol{\Gamma}_\mathrm{H}\left(\boldsymbol{r}_1, \boldsymbol{r}_2, \tau\right) = \langle\!\langle \boldsymbol{H}\left(\boldsymbol{r}_1, t\right) \boldsymbol{H}^\dagger\left(\boldsymbol{r}_2, t-\tau\right)\rangle\!\rangle = \lim_{T\to\infty} \frac{1}{2T} \int_{-T}^{T} \boldsymbol{h}\left(\boldsymbol{r}_1, t\right) \boldsymbol{h}^\dagger\left(\boldsymbol{r}_2, t-\tau\right)\, \mathrm{d}t\,. \tag{3.154}$$

By expressing the resulting observed random field $\boldsymbol{H}$ in terms of an integral over a dyadic Green's function, as in (3.57), one obtains for the mean value $\boldsymbol{m}_\mathrm{H}$

$$\begin{aligned}
\boldsymbol{m}_\mathrm{H}\left(\boldsymbol{r}\right) &= \lim_{T\to\infty} \frac{1}{2T} \int_{-T}^{T} \iiint_{V'} \int_{-\infty}^{\infty} \boldsymbol{G}_\mathrm{HJ}\left(\boldsymbol{r}-\boldsymbol{r}', t-t'\right) \boldsymbol{j}\left(\boldsymbol{r}', t'\right)\, \mathrm{d}t'\, \mathrm{d}^3 r'\, \mathrm{d}t \\
&= \iiint_{V'} \int_{-\infty}^{\infty} \boldsymbol{G}_\mathrm{HJ}\left(\boldsymbol{r}-\boldsymbol{r}', t-t'\right) \langle\!\langle \boldsymbol{J}\left(\boldsymbol{r}', t'\right)\rangle\!\rangle\, \mathrm{d}t'\, \mathrm{d}^3 r' \\
&= \iiint_{V'} \int_{-\infty}^{\infty} \boldsymbol{G}_\mathrm{HJ}\left(\boldsymbol{r}-\boldsymbol{r}', t-t'\right) \boldsymbol{m}_\mathrm{J}\left(\boldsymbol{r}'\right)\, \mathrm{d}t'\, \mathrm{d}^3 r'\,.
\end{aligned} \tag{3.155}$$

For the correlation dyadic of the observed field $\boldsymbol{\Gamma}_{\mathrm{H}}$, we have accordingly [108]

$$\begin{aligned}
\boldsymbol{\Gamma}_{\mathrm{H}}\left(\boldsymbol{r}_1,\boldsymbol{r}_2,\tau\right) &= \lim_{T\to\infty}\frac{1}{2T}\int_{-T}^{T}\iiint_{V'}\int_{-\infty}^{\infty}\iiint_{V'}\int_{-\infty}^{\infty}\boldsymbol{G}_{\mathrm{HJ}}\left(\boldsymbol{r}_1-\boldsymbol{r}_1',t-t'\right)\boldsymbol{j}\left(\boldsymbol{r}_1',t'\right)\boldsymbol{j}^{\dagger}\left(\boldsymbol{r}_2',\tau'-\tau\right)\times\\
&\quad\times\boldsymbol{G}_{\mathrm{HJ}}^{\dagger}\left(\boldsymbol{r}_2-\boldsymbol{r}_2',t-\tau'\right)\,\mathrm{d}\tau'\,\mathrm{d}^3r_2'\,\mathrm{d}t'\,\mathrm{d}^3r_1'\,\mathrm{d}t\\
&= \iiint_{V'}\int_{-\infty}^{\infty}\iiint_{V'}\int_{-\infty}^{\infty}\boldsymbol{G}_{\mathrm{HJ}}\left(\boldsymbol{r}_1-\boldsymbol{r}_1',t-t'\right)\left\langle\!\left\langle\boldsymbol{J}\left(\boldsymbol{r}_1',t'\right)\boldsymbol{J}^{\dagger}\left(\boldsymbol{r}_2',\tau'-\tau\right)\right\rangle\!\right\rangle\times\\
&\quad\times\boldsymbol{G}_{\mathrm{HJ}}^{\dagger}\left(\boldsymbol{r}_2-\boldsymbol{r}_2',t-\tau'\right)\,\mathrm{d}\tau'\,\mathrm{d}^3r_2'\,\mathrm{d}t'\,\mathrm{d}^3r_1'\\
&= \iiint_{V'}\int_{-\infty}^{\infty}\iiint_{V'}\int_{-\infty}^{\infty}\boldsymbol{G}_{\mathrm{HJ}}\left(\boldsymbol{r}_1-\boldsymbol{r}_1',\tau''\right)\boldsymbol{\Gamma}_{\mathrm{J}}\left(\boldsymbol{r}_1',\boldsymbol{r}_2',\tau-\tau'\right)\times\\
&\quad\times\boldsymbol{G}_{\mathrm{HJ}}^{\dagger}\left(\boldsymbol{r}_2-\boldsymbol{r}_2',\tau'-\tau''\right)\,\mathrm{d}\tau'\,\mathrm{d}^3r_2'\,\mathrm{d}\tau''\,\mathrm{d}^3r_1'\,.
\end{aligned}\tag{3.156}$$

These results are similar to the results obtained for non-stationary and non-ergodic Gaussian random fields in section 3.6. Nevertheless, these results are equally important, as they have been obtained in a completely different way. This approach was also used in previous work by Russer, Haider, and Russer [7], [15], [16] for introducing propagation of stationary ergodic Gaussian random fields from samples obtained by near-field scanning. On the one hand, this is a very practical approach, as all statistical parameters needed are self-consistently obtained from known field samples. On the other hand, it is rather difficult to generalize this approach to arbitrary statistics. For stationary ergodic random fields, we can infer the statistical parameters directly from sampled data, where the ensemble averages can be replaced by time averages. Thus, the results in equations (3.155) and (3.156) give an important practical guideline on how to propagate statistical parameters of sampled Gaussian ergodic fields. Anyway, we must assume ergodicity for considering practical measurements, when there is no a-priori knowledge about the characteristic functionals of the random fields. Hence, in the practical setting, where the statistics of the sources are unknown, we must assume a statistical model, e.g. Gaussian statistics, to be able to estimate the statistical parameters from ergodic field samples. The mean value, which is constant in the temporal coordinate, as well as the correlation dyadic of the source field, can be calculated from a sufficiently long recorded sample of the random field at each point, or at each pair of points in space, respectively. Practical examples of stochastic electromagnetic field propagation are presented in chapter 5.

The correlation dyadics for the source field and for the observed field are given in terms of a $\mathbb{R}^3\times\mathbb{R}^3\times\mathbb{R}\to\mathbb{R}^3\times\mathbb{R}^3$ dyadic function. The components of the dyadic represent the correlations between the different field components. In component notation, the correlation dyadics for the source field and for the observed field are given by

$$\boldsymbol{\Gamma}_{\mathrm{J}}\left(\boldsymbol{r}_1,\boldsymbol{r}_2,\tau\right)=\begin{bmatrix}\Gamma_{\mathrm{J}\,xx}\left(\boldsymbol{r}_1,\boldsymbol{r}_2,\tau\right) & \Gamma_{\mathrm{J}\,xy}\left(\boldsymbol{r}_1,\boldsymbol{r}_2,\tau\right) & \Gamma_{\mathrm{J}\,xz}\left(\boldsymbol{r}_1,\boldsymbol{r}_2,\tau\right)\\ \Gamma_{\mathrm{J}\,yx}\left(\boldsymbol{r}_1,\boldsymbol{r}_2,\tau\right) & \Gamma_{\mathrm{J}\,yy}\left(\boldsymbol{r}_1,\boldsymbol{r}_2,\tau\right) & \Gamma_{\mathrm{J}\,yz}\left(\boldsymbol{r}_1,\boldsymbol{r}_2,\tau\right)\\ \Gamma_{\mathrm{J}\,zx}\left(\boldsymbol{r}_1,\boldsymbol{r}_2,\tau\right) & \Gamma_{\mathrm{J}\,zy}\left(\boldsymbol{r}_1,\boldsymbol{r}_2,\tau\right) & \Gamma_{\mathrm{J}\,zz}\left(\boldsymbol{r}_1,\boldsymbol{r}_2,\tau\right)\end{bmatrix},\tag{3.157}$$

and

$$\boldsymbol{\Gamma}_{\mathrm{H}}\left(\boldsymbol{r}_1,\boldsymbol{r}_2,\tau\right)=\begin{bmatrix}\Gamma_{\mathrm{H}\,xx}\left(\boldsymbol{r}_1,\boldsymbol{r}_2,\tau\right) & \Gamma_{\mathrm{H}\,xy}\left(\boldsymbol{r}_1,\boldsymbol{r}_2,\tau\right) & \Gamma_{\mathrm{H}\,xz}\left(\boldsymbol{r}_1,\boldsymbol{r}_2,\tau\right)\\ \Gamma_{\mathrm{H}\,yx}\left(\boldsymbol{r}_1,\boldsymbol{r}_2,\tau\right) & \Gamma_{\mathrm{H}\,yy}\left(\boldsymbol{r}_1,\boldsymbol{r}_2,\tau\right) & \Gamma_{\mathrm{H}\,yz}\left(\boldsymbol{r}_1,\boldsymbol{r}_2,\tau\right)\\ \Gamma_{\mathrm{H}\,zx}\left(\boldsymbol{r}_1,\boldsymbol{r}_2,\tau\right) & \Gamma_{\mathrm{H}\,zy}\left(\boldsymbol{r}_1,\boldsymbol{r}_2,\tau\right) & \Gamma_{\mathrm{H}\,zz}\left(\boldsymbol{r}_1,\boldsymbol{r}_2,\tau\right)\end{bmatrix},\tag{3.158}$$

respectively.

4 Characterization of Stochastic Electromagnetic Fields

4.1 Near-Field Scanning

In chapter 3, the theoretical framework for describing stochastic electromagnetic fields in space and time has been introduced. If the characteristic functional, i.e. the measure on the probability space associated with the random field is known, we have shown a way how to propagate this statistical information through space and time, using Maxwell's equations. The last section 3.7 of the previous chapter introduced the concept of ergodicity, which is essential for an experimental characterization of stochastic electromagnetic fields. In real-world applications, however, there is generally no a-priori knowledge of the characteristic functional, i.e. the probability model of the emitted random field. The stochastic model needs to be chosen according to the observed fields. In general, one can argue by the central limit theorem (see Theorem 2.1), that there should be a Gaussian probability distribution of the source field, close to a device under test, as long as the total number of actual independent sources is large enough, where the total source field is given by a superposition of the individual independent fields. The statistical parameters, in the Gaussian case the mean value and the correlation dyadic, need to be determined from recorded ergodic field samples, in order to give a complete description of the random electromagnetic field.

By the uniqueness theorem (Theorem 3.1), and by the equivalence principle (see section 3.5), the fields in a source-free region $V \subset \mathbb{R}^3$ are uniquely determined, if the tangential field components at the boundary ∂V are known. These tangential field components can then be converted to equivalent Huygens sources, according to equations (3.128) and (3.129). Similar to actual source distributions, the equivalent sources may be propagated either analytically or numerically, in order to determine the probability measure of the random field in the source-free region V. It is, therefore, possible to completely characterize the probability distributions of the random field in V, as long as the characteristic functional, or a parametric description of the characteristic functional of the tangential electromagnetic field components at the boundary ∂V is known. With the assumption that the underlying statistics are stationary and ergodic, a parametric description of the probability distribution can be given by measuring the tangential electromagnetic field components at the boundary surface ∂V and computing the mean value and correlation dyadic from the ergodic field samples according to section 3.7. As for stationary signals, the mean value of the source field is a constant in time, we will focus on the second-order moments, i.e. the correlation dyadics for giving a complete characterization of the stochastic electromagnetic field in V.

The tangential field components of the electromagnetic field at the boundary surface ∂V, radiated from a device under test can be obtained by near-field scanning. Near-field scanning is a well-established technique for antenna measurements [109], [110] and for assessing the field radiated by electronic components in terms of electromagnetic interference (EMI) and electromagnetic compatibility (EMC) [111]. While in the antenna measurement scenario one is primarily interested in the resulting far-field pattern, which can be determined from near-field scanning of the antenna aperture, where the antenna under test is excited with a known deterministic source signal, the main interest in terms of EMI/EMC related scenarios is to identify spatially resolved hot-spots of noisy electromagnetic emissions. For the measurement of electromagnetic emissions in the frequency range of $0.1\,\mathrm{MHz}$ to $6\,\mathrm{GHz}$, there is an international IEC standard [111], describing the measurement procedure by the so-called surface scan method. The standard proposes an automated software-controlled probe positioning system with an accuracy that is greater than the minimum step size of the desired measurement grid, while the measurement grid size, the grid spacing, and the probe height are not further specified and depend on the actual application. Furthermore, the standard specifies near-field probes and calibration strategies for measuring electric, magnetic or combined electromagnetic near-field components. For recording the probe signals, frequency-domain measurement equipment, e.g. a spectrum analyzer, an EMI receiver, or a vector

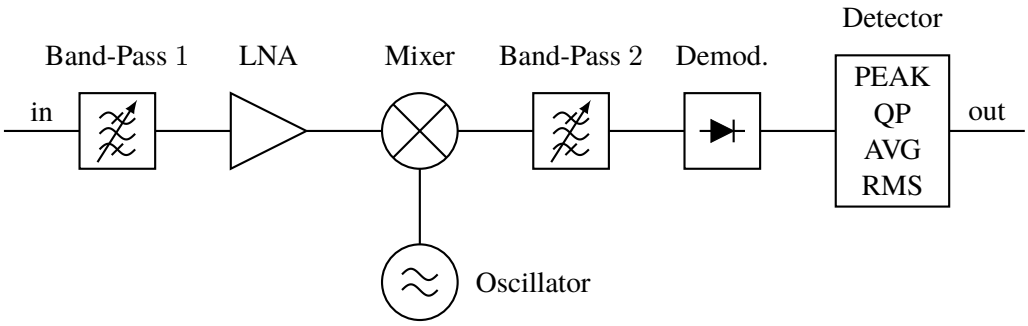

Figure 4.1 Block Diagram of an EMI Receiver.

network analyzer, with a resolution bandwidth of $9\,\mathrm{kHz}$ or $10\,\mathrm{kHz}$ and a video bandwidth of at least three times the resolution bandwidth, is proposed. The RF measurement instrument should be configured to use a peak detector. The dwell time for each measurement point should be long enough to cover at least six iterations of the main code loop of the test firmware programmed to the device under test. In the standard [111] it is also mentioned that the amount of data recorded for a complete scan may be extensive, while the overall measurement time depends on the number of frequencies, the number of scan locations and the capability of the data collection system.

It is pretty obvious that the setting of the standard [111] does not fit the scenario of propagating the statistical parameters obtained from recorded samples of the tangential field components of the electromagnetic field on a boundary surface ∂V into the volume V. Indeed, the standard focuses on creating color-enhanced heat-maps of electromagnetic emissions, and thus disregards phase information, which is inevitable for field propagation. Though it is suggested that one can also obtain phase information by putting a second reference probe for phase synchronous measurements, the main focus of the standard is clearly the identification of EMI sources, rather than a prediction of the field distribution away from the scan plane. Additionally, the peak detector, which neglects the average behavior in favor of the maximum values measured, cannot be used for obtaining accurate time averages. Hence, we propose some amendments to the standard, which are outlined in the following.

4.1.1 Time-Domain Measurements

Since noise is inherently broadband, a characterization over a wide frequency range is desirable. For frequency-domain measurements, this means that the overall dwell time at each scanning location will be multiplied by the number of frequency bands considered. Therefore, ultra-broadband measurements probably won't be feasible using standard frequency-domain measurement devices. Compared to the measurement procedure outlined in [109] or [111] using frequency-domain measurement equipment, time-domain measurements [112]–[115] can effectively reduce the overall measurement time by a reported factor of 8000 [107], [116], [117]. Traditionally, broadband measurements were carried out using superheterodyne receivers in the context of characterizing EMI. The operation principle of an EMI receiver will be outlined in the following. A variable local oscillator within the EMI receiver provides a known reference frequency. The measurement signal, as well as the reference signal, generated by the local oscillator, are mixed and thus transferred to a lower fixed intermediate frequency. The mixing of signals with two different frequencies, which generates a bunch of new signals, e.g. one with the difference and one with the sum of the two input frequencies is referred to as the superheterodyne principle. A block diagram depicting the working principle of a superheterodyne EMI receiver is given in Figure 4.1. The signal picked up by the measurement probe is fed into the input of the EMI receiver and is then filtered by the first tuneable band-pass filter *Band-Pass 1*. This RF preselection band-pass filter at the input limits the input signal to a frequency range around the desired measurement frequency. The signal may be amplified by a low noise amplifier (LNA), in order to have a signal amplitude which is higher than the mixer's noise level. In the next stage, a local oscillator reference frequency signal is mixed with the band-pass filtered input signal, generating signals at the sum of input and reference frequency, and at the difference of the input and reference frequencies, through the non-linearity of the mixer. The mixer may also produce signals at higher-order harmonics. The second band-pass filter *Band-Pass 2* then removes all frequency components but

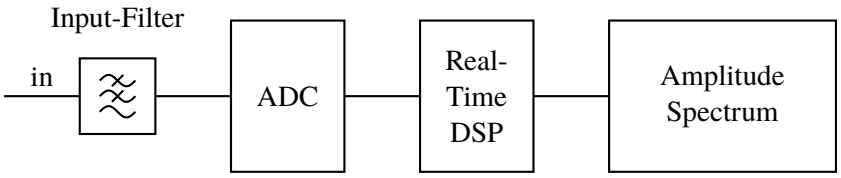

Figure 4.2 Block Diagram of a Time-Domain Measurement System.

the desired intermediate frequency. This filter also determines the bandwidth of the signal recorded by the EMI receiver. In the demodulator, the signal is rectified and further processed in terms of a selected detector mode. The output may be attached to the input of a digital data collection system. As for each frequency, the dwell time can be several seconds depending on the characteristics of the device under test, a broadband measurement run can consume an extensive amount of time.

The enormous time-saving potential of time-domain measurement solutions as reported in [107], [116], [117], along with other benefits, suggests that a time-domain measurement strategy is more promising for characterizing statistical parameters of inherently broadband noisy electromagnetic fields [107], [118], [119]. Figure 4.2 shows a block diagram highlighting the operation principle of a time-domain measurement system, that can be used for characterizing stochastic electromagnetic fields. The probe signal is fed into a low-pass filter (*Input-Filter*) that limits the input bandwidth of the probe signal in order to suppress aliasing effects in the subsequent analog to digital converter block (*ADC*). The ADC samples the signal at a given sampling rate $F_\mathrm{S} = \frac{1}{T_\mathrm{S}}$ and quantizes the sampled signal to a digital output with a certain resolution. The digital signal is further processed by a real-time digital signal processor, *Real-Time DSP*, which computes the fast Fourier transform (FFT) from the digital samples for providing information on, e.g. the amplitude spectrum of the original probe signal. It is also possible to directly store the sampled digital signals, where any possible signal processing can be done at a later time, which is a great advantage over frequency-domain measurements. For the overall dwell time, it is also sufficient to consider only a few main loop cycles of the test firmware programmed to the device under test, in order to have enough ergodic data samples for appropriate time averaging. The sampling process of a time-continuous signal s can be described by a multiplication of the signal s with a periodic sampling series [107],

$$\mathrm{III}_\mathrm{S}(t) = \sum_{n=-\infty}^{\infty} \delta(t - nT_\mathrm{S}) = \frac{1}{T_\mathrm{S}} \sum_{k=-\infty}^{\infty} \mathrm{e}^{\mathrm{i}2\pi k \frac{t}{T_\mathrm{S}}} \,. \tag{4.1}$$

The last equality holds since III_S is periodic with period T_S and can thus be expanded into a Fourier series with constant coefficients $c_k = \frac{1}{T_\mathrm{S}}, \forall k \in \mathbb{Z}$. The Fourier transform of the sampling series III_S is given by

$$\underline{\mathrm{III}}_\mathrm{S}(f) = \frac{1}{T_\mathrm{S}} \int_{-\infty}^{\infty} \sum_{k=-\infty}^{\infty} \mathrm{e}^{\mathrm{i}2\pi k \frac{t}{T_\mathrm{S}}} \mathrm{e}^{-\mathrm{i}2\pi f t} \,\mathrm{d}t = \frac{1}{T_\mathrm{S}} \sum_{k=-\infty}^{\infty} \int_{-\infty}^{\infty} \mathrm{e}^{-\mathrm{i}2\pi \left(f - \frac{k}{T_\mathrm{S}}\right) t} \,\mathrm{d}t = \frac{1}{T_\mathrm{S}} \sum_{k=-\infty}^{\infty} \delta\left(f - \frac{k}{T_\mathrm{S}}\right) . \tag{4.2}$$

The sampled time-domain signal $s(n\Delta T_\mathrm{S})$ at integer multiples of the sampling period T_S is given by

$$s'(t) = s(t) \cdot \mathrm{III}_\mathrm{S}(t) \,. \tag{4.3}$$

The Fourier transform of the sampled signal is given by the convolution of the individual spectra of the time-domain signal $\underline{s}$ and of the sampling series $\underline{\mathrm{III}}_\mathrm{S}$. Using (4.2), it is clear that the spectrum $\underline{s}'$ of the periodically sampled time-domain signal s' is a continuous function of the signal frequency f, and is equal to

$$\underline{s}'(f) = \sum_{n=-\infty}^{\infty} \int_{-\infty}^{\infty} \underline{s}(f - f') \, \delta\left(f' - \frac{k}{T_\mathrm{S}}\right) \mathrm{d}f' = \sum_{n=-\infty}^{\infty} \underline{s}\left(f - \frac{k}{T_\mathrm{S}}\right) . \tag{4.4}$$

Therefore, ideal time-sampling corresponds to infinitely reproducing the spectrum of the original, time-continuous signal at multiples of the sampling frequency $F_\mathrm{S} = \frac{1}{T_\mathrm{S}}$.

This correspondence provides us with a criterion on how to choose the sampling rate and how to design the input filter in Figure 4.2, according to the desired frequency range of the input signal that is to be characterized by time-domain sampling. This criterion is given by the following theorem [120], [121].

Theorem 4.1 (Nyquist–Shannon Sampling Theorem)**.** *Let $s \in L^1$ be a band-limited signal with band-limit B, i.e. the spectrum $\underline{S}(f_0) = 0$ for $f_0 > B$, where we denote the Fourier transform of s by $\underline{S}$. Then the original signal s can be perfectly reconstructed from the discrete values $s(kT_\mathrm{S})$ for $k \in \mathbb{Z}$, if*

$$\frac{1}{T_\mathrm{S}} > 2B\,.$$

Proof. The band-limited signal s can be represented by the inverse Fourier transform

$$s(t) = \int_{-\infty}^{\infty} \underline{S}(f)\,\mathrm{e}^{\mathrm{i}2\pi ft}\,\mathrm{d}f = \int_{-B}^{B} \underline{S}(f)\,\mathrm{e}^{\mathrm{i}2\pi ft}\,\mathrm{d}f\,.$$

The last step holds, since the signal is band-limited with band-limit B by assumption, i.e. the spectrum $\underline{S}$ vanishes outside the interval $f \in [-B, B]$. We define the periodic continuation $\tilde{\underline{S}}$ of the signal spectrum by $\tilde{\underline{S}}(f) = \tilde{\underline{S}}(f + B)$ and $\tilde{\underline{S}}(f) = \underline{S}(f)$ for $|f| \leq B$. The periodic continuation $\tilde{\underline{s}}$ can be represented as a Fourier series by

$$\tilde{\underline{S}}(f) = \sum_{k=-\infty}^{\infty} c_k \exp\left(\frac{\mathrm{i}2\pi kf}{2B}\right),$$

where the coefficients c_k are given by

$$c_k = \frac{1}{2B}\int_{-B}^{B} \tilde{\underline{S}}(f) \exp\left(-\frac{\mathrm{i}2\pi kf}{2B}\right)\mathrm{d}f = \frac{1}{2B}s\left(-\frac{k}{2B}\right).$$

The last step has been interpreted as an inverse Fourier transform with respect to $-f$. Since the integral is evaluated over the interval $[-B, B]$, the resulting signal is given by the original signal s, evaluated at single points $\frac{k}{2B}$. Hence, the periodic continuation spectrum $\tilde{\underline{S}}(f)$ can be represented by

$$\tilde{\underline{S}}(f) = \sum_{k=-\infty}^{\infty} \frac{1}{2B}s\left(-\frac{k}{2B}\right)\exp\left(\frac{\mathrm{i}2\pi kf}{2B}\right).$$

The original signal $s(t)$ can now be obtained by an inverse Fourier transform, restricted to the interval $[-B, B]$. This already proves the theorem, since an absolutely integrable function is completely characterized by its Fourier transform. Nevertheless, one can further derive a closed method for obtaining the original band-limited time-continuous signal s from only a discrete set of signal samples. The inverse Fourier transform of $\tilde{\underline{S}}$ is given by

$$s(t) = \int_{-B}^{B}\left(\sum_{k=-\infty}^{\infty} \frac{1}{2B}s\left(-\frac{k}{2B}\right)\exp\left(\frac{\mathrm{i}2\pi kf}{2B}\right)\right)\mathrm{e}^{\mathrm{i}2\pi ft}\,\mathrm{d}f\,.$$

After some rearrangement, we obtain

$$\begin{aligned} s(t) &= \frac{1}{2B}\sum_{k=-\infty}^{\infty} s\left(-\frac{k}{2B}\right)\int_{-B}^{B}\mathrm{e}^{\mathrm{i}2\pi f\left(\frac{k}{2B}+t\right)}\,\mathrm{d}f \\ &= \frac{1}{2B}\sum_{k=-\infty}^{\infty} s\left(-\frac{k}{2B}\right)\frac{\mathrm{e}^{\mathrm{i}2\pi B\left(\frac{k}{2B}+t\right)} - \mathrm{e}^{-\mathrm{i}2\pi B\left(\frac{k}{2B}+t\right)}}{\mathrm{i}2\pi\left(\frac{k}{2B}+t\right)} \\ &= \sum_{k=-\infty}^{\infty} s\left(\frac{k}{2B}\right)\frac{\sin\left(\pi\left(2Bt-k\right)\right)}{\pi\left(2Bt-k\right)}\,. \end{aligned}$$

The last statement is a discrete convolution of the discrete samples $s\left(\frac{k}{2B}\right)$ with the so-called sinc-kernel, which reproduces the original signal. □

The input filter in Figure 4.2 needs to limit the measured signal to a maximum frequency of $\frac{F_S}{2}$ as otherwise there will be aliasing effects, i.e. artifacts that occur due to spectral overlaps of the frequency-shifted spectral components, according to (4.4).

4.1.2 Measurement Setup

Characterizing stochastic electromagnetic fields slightly differs from both cases introduced above, from the near-field antenna scanning case, where one is primarily interested in the far-field radiation pattern, and also from the near-field EMI characterization case, where the focus is on the identification of radiation hot-spots. However, one can use existing literature [109], [110], [122] and existing standards [111] as a starting point and as a guideline for developing a near-field scanning system for characterizing stochastic electromagnetic fields [118].

In contrast to EMI hot-spot identification, phase information is relevant in order to be able to propagate the statistical parameters measured at the scan-plane ∂V into the source-free volume V above ∂V. In addition, as already mentioned, one cannot simply specify phase values and amplitudes for stochastic electromagnetic fields, as those quantities are random fields that follow certain distributions. Also a stationary phase reference, as suggested in [111], [123] is not sufficient for characterizing noisy electromagnetic fields. For a complete characterization of the statistics of stochastic electromagnetic radiation, one needs to obtain enough information for a parametric estimation of a pre-assigned characteristic functional of the random field at the scan plane. Reconstruction of statistical parameters is only possible for stationary, ergodic random fields, as discussed in section 3.7. Nevertheless, if a full statistical characterization is not necessary, statements regarding the spatial energy distribution of random fields, given in terms of spatial auto-correlation functions can be made for the broader class of wide-sense stationary random fields (see Definition 2.29). For Gaussian random fields, wide-sense stationarity implies stationarity in the strict sense, and thus, a complete statistical characterization of the probability distribution of the field is possible by characterizing first and second order moments. For obtaining second order moments, i.e. spatial correlation functions, one needs to synchronously obtain field samples at each pair of points on the scan plane, and subsequently calculate auto- and cross-correlation functions.

For obtaining field samples simultaneously at each pair of points on the scan plane, an automated two-probe near-field scanning system has been proposed in [124], [125]. In such a system, near-field probes are automatically positioned on a predefined measurement grid and the probe signal is sampled time-synchronized, using a multi-channel digital time-domain oscilloscope. Now suppose we have a predefined measurement grid of N spatial sampling points. The number of multi-channel measurements, required for calculating spatial correlation functions is given by the number of possible point pairs of the measurement grid. Since correlation functions of pairs (m, n) can be obtained from the same data as correlation functions for points (n, m), the total number of point pairs to be measured is given by

$$N_{\text{pairs}} = \frac{N\,(N-1)}{2}\,. \tag{4.5}$$

For a complete characterization, one needs to take into account cross-correlation functions between all possible field orientations, i.e. xx, xy, yx, and yy. Thus, four measurements need to be taken for each spatial point pair, in order to be able to compute all components of the spatial correlation matrix. Thus, the total number of measurements scales with $\mathcal{O}\left(N^2\right)$, which yields extensive measurement times and data storage requirements. A possible strategy for data reduction of sampled stochastic electromagnetic fields will be discussed in chapter 7.

The two-probe scanning system, as proposed in [118], [124], [125] is schematically depicted in Figure 4.3. Thereby, two magnetic near-field loop probes, *Field Probe 1* and *Field Probe 2* are precisely positioned according to a software-defined measurement grid by the positioning elements *Positioning Element 1* and *Positioning Element 2*. As suggested in [111], the accuracy of the spatial positioning must be larger than the desired spatial resolution, which needs to be chosen according to the *Device under Test*. Depending on the number of channels, that can be measured synchronously, one might need a *Switch*, in order to be able to record field samples simultaneously for all vectorial field components. The probe signals are low-pass filtered by *Channel Filter 1* and *Channel Filter 2* for avoiding aliasing effects and are then digitized by the *ADCs*.

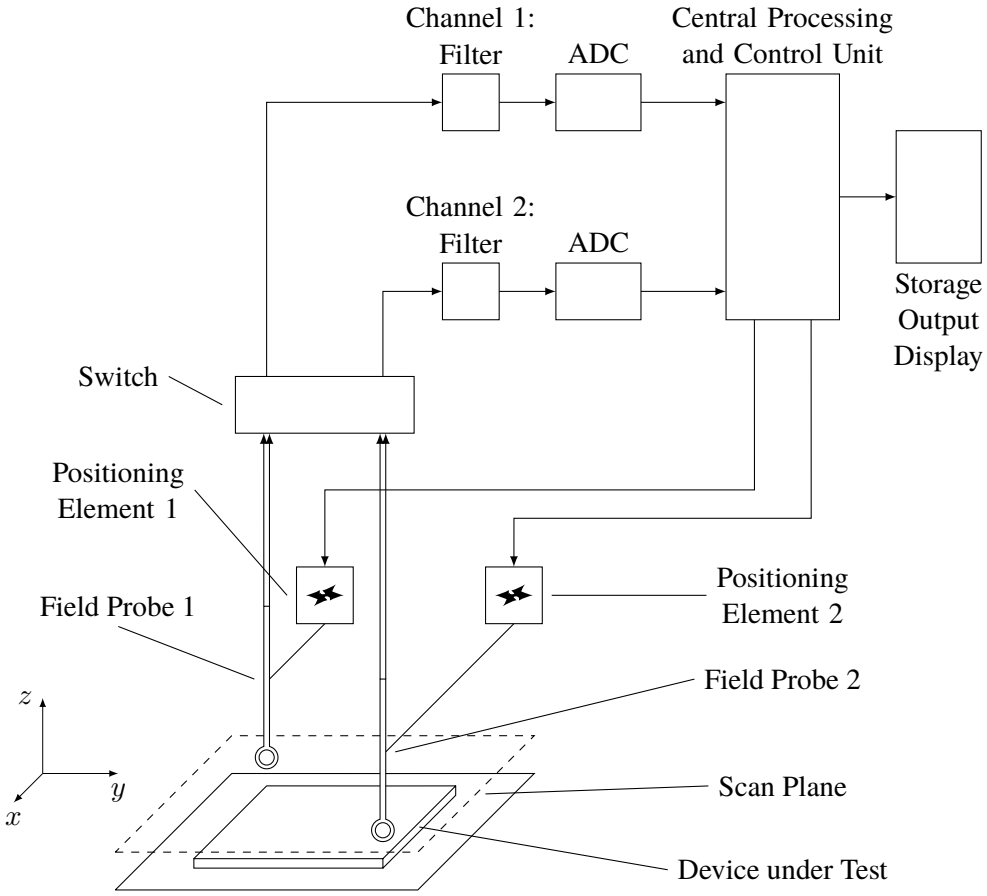

Figure 4.3 Near-field scanning Measurement System (adopted from [124]).

The whole measurement process is controlled by the *Central Processing and Control Unit*. The recorded field samples can either be processed directly after sampling, or one can choose to store the raw data for later post-processing.

For experimentally characterizing stochastic electromagnetic fields, such a near-field scanning solution has been implemented. Figure 4.4 depicts the realization of an automated two probe measurement system. The scanner is mainly composed of plastic in order to not interfere with the radiated electromagnetic fields. The system uses four stepper motors coupled to trapezoidal threads for two independent probe holders in x- and y-direction, respectively. The steppers are controlled using commercially available iSMT stepper drivers from ELV. A stepper control software has been implemented in MATLAB for positioning the probes on a predefined measurement grid. Having two probes moving independently poses the risk of collision between moving parts in the scanning system. This can be avoided, by designing the control system in such a way, that the software is aware of a possible collision for given probe paths and can take the required countermeasures. A collision detection system can be based on detecting overlaps between oriented bounding boxes around the probe geometry [126]. Fast intersection methods, based on the separating axis theorem have been proposed in [127].

4.2 Probe Characterization

For the measurement procedure described so far, ultra-wideband magnetic field probes for scanning the tangential magnetic field in a plane above the device under test have been proposed. To eliminate the influence of the probes and other parts of the measurement setup, the measurement results have to be de-embedded [128], [129]. Based on the measurement results of the probes on a standardized test structure [111], the transfer function of a probe can be determined. The inverse transfer function of the probe can be used to transform the measured signal, such that the measurement error due to the effects of the probes can be eliminated. Typically, microwave measurement

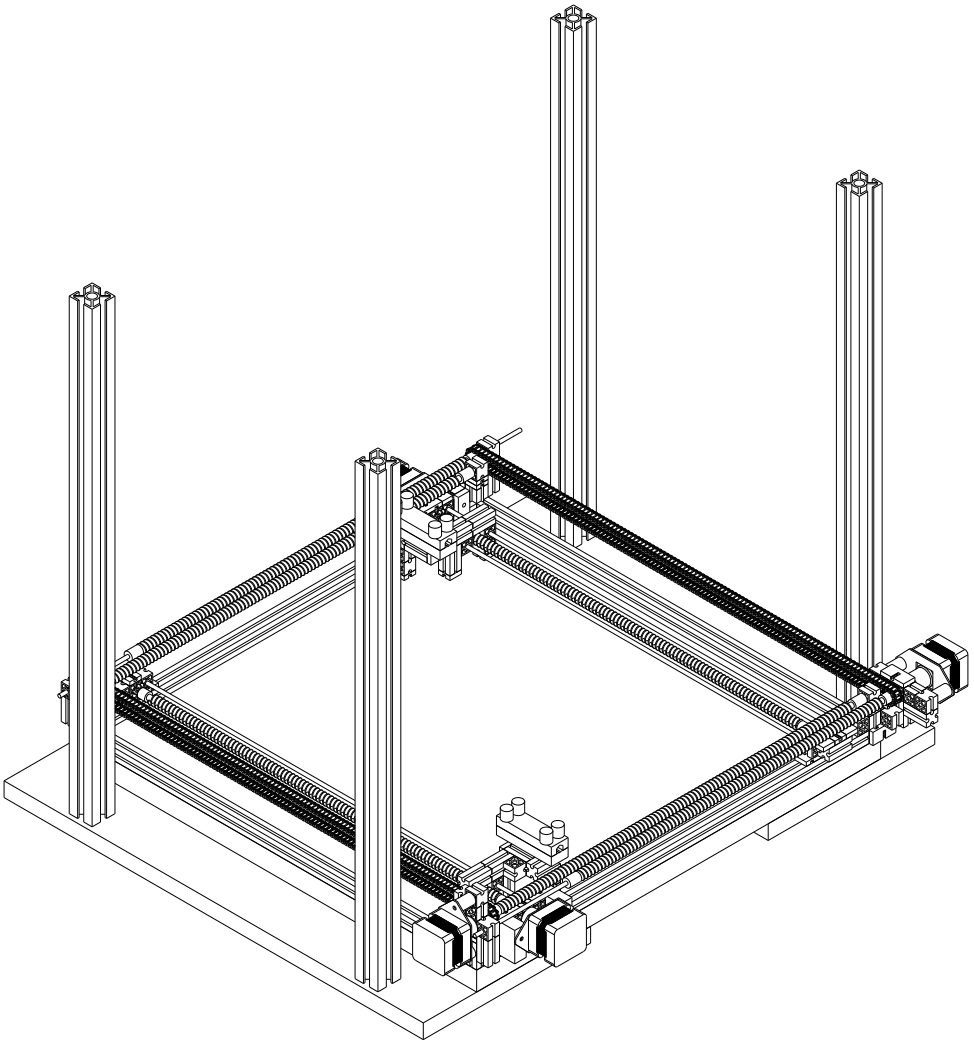

Figure 4.4 3D model of in-house built two probe near-field scanning Measurement System.

setups are described in terms of S-parameters, hence, it is advantageous to formulate possible de-embedding strategies in terms of ratios of transmitted and reflected wave amplitudes in the frequency-domain [129]–[131]. Nevertheless, as we have proposed time-domain measurements for determining the statistical parameters of random electromagnetic fields, also the time-domain transfer function, i.e. the impulse response of the probes is important for us in order to perform a deconvolution of the obtained measurement results.

4.2.1 Frequency-Domain Characterization

For determining the frequency-domain characteristics of a magnetic near-field probe, it is proposed in Annex C of the IEC standard 61967-3 [111] to use a measurement setup similar to the one shown in Figure 4.5. The setup consists of a two-layer PCB with a microstrip line structure with a characteristic impedance of $50\,\Omega$, which is on the one side connected to port 1 of a Keysight E5063A VNA and terminated with a matched load on the other side. Note that the standard suggests using a spectrum analyzer or receiver along with a signal generator with an output power of $0\,\mathrm{dBm}$, instead of a VNA. The output power P_{out} of the VNA at port 1 is set to $0\,\mathrm{dBm}$, to meet this condition. The measurement cables, connecting port 1 of the VNA to the PCB, and port 2 to the magnetic field probe have been calibrated out, such that we know the voltages and currents at the input ports of

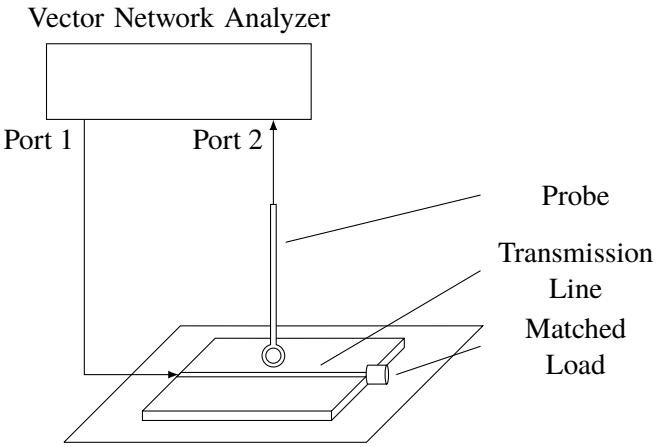

Figure 4.5 Block diagram of the frequency-domain measurement setup for obtaining probe characteristics (adopted from [129]).

both, PCB and magnetic loop probe. The voltages and currents can be obtained from the incident and reflected power waves, $\underline{a}_\nu$ and $\underline{b}_\nu$ respectively, by

$$\underline{V}_\nu = \sqrt{Z_0}\,(\underline{a}_\nu + \underline{b}_\nu)\ , \tag{4.6}$$

$$\underline{I}_\nu = \frac{1}{\sqrt{Z_0}}\,(\underline{a}_\nu - \underline{b}_\nu)\ , \tag{4.7}$$

where $\nu \in \{1, 2\}$, and with

$$\begin{bmatrix}\underline{b}_1\\ \underline{b}_2\end{bmatrix} = \begin{bmatrix}\underline{S}_{11} & \underline{S}_{12}\\ \underline{S}_{21} & \underline{S}_{22}\end{bmatrix}\begin{bmatrix}\underline{a}_1\\ \underline{a}_2\end{bmatrix}\ . \tag{4.8}$$

As the input power, and thus $|\underline{a}_1|$ is known, we can determine voltages and currents from the S-parameters, measured by the VNA. The measured magnitudes and phases obtained according to the measurement setup, as given in Figure 4.5, can be seen in Figure 4.6. From the magnitude of S_{22} in Figure 4.6a, one can see that the probe itself, connected to port 2, has almost flat frequency characteristics over the whole band from $0\,\mathrm{GHz}$ to $10\,\mathrm{GHz}$. As also shown in [129], the measured phase-characteristics in Figure 4.6b reveal a significant delay between the signals transmitted at port 1 and received at port 2 of the VNA. From the voltages and currents at port 1 and port 2 of the VNA, we can calculate the correction factor according to [132]. Figure 4.7 shows the correction factor obtained by measurement, as well as the correction factor that the manufacturer provides in the datasheet of the probes [133]. Considering the slightly different measurement setup, the results are in good agreement. Note that we use a slightly different convention for denoting the calibration factor, compared to the standards [111], [132] and compared to the datasheet of the Langer probes [133]. In the standard, the probe calibration factor is regarded as a multiplicative factor, that transforms the voltage measured at the instrument to the actual magnetic field, which induces the voltage in the loop probe. However, we use the convention, that we treat the loop probe together with the transmission line and the free-space propagation in the measurement setup described in Figure 4.5 as a linear time-invariant (LTI) system, and we regard the correction factor in Figure 4.7 as a frequency-domain impulse response, characterizing the whole system.

4.2.2 Time-Domain Characterization

For time-domain measurements, as proposed in section 4.1, it is often not sufficient to have only the magnitudes of the probe correction factors, as described in the previous section and given by Figure 4.7. For a full time-domain de-embedding procedure, we need to have the complete time-domain impulse response, describing the LTI system, formed by the magnetic near-field probes. The magnetic fields through the loop of the near-field probe, or the currents in the transmission line, respectively, can then be obtained by a de-convolution of the measurement results with the respective impulse response of the system. There are several possibilities to obtain the time-domain impulse response of the system. One could e.g. use the frequency-domain S-parameter

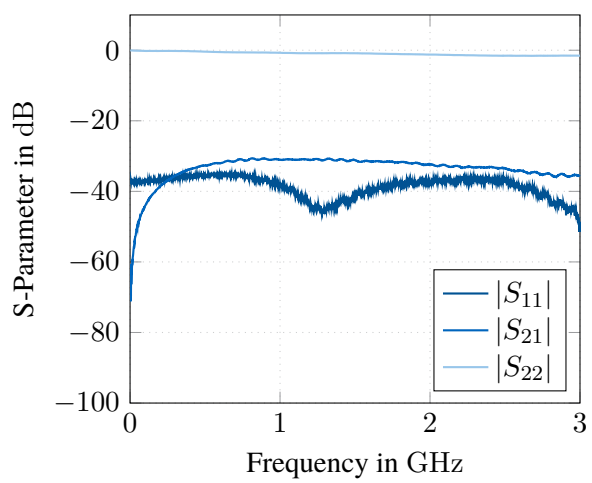

(a) Magnitude of the measured S-parameters of the measurement setup, described in Figure 4.5.

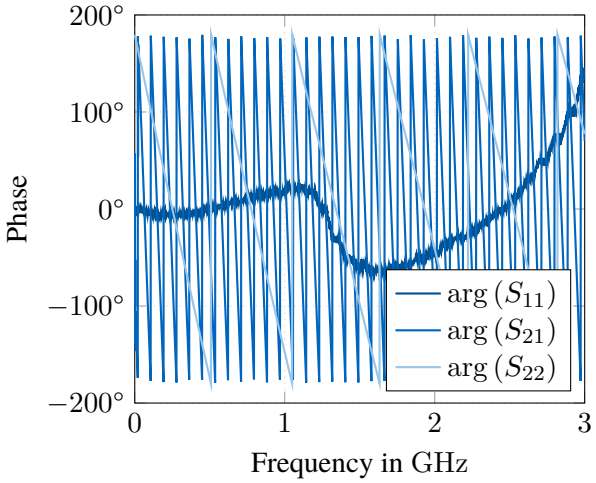

(b) Phase of the measured S-parameters of the measurement setup, described in Figure 4.5.

Figure 4.6 Magnitude and phase of the measured S-parameters of the measurement setup, described in Figure 4.5.

measurements from Figure 4.6b and perform an inverse Fourier transform in order to extract the time-domain characteristics. This approach, nevertheless, has some shortcomings as highlighted in [134]. It is clear from the transmission parameter shown in Figure 4.6 that the frequency-domain response has not sufficiently decayed at a frequency of 10 GHz, and as a consequence, there are some variations in the reconstructed time-domain impulse response. Furthermore, the inverse Fourier transformation might also violate the causality principle. Hence, for obtaining the time-domain impulse response directly, we propose a measurement setup as depicted in Figure 4.8 [129]. We use a Hewlett-Packard 8133A pulse generator that excites the transmission line. For measuring the probe signal, and also the input signal through a power divider, we use a LeCroy SDA-813-A high-speed digital oscilloscope. Furthermore, the probe signal is amplified using a Langer EMV-Technik PA 203 SMA pre-amplifier. As mentioned before, we are modeling the whole structure, including the PCB with the microstrip transmission line and the near-field probe itself as an LTI system. Now let v_{in} be the signal, fed into the transmission line by the pulse generator. The probe voltage v_{P} measured by the oscilloscope can then be described by the convolution

$$v_{\mathrm{P}}(t) = \int_{-\infty}^{\infty} h_{\mathrm{P}}(t-\tau)\, v_{\mathrm{in}}(\tau)\, \mathrm{d}\tau + \eta(t)\ , \tag{4.9}$$

where h_{P} is the impulse response of the probe, including the whole signal path between the output of the pulse generator and the input of the oscilloscope, and η is a random process with zero-mean, modeling the thermal and environmental additive noise. The input signal v_{in}, provided by the pulse generator, can be modeled as a periodic rectangular pulse, with constant amplitude A, period T and pulse width Δ. Hence, the signal is given by

$$v_{\mathrm{in}}(t) = \sum_{n=-\infty}^{\infty} A \cdot \mathrm{rect}\left(\frac{t-nT}{\Delta}\right), \tag{4.10}$$

where $\mathrm{rect}(x)$ is a rectangular unit pulse, defined by

$$\mathrm{rect}(x) = \begin{cases} 1 & \text{for} \quad |x| \leq \frac{1}{2}\,, \\ 0 & \text{for} \quad |x| > \frac{1}{2}\,. \end{cases} \tag{4.11}$$

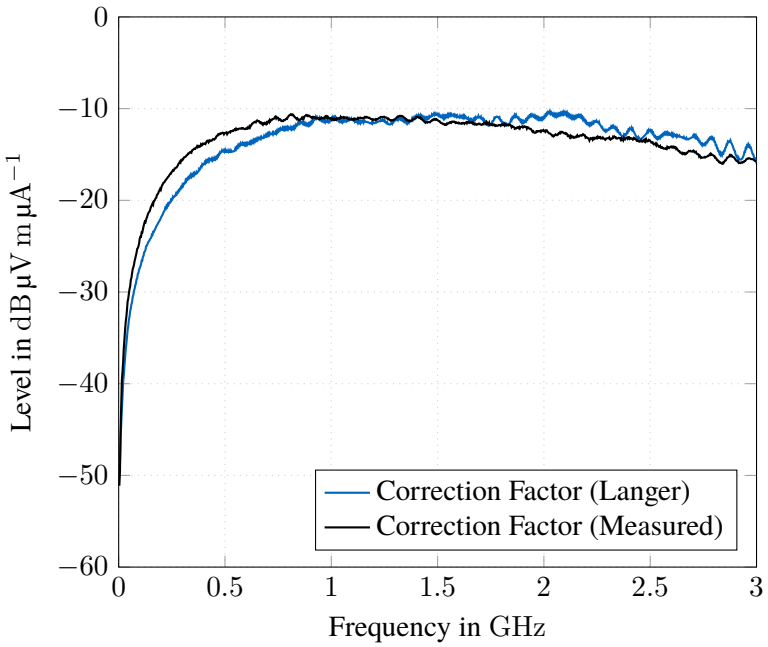

Figure 4.7 Calibration Curve for Langer EMV-Technik RF-R50-1 near-field magnetic loop probe [133].

In order to reduce the influence of the additive zero-mean noise η, which corrupts our system, we perform cyclic averaging. The synchronously registered averaged probe voltage v_{P} for a single period T is given by [129]

$$\langle\!\langle v_{\mathrm{out}}(t) \rangle\!\rangle \approx \frac{1}{M} \sum_{m=1}^{M} v_{\mathrm{out}}(t - mT) \,, \qquad \text{for } 0 \leq t < T \,, \tag{4.12}$$

where M is the number of periods with length T, recorded by the oscilloscope. The cyclic average over the duration of one period of the response to the rectangular pulse, generated by the pulse generator, is given in Figure 4.9. The pulse duration of the input pulse is equal to $\Delta = 5\,\mathrm{ns}$, the period $T = 80\,\mathrm{ns}$ and the amplitude $A = 5\,\mathrm{V}$.

From Figure 4.9, one can see that the pulse duration of the averaged response is approximately $2\,\mathrm{ns}$ which is smaller than the pulse duration of the input pulse. Hence, it can be reasonably argued that the averaged response from Figure 4.9 actually represents the step response of the system when only taking the first pulse up to $t = 5\,\mathrm{ns}$ into account. It is well known that we can extract the impulse response of the system by taking the temporal derivative of the step response [129]. This fact is denoted by the following short theorem.

Theorem 4.2. *Let H be the step response of a linear time-invariant system. The impulse response h of the system can then be obtained by*

$$h(t) = \frac{\mathrm{d}H(t)}{\mathrm{d}t} \,.$$

Proof. The step response H of a linear time-invariant system with impulse response h can be written as

$$H(t) = \int_{-\infty}^{\infty} h(\tau)\, U(t - \tau)\, \mathrm{d}\tau \,,$$

where $U(x)$ is the Heaviside unit step function. Now taking the temporal derivative on both sides yields

$$\frac{\mathrm{d}H(t)}{\mathrm{d}t} = \frac{\mathrm{d}}{\mathrm{d}t} \int_{-\infty}^{\infty} h(\tau)\, U(t - \tau)\, \mathrm{d}\tau = \int_{-\infty}^{\infty} h(\tau)\, \frac{\mathrm{d}}{\mathrm{d}t} U(t - \tau)\, \mathrm{d}\tau = \int_{-\infty}^{\infty} h(\tau)\, \delta(t - \tau)\, \mathrm{d}\tau = h(t) \,,$$

where we have used that the derivative of the Heaviside function is given by the Dirac delta function and that the Dirac delta function is an identity under the convolution. This completes the proof. □

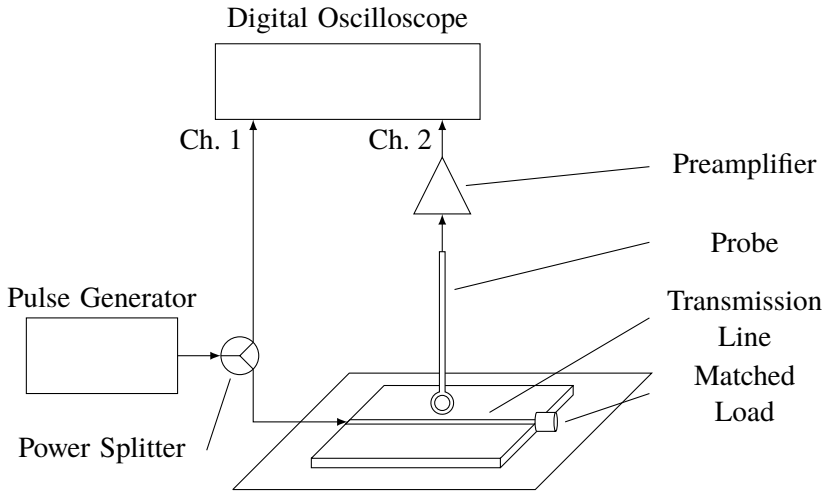

Figure 4.8 Block diagram of the time-domain measurement setup for obtaining probe characteristics (adopted from [129]).

According to Theorem 4.2, we take the numerical derivative of the step response, given in Figure 4.9 and obtain the impulse response, which is depicted in Figure 4.10. The impulse response itself is a dimensionless quantity, as it relates voltages at the input side to voltages at the output of the LTI system. In order to compare both, time-domain and frequency-domain approaches, we have calculated the Fourier transform of the impulse response. The magnitude and phase of the Fourier transformed linear time-invariant system can be seen in Figure 4.11. Comparing Figure 4.11a, to the probe correction factors obtained in the frequency-domain from the previous subsection, we can see that the agreement between the two curves is reasonably good. Additionally, we have also plotted the phase distribution over frequency in Figure 4.11b, which can also provide valuable information for the de-embedding strategy.

4.3 On the Spatial Distribution of Spectral Energy

The spatial distribution of the spectral energy density using principal components is discussed in [135][1]. We consider a setup given by a two-dimensional array consisting of $p = m' \times n'$ Hertzian dipoles of length l, oriented in x-direction. The currents $\{I_j\}_{j=1}^{p}$ in the dipoles are governed by Gaussian random processes with zero mean and are described by the correlation matrix $\boldsymbol{C}_I$ [16]. The location $\left(x'_j, y'_j\right)$ of the j-th dipole on the source-plane $z' = 0$ is

$$x'_j = x'_0 + \left\lfloor \frac{j-1}{m'} \right\rfloor \Delta x' \,, \tag{4.13}$$

$$y'_j = y'_0 + \left[(j-1) \bmod n'\right] \Delta y' \,, \tag{4.14}$$

with $j \in \{1, \ldots, p\}$. Here, $\lfloor \cdot \rfloor$ denotes the floor operation, i.e. the next smaller integer number, and a mod b is the modulo division of a and b. In order to investigate the propagation of stochastic electromagnetic fields, we define a sampling grid, consisting of $q = m \times n$ observations on a plane at a distance of $z = h$ from the source plane. The spatial location (x_j, y_j) of the j-th observation point is analogous to (4.13) and (4.14), where the location of the initial point (x_0, y_0) and the horizontal and vertical grid-spacing Δx and Δy may differ from the source-grid parameters.

After choosing a finite set of source and observation points, the method of moments (see section 5.1.1) can be applied to transfer the field problem to a network problem [136]. The mapping information obtained in form of the moment matrix also provides the information how to transform the correlation information describing

[1] The results presented in this section have been published under IEEE copyright in M. Haider, J. A. Russer, A. Baev, *et al.*, "Principal component analysis applied in modeling of stochastic electromagnetic field propagation", in *47th European Microwave Conference (EuMC)*, Oct. 2017, pp. 1–4. The content (text and figures) is reproduced with permission of IEEE.

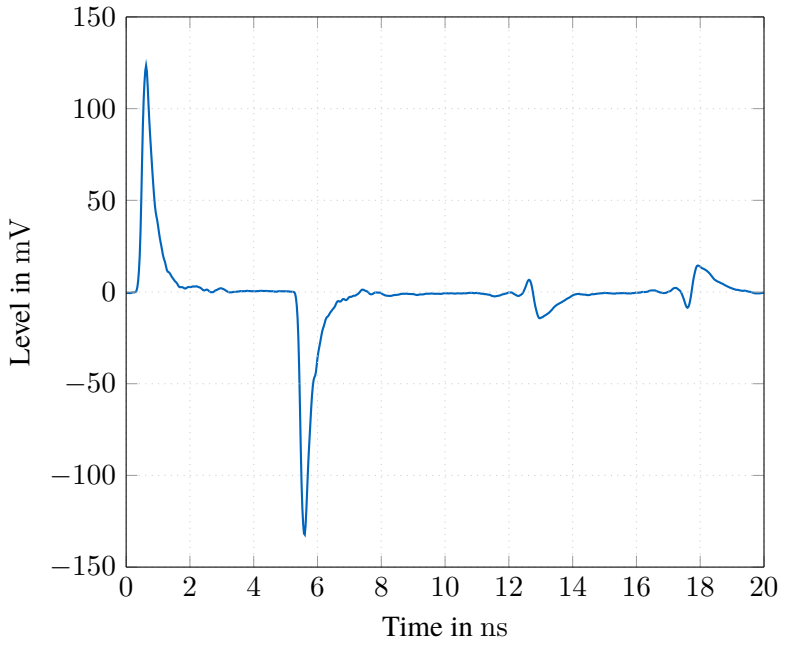

Figure 4.9 Measured step response of the Langer EMV-Technik RF-R50-1 near-field magnetic loop probe with PA 203 SMA amplifier.

stationary stochastic EM fields. For our considerations, we use the free-space dyadic Green's function, also accounting for the near-field contributions, together with point-matching [137] to obtain a generalized impedance matrix $\underline{\boldsymbol{Z}}(\omega)$ relating the vector of generalized source currents $\underline{\boldsymbol{I}}_{\mathrm{T}}(\omega)$ to a vector of generalized voltages $\underline{\boldsymbol{V}}_{\mathrm{T}}(\omega)$ on the observation plane [16]. The subscript $_{\mathrm{T}}$ denotes the time-windowed signal for which a spectrum can be defined (see section 3.6.3). The (m,n)-th element $\underline{Z}_{mn}$ of the generalized impedance matrix $\underline{\boldsymbol{Z}}(\omega)$, relating the n-th source-current to the m-th observation, is given by

$$\underline{Z}_{mn}(h,k) = \frac{lZ_0}{4\pi k}\mathrm{e}^{-\mathrm{i}k\sqrt{(x_m-x_n')^2+(y_m-y_n')^2+h^2}}\Big[g_1\left(x_m-x_n',y_m-y_n',h,k\right)\left(x_m-x_n'\right)^2 + g_2\left(x_m-x_n',y_m-y_n',h,k\right)\Big]\,, \tag{4.15}$$

where Z_0 is the free space wave impedance and $k = 2\pi f/c_0$ is the wave number, c_0 is the speed of light in vacuum. In (4.15), we use g_1 and g_2 given by

$$g_1(x,y,z,k) = -\frac{3\mathrm{i}}{\|\boldsymbol{r}\|^5} - \frac{3k}{\|\boldsymbol{r}\|^4} + \frac{\mathrm{i}k^2}{\|\boldsymbol{r}\|^3}\,, \tag{4.16}$$

$$g_2(x,y,z,k) = -\frac{\mathrm{i}k^2}{\|\boldsymbol{r}\|} + \frac{k}{\|\boldsymbol{r}\|^2} + \frac{\mathrm{i}}{\|\boldsymbol{r}\|^3}\,, \tag{4.17}$$

with $\|\boldsymbol{r}\| = \sqrt{x^2+y^2+z^2}$. In the following, let us consider uncorrelated currents at a single frequency with unit variance. Using the generalized impedance matrix $\underline{\boldsymbol{Z}}$ assembled from (4.15), we can propagate the electric field generated by the source dipole currents to observation-planes at different heights h_i. The observations are related to the sources by

$$\underline{\boldsymbol{V}}_{\mathrm{T}}^{h_i}(\omega) = \underline{\boldsymbol{Z}}(h_i,\omega/c_0)\,\underline{\boldsymbol{I}}_{\mathrm{T}}(\omega)\,. \tag{4.18}$$

The subscript $_{\mathrm{T}}$ denotes the spectrum of the time-windowed signals. Figure 4.12 shows the amplitudes of the propagated electric field at different heights h_i for a single realization of the stochastic source currents $\underline{\boldsymbol{I}}_{\mathrm{T}}$. To compute the stochastic field, an ensemble average of the propagation of different realizations of $\underline{\boldsymbol{I}}_{\mathrm{T}}$ has to be formed.

Stochastic EM fields with Gaussian probability distribution can be described by second-order statistics, as shown in chapter 3. We calculate auto- and cross-correlation spectra of fields at different heights using a method

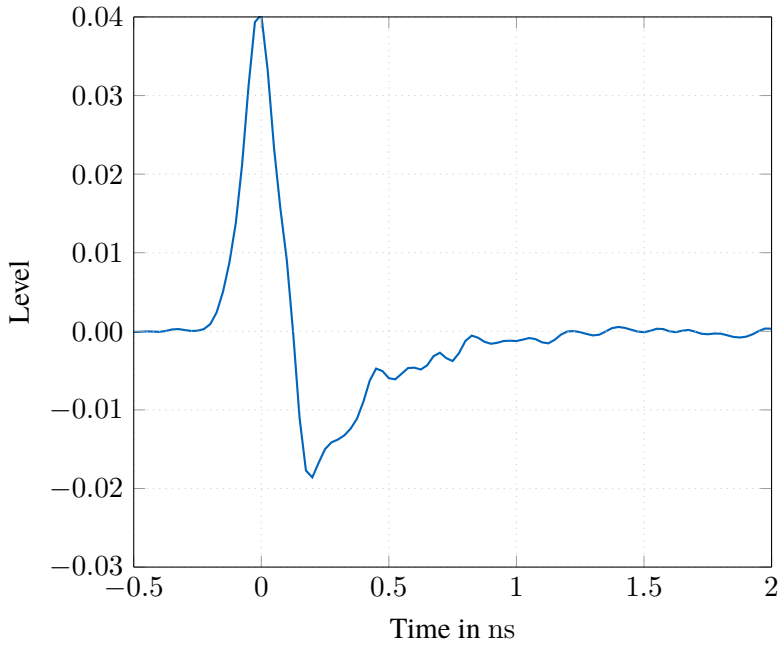

Figure 4.10 Impulse response of the Langer EMV-Technik RF-R50-1 near-field magnetic loop probe with PA 203 SMA amplifier, obtained by taking the numerical derivative of the measured step response, given in Figure 4.9.

of moments based propagation scheme for correlation matrices utilizing the deterministic impedance matrix, assembled from (4.15). Correlation matrices for generalized voltages $\underline{\boldsymbol{V}}_{\mathrm{T}}$ and generalized currents $\underline{\boldsymbol{I}}_{\mathrm{T}}$, as defined in [16], can be obtained by the ensemble averages

$$\underline{\boldsymbol{C}}_{\mathrm{I}}(\omega) = \lim_{T\to\infty} \frac{1}{2T} \left\langle\!\!\left\langle \underline{\boldsymbol{I}}_{\mathrm{T}}(\omega)\, \underline{\boldsymbol{I}}_{\mathrm{T}}^{\dagger}(\omega) \right\rangle\!\!\right\rangle , \tag{4.19}$$

$$\underline{\boldsymbol{C}}_{\mathrm{V}}(\omega) = \lim_{T\to\infty} \frac{1}{2T} \left\langle\!\!\left\langle \underline{\boldsymbol{V}}_{\mathrm{T}}(\omega)\, \underline{\boldsymbol{V}}_{\mathrm{T}}(\omega) \right\rangle\!\!\right\rangle . \tag{4.20}$$

Using (4.18), (4.19) and (4.20), we obtain a propagation rule for the correlation matrices [16], given by

$$\underline{\boldsymbol{C}}_{\mathrm{V}}^{h_i}(\omega) = \underline{\boldsymbol{Z}}(h_i, \omega/c_0)\, \underline{\boldsymbol{C}}_{\mathrm{I}}(\omega)\, \underline{\boldsymbol{Z}}^{\dagger}(h_i, \omega/c_0) \ . \tag{4.21}$$

For $\underline{\boldsymbol{C}}_{\mathrm{I}}(\omega)$ is equal to unity, which is the case for completely uncorrelated source currents $\underline{I}_m$, we get

$$\underline{\boldsymbol{C}}_{\mathrm{V}}^{h_i}(\omega) = \underline{\boldsymbol{Z}}(h_i, \omega/c_0)\, \underline{\boldsymbol{Z}}^{\dagger}(h_i, \omega/c_0) \ . \tag{4.22}$$

Using (4.15), the elements of the correlation matrix $\underline{\boldsymbol{C}}_{\mathrm{V}}^{h_i}(\omega)$ can be calculated by

$$\underline{C}_{\mathrm{V},mn}^{h_i}(\omega) = \sum_{\nu=1}^{N} \underline{Z}_{m\nu}(h_i, \omega/c_0)\, \underline{Z}_{\nu n}^{*}(h_i, \omega/c_0) \ . \tag{4.23}$$

Using a cumulative percentage of total variance criterion, as specified in [138] and later on in 7, we can evaluate the number of principal components to retain for different heights h_i and different frequencies $\omega = 2\pi f$ for the proposed setup.

4.3.1 Required Principal Components and Energy Considerations

We specify an array of source points, modeled by Hertzian dipoles oriented in x-direction, on an $m' = 8$ by $n' = 8$ grid with a grid point spacing of $\Delta x' = \Delta y' = 1\,\mathrm{cm}$. With all source dipole currents chosen to be uncorrelated, the correlation matrix describing these sources is a 64×64 matrix of full rank. Hence, we require 64 principal components to account for 100% of the variance. In the following, we investigate how the number

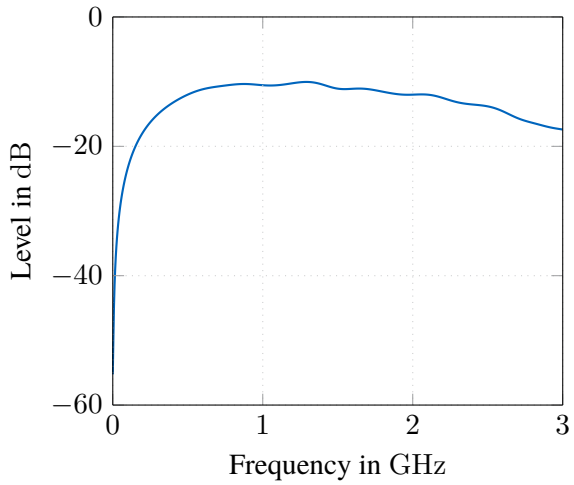

(a) Magnitude of the Fourier transformed impulse response, obtained by measurement.

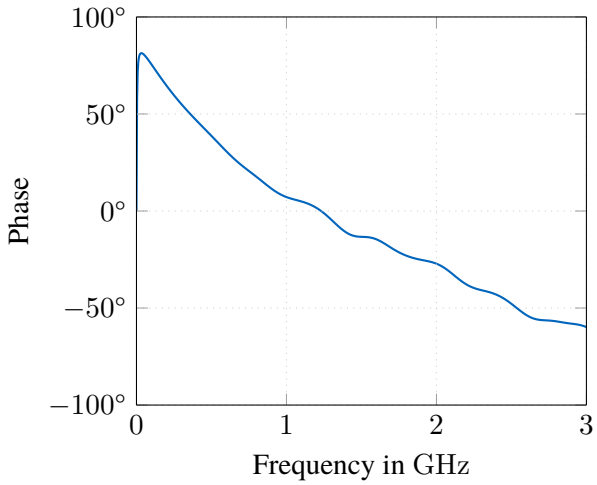

(b) Phase of the Fourier transformed impulse response, obtained by measurement.

Figure 4.11 Magnitude and phase of the Fourier transformed impulse response, obtained by measurement.

of principal components necessary to explain 99% of the total variance changes, if we consider sampling grids of the same size and spacing as the source grid, i.e. $\Delta x = \Delta y = \Delta x' = \Delta y' = 1\,\mathrm{cm}$ and $m = m' = 8$ and $n = n' = 8$, at various heights h_i above the source plane where the $\underline{E}_x$-field was sampled. Figure 4.13 shows the estimated numbers of principal components to retain in order to explain 99% of total variance for each height for source excitations at $1\,\mathrm{GHz}$ and $10\,\mathrm{GHz}$. To perform this estimate on the number of principal components, we consider the total EM field energy in each observation plane at $z = h_i$. For this estimation, we numerically propagate the field correlations of the noisy sources and use a finely resolved grid on the observation plane which considerably exceeds the $7 \times 7\,\mathrm{cm}^2$ area used for the sources at $z = h_0$, such that effectively all energy radiated into the observation plane at h_i is also sampled. The spectral energy density (SED) is closely related to the auto-correlation spectrum for each field sampling point on the observation plane. The EM field energy obtained by integrating the energy density over the $7 \times 7\,\mathrm{cm}^2$ area of interest at $z = h_i$ is compared to the total energy on the observation plane $z = h_i$. This ratio between the energy on the $7 \times 7\,\mathrm{cm}^2$ area to the total energy in the plane, gives a proper estimate for the number of principal components to retain, in order to account for 99% of total variation for each height h_i.

Figure 4.13 also shows the actual number of PCs which need to be retained in order to account for 99% of the variance, and hence also for 99% of the SED of the stochastic EM field, obtained by performing principal component analysis on the matrices $\underline{\boldsymbol{C}}_{\mathrm{V}}^{h_i}$, given by (4.22). Here, we consider sampling grids of the same size and resolution as the source grid. For terminating the algorithm after a certain percentage of total variation we use the cumulative percentage of total variance (CPTV) criterion from [138], which will be later on described in chapter 7.

4.3.2 Transverse Coherence

With increasing distance from the source plane, which can be considered an aperture, the number of principal components required to explain the variance on a sampling grid of constant size decreases, while at the same time the spatial angle observed, and hence, the number of transverse modes to be resolved, decreases as well. To estimate the number of principal components required for explaining 99.9% of the variance at sampling grids at a height $z = h_i$ and at height $z = h_0$, we give an estimate on how many transverse modes we can resolve on the given sampling point grid. The EM field is originating from an aperture A_{s}. This is a worst-case estimate, i.e. indicating how many principal components we will need at most to give an accurate description of the correlation matrix. The estimate will be good in the far-field and we assume the transverse component of the propagation vector $\boldsymbol{k}$ to be small in magnitude compared to its overall wave number k_0. The space angle

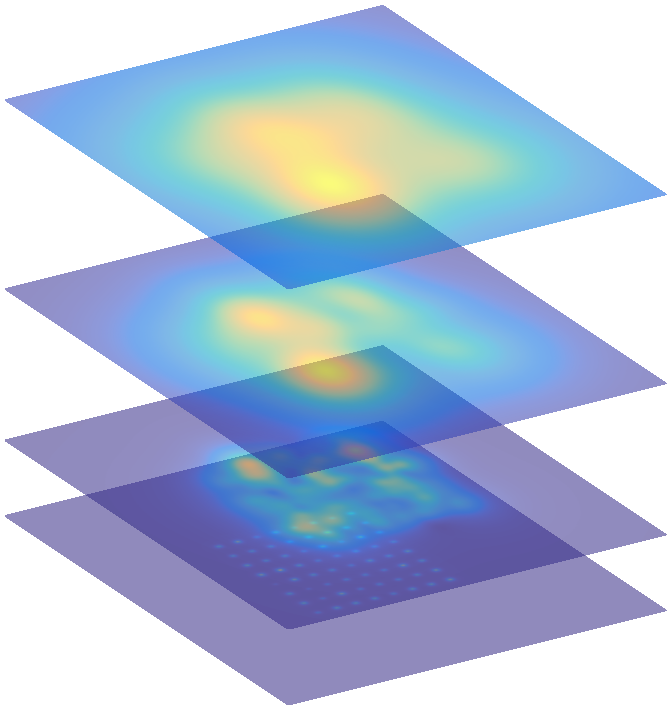

Figure 4.12 Electric field magnitudes of the propagated EM field for a single realization, normalized within each observation plane, at heights $h_0 = 0\,\mathrm{mm}$, $h_1 = 10\,\mathrm{mm}$, $h_2 = 30\,\mathrm{mm}$, and $h_3 = 55\,\mathrm{mm}$. The sources are modeled as 64 small dipole antennas, excited by uncorrelated currents, radiating in free space (from [135]).

containing one emitted mode is given by $\Omega_\mathrm{c} = \lambda_0^2/A_\mathrm{s}$, where $\lambda_0 = 2\pi/k_0$ and, for our case, $A_s = 7 \times 7\mathrm{cm}^2$. The number of transverse modes N_tr which can be resolved in a distance r from the aperture on an area A_s will be

$$N_\mathrm{tr} = \frac{A_\mathrm{s}^2}{r^2\lambda_0^2}\,. \tag{4.24}$$

For our numerical example, where only the $\underline{E}_x$-field is sampled, the number of transverse modes to be detected is $N_\mathrm{tr}/2$. Hence, at a distance r, the number of principal components required for a full description of our correlation matrix is given by $N_\mathrm{tr}/2$ while at the same time the number of principal components in our estimate cannot exceed the maximum rank of the correlation matrix, which is in our example 64. The function

$$\min\left(\frac{N_\mathrm{tr}}{2}, 64\right)\,, \tag{4.25}$$

provides a qualitative good estimate for the maximum number of principal components required. At lower frequencies, when the far-field assumption is less justified, the number of PCs required may exceed the number from this estimate based on counting transverse modes.

4.4 Source Localization

Source localization has been treated extensively in [139][2]. In the design process of a system, noisy fields can be characterized by measurement and subsequent evaluation of correlation spectra of the EM field in a chosen scanning plane of a device under test. The correlation spectra may be propagated in the source-free volume

[2]The results presented in this section have been published under IEEE copyright in M. Haider and J. A. Russer, "Equivalent source localization for stochastic electromagnetic fields", in *International Conference on Electromagnetics in Advanced Applications (ICEAA)*, Sep. 2017, pp. 1486–1489. DOI: 10.1109/ICEAA.2017.8065563. The content (text and figures) is reproduced with permission of IEEE.

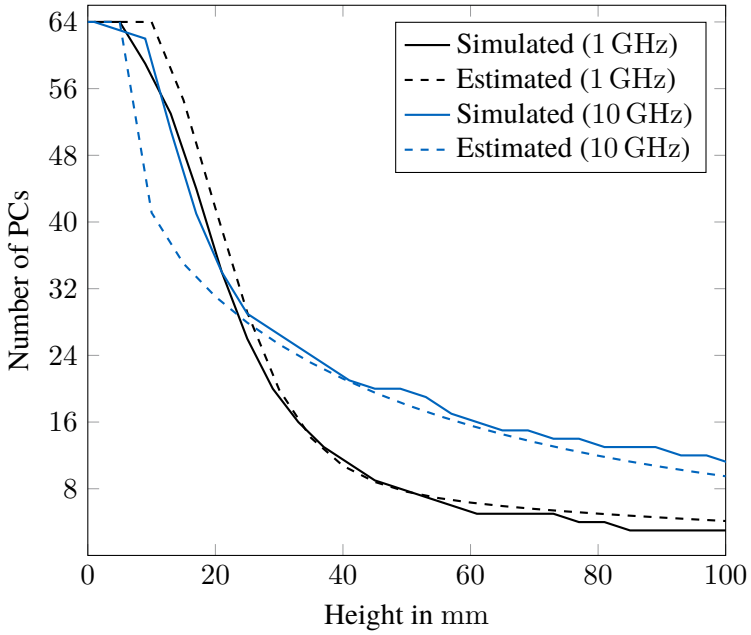

Figure 4.13 Number of dominant principal components vs. height of observation plane obtained by numerical propagation of the field-field correlations on a constant sized observation grid, by estimation of field energy within the observation window. (from [135]).

above the scan plane, and hence, the noise energy can be computed for close-by components. However, it is also of interest to obtain exact locations of noise sources that gave rise to the noisy field characterized in the aforementioned scanning plane. In this way, insight is gained to the actual sources of EMI and strategies to avoid or suppress disturbances can be devised. A simplified model can be established, based on equivalent point sources, where the locations of these sources are calculated from data obtained by e.g. near-field scanning of the device under test [140]. This helps in identifying hot-spots of concentrated radiated energy on the device under test. To achieve a reliable localization of sources of electromagnetic interference, the spatial correlations of the field observations at some distance of the actual device under test must be considered. This problem, i.e. estimating the locations of radiating EMI sources, is strongly related to the problem of direction of arrival estimation. There are well established algorithms available [141], [142], performing very efficiently under far-field conditions. Direction of arrival estimation has been also considered using neural networks for noisy EM fields in [143]. Another interesting approach is given in [144], where the authors perform a characterization of noisy electromagnetic fields by a cross spectral density eigenvalue analysis. Work on source identification for stochastic electromagnetic fields has been done in [134], [145]–[148]. The problem of finding locations of equivalent dipoles can be split into four steps. First, find an appropriate Green's function for a dense grid of potential source points giving rise to an EM field at all specified observation points. Also for complex geometries appropriate numerical Green's functions can be found by using full-wave numerical EM modeling tools. The second step is to form an inverse-propagator for the known Green's function. With this, the stochastic EM fields, described by spatial correlations, can be propagated back to the source plane. In the third step, an estimation of the model order needs to be performed [30]. Finally, equivalent sources are identified based on the data obtained by the inverse-propagation.

We discuss a method for source localization by obtaining inverse-propagation operators for arbitrary geometries and present a numerical propagator for free-space, based on the discretization of the free-space Green's dyadic for the EM field. Based on the back-propagated data, a two-dimensional optimization problem is formulated for finding the locations of equivalent dipole sources. Finally, a numerical example is presented.

Numerical EM field solvers can provide numerical Green's functions for arbitrary structures. Here, we use a numerical near-field propagator for free-space based on the free-space Green's dyadic relating the current

density in a source region to the excited magnetic fields. The magnetic field $\underline{\boldsymbol{H}}(\boldsymbol{r},\omega)$ due to a current density $\underline{\boldsymbol{J}}(\boldsymbol{r}',\omega)$ is given by

$$\underline{\boldsymbol{H}}(\boldsymbol{r},\omega) = \iiint_{V'} \underline{\boldsymbol{G}}_{\mathrm{HJ}}(\boldsymbol{r},\boldsymbol{r}',\omega)\,\underline{\boldsymbol{J}}(\boldsymbol{r}',\omega)\,\mathrm{d}^3 r' . \tag{4.26}$$

For free space, we know an analytic expression for the magnetic field Green's dyadic, given by [16]

$$\underline{\boldsymbol{G}}_{\mathrm{HJ}}(\boldsymbol{r},\omega) = \frac{\beta^2}{4\pi}\boldsymbol{x}\times\mathbf{1}\frac{1+\mathrm{i}\beta\|\boldsymbol{r}\|}{\beta^2\|\boldsymbol{r}\|^3}\mathrm{e}^{-\mathrm{i}\beta\|\boldsymbol{r}\|} , \tag{4.27}$$

with the unit dyadic $\mathbf{1}$, $\|\boldsymbol{r}\| = \sqrt{x^2+y^2+z^2}$, the phase coefficient $\beta = \omega/c_0$, and the free-space speed of light c_0. We can decompose the magnetic field as well as the current density into a set of basis functions $\boldsymbol{u}_m(\boldsymbol{r})$,

$$\underline{\boldsymbol{H}}(\boldsymbol{r},\omega) = \sum_{m=1}^{N_{\mathrm{o}}} \underline{I}_m^{(o)}(\omega)\,\boldsymbol{u}_m(\boldsymbol{r}) , \tag{4.28}$$

$$\underline{\boldsymbol{J}}(\boldsymbol{r},\omega) = \sum_{n=1}^{N_{\mathrm{s}}} \underline{I}_n^{(s)}(\omega)\,\boldsymbol{u}_n(\boldsymbol{r}) , \tag{4.29}$$

where N_{o}, N_{s} denotes the number of expansion functions for the observation and source plane, respectively, and the expansion coefficients are termed as generalized currents $\underline{I}_n$. A superscript o or s denotes the association of the expansion function with points on the observation or source plane, respectively. We use Dirac delta distributions for both, weighting and testing functions, which corresponds to the point-matching scheme for the method of moments (MoM), hence

$$\underline{\boldsymbol{H}}(\boldsymbol{r},\omega) = \sum_{n=1}^{N_{\mathrm{o}}} \underline{I}_m^{(\mathrm{o})}(\omega)\,\delta(\boldsymbol{r}-\boldsymbol{r}_m) , \tag{4.30}$$

$$\underline{\boldsymbol{J}}(\boldsymbol{r},\omega) = \sum_{n=1}^{N_{\mathrm{s}}} \underline{I}_n^{(\mathrm{s})}(\omega)\,dirac(\boldsymbol{r}-\boldsymbol{r}_n) . \tag{4.31}$$

Inserting (4.30) and (4.31) into (4.26) and applying an inner product with $\delta(\boldsymbol{r}-\boldsymbol{r}_m)$, we obtain

$$\underline{I}_m^{(\mathrm{o})}(\omega) = \sum_{n=1}^{N_{\mathrm{s}}} \underline{\boldsymbol{G}}_{\mathrm{HJ}}(\boldsymbol{r}_m-\boldsymbol{r}_n',\omega)\,\underline{I}_n^{(\mathrm{s})}(\omega) . \tag{4.32}$$

In the following, we assume that observation and source plane are oriented in xy-direction while the distance between source and observation plane $h = (z-z')$ is fixed, and we obtain basis function expansions in the xy-plane for (4.32) with a fixed frequency ω by

$$\underline{I}_{m,x}^{(\mathrm{o})} = \sum_{n=1}^{N} \underline{\tilde{M}}(\boldsymbol{r}_m,\boldsymbol{r}_n')\left[\underline{I}_{n,z}^{(\mathrm{s})}(y_m-y_n') - \underline{I}_{n,y}^{(\mathrm{s})}h\right] , \tag{4.33}$$

$$\underline{I}_{m,y}^{(\mathrm{o})} = \sum_{n=1}^{N} \underline{\tilde{M}}(\boldsymbol{r}_m,\boldsymbol{r}_n')\left[\underline{I}_{n,x}^{(\mathrm{s})}h - \underline{I}_{n,z}^{(\mathrm{s})}(x_m-x_n')\right] . \tag{4.34}$$

Here, we have introduced the function

$$\underline{\tilde{M}}(\boldsymbol{r}_m,\boldsymbol{r}_n') = \frac{\beta^2}{4\pi}\frac{1+\mathrm{i}\beta\|\boldsymbol{r}_m-\boldsymbol{r}_n'\|}{\beta^2\|\boldsymbol{r}_m-\boldsymbol{r}_n'\|^3}\mathrm{e}^{-\mathrm{i}\beta\|\boldsymbol{r}_m-\boldsymbol{r}_n'\|} . \tag{4.35}$$

For the equivalent source localization, planar structures radiating EMI are assumed, i.e. $\underline{I}_{n,z}^{(\mathrm{s})} = 0$. The frequency dependent correlations between generalized currents can be obtained by

$$\underline{C}_{ij,mn}^{(\mathrm{o})} = \lim_{T\to\infty}\frac{1}{2T}\left\langle\!\!\left\langle \underline{I}_{m,i}^{(\mathrm{o})}\underline{I}_{n,j}^{(\mathrm{o})*}\right\rangle\!\!\right\rangle , \tag{4.36}$$

$$\underline{C}_{ij,mn}^{(\mathrm{s})} = \lim_{T\to\infty}\frac{1}{2T}\left\langle\!\!\left\langle \underline{I}_{m,i}^{(\mathrm{s})}\underline{I}_{n,j}^{(\mathrm{s})*}\right\rangle\!\!\right\rangle , \tag{4.37}$$

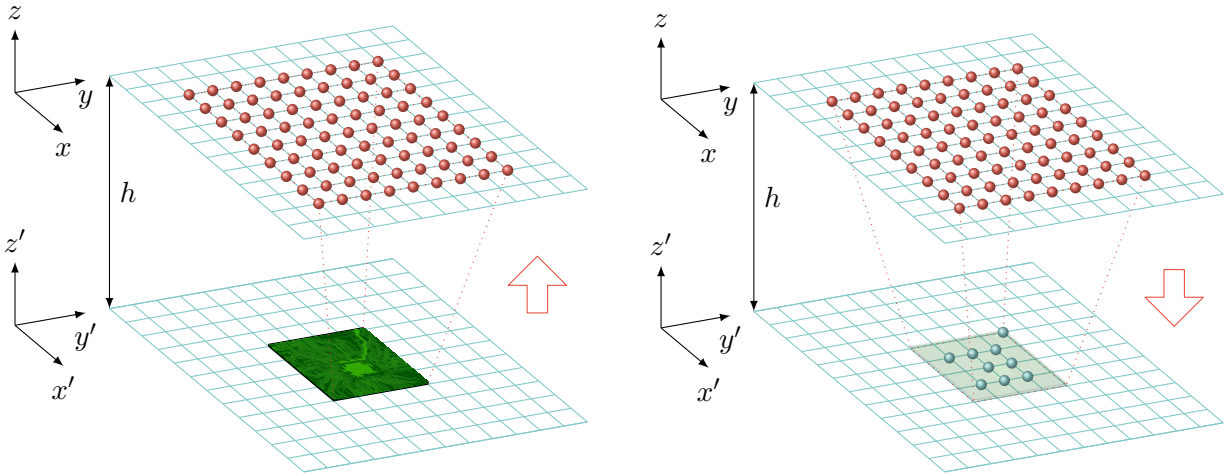

(a) Near-field scanning scheme.

(b) Source estimation based on scanned data.

Figure 4.14 Near-field sampling on a plane above the DUT (a) and source estimation based on sampled data (b) (from [139]).

with $i, j \in \{x, y\}$. These correlations can be summarized in the matrices $\underline{\boldsymbol{C}}_{ij}^{(\mathrm{o})}$ and $\underline{\boldsymbol{C}}_{ij}^{(\mathrm{s})}$. With $\underline{M}_{mn} = h \cdot \underline{\tilde{M}}\left(\boldsymbol{r}_m, \boldsymbol{r}_n\right)$ we find

$$\underline{C}_{xx,mn}^{(\mathrm{o})} = \sum_{k=1}^{N_\mathrm{s}} \sum_{l=1}^{N_\mathrm{s}} \underline{M}_{mk} \underline{M}_{nl} \underline{C}_{yy,kl}^{(\mathrm{s})} \,, \tag{4.38}$$

$$\underline{C}_{xx,mn}^{(\mathrm{o})} = \sum_{k=1}^{N_\mathrm{s}} \sum_{l=1}^{N_\mathrm{s}} \underline{M}_{mk} \underline{M}_{nl} \underline{C}_{xx,kl}^{(\mathrm{s})} \,. \tag{4.39}$$

This can be re-formulated in matrix-vector notation as

$$\underline{\boldsymbol{C}}_{xx}^{(\mathrm{o})} = \underline{\boldsymbol{M}}\, \underline{\boldsymbol{C}}_{yy}^{(\mathrm{s})}\, \underline{\boldsymbol{M}}^{\dagger} \,, \qquad \underline{\boldsymbol{C}}_{yy}^{(\mathrm{o})} = \underline{\boldsymbol{M}}\, \underline{\boldsymbol{C}}_{xx}^{(\mathrm{s})}\, \underline{\boldsymbol{M}}^{\dagger} \,. \tag{4.40}$$

4.4.1 The Inverse Problem

With a suitable matrix inverse $\underline{\boldsymbol{M}}^{-1}$, we can obtain

$$\underline{\boldsymbol{M}}^{-1} \underline{\boldsymbol{C}}_{xx}^{(\mathrm{o})} \left(\underline{\boldsymbol{M}}^{\dagger}\right)^{-1} = \underline{\boldsymbol{M}}^{-1} \underline{\boldsymbol{M}}\, \underline{\boldsymbol{C}}_{yy}^{(\mathrm{s})}\, \underline{\boldsymbol{M}}^{\dagger} \left(\underline{\boldsymbol{M}}^{\dagger}\right)^{-1} \,, \tag{4.41}$$

$$\underline{\boldsymbol{M}}^{-1} \underline{\boldsymbol{C}}_{yy}^{(\mathrm{o})} \left(\underline{\boldsymbol{M}}^{\dagger}\right)^{-1} = \underline{\boldsymbol{M}}^{-1} \underline{\boldsymbol{M}}\, \underline{\boldsymbol{C}}_{xx}^{(\mathrm{s})}\, \underline{\boldsymbol{M}}^{\dagger} \left(\underline{\boldsymbol{M}}^{\dagger}\right)^{-1} \,. \tag{4.42}$$

In general, the transformation matrix $\underline{\boldsymbol{M}} \in \mathbb{C}^{N_\mathrm{o} \times N_\mathrm{s}}$ is not a square matrix, i.e. the number of observations is different from the number of sources. Thus, the existence of a matrix inverse $\underline{\boldsymbol{M}}^{-1}$ is not granted. Now, a dense grid in the observation plane can be defined, where the matrix elements of $\underline{\boldsymbol{M}}$ are calculated for each (x'_n, y'_n) and all the known observation points. The inverse problem is then solved by calculating the Moore-Penrose pseudo inverse $\underline{\boldsymbol{M}}^{+}$, defined by [149]

$$\underline{\boldsymbol{M}}\, \underline{\boldsymbol{M}}^{+} \underline{\boldsymbol{M}} = \underline{\boldsymbol{M}} \,, \qquad \underline{\boldsymbol{M}}^{+} \underline{\boldsymbol{M}}\, \underline{\boldsymbol{M}}^{+} = \underline{\boldsymbol{M}}^{+} \,, \tag{4.43}$$

$$\left(\underline{\boldsymbol{M}}\, \underline{\boldsymbol{M}}^{+}\right)^{\dagger} = \underline{\boldsymbol{M}}\, \underline{\boldsymbol{M}}^{+} \,, \qquad \left(\underline{\boldsymbol{M}}^{+} \underline{\boldsymbol{M}}\right)^{\dagger} = \underline{\boldsymbol{M}}^{+} \underline{\boldsymbol{M}} \,. \tag{4.44}$$

We can therefore find an optimal solution to the inverse problem by means of the Moore-Penrose pseudo inverse

$$\underline{\boldsymbol{C}}_{xx}^{(\mathrm{s})} = \underline{\boldsymbol{M}}^{+} \underline{\boldsymbol{C}}_{yy}^{(\mathrm{o})} \left(\underline{\boldsymbol{M}}^{\dagger}\right)^{+} \,, \qquad \underline{\boldsymbol{C}}_{yy}^{(\mathrm{s})} = \underline{\boldsymbol{M}}^{+} \underline{\boldsymbol{C}}_{xx}^{(\mathrm{o})} \left(\underline{\boldsymbol{M}}^{\dagger}\right)^{+} \,. \tag{4.45}$$

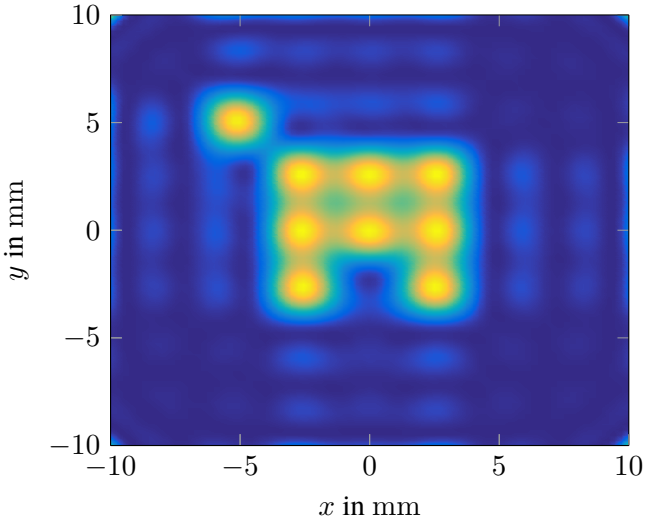

Figure 4.15 Result of the inverse problem for numerical back-propagation in Matlab (from [139]).

4.4.2 Equivalent Source Localization

The actual equivalent source localization poses an optimization problem. Given the correlation matrix in the source plane as the solution of the inverse problem, the hot-spots of radiated energy need to be identified. This can be done by finding the locations (x', y'), such that the energy, given by the diagonal elements of $\underline{\boldsymbol{C}}_{xx}^{(\mathrm{s})}$ and $\underline{\boldsymbol{C}}_{yy}^{(\mathrm{s})}$ is maximized. The first equivalent source location is given by the largest maximum. In order to find the total number of sources, we must employ a criterion for estimating the model order. We use principal component analysis, with a predefined cumulative percentage of total variance criterion [38], as we will later introduce in chapter 7. The number of dominant principal components corresponds to the number of independent sources and hence gives a good estimate of the model order. The two-dimensional local maxima can be identified in terms of the two-dimensional optimization problem

$$\left(x', y'\right) = \left(x'_n, y'_n\right),\, n \leq N \,\middle|\, \underset{n \leq N}{\arg\max} \left(\underline{C}_{ii,nn}^{(\mathrm{s})}\right) \,. \tag{4.46}$$

With all local maxima known, the largest N extrema are chosen, where N corresponds to the result of the model order estimation, based on principal component analysis. Figure 4.14 illustrates the scheme for sampling the field originating from the device under test and subsequent source localization.

4.4.3 Numerical Example

Based on the free-space numerical propagator, given by (4.35), we investigate a numerical example. Numerical propagators can be obtained for arbitrary geometries from full-wave analysis. We chose a known set of sources in free-space on the source plane and propagated the stochastic magnetic field correlation matrix to the observation plane. In order to resemble a real measurement, Gaussian noise is added to the observed signals. Subsequently, we assume that the locations of the sources are unknown. Figure 4.15 shows the sampling points in the xy-observation plane and noisy sources in the $x'y'$-plane, with currents oriented in x-direction. A dense grid of possible source points is created on the source plane, where we calculate the necessary matrix elements of the numerical propagator for each single grid point. Afterwards, we form the Moore-Penrose pseudo inverse and pre- and post-multiply it to the noisy observation correlation matrix according to (4.45). In this way, we obtain an estimate for the energy distribution in the source plane. By performing a principal component analysis, we obtain a measure for the model order and can identify the locations of equivalent dipole sources. Results shown in Figure 4.15 demonstrate an accurate source localization.

5 Propagation of Stochastic Electromagnetic Fields

5.1 Frequency-Domain Propagation

5.1.1 The Method of Moments (MoM)

The method of moments is a very general procedure for turning field problems into network problems, i.e. algebraic equations that can be solved numerically [136], [137]. The method of moments has been used to generalize a whole subset of frequently used numerical methods, such as FDTD [150] and TLM [151]. As both methods mentioned are indeed time-domain methods, one should note that the method of moments is not exclusively a frequency-domain method, but a general concept for obtaining discretized field equations. We decided to introduce the method of moments in the frequency-domain propagation chapter, because in electromagnetics the method of moments is primarily, but not exclusively used in the frequency-domain [137]. Let $\mathcal{H}$ be a Hilbert space according to Definition 2.8. The most general formulation of a linear equation relating elements of the Hilbert space $\mathcal{H}$ is given in terms of a linear operator $L : \mathcal{H} \to \mathcal{H}$. The linear operator L can be applied to a function $f \in \mathcal{H}$, which yields a new function $g \in \mathcal{H}$,

$$Lf = g\,. \tag{5.1}$$

If there is one unique function $f \in \mathcal{H}$ for all $g \in \mathcal{H}$ under the action of L, then (5.1) constitutes a bijective mapping and there exists an inverse operator L^{-1} with

$$f = L^{-1}g\,. \tag{5.2}$$

Any analytic function f can be expanded into a series of basis functions u_n with $n \in \{1, \ldots, N\}$, as given in

$$f = \sum_{n=1}^{\infty} a_n u_n\,, \tag{5.3}$$

where the limit of the sum may be truncated after a finite index N for numerical feasibility. Anyway, we can assume N to be finite, and treat the finite series expansion as an arbitrarily precise approximation to the analytic function f. Inserting the series expansion from (5.3) into the linear equation (5.1), we have

$$Lf = L\left(\sum_{n=1}^{N} a_n u_n\right) = \sum_{n=1}^{N} a_n L u_n = g\,. \tag{5.4}$$

Also the resulting function g can be expanded into a set of testing functions w_m with $m \in \{1, \ldots, M\}$, such that

$$g = \sum_{m=1}^{M} b_m w_m\,. \tag{5.5}$$

If the set of testing functions $\{w_m\}_{m=1}^{M}$ spans the Hilbert space $\mathcal{H}$, the coefficients b_m of the function g, with respect to the series expansion in (5.5), can be determined by an inner product

$$b_m = \langle w_m, g \rangle\ . \tag{5.6}$$

By applying the inner product to the series expansion of the linear equation in (5.4), we obtain a set of algebraic equations, relating the expansion coefficients a_n of the analytic function $f \in \mathcal{H}$ to the expansion coefficients b_m of the function $g \in \mathcal{H}$. The set of linear algebraic equations expressing this relation is given by [45]

$$\left\langle w_m, \sum_{n=1}^{N} a_n L u_n \right\rangle = \sum_{n=1}^{N} a_n \langle w_m, L u_n \rangle = \langle w_m, g \rangle = b_m\,. \tag{5.7}$$

The linear set of algebraic equations, given in terms of (5.7), can be written in matrix-vector form as

$$\boldsymbol{L}\boldsymbol{a} = \boldsymbol{b}\,, \tag{5.8}$$

with the coefficient vectors $\boldsymbol{a}$ and $\boldsymbol{b}$ of the series expansions, and the matrix $\boldsymbol{L}$, representing the expansion of the linear operator L. The result of this matrix-vector multiplication is given element-wise by

$$\begin{bmatrix} \langle w_1, Lu_1\rangle & \langle w_1, Lu_2\rangle & \cdots & \langle w_1, Lu_N\rangle \\ \langle w_2, Lu_1\rangle & \langle w_2, Lu_2\rangle & \cdots & \langle w_2, Lu_N\rangle \\ \vdots & \vdots & \ddots & \vdots \\ \langle w_M, Lu_1\rangle & \langle w_M, Lu_2\rangle & \cdots & \langle w_M, Lu_N\rangle \end{bmatrix} \begin{bmatrix} a_1 \\ a_2 \\ \vdots \\ a_N \end{bmatrix} = \begin{bmatrix} \langle w_1, g\rangle \\ \langle w_2, g\rangle \\ \vdots \\ \langle w_M, g\rangle \end{bmatrix} = \begin{bmatrix} b_1 \\ b_2 \\ \vdots \\ b_M \end{bmatrix}. \tag{5.9}$$

Although the method of moments found widespread applications in solving problems in electromagnetics [137], it is a very general mathematical procedure to approximate analytic equations by a finite set of algebraic equations, which can be solved numerically, as mentioned before.

5.1.2 Stochastic Field Propagation by the Method of Moments

The general idea of propagating a stochastic field, as described in section 3.1, is first constructing a probability measure on the space of fields X, representing the possible realizations of the random source field by means of the family of all finite dimensional probability distributions, using Theorem 2.2. By requiring separability, Theorem 2.3 ensures the existence of a probability measure also for continuous index sets. For any probability measure $\tilde{P}$, we can construct a characteristic functional χ on X with respect to $\tilde{P}$, which carries all statistical information and thus uniquely determines the random field. The second step is to model the propagation of the field by a linear operator that maps the random source field to the observed random field. We discussed the transformation of characteristic functionals under linear operators in section 3.1.2 and the special case of the linear transformation of Gaussian random fields in section 3.2. In the general case, as can be seen from equation (3.18), the transformation of the characteristic functional of the random source field to the characteristic functional of the observed field is not linear, as the adjoint linear operator in (3.18) appears in the argument of the functional χ_X. This renders the direct numerical propagation of characteristic functionals a very difficult problem, as it involves solving non-linear equations. However, for Gaussian random fields, which we will consider in the following, the characteristic functionals only depend on two statistical parameters, i.e. mean function and correlation dyadic, which transform linearly. Thus, we can restrict ourselves to solving linear equations for propagating those statistical parameters. Also for other than Gaussian statistics, it seems to be beneficial to investigate the transformation of statistical parameters instead of propagating characteristic functionals themselves. For now and in the following, we consider an electromagnetic random source field which is assumed to be stationary, ergodic, and Gaussian distributed. The characteristic functional χ_{J} of the random source current density is given in the frequency-domain by the parameters $\underline{\boldsymbol{m}}_{\mathrm{J}}(\boldsymbol{r}')$ and $\underline{\boldsymbol{\Gamma}}_{\mathrm{J}}(\boldsymbol{r}'_1, \boldsymbol{r}'_2, \omega)$. Without loss of generality we set $\underline{\boldsymbol{m}}_{\mathrm{J}}(\boldsymbol{r}')$ to zero for all $\boldsymbol{r}'$. The propagation of the stochastic electromagnetic field is modeled by a linear integral operator with integral kernel $\underline{\boldsymbol{G}}_{\mathrm{HJ}}(\boldsymbol{r}, \boldsymbol{r}', \omega)$, given by the Green's function of the spatial region under consideration. Hence we have

$$\underline{\boldsymbol{\Gamma}}_{\mathrm{H}}(\boldsymbol{r}_1, \boldsymbol{r}_2, \omega) = \iiint_{V'} \iiint_{V'} \underline{\boldsymbol{G}}_{\mathrm{HJ}}(\boldsymbol{r}_1 - \boldsymbol{r}'_1, \omega)\, \underline{\boldsymbol{\Gamma}}_{\mathrm{J}}(\boldsymbol{r}'_1, \boldsymbol{r}'_2, \omega)\, \underline{\boldsymbol{G}}^{\dagger}_{\mathrm{HJ}}(\boldsymbol{r}_2 - \boldsymbol{r}'_2, \omega)\, \mathrm{d}^3 r'_1\, \mathrm{d}^3 r'_2\,. \tag{5.10}$$

We expand the source correlation dyadic $\underline{\boldsymbol{\Gamma}}_{\mathrm{J}}$ into a series of orthogonal spatial basis functions $\boldsymbol{u}_k(\boldsymbol{r}'_1)$ and $\boldsymbol{u}_l(\boldsymbol{r}'_2)$, such that

$$\underline{\boldsymbol{\Gamma}}_{\mathrm{J}}(\boldsymbol{r}'_1, \boldsymbol{r}'_2, \omega) = \sum_{k=1}^{N} \sum_{l=1}^{N} \underline{C}_{\mathrm{J}\,kl}(\omega)\, \boldsymbol{u}_k(\boldsymbol{r}'_1)\, \boldsymbol{u}^{\dagger}_l(\boldsymbol{r}'_2)\,. \tag{5.11}$$

Also the observed correlation dyadic $\underline{\boldsymbol{\Gamma}}_{\mathrm{H}}$ is expanded into a series of orthogonal testing functions $\boldsymbol{w}_m(\boldsymbol{r}_1)$ and $\boldsymbol{w}_n(\boldsymbol{r}_2)$, which is given by

$$\underline{\boldsymbol{\Gamma}}_{\mathrm{H}}(\boldsymbol{r}_1, \boldsymbol{r}_2, \omega) = \sum_{m=1}^{M} \sum_{n=1}^{M} \underline{C}_{\mathrm{H}\,mn}(\omega)\, \boldsymbol{w}_m(\boldsymbol{r}_1)\, \boldsymbol{w}^{\dagger}_n(\boldsymbol{r}_2)\,. \tag{5.12}$$

Inserting the series expansions (5.11) and (5.12) into the propagation equation for the correlation dyadic (5.10) yields

$$\sum_{m=1}^{M}\sum_{n=1}^{M}\underline{C}_{\mathrm{H}\,mn}\left(\omega\right)\boldsymbol{w}_m\left(\boldsymbol{r}_1\right)\boldsymbol{w}_n^{\dagger}\left(\boldsymbol{r}_2\right)=\sum_{k=1}^{N}\sum_{l=1}^{N}\underline{C}_{\mathrm{J}\,kl}\left(\omega\right)\iiint_{V'}\iiint_{V'}\underline{\boldsymbol{G}}_{\mathrm{HJ}}\left(\boldsymbol{r}_1-\boldsymbol{r}_1',\omega\right)\boldsymbol{u}_k\left(\boldsymbol{r}_1'\right)\boldsymbol{u}_l^{\dagger}\left(\boldsymbol{r}_2'\right)\times \\ \times\,\underline{\boldsymbol{G}}_{\mathrm{HJ}}^{\dagger}\left(\boldsymbol{r}_2-\boldsymbol{r}_2',\omega\right)\,\mathrm{d}^3r_1'\,\mathrm{d}^3r_2'\,. \tag{5.13}$$

By applying two inner products, one with $\boldsymbol{w}_p\left(\boldsymbol{r}_1\right)$ and one with $\boldsymbol{w}_q^{\dagger}\left(\boldsymbol{r}_2\right)$, and by using the orthogonality of the testing functions, we obtain

$$\underline{C}_{\mathrm{H}\,mn}\left(\omega\right)=\sum_{k=1}^{N}\sum_{l=1}^{N}\underline{C}_{\mathrm{J}\,kl}\left(\omega\right)\iiint_{V}\iiint_{V}\iiint_{V'}\iiint_{V'}\boldsymbol{w}_m^{\dagger}\left(\boldsymbol{r}_1\right)\underline{\boldsymbol{G}}_{\mathrm{HJ}}\left(\boldsymbol{r}_1-\boldsymbol{r}_1',\omega\right)\boldsymbol{u}_k\left(\boldsymbol{r}_1'\right)\boldsymbol{u}_l^{\dagger}\left(\boldsymbol{r}_2'\right)\times \\ \times\,\underline{\boldsymbol{G}}_{\mathrm{HJ}}^{\dagger}\left(\boldsymbol{r}_2-\boldsymbol{r}_2',\omega\right)\boldsymbol{w}_n\left(\boldsymbol{r}_2\right)\,\mathrm{d}^3r_1'\,\mathrm{d}^3r_2'\,\mathrm{d}^3r_1\,\mathrm{d}^3r_2\,. \tag{5.14}$$

Thus we have

$$\underline{C}_{\mathrm{H}\,mn}\left(\omega\right)=\sum_{k=1}^{N}\sum_{l=1}^{N}\underline{C}_{\mathrm{J}\,kl}\left(\omega\right)\underline{M}_{mk}\left(\omega\right)\underline{M}_{ln}^{*}\left(\omega\right)\,, \tag{5.15}$$

with

$$\underline{M}_{ij}\left(\omega\right)=\iiint_{V}\iiint_{V'}\boldsymbol{w}_i^{\dagger}\left(\boldsymbol{r}\right)\underline{\boldsymbol{G}}_{\mathrm{HJ}}\left(\boldsymbol{r}-\boldsymbol{r}',\omega\right)\boldsymbol{u}_j\left(\boldsymbol{r}'\right)\mathrm{d}^3r'\,\mathrm{d}^3r\,. \tag{5.16}$$

The series expansions of the source and observation correlation dyadics yielded an algebraic equation, relating discrete correlation matrices of frequency-dependent expansion coefficients using an expansion of the Green's dyadic. Finally, equation (5.16) can be written in matrix notation as

$$\underline{\boldsymbol{C}}_{\mathrm{H}}\left(\omega\right)=\underline{\boldsymbol{M}}\left(\omega\right)\underline{\boldsymbol{C}}_{\mathrm{J}}\left(\omega\right)\underline{\boldsymbol{M}}^{\dagger}\left(\omega\right)\,. \tag{5.17}$$

This method is very powerful in propagating correlation information, which shall be illustrated by a numerical example. The accuracy of the solutions generated by the method of moments is dependent on the choice of basis and testing functions [137]. For complex problems, it is desirable to obtain approximate solutions by using subsectional basis functions, i.e. basis functions that are non-vanishing only on a finite subsection of the source-domain V'. The same holds for the testing functions. In the following numerical example, we use three-dimensional unit step functions as basis functions, and Dirac delta distributions as testing functions, which corresponds to the point-matching approximation [137], [152].

5.1.3 Numerical Example

Numerical studies on the near-field to far-field propagation of correlation information have been performed in [152][1]. As a device under test (DUT), we consider an Atlys Spartan-6 board, which is programmed to send a Gaussian pseudo-random bit sequence along a transmission line on the printed circuit board (PCB)). For a complete characterization of the radiated EMI of the DUT, we need knowledge of the tangential electromagnetic field components on all possible pairs of measurement points simultaneously, according to section 3.2. Even for moderate numbers of sampling points, this would result in a very large number of measurements and hence, in an immense amount of data. Techniques for reducing the amount of data for two-probe near-field measurements have been discussed in [38] and will be presented in chapter 7.

[1]The numerical example presented in this section was published under IEEE copyright in M. Haider, A. Baev, Y. Kuznetsov, *et al.*, "Near-field to far-field propagation of correlation information for noisy electromagnetic fields", in *48th European Microwave Conference (EuMC)*, Sep. 2018, pp. 1190–1193. DOI: 10.23919/EuMC.2018.8541636. The content (text and figures) is reproduced with permission of IEEE.

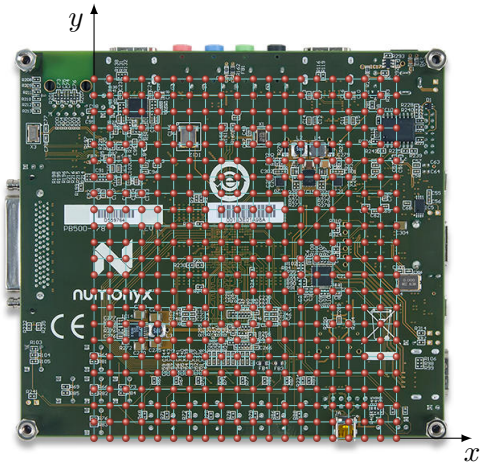

Figure 5.1 Near-field scan plane above Atlys Spartan-6 Board (from [152]).

With the following numerical example, we want to compare correlation data of the sampled electromagnetic far-field obtained by measurement, and far-field correlation data obtained by numerical propagation of the near-field scan data, by means of the method of moments. To this end, we prepared a test case by propagating a defined pseudo-random bit sequence along one signal transmission line of the PCB. This well-defined scenario allows us to keep the reference probe stationary and hence reduces the number of measurements required. The data signal propagating on the PCB can be written as

$$s_T(t) = \sum_{n=0}^{N-1} a_n \cdot \operatorname{rect}\left(\frac{t - n\Delta}{\Delta}\right), \tag{5.18}$$

where $\operatorname{rect}\left(\frac{t-n\Delta}{\Delta}\right)$ are rectangular pulses with duration Δ and the coefficients $a_n \in \{\pm 1\}$ are given by a pseudo random M-sequence with delta-correlation properties [153].

The time-domain near-field measurement setup comprises two RF-R 50-1 H-field probes from Langer EMV Technik, which are connected to port 1 and port 3 of a Lecroy SDA-813-Zi-A high sampling rate digital oscilloscope. We used our in-house scanning system, described in section 4.1.2, to spatially scan the DUT on a rectangular 20×23 measurement grid with a $5\,\mathrm{mm}$ horizontal and vertical spacing at a height of about $2\,\mathrm{mm}$. The measurement grid relative to the DUT can be seen in Figure 5.1. Figure 5.2 shows the concept of near-field scanning above the DUT. We define the correlation function $c_{ij}(\tau, t)$ of two random signals $s_i(t)$ and $s_j(t)$ by

$$c_{ij}(\tau, t) = \langle\!\langle s_i(t)\, s_j(t-\tau) \rangle\!\rangle, \tag{5.19}$$

where c_{ii} is the auto-correlation function, c_{ij} with $i \neq j$ is the cross-correlation function (CCF), and the brackets $\langle\!\langle \ldots \rangle\!\rangle$ denote the forming of an ensemble average [20]. If the mean values of two signals $\langle\!\langle s_i(t) \rangle\!\rangle$, $\langle\!\langle s_i(t) \rangle\!\rangle$ and their correlation functions $\langle\!\langle s_i(t)\, s_j(t-\tau) \rangle\!\rangle$ are periodic with a period T_0, the signals s_i and s_j are second-order cyclostationary in the wide sense, according to Definition 2.31.

The magnetic field excited by a certain current distribution is given through convolution with a dyadic Green's function. For free space, the dyadic Green's function for the magnetic field is given by [102]

$$\underline{\boldsymbol{G}}_{\mathrm{HJ}}(\boldsymbol{r}, \omega) = \frac{1}{4\pi} \boldsymbol{r} \times \mathbf{1} \frac{c_0 + \mathrm{i}\omega \|\boldsymbol{r}\|}{c_0 \|\boldsymbol{r}\|^3} \mathrm{e}^{-\mathrm{i}\omega \frac{\|\boldsymbol{r}\|}{c_0}}, \tag{5.20}$$

with

$$\boldsymbol{r} \times \mathbf{1} = \begin{bmatrix} 0 & -z & y \\ z & 0 & -x \\ -y & x & 0 \end{bmatrix}, \tag{5.21}$$

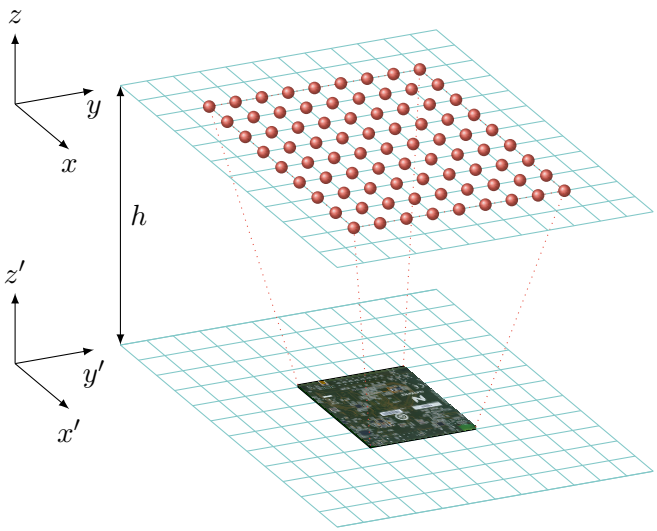

Figure 5.2 Near-field scanning scheme for a DUT at measurement height h (from [152]).

where $\|\boldsymbol{r}\|^2 = x^2 + y^2 + z^2$, and c_0 as the free-space velocity of light. In the context of the MoM, we expand the current density $\underline{\boldsymbol{J}}(\boldsymbol{r}', \omega)$ and the magnetic field $\underline{\boldsymbol{H}}(\boldsymbol{r}, \omega)$ into orthogonal basis functions $\{\boldsymbol{u}_n\}_{n=0}^{N}$ and $\{\boldsymbol{w}_m\}_{m=0}^{M}$,

$$\underline{\boldsymbol{J}}(\boldsymbol{r}', \omega) = \sum_{n=1}^{N} \underline{I}_{\mathrm{J}\,n}(\omega)\, \boldsymbol{u}_n(\boldsymbol{r}') \;, \tag{5.22}$$

$$\underline{\boldsymbol{H}}(\boldsymbol{r}, \omega) = \sum_{m=1}^{M} \underline{I}_{\mathrm{H}\,m}(\omega)\, \boldsymbol{w}_m(\boldsymbol{r}) \;. \tag{5.23}$$

Note that the expansion functions $\boldsymbol{u}_n(\boldsymbol{r}')$ and $\boldsymbol{w}_m(\boldsymbol{r})$ are solely space dependent, while the expansion coefficients $\underline{I}_{\mathrm{J}\,n}(\omega)$ and $\underline{I}_{\mathrm{H}\,m}(\omega)$ only depend on frequency. With this, and with a suitable inner product, we can write (3.113) as

$$\underline{I}_{\mathrm{H}\,m}(\omega) = \sum_{n=1}^{N} \underline{I}_{\mathrm{J}\,n}(\omega) \iiint_V \iiint_{V'} \boldsymbol{w}_m^{\dagger}(\boldsymbol{r})\, \underline{\boldsymbol{G}}_{\mathrm{HJ}}(\boldsymbol{r} - \boldsymbol{r}', \omega)\, \boldsymbol{u}_n(\boldsymbol{r}')\, \mathrm{d}^3 r'\, \mathrm{d}^3 r \;, \tag{5.24}$$

according to section 5.1.1. We summarize the expansion coefficients for the source current density in the vector $\underline{\boldsymbol{I}}_{\mathrm{J}}(\omega)$, the coefficients for the observed magnetic field in the vector $\underline{\boldsymbol{I}}_{\mathrm{H}}(\omega)$, and the numerical propagator in the matrix $\underline{\boldsymbol{M}}(\omega)$. With this, the relation in (5.24) can be simplified to

$$\underline{\boldsymbol{I}}_{\mathrm{H}}(\omega) = \underline{\boldsymbol{M}}(\omega)\, \underline{\boldsymbol{I}}_{\mathrm{J}}(\omega) \;. \tag{5.25}$$

For any discrete set of source points in V' on a grid with x-spacing Δ_x' and y-spacing Δ_y', we use the subsectional expansion functions

$$\boldsymbol{u}_n(\boldsymbol{r}') = \begin{cases} \frac{1}{\Delta_x' \Delta_y'} & \text{for} \quad \boldsymbol{r}' \in U_n \\ 0 & \text{otherwise} \end{cases} \;, \tag{5.26}$$

where U_n is the neighborhood around a grid point $\boldsymbol{r}_n' \in V'$ defined by

$$U_n = \left\{ \boldsymbol{r}' \in \mathbb{R}^3,\, \boldsymbol{r}_n' \in V' : x_n' - \frac{\Delta_x'}{2} \leq x' \leq x_n' + \frac{\Delta_x'}{2} \wedge y_n' - \frac{\Delta_y'}{2} \leq y' \leq y_n' + \frac{\Delta_y'}{2} \wedge z' = 0 \right\} . \tag{5.27}$$

For a discrete set of observation points in V, we use Dirac delta distributions as expansion functions, i.e.

$$\boldsymbol{w}_m(\boldsymbol{r}) = \delta(\boldsymbol{r} - \boldsymbol{r}_m) \;, \qquad \forall \boldsymbol{r}_m \in V \;, \tag{5.28}$$

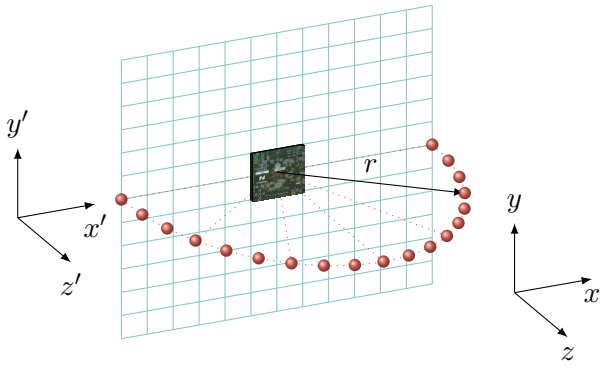

Figure 5.3 Far-field propagation of measured data (from [152]).

which corresponds to the point-matching approximation [137]. Thus, we obtain a free-space numerical Green's propagator $\underline{\boldsymbol{M}}\,(\omega)$ by inserting the expression for $\underline{\boldsymbol{G}}_{\mathrm{HJ}}\,(\boldsymbol{r}-\boldsymbol{r}',\omega)$ from (5.20) into (5.24) and solving the integrals

$$\underline{M}_{mn}\,(\omega) = \frac{1}{4\pi\Delta_x'\Delta_y'} \iiint_{U_n} \left[(\boldsymbol{r}_m - \boldsymbol{r}') \times \mathbf{1}\right] \frac{c_0 + \mathrm{i}\omega\,\|\boldsymbol{r}_m - \boldsymbol{r}'\|}{c_0\,\|\boldsymbol{r}_m - \boldsymbol{r}'\|^3} \mathrm{e}^{-\mathrm{i}\frac{\omega}{c_0}\|\boldsymbol{r}_m - \boldsymbol{r}'\|}\,\mathrm{d}^3 r'\,. \tag{5.29}$$

Using (5.24) and (5.29), we can calculate the magnetic field at each observation point $\boldsymbol{r}_m \in U_m$. The correlation dyadics of the source currents $\boldsymbol{\Gamma}_{\mathrm{J}}\,(\boldsymbol{r}_1', \boldsymbol{r}_2', \omega)$ and the field-field correlation dyadic of the magnetic field $\boldsymbol{\Gamma}_{\mathrm{H}}\,(\boldsymbol{r}_1, \boldsymbol{r}_2, \omega)$ are given by [16]

$$\underline{\boldsymbol{\Gamma}}_{\mathrm{J}}\,(\boldsymbol{r}_1', \boldsymbol{r}_2', \omega) = \left\langle\!\left\langle \underline{\boldsymbol{J}}\,(\boldsymbol{r}_1', \omega)\,\underline{\boldsymbol{J}}^{\dagger}\,(\boldsymbol{r}_2', \omega)\right\rangle\!\right\rangle, \tag{5.30}$$

$$\underline{\boldsymbol{\Gamma}}_{\mathrm{H}}\,(\boldsymbol{r}_1, \boldsymbol{r}_2, \omega) = \left\langle\!\left\langle \underline{\boldsymbol{H}}\,(\boldsymbol{r}_1, \omega)\,\underline{\boldsymbol{H}}^{\dagger}\,(\boldsymbol{r}_2, \omega)\right\rangle\!\right\rangle. \tag{5.31}$$

The correlation dyadic for the observation points $\boldsymbol{r}_1$ and $\boldsymbol{r}_2$ (5.31) can be obtained from the correlation dyadic of the source currents (5.30) according to (3.150) for ergodic fields by

$$\underline{\boldsymbol{\Gamma}}_{\mathrm{H}}\,(\boldsymbol{r}_1, \boldsymbol{r}_2, \omega) = \iiint_{V'} \iiint_{V'} \underline{\boldsymbol{G}}_{\mathrm{HJ}}\,(\boldsymbol{r}_1 - \boldsymbol{r}_1', \omega)\,\underline{\boldsymbol{\Gamma}}_{\mathrm{J}}\,(\boldsymbol{r}_1', \boldsymbol{r}_2', \omega)\,\underline{\boldsymbol{G}}_{\mathrm{HJ}}^{\dagger}\,(\boldsymbol{r}_2 - \boldsymbol{r}_2', \omega)\,\mathrm{d}^3 r_1'\,\mathrm{d}^3 r_2'\,. \tag{5.32}$$

With the numerical propagator from (5.29) and with (5.11) to (5.17), we can calculate the correlations of the magnetic field at the observation points by

$$\underline{\boldsymbol{C}}_{\mathrm{H}}\,(\omega) = \underline{\boldsymbol{M}}\,(\omega)\,\underline{\boldsymbol{C}}_{\mathrm{J}}\,(\omega)\,\underline{\boldsymbol{M}}^{\dagger}\,(\omega)\,, \tag{5.33}$$

with $\underline{\boldsymbol{C}}_{\mathrm{H}}\,(\omega) = \left\langle\!\left\langle \underline{\boldsymbol{I}}_{\mathrm{H}}\,(\omega)\,\underline{\boldsymbol{I}}_{\mathrm{H}}^{\dagger}\,(\omega)\right\rangle\!\right\rangle$ and $\underline{\boldsymbol{C}}_{\mathrm{J}}\,(\omega) = \left\langle\!\left\langle \underline{\boldsymbol{I}}_{\mathrm{J}}\,(\omega)\,\underline{\boldsymbol{I}}_{\mathrm{J}}^{\dagger}\,(\omega)\right\rangle\!\right\rangle$.

By introducing a Huygens surface at the scan plane $z = 0$, the measured near-field data is propagated using the numerical MoM propagator from (5.29), which was implemented in Matlab. The time-domain near-field data is first Fourier transformed and then propagated to a spherical grid of observation points in the far-field at a distance of $r = 3\,\mathrm{m}$. The Fourier transform is necessary since the numerical propagator is given in the frequency-domain, whereas we have recorded time-domain samples. The Fourier transform is calculated according to

$$\underline{I}_{\mathrm{H}\,m}\,(\omega) = \lim_{T\to\infty} \frac{1}{2T} \int_{-T}^{T} I_{\mathrm{H}\,m}\,(t)\,\mathrm{e}^{\mathrm{i}\omega t}\,\mathrm{d}t\,. \tag{5.34}$$

A pure time-domain free-space Green's propagator has been described in [7], [98], and was applied in [7] for propagating correlation information solely in time-domain. We will show an example for time-domain numerical propagation in 5.2. The sample points in the plane $z = 0$ are given by $r = 3\,\mathrm{m}$, $\vartheta = \left[-\frac{\pi}{2}, \frac{\pi}{2}\right]$ in $5°$ steps, and $\varphi = 0°$. The numerical Green's function is evaluated for each source integral and all observation

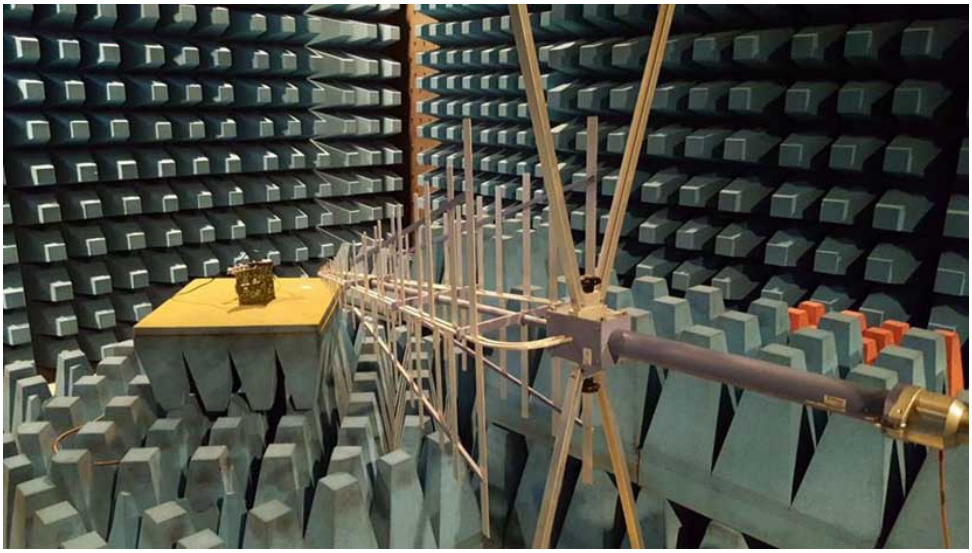

Figure 5.4 The device under test on a rotating table in an anechoic chamber, together with the receiving antenna (from [152]).

points in the frequency-domain, for 131,073 frequency steps. The spatial arrangement of the observation points for the numerical propagation can be seen in Figure 5.3.

The frequency-domain data of the propagated, synchronized, and averaged near-field is then inversely Fourier transformed and correlated with the initial pseudo-random bit sequence. The correlation is given by

$$C_{s_T, I_{\mathrm{H}\,m}}(\tau) = \int_{-\infty}^{\infty} I_{\mathrm{H}\,m}(t)\, s_T(t-\tau)\, \mathrm{d}t\,. \tag{5.35}$$

For comparison, far-field measurements at $3\,\mathrm{m}$ distance are performed inside an anechoic chamber where the DUT is mounted on a rotating table. Figure 5.4 shows the DUT in the anechoic chamber. The angle between the normal to the surface of the PCB and the antenna's axis is rotated from $-90°$ to $90°$ while a reference probe is situated on the opposite side of the PCB. Correlation data which was obtained thereby is shown in Figures 5.5a, 5.5c and 5.5b, 5.5d for horizontal and vertical polarization. One can see good agreement between the correlation coefficients of the measured and the numerically propagated field data. In Figures. 5.5a and 5.5c one can see the angular dependency for the horizontal field component, while in Figures 5.5b and 5.5d no strong angular dependence can be observed.

5.2 Time-Domain Propagation

5.2.1 Time-Domain Green's Functions

In section 3.5, we have introduced the concept of time-domain Green's functions for propagating a known source distribution in a volume V' to an observed field at points in a volume V. We consider electric polarization densities $\boldsymbol{P}_{\mathrm{e}}$ as sources and we observe a magnetic field $\boldsymbol{H}$ at distinct points of interest. The relationship between source polarization density and observed magnetic field is given in terms of a Green's dyadic $\boldsymbol{G}_{\mathrm{HP_e}}$. For propagating correlation dyadics, describing stationary ergodic Gaussian stochastic electromagnetic fields, we consider equation (3.156) in component notation

$$\begin{aligned}\Gamma_{\mathrm{H}\,\mu\nu}(\boldsymbol{r}_1, \boldsymbol{r}_2, \tau) = \sum_{\kappa\in\{x,y,z\}} \sum_{\lambda\in\{x,y,z\}} \iiint_{V'} \iiint_{V'} \int_{-\infty}^{\infty} \int_{-\infty}^{\infty} G_{\mathrm{HP_e}\,\mu\kappa}(\boldsymbol{r}_1 - \boldsymbol{r}_1', \tau'') \times \\ \times\, \Gamma_{\mathrm{P_e}\,\kappa\lambda}(\boldsymbol{r}_1', \boldsymbol{r}_2', \tau - \tau')\, G_{\mathrm{HP_e}\,\nu\lambda}(\boldsymbol{r}_2 - \boldsymbol{r}_2', \tau' - \tau'')\, \mathrm{d}\tau'\, \mathrm{d}\tau''\, \mathrm{d}^3 r_2'\, \mathrm{d}^3 r_1'\,.\end{aligned} \tag{5.36}$$

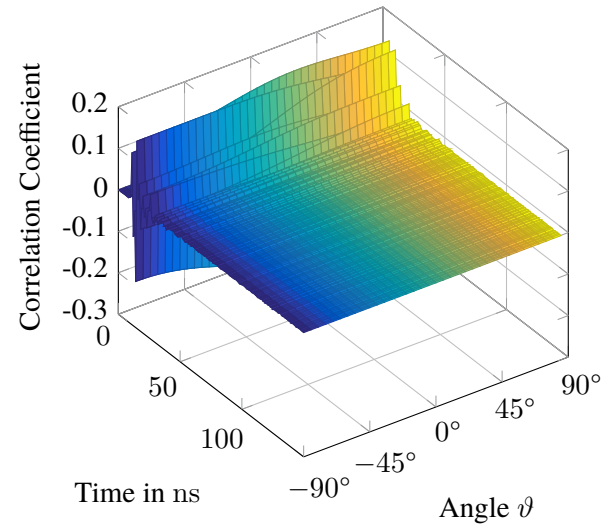

(a) Propagated far-field CCF for horizontal polarization.

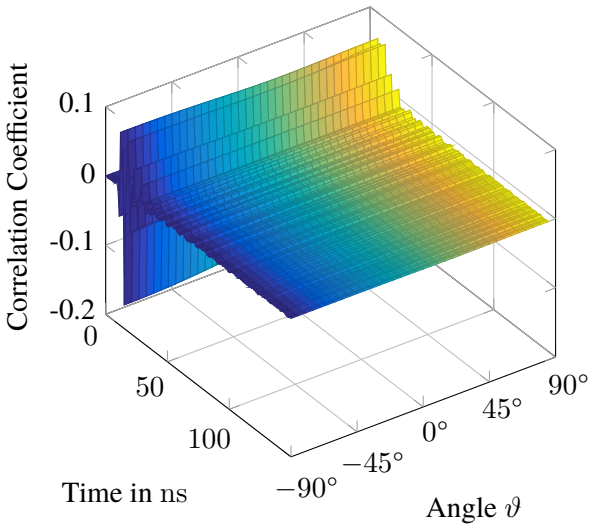

(b) Propagated far-field CCF for vertical polarization.

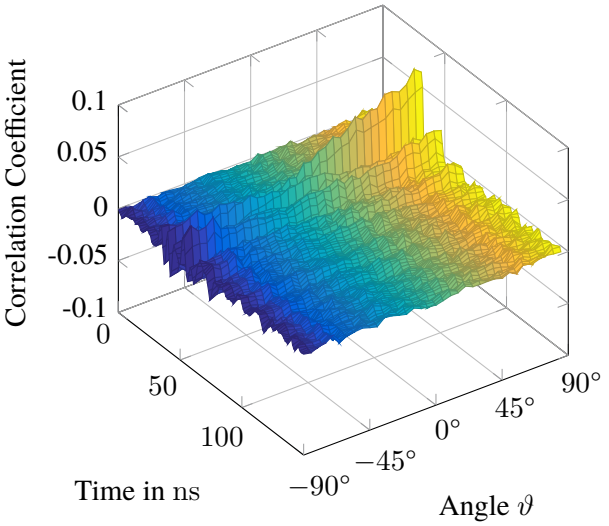

(c) Measured far-field CCF for horizontal polarization.

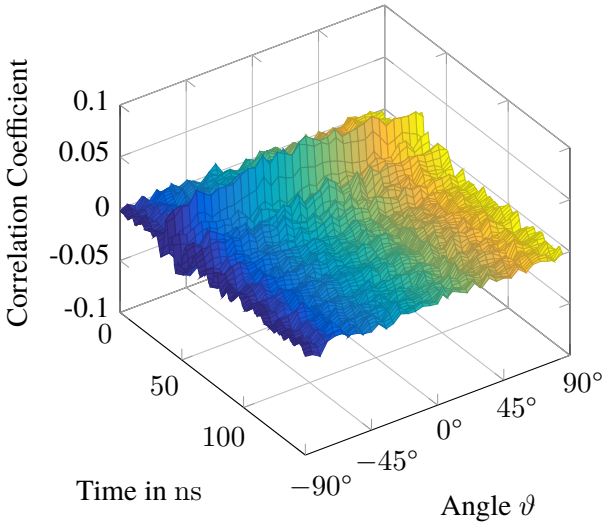

(d) Measured far-field CCF for vertical polarization.

Figure 5.5 Angular distributions of propagated and measured CCF at a distance of 3 m for both polarizations (from [152]).

At least for (wide-sense) stationary fields, where the correlation dyadic is only dependent on the time difference τ, as we described in 3.3, we can define a single rank-4-tensor $K_{\mathrm{HP_e}\,\mu\kappa\lambda\nu}$, describing the propagation of correlation dyadics [7]. We refer to the rank-4-tensor as Green's correlation tensor, which relates the correlation dyadic $\Gamma_{\mathrm{H}\,\mu\nu}$ of the observed field to the correlation dyadic of the source fields $\Gamma_{\mathrm{P_e}\,\mu\nu}$. Note that only a single temporal convolution with the rank-4-tensor $K_{\mathrm{HP_e}\,\mu\kappa\lambda\nu}$ is necessary in order to propagate from the source correlations to the correlation dyadic of the observed field. The Green's correlation tensor is defined by

$$K_{\mathrm{HP_e}\,\mu\kappa\lambda\nu}\left(\boldsymbol{r}_1,\boldsymbol{r}_2,\tau\right) = \int_{-\infty}^{\infty} G_{\mathrm{HP_e}\,\mu\kappa}\left(\boldsymbol{r}_1,\tau'\right) G_{\mathrm{HP_e}\,\nu\lambda}\left(\boldsymbol{r}_2,\tau-\tau'\right)\,\mathrm{d}\tau'\,. \tag{5.37}$$

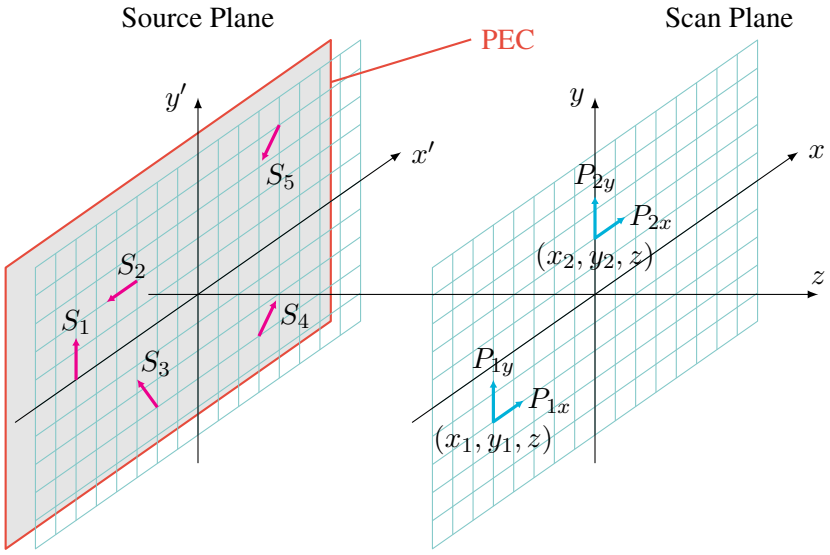

Figure 5.6 Planar array of $N = 5$ stochastic sources sampled at a sampling plane parallel to the source plane (from [7]).

Inserting equation (5.37) into (5.36) results in a correlation propagation scheme exhibiting only a single temporal convolution

$$\Gamma_{\mathrm{H}\,\mu\nu}\left(\boldsymbol{r}_1, \boldsymbol{r}_2, \tau\right) = \sum_{\kappa\in\{x,y,z\}} \sum_{\lambda\in\{x,y,z\}} \iiint_{V'} \iiint_{V'} \int_{-\infty}^{\infty} K_{\mathrm{HP_e}\,\mu\kappa\lambda\nu}\left(\boldsymbol{r}_1 - \boldsymbol{r}_1', \boldsymbol{r}_2 - \boldsymbol{r}_2', \tau'\right) \times$$
$$\times\, \Gamma_{\mathrm{P_e}\,\kappa\lambda}\left(\boldsymbol{r}_1', \boldsymbol{r}_2', \tau - \tau'\right)\, \mathrm{d}\tau'\, \mathrm{d}^3 r_2'\, \mathrm{d}^3 r_1' \,. \tag{5.38}$$

In the following, we consider three examples from [7], which are chosen to demonstrate the time-domain propagation of correlation information, based on Green's functions for polarization densities.

5.2.2 Near-Field Distribution Excited by Sources in a Plane

Figure 5.6 shows an arrangement of $N = 5$ random dipole sources $S_1 \ldots S_5$ located in the plane $z = 0$ at positions $\boldsymbol{r}_\nu = [x_\nu, y_\nu, 0]^{\mathrm{T}}$ with $\nu = 1 \ldots N$. Impressing an electric current $i_\nu(t)$ into the ν-th dipole with a small length l_ν, we can calculate the electric polarization $p_{\mathrm{e}\,\nu}$ of the ν-th dipole by

$$p_{\mathrm{e}\,\nu}(t) = l_\nu \int_0^t i_\nu\left(t'\right)\, \mathrm{d}t' \,. \tag{5.39}$$

Assuming a spherical coordinate system, the orientation of each dipole is characterized by the azimuth and elevation angles φ_ν and ϑ_ν, respectively, with respect to the z-axis. The electric polarization density $\boldsymbol{P}_{\mathrm{e}}(\boldsymbol{r}, t)$ of all dipoles is given by the sum

$$\boldsymbol{P}_{\mathrm{e}}(\boldsymbol{r}, t) = \sum_{\nu=1}^{N} p_{\mathrm{e}\,\nu}(t)\, \boldsymbol{\Omega}_\nu \delta\left(\boldsymbol{r} - \boldsymbol{r}_\nu\right) \,, \tag{5.40}$$

where $\delta(\boldsymbol{r})$ is the three-dimensional Dirac delta distribution. The normalized orientation vector $\boldsymbol{\Omega}_\nu$, given by

$$\boldsymbol{\Omega}_\nu = \begin{bmatrix} \sin\vartheta_\nu \cos\varphi_\nu \\ \sin\vartheta_\nu \sin\varphi_\nu \\ \cos\vartheta_\nu \end{bmatrix} \,, \tag{5.41}$$

describes the angular orientation of the ν-th dipole.

The time-domain correlation dyadic $\mathbf{\Gamma}_{\mathrm{P_e}}\left(\boldsymbol{r}_1, \boldsymbol{r}_2, \tau\right)$ of the stochastic electric polarization density vectors at the locations $\boldsymbol{r}_1$ and $\boldsymbol{r}_2$ is given by

$$\mathbf{\Gamma}_{\mathrm{P_e}}\left(\boldsymbol{r}_1, \boldsymbol{r}_2, \tau\right) = \sum_{\mu=1}^{N} \sum_{\nu=1}^{N} c_{\mathrm{p_e}\,\mu\nu}\left(\tau\right) \mathbf{\Omega}_\mu \mathbf{\Omega}_\nu^{\mathrm{T}} \delta\left(\boldsymbol{r}_1 - \boldsymbol{r}_\mu\right) \delta\left(\boldsymbol{r}_2 - \boldsymbol{r}_\nu\right) , \tag{5.42}$$

with the correlation matrix elements of the electric dipole moments

$$c_{\mathrm{p_e}\,\mu\nu}\left(\tau\right) = \left\langle\!\left\langle p_{\mathrm{e}\,\mu}\left(t\right) p_{\mathrm{e}\,\nu}\left(t-\tau\right)\right\rangle\!\right\rangle . \tag{5.43}$$

Consider an even simpler example with only two point-like electric dipole sources located at $\boldsymbol{r}_- = \left[-a, 0, 0\right]^{\mathrm{T}}$ and $\boldsymbol{r}_+ = \left[a, 0, 0\right]^{\mathrm{T}}$. Let both dipoles be oriented in y-direction such that $\vartheta_\nu = \varphi_\nu = \pi/2$. In this case we obtain $\mathbf{\Omega}_\nu = \left[0, 1, 0\right]^{\mathrm{T}}$ for $\nu \in \{\pm\}$, and hence, the source polarization dyadic $\mathbf{\Gamma}_{\mathrm{P_e}}\left(\boldsymbol{r}_1, \boldsymbol{r}_2, \tau\right)$ exhibits the single component

$$\mathbf{\Gamma}_{\mathrm{P_e}\,yy}\left(\boldsymbol{r}_1, \boldsymbol{r}_2, \tau\right) = \sum_{\mu\in\{\pm\}} \sum_{\nu\in\{\pm\}} c_{\mathrm{p_e}\,\mu\nu}\left(\tau\right) \delta\left(\boldsymbol{r}_1 - \boldsymbol{r}_\mu\right) \delta\left(\boldsymbol{r}_2 - \boldsymbol{r}_\nu\right) . \tag{5.44}$$

It is easy to prove that $c_{\mathrm{p_e}\,\nu\mu}\left(\tau\right) = c_{\mathrm{p_e}\,\mu\nu}\left(-\tau\right)$, by reversing the indices in equation (5.43). For propagating the correlation dyadic of the electric source polarization density $\mathbf{\Gamma}_{\mathrm{P_e}}$ to arbitrary observation points, we consider a propagation scheme as given in (5.38). The resulting electric and magnetic field correlation dyadics are thus obtained by

$$\Gamma_{\mathrm{H}\,\mu\nu}\left(\boldsymbol{r}_1, \boldsymbol{r}_2, \tau\right) = \iiint_{V'} \iiint_{V'} \int_{-\infty}^{\infty} K_{\mathrm{HP_e}\,\mu yy\nu}\left(\boldsymbol{r}_1 - \boldsymbol{r}_1', \boldsymbol{r}_2 - \boldsymbol{r}_2', \tau'\right) \Gamma_{\mathrm{P_e}\,yy}\left(\boldsymbol{r}_1', \boldsymbol{r}_2', \tau - \tau'\right) \mathrm{d}^3 r_1' \, \mathrm{d}^3 r_2' \, \mathrm{d}\tau' , \tag{5.45}$$

$$\Gamma_{\mathrm{E}\,\mu\nu}\left(\boldsymbol{r}_1, \boldsymbol{r}_2, \tau\right) = \iiint_{V'} \iiint_{V'} \int_{-\infty}^{\infty} K_{\mathrm{EP_e}\,\mu yy\nu}\left(\boldsymbol{r}_1 - \boldsymbol{r}_1', \boldsymbol{r}_2 - \boldsymbol{r}_2', \tau'\right) \Gamma_{\mathrm{P_e}\,yy}\left(\boldsymbol{r}_1', \boldsymbol{r}_2', \tau - \tau'\right) \mathrm{d}^3 r_1' \, \mathrm{d}^3 r_2' \, \mathrm{d}\tau' , \tag{5.46}$$

where the non-vanishing Green's Correlation rank-4-tensor components of (5.45) and (5.46) are given by

$$K_{\mathrm{HP_e}\,\mu yy\nu}\left(\boldsymbol{r}_1, \boldsymbol{r}_2, \tau\right) = \int_{-\infty}^{\infty} G_{\mathrm{HP_e}\,\mu y}\left(\boldsymbol{r}_1, \tau'\right) G_{\mathrm{HP_e}\,\nu y}\left(\boldsymbol{r}_2, \tau - \tau'\right) \mathrm{d}\tau' , \tag{5.47}$$

$$K_{\mathrm{EP_e}\,\mu yy\nu}\left(\boldsymbol{r}_1, \boldsymbol{r}_2, \tau\right) = \int_{-\infty}^{\infty} G_{\mathrm{EP_e}\,\mu y}\left(\boldsymbol{r}_1, \tau'\right) G_{\mathrm{EP_e}\,\nu y}\left(\boldsymbol{r}_2, \tau - \tau'\right) \mathrm{d}\tau' . \tag{5.48}$$

The Green's functions in equations (5.47) and (5.48) are given by equations (3.74) and (3.77) for free space. In component notation, these are given by

$$G_{\mathrm{HP_e}\,\mu\kappa}\left(\boldsymbol{r}, \tau\right) = \frac{1}{4\pi} \sum_{\nu\in\{x,y,z\}} \epsilon_{\mu\kappa\nu} r_\nu \left[\frac{1}{\left\|\boldsymbol{r}\right\|^3} \delta'\left(\tau - \frac{\left\|\boldsymbol{r}\right\|}{c_0}\right) - \frac{1}{c_0 \left\|\boldsymbol{r}\right\|^2} \delta''\left(\tau - \frac{\left\|\boldsymbol{r}\right\|}{c_0}\right)\right] , \tag{5.49}$$

$$\begin{aligned} G_{\mathrm{EP_e}\,\mu\kappa}\left(\boldsymbol{r}, \tau\right) = \frac{\mu_0}{4\pi} \sqrt{\frac{\mu_0}{\varepsilon_0}} \Bigg[& \left(\delta_{\mu\kappa} - 3\frac{r_\mu r_\kappa}{\left\|\boldsymbol{r}\right\|^2}\right) \left(\frac{c_0 \delta'\left(\tau - \frac{\left\|\boldsymbol{r}\right\|}{c}\right)}{\left\|\boldsymbol{r}\right\|^2} + \frac{c_0^2 \delta\left(c_0\tau - \left\|\boldsymbol{r}\right\|\right)}{\left\|\boldsymbol{r}\right\|^3}\right) \\ & + \left(\delta_{\mu\kappa} - \frac{r_\mu r_\kappa}{\left\|\boldsymbol{r}\right\|^2}\right) \left(\frac{\delta''\left(\tau - \frac{\left\|\boldsymbol{r}\right\|}{c_0}\right)}{\left\|\boldsymbol{r}\right\|}\right) \Bigg] , \end{aligned} \tag{5.50}$$

where $\epsilon_{\mu\kappa\nu}$ is the Levi-Civita complete antisymmetric tensor exhibiting the value $+1$ if $\mu\kappa\nu$ is an even permutation of $\{x, y, z\}$, the value -1 if $\mu\kappa\nu$ is an odd permutation of $\{x, y, z\}$ and the value 0 if at least two indices are identical.

In the following, we focus on the magnetic field correlations only. Inserting (5.49) into (5.47) and applying the relation

$$\int_{-\infty}^{\infty} \delta^{(m)}\left(t'\right) \delta^{(n)}\left(t - t'\right) \, \mathrm{d}t' = \delta^{((m+n)}\left(t\right) \tag{5.51}$$

for the convolution of the m-th with the n-th derivative of the Dirac delta distribution, we obtain for the Green's correlation rank-4-tensor of the magnetic field

$$\begin{aligned} K_{\mathrm{HP_e}\,\mu y y \nu}\left(\boldsymbol{r}_1, \boldsymbol{r}_2, \tau\right) = & \sum_{\kappa \in \{x,z\}} \sum_{\lambda \in \{x,z\}} \frac{\epsilon_{\mu y \kappa} \epsilon_{\nu y \lambda} r_{1\,\kappa} r_{2\,\lambda}}{16\pi^2 \left\|\boldsymbol{r}_1\right\|^3 \left\|\boldsymbol{r}_2\right\|^3} \left[\delta^{(2)}\left(\tau - \frac{\left|\left\|\boldsymbol{r}_1\right\| - \left\|\boldsymbol{r}_2\right\|\right|}{c_0}\right)\right. \\ & \left. - \frac{\left\|\boldsymbol{r}_1\right\| + \left\|\boldsymbol{r}_2\right\|}{c_0} \delta^{(3)}\left(\tau - \frac{\left|\left\|\boldsymbol{r}_1\right\| - \left\|\boldsymbol{r}_2\right\|\right|}{c_0}\right) + \frac{\left\|\boldsymbol{r}_1\right\| \left\|\boldsymbol{r}_2\right\|}{c_0^2} \delta^{(4)}\left(\tau - \frac{\left|\left\|\boldsymbol{r}_1\right\| - \left\|\boldsymbol{r}_2\right\|\right|}{c_0}\right)\right] . \end{aligned} \tag{5.52}$$

Inserting (5.44) and (5.52) into (5.45) yields

$$\begin{aligned} \Gamma_{\mathrm{H}\,\mu\nu}\left(\boldsymbol{r}_1, \boldsymbol{r}_2, \tau\right) = & \iiint_{V'} \iiint_{V'} \int_{-\infty}^{\infty} \sum_{\kappa \in \{x,z\}} \sum_{\lambda \in \{x,z\}} \frac{\epsilon_{\mu y \kappa} \epsilon_{\nu y \lambda} \left(r_{1\,\kappa} - r'_{1\,\kappa}\right) \left(r_{2\,\lambda} - r'_{2\,\lambda}\right)}{16\pi^2 \left\|\boldsymbol{r}_1 - \boldsymbol{r}'_1\right\|^3 \left\|\boldsymbol{r}_2 - \boldsymbol{r}'_2\right\|^3} \times \\ & \times \left[\delta^{(2)}\left(\tau' - \frac{\left|\left\|\boldsymbol{r}_1 - \boldsymbol{r}'_1\right\| - \left\|\boldsymbol{r}_2 - \boldsymbol{r}'_2\right\|\right|}{c_0}\right)\right. \\ & - \frac{\left\|\boldsymbol{r}_1 - \boldsymbol{r}'_1\right\| + \left\|\boldsymbol{r}_2 - \boldsymbol{r}'_2\right\|}{c_0} \delta^{(3)}\left(\tau' - \frac{\left|\left\|\boldsymbol{r}_1 - \boldsymbol{r}'_1\right\| - \left\|\boldsymbol{r}_2 - \boldsymbol{r}'_2\right\|\right|}{c_0}\right) \\ & \left. + \frac{\left\|\boldsymbol{r}_1 - \boldsymbol{r}'_1\right\| \left\|\boldsymbol{r}_2 - \boldsymbol{r}'_2\right\|}{c_0^2} \delta^{(4)}\left(\tau' - \frac{\left|\left\|\boldsymbol{r}_1 - \boldsymbol{r}'_1\right\| - \left\|\boldsymbol{r}_2 - \boldsymbol{r}'_2\right\|\right|}{c_0}\right)\right] \times \\ & \times \sum_{\xi \in \{\pm\}} \sum_{\eta \in \{\pm\}} c_{\mathrm{p_e}\,\xi\eta}\left(\tau - \tau'\right) \delta\left(\boldsymbol{r}'_1 - \boldsymbol{r}_\xi\right) \delta\left(\boldsymbol{r}'_2 - \boldsymbol{r}_\eta\right) \, \mathrm{d}^3 r'_1 \, \mathrm{d}^3 r'_2 \, \mathrm{d}\tau' . \end{aligned} \tag{5.53}$$

Performing the integration over the primed spatial coordinates $\boldsymbol{r}'_1$ and $\boldsymbol{r}'_2$, we obtain

$$\begin{aligned} \Gamma_{\mathrm{H}\,\mu\nu}\left(\boldsymbol{r}_1, \boldsymbol{r}_2, \tau\right) = & \sum_{\kappa \in \{x,z\}} \sum_{\lambda \in \{x,z\}} \sum_{\xi \in \{\pm\}} \sum_{\eta \in \{\pm\}} \frac{\epsilon_{\mu y \kappa} \epsilon_{\nu y \lambda} \left(r_{1\,\kappa} - r_{\xi\,\kappa}\right) \left(r_{2\,\lambda} - r_{\eta\,\lambda}\right)}{16\pi^2 \left\|\boldsymbol{r}_1 - \boldsymbol{r}_\xi\right\|^3 \left\|\boldsymbol{r}_2 - \boldsymbol{r}_\eta\right\|^3} \times \\ & \times \int_{-\infty}^{\infty} \left[\delta^{(2)}\left(\tau' - \frac{\left|\left\|\boldsymbol{r}_1 - \boldsymbol{r}_\xi\right\| - \left\|\boldsymbol{r}_2 - \boldsymbol{r}_\eta\right\|\right|}{c_0}\right)\right. \\ & - \frac{\left\|\boldsymbol{r}_1 - \boldsymbol{r}_\xi\right\| + \left\|\boldsymbol{r}_2 - \boldsymbol{r}_\eta\right\|}{c_0} \delta^{(3)}\left(\tau' - \frac{\left|\left\|\boldsymbol{r}_1 - \boldsymbol{r}_\xi\right\| - \left\|\boldsymbol{r}_2 - \boldsymbol{r}_\eta\right\|\right|}{c_0}\right) \\ & \left. + \frac{\left\|\boldsymbol{r}_1 - \boldsymbol{r}_\xi\right\| \left\|\boldsymbol{r}_2 - \boldsymbol{r}_\eta\right\|}{c_0^2} \delta^{(4)}\left(\tau' - \frac{\left|\left\|\boldsymbol{r}_1 - \boldsymbol{r}_\xi\right\| - \left\|\boldsymbol{r}_2 - \boldsymbol{r}_\eta\right\|\right|}{c_0}\right)\right] \times \\ & \times c_{\mathrm{p_e}\,\xi\eta}\left(\tau - \tau'\right) \mathrm{d}\tau' . \end{aligned} \tag{5.54}$$

Table 5.1 Cases of Correlation

Fully correlated in-phase	$c^{pe}_{-+}(\tau) = c^{pe}_{+-}(-\tau) = c^{pe}_{++}(\tau)$
Fully correlated anti-phase	$c^{pe}_{-+}(\tau) = c^{pe}_{+-}(-\tau) = -c^{pe}_{++}(\tau)$
Uncorrelated	$c^{pe}_{-+}(\tau) = c^{pe}_{+-}(\tau) = 0$

The resulting correlation dyadic of the magnetic field is finally obtained by performing the integration over τ'. This yields

$$\begin{aligned}\Gamma_{\mathrm{H}\,\mu\nu}(\boldsymbol{r}_1,\boldsymbol{r}_2,\tau) = \sum_{\kappa\in\{x,z\}}\sum_{\lambda\in\{x,z\}}\sum_{\xi\in\{\pm\}}\sum_{\eta\in\{\pm\}} \frac{\epsilon_{\mu y\kappa}\epsilon_{\nu y\lambda}\left(r_{1\,\kappa}-r_{\xi\,\kappa}\right)\left(r_{2\,\lambda}-r_{\eta\,\lambda}\right)}{16\pi^2 r^3_{\xi\mapsto 1} r^3_{\eta\mapsto 2}}\times \\ \times\left[c^{(2)}_{\mathrm{p_e}\,\xi\eta}\left(\tau-\frac{|r_{\xi\mapsto 1}-r_{\eta\mapsto 2}|}{c_0}\right)-\frac{r_{\xi\mapsto 1}+r_{\eta\mapsto 2}}{c_0}c^{(3)}_{\mathrm{p_e}\,\xi\eta}\left(\tau-\frac{|r_{\xi\mapsto 1}-r_{\eta\mapsto 2}|}{c_0}\right)\right. \\ \left.+\frac{r_{\xi\mapsto 1}r_{\eta\mapsto 2}}{c_0}c^{(4)}_{\mathrm{p_e}\,\xi\eta}\left(\tau-\frac{|r_{\xi\mapsto 1}-r_{\eta\mapsto 2}|}{c_0}\right)\right], \end{aligned} \tag{5.55}$$

with the propagation distance functionals $r_{\xi\mapsto 1} = \|\boldsymbol{r}_1-\boldsymbol{r}_\xi\|$ and $r_{\eta\mapsto 2} = \|\boldsymbol{r}_2-\boldsymbol{r}_\eta\|$. Due to the sparsity of the resulting matrices, the sums over the Levi-Civita symbols can be simplified to

$$\begin{aligned}\sum_{\kappa\in\{x,z\}}\sum_{\lambda\in\{x,z\}}\epsilon_{\mu y\kappa}\epsilon_{\nu y\lambda}\left(r_{1\,\kappa}-r_{\xi\,\kappa}\right)\left(r_{2\,\lambda}-r_{\eta\,\lambda}\right) &= \delta_{\mu x}\delta_{\mu x}\left(r_{1\,x}-r_{\xi\,x}\right)\left(r_{2\,x}-r_{\eta\,x}\right) \\ &\quad-\delta_{\mu x}\delta_{\mu z}\left(r_{1\,x}-r_{\xi\,x}\right)\left(r_{2\,z}-r_{\eta\,z}\right) \\ &\quad-\delta_{\mu z}\delta_{\mu x}\left(r_{1\,z}-r_{\xi\,z}\right)\left(r_{2\,x}-r_{\eta\,x}\right) \\ &\quad+\delta_{\mu z}\delta_{\mu z}\left(r_{1\,z}-r_{\xi\,z}\right)\left(r_{2\,z}-r_{\eta\,z}\right). \end{aligned} \tag{5.56}$$

With this, we can now write equation (5.55) in matrix-vector notation as

$$\begin{aligned}\boldsymbol{\Gamma}_{\mathrm{H}}(\boldsymbol{r}_1,\boldsymbol{r}_2,\tau) = \sum_{\xi\in\{\pm\}}\sum_{\eta\in\{\pm\}}\frac{1}{16\pi^2 r^3_{\xi\mapsto 1} r^3_{\eta\mapsto 2}}\left[c^{(2)}_{\mathrm{p_e}\,\xi\eta}\left(\tau-\frac{|r_{\xi\mapsto 1}-r_{\eta\mapsto 2}|}{c_0}\right)\right. \\ \left.-\frac{r_{\xi\mapsto 1}+r_{\eta\mapsto 2}}{c_0}c^{(3)}_{\mathrm{p_e}\,\xi\eta}\left(\tau-\frac{|r_{\xi\mapsto 1}-r_{\eta\mapsto 2}|}{c_0}\right)+\frac{r_{\xi\mapsto 1}r_{\eta\mapsto 2}}{c_0}c^{(4)}_{\mathrm{p_e}\,\xi\eta}\left(\tau-\frac{|r_{\xi\mapsto 1}-r_{\eta\mapsto 2}|}{c_0}\right)\right]\times \\ \times\begin{bmatrix}\left(r_{1\,x}-r_{\xi\,x}\right)\left(r_{2\,x}-r_{\eta\,x}\right) & 0 & -\left(r_{1\,x}-r_{\xi\,x}\right)\left(r_{2\,z}-r_{\eta\,z}\right)\\ 0 & 0 & 0\\ -\left(r_{1\,z}-r_{\xi\,z}\right)\left(r_{2\,x}-r_{\eta\,x}\right) & 0 & \left(r_{1\,z}-r_{\xi\,z}\right)\left(r_{2\,z}-r_{\eta\,z}\right)\end{bmatrix}. \end{aligned} \tag{5.57}$$

Let us assume both sources to be Gaussian noise sources. We will consider three cases of correlation between the two sources according to Table 5.1. Using equation 5.57 on the correlation matrices of two Gaussian noise processes, one for each source at $\boldsymbol{r}_\pm$, we can compute $\boldsymbol{\Gamma}_{\mathrm{H}}(\boldsymbol{r}_1,\boldsymbol{r}_2,\tau)$ numerically. The expectation value of the magnetic energy density is given by the trace of $\boldsymbol{\Gamma}_{\mathrm{H}}(\boldsymbol{r}_1,\boldsymbol{r}_2,\tau)$ as

$$\left\langle\!\left\langle W_{\mathrm{mag}}(\tau)\right\rangle\!\right\rangle = \frac{\mu}{2}\left\langle\!\left\langle \boldsymbol{H}^2(\boldsymbol{r},t)\right\rangle\!\right\rangle = \frac{\mu}{2}\mathrm{Tr}\left(\boldsymbol{\Gamma}_{\mathrm{H}}(\boldsymbol{r},\boldsymbol{r},\tau)\right). \tag{5.58}$$

The angular distribution of the auto-correlation functions of the field observed in this numerical example is plotted in Figure 5.7. Here it was assumed that $a = 2.5\,\mathrm{cm}$, and the field was observed over the azimuth angle θ at a distance of $r = 15\,\mathrm{cm}$ from the origin (see also Figure 5.6). The source field is generated by Gaussian noise which was sampled at a sampling rate of $10\,\mathrm{GS\,s^{-1}}$. As expected, values for the auto-correlation function exhibit a maximum for $\tau = 0$, $\theta = 0°$ for the case of fully in-phase correlated noise, a minimum for the case of anti-phase correlated sources, and an intermediate value for uncorrelated sources.

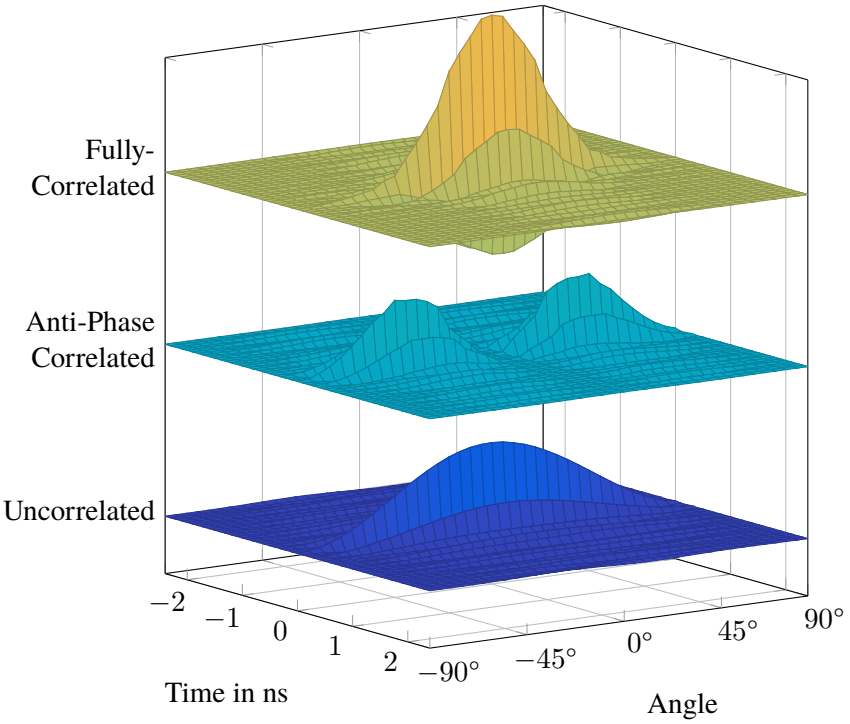

Figure 5.7 Angular distribution of the auto-correlation function at a distance of $15\,\mathrm{cm}$ for the case of correlated in-phase, correlated anti-phase, and uncorrelated sources (from [7]).

5.2.3 Plane Wave Incident on a Circular Sensor Array

As our next example, we consider a plane wave incident on a circular array of $m = 6$ sensors, denoted by $A_1 \ldots A_m$ as depicted in Figure 5.8. This example is similar to the one presented in [154]. Figures 5.9a and 5.9b show the auto-correlation spectrum and the auto-correlation function of a stationary Gaussian noise wave with the spectrum centered around the frequency f_0 and the variances $\sigma_t f_0 = 2$ and $\sigma_t f_0 = 10$, respectively. For the spectrum of the Gaussian random process, we assume a Gaussian-shaped spectrum centered around the frequency f_0, which can be described by the auto-correlation spectrum and by the auto-correlation function

$$\underline{C}_{\mathrm{E}\,xx}(f) = \frac{1}{2}\sqrt{\pi}\sigma_t C_0 \left[\mathrm{e}^{-(f-f_0)^2\sigma_t^2} + \mathrm{e}^{-(f+f_0)^2\sigma_t^2}\right], \tag{5.59}$$

$$c_{\mathrm{E}\,xx}(\tau) = C_0 \cos(2\pi f_0 \tau)\, \mathrm{e}^{\frac{-\tau^2}{\sigma_t^2}}. \tag{5.60}$$

Antenna diagrams for an incident harmonic plane wave with frequency $f_0 = c_0/a$ and incident Gaussian noise plane waves with center frequency $f_0 = c_0/a$ and variable spectral width are shown in Figure 5.10. In the remainder of this example, the radius of the circular sensor array is chosen to $a = 60\,\mathrm{cm}$. The incident wave represents a random wireless data transmission at a center frequency of $2.4\,\mathrm{GHz}$. A QPSK modulated random bit sequence, representing the payload data, is combined with a deterministic frame header and transmit-filtered with a root raised cosine pulse-shape filter to form the transmit data stream [155]. A signal source is modeled as a point source at a distance of $1000\,\mathrm{m}$ from the array center, where the polarization density of the point source is the up-converted data stream with normalized signal amplitude. Two realizations of the QPSK-modulated, transmit-filtered and up-converted data stream are depicted in Figure 5.11. The sensed electromagnetic signals at the elements of the circular array are computed by equation (3.73), and the signal correlations by equation (3.156), respectively. The signals $s_{m\,T}(t)$ at the sensors are summarized in a signal vector $\boldsymbol{s}_T(t)$. The index $_T$ denotes time-windowing of the signal [107], as discussed earlier in subsection 3.6.3.

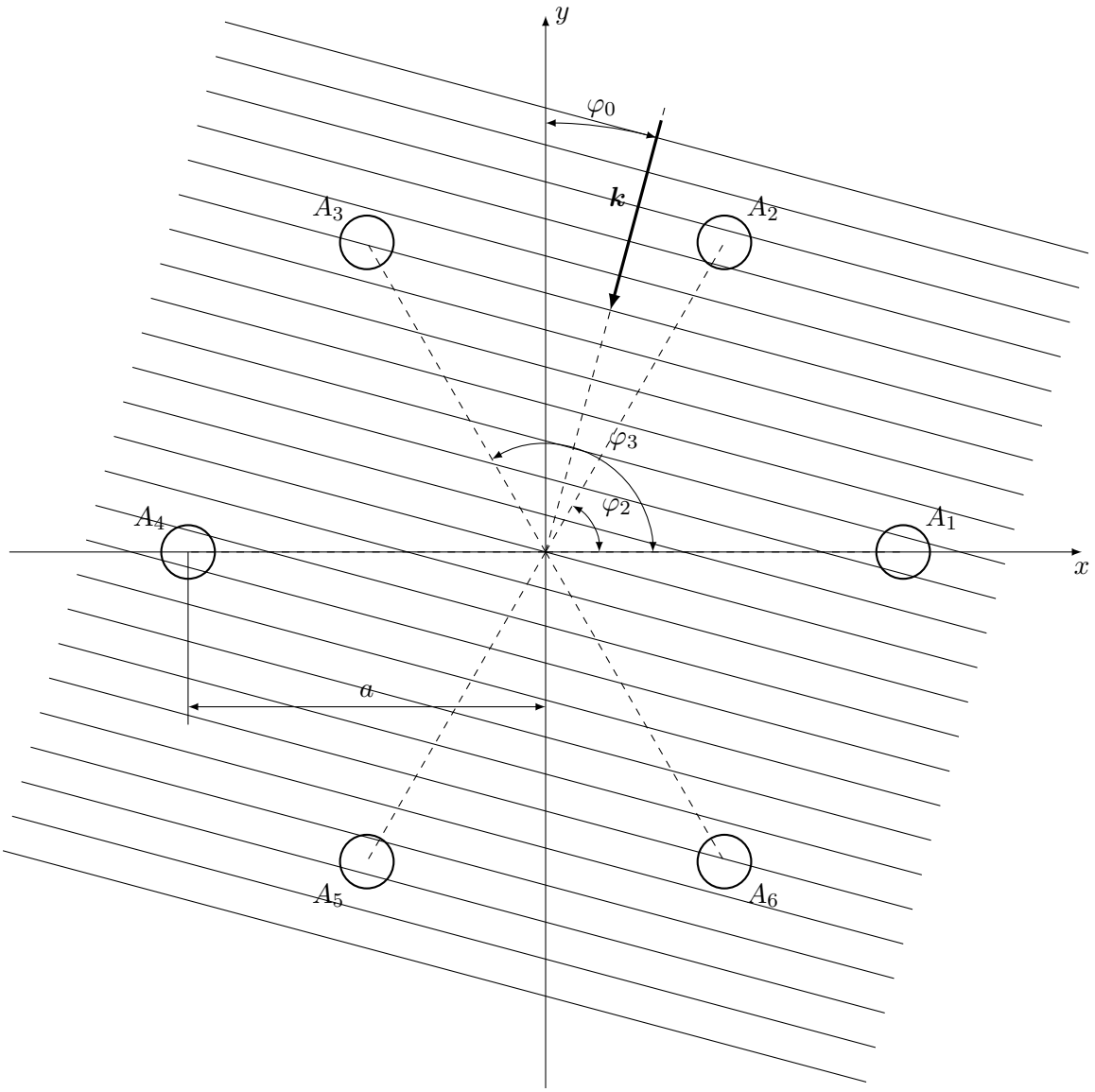

Figure 5.8 Circular antenna array with $m = 6$ sensors. The sensors are organized in a hexagonal shape, where the outer radius is given by a. Plane waves are incident to the array at an angle of φ_0.

We implement a time-domain steering vector matrix as [154]

$$\boldsymbol{a}\left(t, \varphi_1, \ldots, \varphi_m\right) = \begin{bmatrix} \delta\left(t-\tau_{11}\right) & \delta\left(t-\tau_{12}\right) & \cdots & \delta\left(t-\tau_{1m}\right) \\ \delta\left(t-\tau_{21}\right) & \delta\left(t-\tau_{22}\right) & \cdots & \delta\left(t-\tau_{2m}\right) \\ \vdots & \vdots & \ddots & \vdots \\ \delta\left(t-\tau_{n1}\right) & \delta\left(t-\tau_{n2}\right) & \cdots & \delta\left(t-\tau_{nm}\right) \end{bmatrix}, \tag{5.61}$$

where $\tau_{\mu\nu} = \tau_a\left(\cos\varphi_\mu - \cos\varphi_\nu\right)$, $\tau_a = a/c_0$, φ_μ is the steering angle, and φ_ν is the angle attributed to the m-th sensor element. With this steering matrix implemented, we obtain an antenna output vector

$$\boldsymbol{v}_T\left(t\right) = \int_{-\infty}^{\infty} \boldsymbol{a}\left(t-\tau, \varphi_1, \ldots, \varphi_m\right) \boldsymbol{s}_T\left(\tau\right)\, \mathrm{d}\tau\,. \tag{5.62}$$

The correlation function of the antenna signals $v_{\nu T}\left(t\right)$ and $v_{\kappa T}\left(t\right)$ is given by

$$c_{\mathrm{v}\,\nu\kappa}\left(\tau\right) = \lim_{T\to\infty} \frac{1}{2T} \int_{-\infty}^{\infty} v_{\nu T}\left(t\right) v_{\kappa T}\left(t-\tau\right)\, \mathrm{d}t\,, \tag{5.63}$$

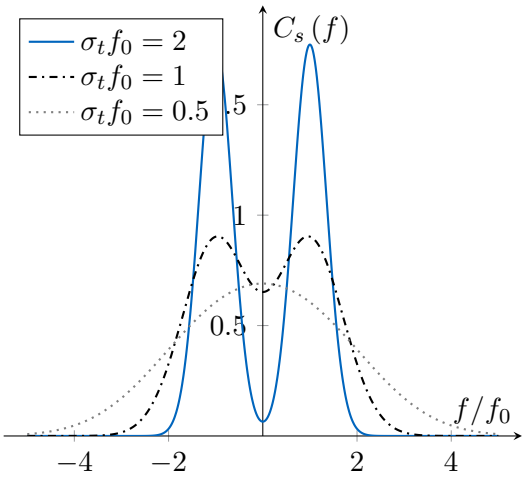

(a) Auto-correlation spectrum of a stationary Gaussian noise wave.

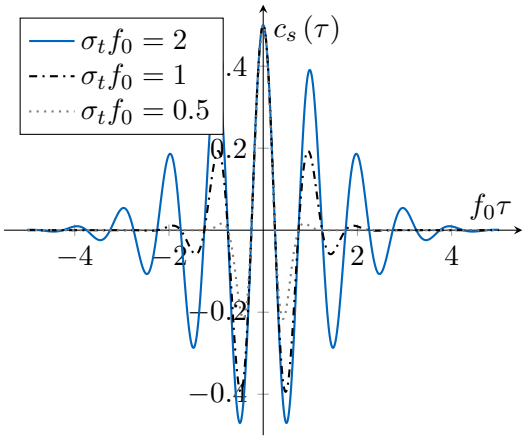

(b) Auto-correlation function of a stationary Gaussian noise wave.

Figure 5.9 Auto-correlation spectrum and auto-correlation function of a Gaussian noise wave. Both, spectrum and correaltion function are plotted for variances of $\sigma_t f_0 = 0.5$, $\sigma_t f_0 = 1$, and $\sigma_t f_0 = 2$ (from [7]).

and the time-domain steering vector matrix is given by

$$\boldsymbol{a}\left(t, \varphi_1, \ldots, \varphi_m\right) = \left[\boldsymbol{a}_1\left(t, \varphi_1\right), \ldots, \boldsymbol{a}_m\left(t, \varphi_m\right)\right] , \tag{5.64}$$

with the time-domain steering vectors

$$\boldsymbol{a}_\mu\left(t, \theta_\mu\right) = \begin{bmatrix} \delta\left(t - \tau_a\left(\cos\varphi_\mu - \cos\varphi_1\right)\right) \\ \delta\left(t - \tau_a\left(\cos\varphi_\mu - \cos\varphi_2\right)\right) \\ \vdots \\ \delta\left(t - \tau_a\left(\cos\varphi_\mu - \cos\varphi_n\right)\right) \end{bmatrix} . \tag{5.65}$$

In two example cases, a single QPSK source, located at an angle of 120°, is excited, or two QPSK sources with different, independent data streams, located at the angles 45° and 270°, are excited. The observed auto-correlation function according to equation (5.63), for changing steering angles φ_μ, is assessed. The maximum of the auto-correlation function shows the direction of arrival of the incident wave, as shown in Figure 5.12. It is shown that the maximum in the auto-correlation function over all steering angles clearly identifies the direction of the source.

5.2.4 Propagation of Field Correlation

In an experimental setup, we have computed cross-correlations pertaining to the far-field from experimental near-field scanning data of a digital circuit board under test, an Atlys Spartan-6 board, and compared it to cross-correlations obtained from measurements performed directly in the far-field. Measurements for the far-field were taken in an anechoic chamber [152]. The presented time-domain propagator for field correlations has been applied to the scanned near-field data, in order to predict the measured far-field cross-correlations. For the far-field measurements in the anechoic chamber, a reference probe was placed close to the device under test (DUT) for obtaining a synchronization signal of the cyclostationary process occurring on the board. Using this reference signal, we can synchronize the obtained far-field measurement curves and perform cyclic averaging with the cycle period of the underlying cyclostationary process. Cross-correlations are formed with a known pseudo-random bit sequence governing the data transfer process on the device under test. Figure 5.13 shows the angular dependence of the cross-correlation function (CCF) obtained from numerically propagated far-field observations with the reference pseudo-random bit sequence and cross-correlations obtained with measured far-field data. Both, the measured and the numerically propagated CCFs plotted show a qualitatively good

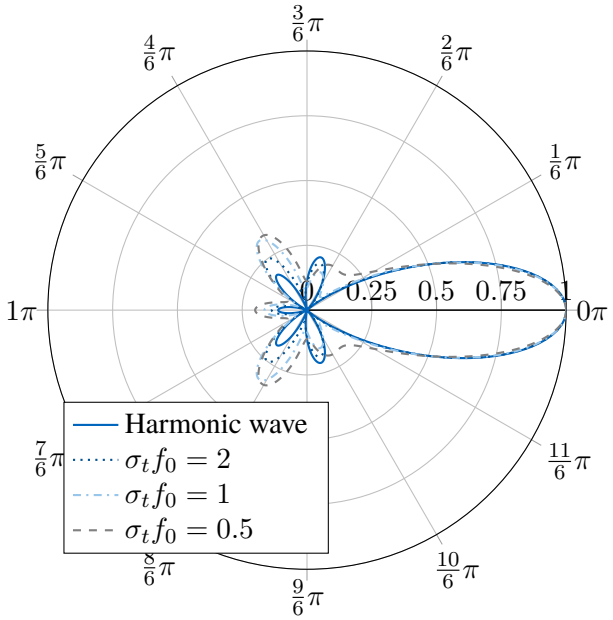

Figure 5.10 Antenna diagrams of an incident plane wave with frequency $f_0 = c_0/a$, and incident Gaussian noise plane waves with Gaussian spectrum, centered around the frequency $f_0 = c_0/a$ with spectral widths $\sigma_t f_0 = 2$, $\sigma_t f_0 = 1$, and $\sigma_t f_0 = 0.5$.

agreement, while their magnitudes deviate, which may be attributed to the fact that cables have not been de-embedded and probe compensation for the logarithmic periodic sensing antenna has not been taken into account in these measurements.

5.2.5 Correlation Transmission Line Matrix Method (CTLM)

The correlation transmission line matrix (CTLM) method for numerical propagation of stochastic electromagnetic fields is an extension to the discrete-time transmission line matrix (TLM) method [21], [22], which is a well established numerical method for solving Maxwell's equations [156]. The TLM method relies on the analogy between electromagnetic fields, propagating in space and time, and voltages and currents propagating through a mesh of transmission lines [157]. Based on this analogy, the TLM method has been first proposed in [158]. It has been shown in [151], that the TLM method can be derived by expanding Maxwell's equations at the boundary surfaces into a set of triangular basis functions for the time coordinate and for the tangential spatial coordinates, and into step functions for the perpendicular spatial coordinate, respectively. Field samples can be taken in the center of the boundary surface, which is referred to as finite difference approximation, or by taking an average over a certain surface area, which is called finite integration approximation [83]. For simplicity, we assume free-space propagation in the following, although the TLM scheme is general enough to treat arbitrary geometries with different material parameters. Material parameters and losses are incorporated by loading each TLM node with a certain load impedance Z and modifying the scattering matrix $\boldsymbol{S}$ in each node accordingly [156].

The three-dimensional condensed node [151], used in TLM, is depicted in Figure 5.14. In TLM, one considers twelve wave-amplitudes, incident at each node, summarized in a vector $\boldsymbol{a}$, and twelve scattered wave-amplitudes, summarized in a vector $\boldsymbol{b}$. The wave-amplitudes are mapped to the electric and magnetic field vectors using the cell-boundary-mapping introduced in [151]. The cell-boundary-mapping ensures a bijective one-to-one mapping between the twenty-four tangential electric and magnetic field components sampled at the six boundary surfaces of a TLM cell and the twenty-four wave pulse amplitudes incident on the respective TLM node and scattered from it.

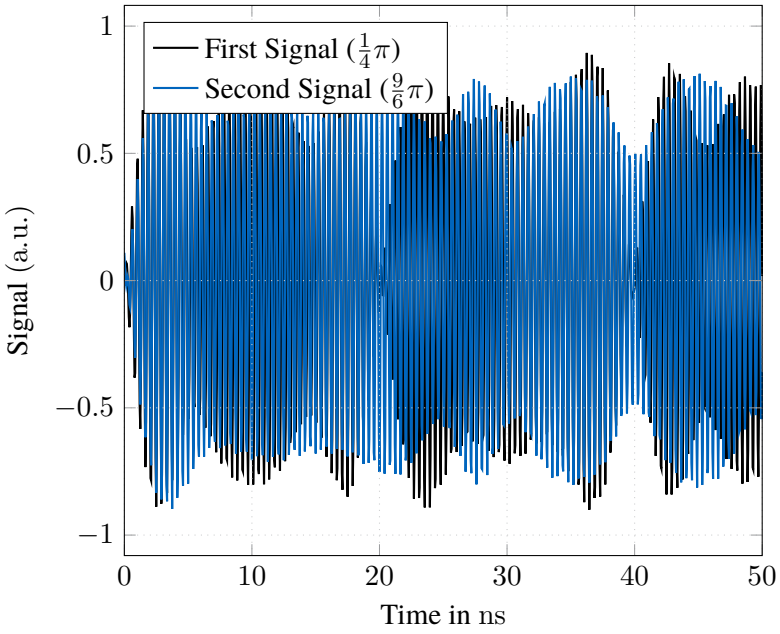

Figure 5.11 Two realizations of the incident QPSK modulated signals, generated from pseudo-random bit sequences. The first signal is incident at an angle of $\frac{1}{4}\pi$ and the second signal generates an incident wave at an angle of $\frac{9}{6}\pi$ (from [7]).

Now let $x\,[n]$ denote a discrete-time signal given by the sampled values of the signal at time instances nT_S, where T_S is the sampling rate of the sampled real signal s. The correlation function of two time-discrete signals $x_i\,[n]$ and $x_j\,[n]$ is given by

$$c_{ij}^{x}\,[n, n+m] = \langle\!\langle x_i\,[n]\, x_j\,[n+m] \rangle\!\rangle\,. \tag{5.66}$$

For stationary ergodic processes, as we will consider in the following, the correlation function $c_{ij}^{x}\,[n, n+m]$ is independent of the absolute time argument nT_s, as can be easily verified as a consequence of Definition 2.28. For ergodic processes (Definition 2.32), the ensemble average is identical to the time average of a finite sequence of time samples. Hence we can write

$$c_{ij}^{x}\,[m] = \langle\!\langle x_i\,[n]\, x_j\,[n+m] \rangle\!\rangle = \lim_{N\to\infty} \frac{1}{2N-1} \sum_{n=-N}^{N} x_i\,[n]\, x_j\,[n+m]\;. \tag{5.67}$$

For a time-discrete linear shift invariant (LSI) system, the output signal $y_i\,[n]$ is obtained from the input signal $x_j\,[n]$ by discrete convolution with the impulse response $h_{ij}\,[n]$. Hence, correlations of the signals at the output side are obtained from correlations at the input boundary by means of the correlation transfer function [21]

$$k_{pq\,rs}^{y}\,[l] = \sum_{k=-\infty}^{\infty} h_{pr}\,[k]\, h_{qs}\,[l+k]\;. \tag{5.68}$$

The propagation of correlation information between two arbitrary spatial nodes p and q is then obtained from the correlations at the boundary nodes r and s by

$$c_{pq}^{y}\,[m] = \sum_{l=-\infty}^{\infty} k_{pq\,rs}\,[l]\, c_{rs}^{x}\,[m-l]\;. \tag{5.69}$$

In terms of the TLM method, these correlation transfer functions $k_{pq\,rs}$ can be obtained by a numerical propagation of wave pulses in a Cartesian mesh of nodes similar, to Figure 5.14. The incident wave pulses on all faces of all nodes can be summarized in a Hilbert space vector ${}_k|\boldsymbol{a}\rangle$, given by [159]

$${}_k|\boldsymbol{a}\rangle = \sum_{l=-\infty}^{\infty} \sum_{m=-\infty}^{\infty} \sum_{n=-\infty}^{\infty} {}_k[a_1, a_2, \ldots, a_{12}]_{l,m,n}^{\mathrm{T}}\; {}_k|l, m, n\rangle\;, \tag{5.70}$$

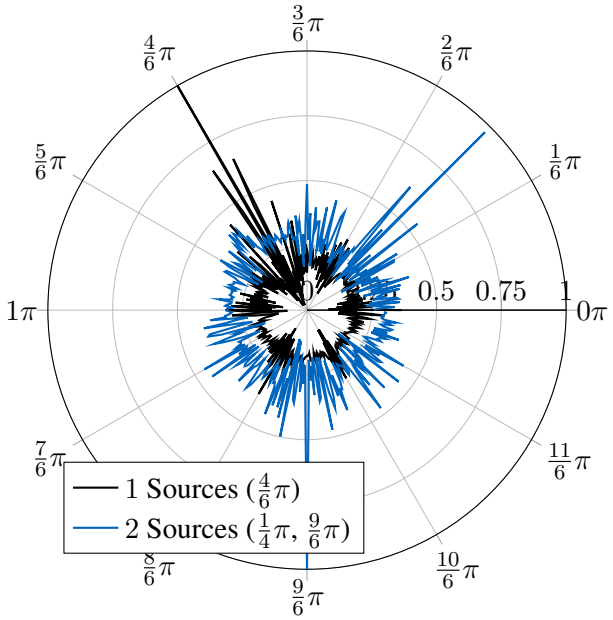

Figure 5.12 Auto-correlation function for changing steering angles. The black curve shows the direction of arrival of a single random QPSK-modulated signal in the direction of 120°. The blue curve shows the obtained auto-correlation functions for two random sources, located at 45° and 270° (from [7]).

where k represents the time step, and l, m, and n represent three-dimensional spatial node indices [159]. Similarly, one can define Hilbert space vectors for all scattered waves at all nodes ${}_k|\boldsymbol{b}\rangle$, given by

$$ {}_k|\boldsymbol{b}\rangle = \sum_{l=-\infty}^{\infty} \sum_{m=-\infty}^{\infty} \sum_{n=-\infty}^{\infty} {}_k[b_1, b_2, \ldots, b_{12}]^{\mathrm{T}}_{l,m,n} \; {}_k|l, m, n\rangle \;, \tag{5.71} $$

The spatial connection of neighboring nodes is modeled by a connection operator $\boldsymbol{\Gamma}$, which connects the scattered waves at one node to the incident waves of the adjacent nodes. The scattering process itself is given by the scattering operator $\boldsymbol{S}$, which models the transformation of incident waves into scattered waves in each TLM

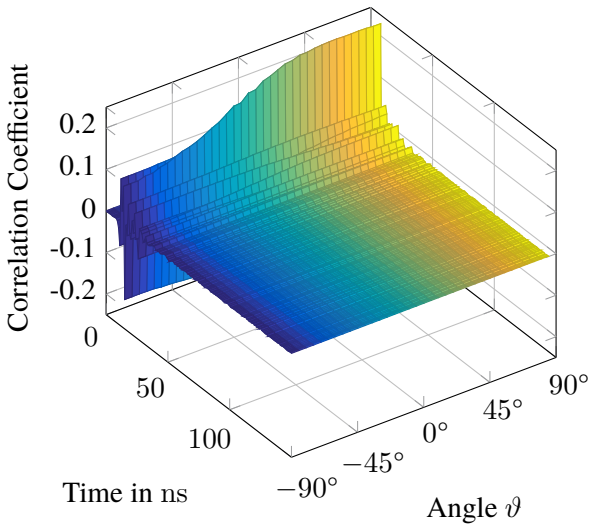

(a) Propagated far-field CCF for horizontal polarization.

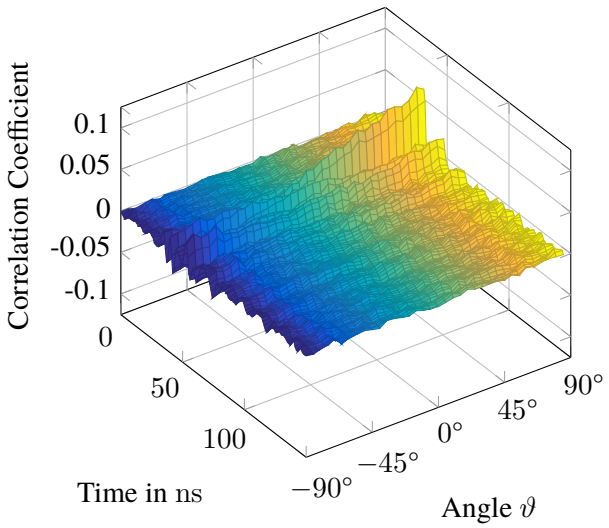

(b) Measured far-field CCF for horizontal polarization.

Figure 5.13 Angular distributions of propagated and measured CCF at 3 m distance for horizontal polarization (from [7]).

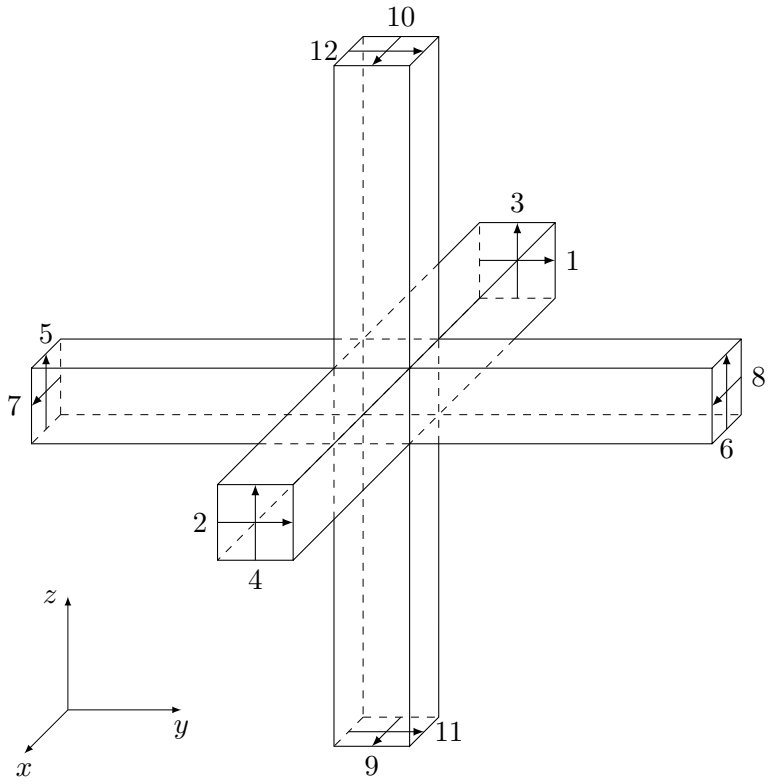

Figure 5.14 TLM unit cell.

node, depending on the respective material parameters. Altogether, the TLM propagation scheme can thus be written as

$$ {}_{k+1}|\boldsymbol{b}\rangle = \boldsymbol{S}_{\,k}|\boldsymbol{a}\rangle \ , \tag{5.72} $$

$$ {}_{k}|\boldsymbol{a}\rangle = \boldsymbol{\Gamma}_{\,k}|\boldsymbol{b}\rangle \ . \tag{5.73} $$

The propagation of pulses of wave amplitudes through the TLM mesh yields a discrete Green's function, also called John's matrix, which relates the wave pulses $\boldsymbol{a}\,[n_i; k']$ incident on a boundary port n_i, at time k' to scattered wave pulses $\boldsymbol{b}\,[l, m, n; k]$, observed at arbitrary observation points given by the spatial node indices l, m, n at time k [160]. Here, $B = \{n_1, n_2, \ldots, n_N\}$ is a set of N boundary nodes, each described by node indices l', m', n'. The discrete-time auto-correlation and cross-correlation functions are obtained similar to (5.68), and are furthermore related to each other through the CTLM method [21] via discrete-time correlation Green's functions $K_{ij\,rs}\,[p]$ by

$$ c^{b}_{ij}\,[q] = \sum_{n_r, n_s \in B} \sum_{p=-\infty}^{\infty} K_{ij\,rs}\,[p]\, c^{a}_{rs}\,[q-p] \ , \tag{5.74} $$

with the correlation Green's function $K_{ij\,pq}$, given as

$$ K_{ij\,pq}\,[k] = \sum_{k'=-\infty}^{\infty} G_{i\,p}\left[k'\right] G_{j\,q}\left[k'+k\right] \ . \tag{5.75} $$

5.3 Phase-Space Approach

5.3.1 Phase-Space Representation of Electromagnetic Fields

Another interesting approach for propagating correlation information of wide-sense stationary stochastic electromagnetic fields (according to Definition 2.29) is given in terms of Wigner distribution functions in phase-space [17], [161]. Using Wigner distribution functions for propagating correlation information of stochastic

electromagnetic fields was first proposed by Gradoni, Creagh, Tanner, *et al.* [17], and proved to be a good approximate method for predicting correlations on different observation planes in the ray-tracing limit [23].

Nevertheless, one must treat this method as an approximate one, as evanescent components may be included by a leading order approximation of the phase-space diffusion [162], whereas a MoM-based numerical propagator directly provides a solution including all the near-field contributions. Also, a numerical propagator based on numerical Green's functions, obtained by the generalized Moments method can be easily computed for arbitrary geometries and materials. However, the phase-space method can be used to reveal directional information on the propagation of electromagnetic energy, which is an added value in the analysis of stochastic electromagnetic fields.

So far, our goal was to find a parametric description of ergodic wide-sense stationary random fields in terms of mean value functions and correlation dyadics. This was done by specifying the tangential field components of radiated electromagnetic fields at a boundary surface ∂V close to a device under test, and thus, by Theorem 3.1 being able to reconstruct the field distribution, and hence the statistical parameters, in the source-free volume V, excluding the source region, i.e. the device under test. For the phase-space approach, we consider only planar boundary surfaces of infinite extent, where we investigate how the correlation information will propagate to other observation planes parallel to the source plane. We implicitly made the assumption of distinct parallel source and observation planes in section 4.4, but the phase-space method explicitly makes use of the fact that correlations are only measured on parallel planes from a theoretical point of view. Suppose that we have field samples of a random magnetic field $\underline{\boldsymbol{H}}$, given in frequency-domain, measured on a two-dimensional spatial sampling grid at locations $\boldsymbol{r} \in \mathbb{R}^2$ in a plane at height $z = 0$. The spatial correlations on any z-plane are given by

$$\underline{\boldsymbol{\Gamma}}_{\mathrm{H}}\left(\boldsymbol{r}_1, \boldsymbol{r}_2, z, \omega\right) = \left\langle\!\left\langle \underline{\boldsymbol{H}}\left(\boldsymbol{r}_1, z, \omega\right) \underline{\boldsymbol{H}}^{\dagger}\left(\boldsymbol{r}_2, z, \omega\right)\right\rangle\!\right\rangle . \tag{5.76}$$

The magnetic field $\underline{\boldsymbol{H}}$ at an arbitrary plane $z > 0$ can be represented in phase-space by a partial spatial Fourier transform [17]

$$\tilde{\boldsymbol{H}}\left(\boldsymbol{p}, z, \omega\right) = \iint_A \mathrm{e}^{-\mathrm{i}k\boldsymbol{p}\cdot\boldsymbol{r}} \underline{\boldsymbol{H}}\left(\boldsymbol{r}, z, \omega\right) \cdot \mathrm{d}\boldsymbol{r} , \tag{5.77}$$

where $k = \sqrt{k_x^2 + k_y^2}$ is the wave number. The respective partial inverse Fourier transform, to retrieve the fields from the phase-space representation is given by

$$\underline{\boldsymbol{H}}\left(\boldsymbol{r}, z, \omega\right) = \left(\frac{k}{2\pi}\right)^2 \iint_A \mathrm{e}^{\mathrm{i}k\boldsymbol{p}\cdot\boldsymbol{r}} \tilde{\boldsymbol{H}}\left(\boldsymbol{p}, z, \omega\right) \cdot \mathrm{d}\boldsymbol{p} . \tag{5.78}$$

In the plane-wave limit, where no evanescent components are present, we can calculate a momentum representation of the magnetic field $\tilde{\boldsymbol{H}}$ from the boundary conditions, given in terms of measured field samples on the plane $z = 0$ at any distance z by

$$\tilde{\boldsymbol{H}}\left(\boldsymbol{p}, z, \omega\right) = \mathrm{e}^{\mathrm{i}kzT(\boldsymbol{p})} \tilde{\boldsymbol{H}}\left(\boldsymbol{p}, 0, \omega\right) , \tag{5.79}$$

with

$$T\left(\boldsymbol{p}\right) = \begin{cases} \sqrt{1 - |\boldsymbol{p}|^2} & \text{for} \quad |\boldsymbol{p}|^2 \leq 1 \\ \mathrm{i}\sqrt{|\boldsymbol{p}|^2 - 1} & \text{for} \quad |\boldsymbol{p}|^2 > 1 \end{cases} . \tag{5.80}$$

Note that the case $|\boldsymbol{p}| > 1$ corresponds to evanescent propagation, which does not have a contribution to the far-field and vanishes in the ray-tracing approximation.

5.3.2 Wigner Functions

In semiclassical quantum mechanics, the Wigner function for an ensemble of single particles describes a quasi-probability distribution of finding a particle in a certain state in phase space [163]. Using the Wigner transform, which is mathematically given by a coordinate transform and a partial Fourier transform with respect to the

transformed variables, positional as well as directional properties can be extracted from the correlation dyadic $\underline{\boldsymbol{\Gamma}}_{\mathrm{H}}$ [17], [23]. For a given correlation dyadic $\underline{\boldsymbol{\Gamma}}_{\mathrm{H}}$, the Wigner function $\mathcal{W}_{\mathrm{H}}$ can be obtained by

$$\mathcal{W}_{\mathrm{H}}\left(\boldsymbol{r}, \boldsymbol{p}, z, \omega\right) = \iint_A \mathrm{e}^{-\mathrm{i}k\boldsymbol{p}\cdot\boldsymbol{s}} \underline{\boldsymbol{\Gamma}}_{\mathrm{H}}\left(\boldsymbol{r} + \frac{\boldsymbol{s}}{2}, \boldsymbol{r} - \frac{\boldsymbol{s}}{2}, z, \omega\right) \cdot \mathrm{d}\boldsymbol{s}\,, \tag{5.81}$$

where k is the wave number and $\boldsymbol{r}$ and $\boldsymbol{s}$ are the transformed spatial variables. The transformed variable $\boldsymbol{r}$ represents the average position of two distinct sampling points $\boldsymbol{r}_1$ and $\boldsymbol{r}_2$ on a plane, and the transformed variable $\boldsymbol{s}$ is given as the difference vector pointing from $\boldsymbol{r}_2$ to $\boldsymbol{r}_1$, i.e.

$$\boldsymbol{r} = \frac{\boldsymbol{r}_1 + \boldsymbol{r}_2}{2}\,, \tag{5.82}$$

$$\boldsymbol{s} = \boldsymbol{r}_1 - \boldsymbol{r}_2\,. \tag{5.83}$$

The conjugate momentum vector $\boldsymbol{p} = [p_x, p_y]^{\mathrm{T}}$ can be interpreted as the normalized components of the wave vector, parallel to the source plane

$$p_x = \sin\vartheta\cos\varphi\,, \tag{5.84}$$

$$p_y = \sin\vartheta\sin\varphi\,, \tag{5.85}$$

with $|\boldsymbol{p}| = \sin\vartheta$, where ϑ is the angle of a ray with respect to the outward normal [23]. In that sense, a notion of the average direction of propagation is assigned to each position $\boldsymbol{r}$. The respective inverse transform, for recovering the correlation dyadic from the Wigner function is given by

$$\underline{\boldsymbol{\Gamma}}_{\mathrm{H}}\left(\boldsymbol{r} + \frac{\boldsymbol{s}}{2}, \boldsymbol{r} - \frac{\boldsymbol{s}}{2}, z, \omega\right) = \left(\frac{k}{2\pi}\right)^2 \iint_A \mathrm{e}^{\mathrm{i}k\boldsymbol{p}\cdot\boldsymbol{s}} \mathcal{W}_{\mathrm{H}}\left(\boldsymbol{r}, \boldsymbol{p}, z, \omega\right)\, \mathrm{d}\boldsymbol{p}\,. \tag{5.86}$$

With respect to the partial spatial Fourier transform in equation (5.77), one can define the momentum representation $\tilde{\boldsymbol{\Gamma}}_{\mathrm{H}}$ of the correlation dyadic $\underline{\boldsymbol{\Gamma}}_{\mathrm{H}}$ by the double spatial partial Fourier transform

$$\tilde{\boldsymbol{\Gamma}}_{\mathrm{H}}\left(\boldsymbol{p}_1, \boldsymbol{p}_2, z, \omega\right) = \iint_A \iint_A \mathrm{e}^{-\mathrm{i}k(\boldsymbol{p}_1\cdot\boldsymbol{r}_1 - \boldsymbol{p}_2\cdot\boldsymbol{r}_2)} \underline{\boldsymbol{\Gamma}}_{\mathrm{H}}\left(\boldsymbol{r}_1, \boldsymbol{r}_2, z, \omega\right)\, \mathrm{d}\boldsymbol{r}_1\, \mathrm{d}\boldsymbol{r}_2\,. \tag{5.87}$$

It can be easily verified, that position and momentum variables enter the Wigner transform symmetrically. Thus, the Wigner transform from (5.81) can also be obtained in momentum representation by

$$\mathcal{W}_{\mathrm{H}}\left(\boldsymbol{r}, \boldsymbol{p}, z, \omega\right) = \left(\frac{k}{2\pi}\right)^2 \iint_A \mathrm{e}^{\mathrm{i}k\boldsymbol{r}\cdot\boldsymbol{q}} \tilde{\boldsymbol{\Gamma}}_{\mathrm{H}}\left(\boldsymbol{p} + \frac{\boldsymbol{q}}{2}, \boldsymbol{p} - \frac{\boldsymbol{q}}{2}, z, \omega\right) \cdot \mathrm{d}\boldsymbol{q}\,, \tag{5.88}$$

with the average momentum variable $\boldsymbol{p}$ and the difference momentum $\boldsymbol{q}$, given according to

$$\boldsymbol{p} = \frac{\boldsymbol{p}_1 + \boldsymbol{p}_2}{2}\,, \tag{5.89}$$

$$\boldsymbol{q} = \boldsymbol{p}_1 - \boldsymbol{p}_2\,. \tag{5.90}$$

The respective inverse transform, for getting back the momentum representation of the correlation dyadic from the Wigner function is given by

$$\tilde{\boldsymbol{\Gamma}}_{\mathrm{H}}\left(\boldsymbol{p} + \frac{\boldsymbol{q}}{2}, \boldsymbol{p} - \frac{\boldsymbol{q}}{2}, z, \omega\right) = \iint_A \mathrm{e}^{-\mathrm{i}k\boldsymbol{r}\cdot\boldsymbol{q}} \mathcal{W}_{\mathrm{H}}\left(\boldsymbol{r}, \boldsymbol{p}, z, \omega\right)\, \mathrm{d}\boldsymbol{r}\,. \tag{5.91}$$

5.3.3 Propagation of Correlation Information Using Wigner Function

Similar to equation (5.79), correlation information on an arbitrary plane can be calculated by propagating boundary data, given at $z = 0$ along the normal direction with

$$\tilde{\boldsymbol{\Gamma}}_{\mathrm{H}}\left(\boldsymbol{p}_1, \boldsymbol{p}_2, z, \omega\right) = \mathrm{e}^{\mathrm{i}kz[T(\boldsymbol{p}_1) - T^*(\boldsymbol{p}_2)]} \tilde{\boldsymbol{\Gamma}}_{\mathrm{H}}\left(\boldsymbol{p}_1, \boldsymbol{p}_2, 0, \omega\right)\,, \tag{5.92}$$

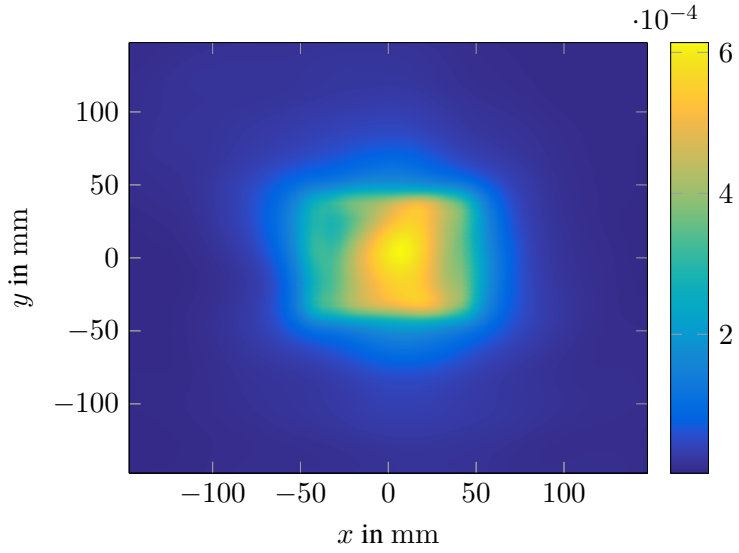

Figure 5.15 Measured spatial energy distribution at the source plane $z' = 10\,\mathrm{mm}$.

where T is given according to (5.80). By inserting (5.92) into (5.88), a transport equation for the Wigner function can be found [17], [23]. It is given by

$$\mathcal{W}_{\mathrm{H}}\left(\boldsymbol{r}, \boldsymbol{p}, z, \omega\right) = \iint_A \iint_A \boldsymbol{G}\left(\boldsymbol{r}, \boldsymbol{p}, \boldsymbol{r}', \boldsymbol{p}', z, \omega\right) \mathcal{W}_{\mathrm{H}}\left(\boldsymbol{r}', \boldsymbol{p}', 0, \omega\right) \,\mathrm{d}\boldsymbol{r}'\,\mathrm{d}\boldsymbol{p}'\,, \tag{5.93}$$

with the dyadic kernel propagator

$$\boldsymbol{G}\left(\boldsymbol{r}, \boldsymbol{p}, \boldsymbol{r}', \boldsymbol{p}', z, \omega\right) = \left(\frac{k}{2\pi}\right)^2 \delta\left(\boldsymbol{p} - \boldsymbol{p}'\right) \mathbf{1} \iint_A \mathrm{e}^{\mathrm{i}k(\boldsymbol{r}-\boldsymbol{r}')\cdot\boldsymbol{q} + \mathrm{i}kz\left(T\left(\boldsymbol{p}+\frac{\boldsymbol{q}}{2}\right) - T^*\left(\boldsymbol{p}-\frac{\boldsymbol{q}}{2}\right)\right)} \,\mathrm{d}\boldsymbol{q}\,, \tag{5.94}$$

for free-space propagation of plane-wave solutions. An approximation to the dyadic propagator can be found by a series expansion of the exponential in (5.94) [23], which yields a Dirac delta distribution

$$\boldsymbol{G}\left(\boldsymbol{r}, \boldsymbol{p}, \boldsymbol{r}', \boldsymbol{p}', z, \omega\right) \approx \delta\left(\boldsymbol{r} - \boldsymbol{r}' - \frac{z\boldsymbol{p}}{T\left(\boldsymbol{p}\right)}\right) \delta\left(\boldsymbol{p} - \boldsymbol{p}'\right) \mathbf{1}\,, \tag{5.95}$$

for propagating waves, and exponential damping

$$\boldsymbol{G}\left(\boldsymbol{r}, \boldsymbol{p}, \boldsymbol{r}', \boldsymbol{p}', z, \omega\right) \approx \mathrm{e}^{-2kz\sqrt{|\boldsymbol{p}|^2 - 1}} \delta\left(\boldsymbol{p} - \boldsymbol{p}'\right) \mathbf{1}\,. \tag{5.96}$$

for the evanescent components. Inserting the approximate propagators (5.95) and (5.96) into the integral equation (5.93) yields an approximate transport scheme for the Wigner function $\mathcal{W}_{\mathrm{H}}$ at the boundary $z = 0$ to any arbitrary plane $z > 0$, given by

$$\mathcal{W}_{\mathrm{H}}\left(\boldsymbol{r}, \boldsymbol{p}, z, \omega\right) \approx \begin{cases} \mathcal{W}_{\mathrm{H}}\left(\boldsymbol{r} - \frac{z\boldsymbol{p}}{T(\boldsymbol{p})}, \boldsymbol{p}, 0, \omega\right) & \text{for} \quad |\boldsymbol{p}| < 1 \\ \mathcal{W}_{\mathrm{H}}\left(\boldsymbol{r}, \boldsymbol{p}, 0, \omega\right) \mathrm{e}^{-2kz\sqrt{|\boldsymbol{p}|^2 - 1}} & \text{for} \quad |\boldsymbol{p}| > 1 \end{cases}. \tag{5.97}$$

5.4 Comparison of Different Propagation Schemes

In the following, we consider a given near-field scan of the y-component of the magnetic field on a boundary surface at $z' = 10\,\mathrm{mm}$. The data set is the same as in [23], [161]. It was obtained using a Langer EMV-Technik RF R50-1 near field probe, scanning above a cavity-backed aperture on a spatial grid of 60×60 points, with

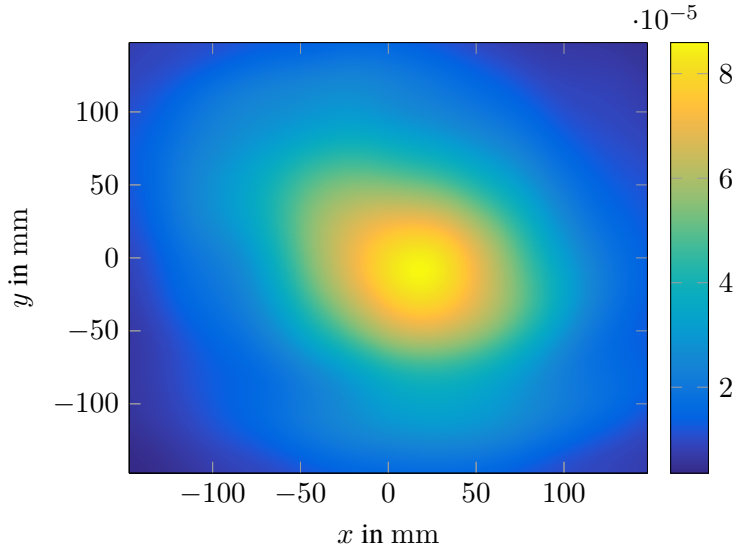

Figure 5.16 Measured spatial energy distribution at the observation plane $z = 100\,\mathrm{mm}$.

a step size of $\Delta = 5\,\mathrm{mm}$ in both, x- and y-direction. The probe was connected to an Agilent E5062A vector network analyzer, which also provided the excitation for the cavity-backed aperture. Since the excitation signal in the VNA is known, a single probe scan is sufficient. The cavity features a mechanical mode stirrer with 36 different paddle positions. Measurements were taken for each paddle position at a fixed frequency of 3 GHz. From this data, with the known phase reference, all spatial correlations have been calculated. The obtained spatial energy density at the source plane is given in Figure 5.15.

The same measurements were performed in a plane at $z = 100\,\mathrm{mm}$ in order to obtain a reference for benchmarking our propagation schemes. The spatial energy distribution for $z = 100\,\mathrm{mm}$ can be seen in Figure 5.16. The source correlation matrix, obtained by measurement, is numerically Wigner transformed by equation (5.81) using implementations of the fast Fourier transform in MATLAB. The numerical Wigner transform of the source correlations is then propagated according to (5.97), using phase-space propagation techniques, discussed in section 5.3. The resulting propagated Wigner transform is then inverse-Wigner-transformed according to (5.86), in order to obtain an approximation for the phase-space propagated correlation matrix at a distance of $z = 100\,\mathrm{mm}$. The spatial energy distribution for the Wigner-propagated correlation matrix is given in Figure 5.17.

For our measurements, we only consider the y-component of the tangential magnetic field. Thus, by $\underline{\boldsymbol{J}} = \boldsymbol{n} \times \underline{\boldsymbol{H}}$ from the equivalence principle in section 3.5.5, the equivalent surface current only exhibits an x-component. Therefore, we only need to consider the following part of the total dyadic Green's function $\underline{\boldsymbol{G}}_{\mathrm{HJ}}$ of the magnetic field

$$\underline{G}^{yx}_{\mathrm{HJ}}\left(\boldsymbol{r}-\boldsymbol{r}',\omega\right) = -\frac{1}{2\pi}\left(z-z'\right)\frac{c_0 - \mathrm{i}\omega\left\|\boldsymbol{r}-\boldsymbol{r}'\right\|}{c_0\left\|\boldsymbol{r}-\boldsymbol{r}'\right\|^3}\mathrm{e}^{-\mathrm{i}\omega\frac{\left\|\boldsymbol{r}-\boldsymbol{r}'\right\|}{c_0}}, \tag{5.98}$$

where a factor of 2 was introduced by image theory since we only consider magnetic field components [102]. We apply the method of moments in order to obtain a set of algebraic equations that can be solved numerically from the analytic equation

$$\underline{\boldsymbol{\Gamma}}^{y}_{\mathrm{H}}\left(\boldsymbol{r}_1,\boldsymbol{r}_2,\omega\right) = \iiint_{V'}\iiint_{V'}\underline{G}^{yx}_{\mathrm{HJ}}\left(\boldsymbol{r}_1-\boldsymbol{r}'_1,\omega\right)\underline{\boldsymbol{\Gamma}}^{x}_{\mathrm{J}}\left(\boldsymbol{r}'_1,\boldsymbol{r}'_2,\omega\right)\underline{G}^{yx\,\dagger}_{\mathrm{HJ}}\left(\boldsymbol{r}_2-\boldsymbol{r}'_2,\omega\right)\,\mathrm{d}^3r'_1\,\mathrm{d}^3r'_2\,. \tag{5.99}$$

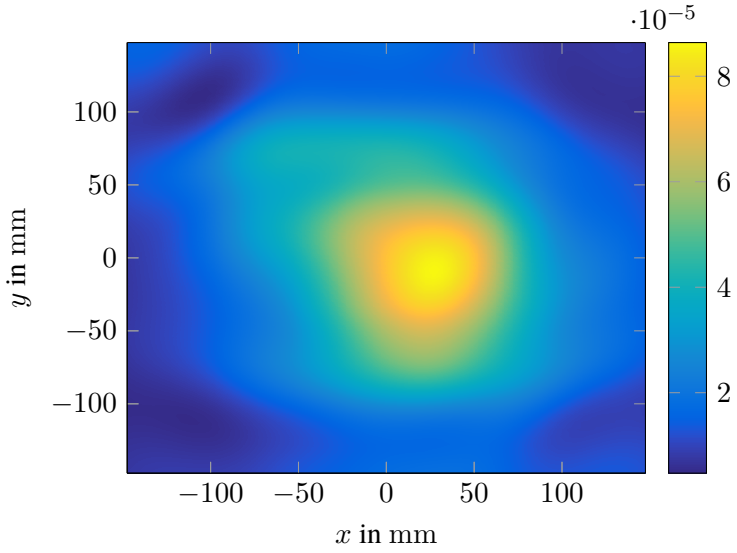

Figure 5.17 Propagated spatial energy distribution at the observation plane $z = 100\,\mathrm{mm}$, using the Wigner function propagation method.

We expand the magnetic field $\underline{H}_y$ and the equivalent source currents $\underline{J}_x$ into a set of basis functions, given by

$$\underline{H}_y(\boldsymbol{r},\omega) = \sum_{m=1}^{M} \underline{I}_{\mathrm{H}\,m}(\omega)\,\delta(\boldsymbol{r}-\boldsymbol{r}_m)\ , \tag{5.100}$$

$$\underline{J}_x(\boldsymbol{r}',\omega) = \sum_{n=1}^{N} \underline{I}_{\mathrm{J}\,n}(\omega)\,u_n(\boldsymbol{r}')\ . \tag{5.101}$$

The basis functions u_n used for expanding the source field $\underline{J}_x$ are given in terms of two-dimensional spatial unit pulse functions as

$$u_n(\boldsymbol{r}') = \begin{cases} \frac{1}{\Delta^2} & \text{for } \boldsymbol{r}' \in U_n \\ 0 & \text{otherwise} \end{cases}\ , \tag{5.102}$$

where the set U_n is the neighborhood of a measurement grid point in the source plane $z = 10\,\mathrm{mm}$, given as

$$U_n = \left\{ \boldsymbol{r}' \in \mathbb{R}^3,\, \boldsymbol{r}'_n \in V' : x'_n - \frac{\Delta}{2} \le x' \le x'_n + \frac{\Delta}{2} \wedge y'_n - \frac{\Delta}{2} \le y' \le y'_n + \frac{\Delta}{2} \wedge z' = 10\,\mathrm{mm} \right\}\ . \tag{5.103}$$

Hence, the basis functions u_n are orthonormal, i.e.

$$\iiint_{V'} u_m^*(\boldsymbol{r}')\,u_n(\boldsymbol{r}')\ \mathrm{d}^3 r' = \delta_{mn}\,. \tag{5.104}$$

Applying the method of moments according to section 5.1.1, we obtain algebraic equations for the expansion coefficients $\underline{I}_{\mathrm{H}\,m}$ and $\underline{I}_{\mathrm{J}\,n}$. Inserting the series expansions (5.100) and (5.101) into equation (3.113) yields

$$\underline{I}_{\mathrm{H}\,m}(\omega) = \sum_{n=1}^{N} \underline{I}_{\mathrm{J}\,n}(\omega) \iiint_{V'} \underline{G}_{\mathrm{HJ}}^{yx}(\boldsymbol{r}_m - \boldsymbol{r}',\omega)\,u_n(\boldsymbol{r}')\ \mathrm{d}^3 r'\,. \tag{5.105}$$

With this discretization scheme, one can define correlation matrices for the expansion coefficients $\underline{I}_{\mathrm{H}\,m}$ and $\underline{I}_{\mathrm{J}\,n}$ in terms of the ergodic expectation values

$$\underline{C}_{\mathrm{H}\,mn}^{y}(\omega) = \langle\!\langle \underline{I}_{\mathrm{H}\,m}(\omega)\,\underline{I}_{\mathrm{H}\,n}^*(\omega) \rangle\!\rangle\,, \tag{5.106}$$

$$\underline{C}_{\mathrm{J}\,mn}^{x}(\omega) = \langle\!\langle \underline{I}_{\mathrm{J}\,m}(\omega)\,\underline{I}_{\mathrm{J}\,n}^*(\omega) \rangle\!\rangle\,. \tag{5.107}$$

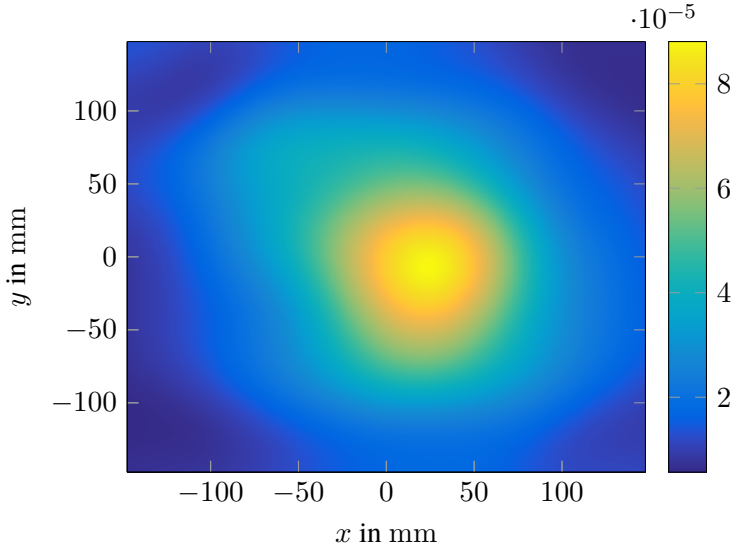

Figure 5.18 Propagated spatial energy distribution at the observation plane $z = 100\,\mathrm{mm}$, using the Method of Moments propagation method.

The discretized correlation matrices can also be directly obtained from the correlation dyadics using

$$\underline{C}^{y}_{\mathrm{H}\,mn}(\omega) = \iiint_V \iiint_V \delta(\boldsymbol{r}_1 - \boldsymbol{r}_m)\,\underline{\boldsymbol{\Gamma}}_{\mathrm{H}}(\boldsymbol{r}_1, \boldsymbol{r}_2, \omega)\,\delta(\boldsymbol{r}_2 - \boldsymbol{r}_n)\,\mathrm{d}^3 r_1\,\mathrm{d}^3 r_2 = \underline{\boldsymbol{\Gamma}}_{\mathrm{H}}(\boldsymbol{r}_m, \boldsymbol{r}_n, \omega)\;, \tag{5.108}$$

$$\underline{C}^{x}_{\mathrm{J}\,mn}(\omega) = \iiint_{V'} \iiint_{V'} u^*_m(\boldsymbol{r}'_1)\,\underline{\boldsymbol{\Gamma}}_{\mathrm{J}}(\boldsymbol{r}'_1, \boldsymbol{r}'_2, \omega)\,u_n(\boldsymbol{r}'_2)\;\mathrm{d}^3 r'_1\,\mathrm{d}^3 r'_2\,. \tag{5.109}$$

Finally, we obtain a numerical propagator similar to (5.29), relating

$$\underline{C}^{y}_{\mathrm{H}\,mn}(\omega) = \sum_{k=1}^{N}\sum_{l=1}^{N} \underline{M}_{mk}(\omega)\,\underline{C}^{x}_{\mathrm{J}\,kl}(\omega)\,\underline{M}^*_{ln}(\omega) \tag{5.110}$$

with

$$\begin{aligned}\underline{M}_{mn}(\omega) &= \iiint_{\partial V'} \underline{G}^{yx}_{\mathrm{HJ}}(\boldsymbol{r}_m - \boldsymbol{r}', \omega)\,u_n(\boldsymbol{r}')\;\mathrm{d}^3 r' \\ &= -\frac{1}{2\pi\Delta^2}\iiint_{U_n}(z_m - z')\,\frac{c_0 - \mathrm{i}\omega\,\|\boldsymbol{r}_m - \boldsymbol{r}'\|}{c_0\,\|\boldsymbol{r}_m - \boldsymbol{r}'\|^3}\mathrm{e}^{-\mathrm{i}\omega\frac{\|\boldsymbol{r}_m - \boldsymbol{r}'\|}{c_0}}\,\mathrm{d}^3 r'\,.\end{aligned} \tag{5.111}$$

Figure 5.18 shows the spatial energy distribution, i.e. the diagonal elements of the correlation matrix $\underline{C}^{y}_{\mathrm{H}\,mn}$, which is a numerically propagated version of the measured source correlation matrix $\underline{C}^{x}_{\mathrm{J}\,mn}$ using the propagation scheme given in equations (5.110) and (5.111).

Both methods compared here show good agreement, qualitatively and quantitatively. The Wigner propagation method needed some post-treatment in order to obtain the correct quantitative values, which, however, can be explained by errors in the numerical implementation. A more detailed comparison of e.g. selected parts of the correlation matrices and computational cost is given in the original paper [23].

5.5 Computer Aided Modelling

The noisy electromagnetic field in the vicinity of an electronic device consists of a superposition of the radiated emissions of all deterministic and random sources present on the device. Hence, field correlations, as well as spatial correlations of the noise sources play an important role in the analysis of signal integrity and

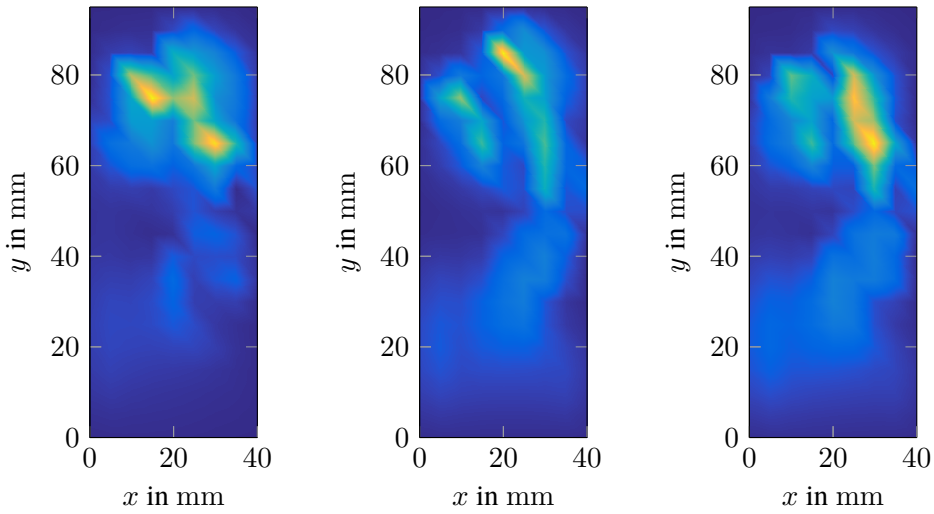

(a) Correlated, in-phase. **(b)** Correlated, anti-phase. **(c)** Uncorrelated

Figure 5.19 Spatial energy distribution $5\ \mathrm{mm}$ above a PCB with two transmission lines excited with in-phase fully correlated signals (a), anti-phase fully correlated signals (b), and completely uncorrelated signals (c) at $2.4\ \mathrm{GHz}$, propagated in CST Microwave Studio.

electromagnetic compatibility, as their characteristics allow a description of how one part of a device influences another. The correlation function of two stationary random processes s_i and s_j is given by [120]

$$c_{\mathrm{s}\,ij}\left(\tau\right) = \left\langle\!\left\langle s_i\left(t\right) s_j\left(t-\tau\right)\right\rangle\!\right\rangle, \tag{5.112}$$

where the brackets $\langle\!\langle \ldots \rangle\!\rangle$ denote the ensemble average. For ergodic random processes, the ensemble average can be substituted by the time average, such that

$$c_{\mathrm{s}\,ij}\left(\tau\right) = \lim_{T\to\infty} \frac{1}{2T} \int_{-T}^{T} s_i\left(t\right) s_j\left(\tau - t\right)\,\mathrm{d}t\,. \tag{5.113}$$

Let us now consider a PCB with N transmission lines, excited with either pairwise correlated, pairwise partially correlated, or uncorrelated stationary ergodic Gaussian random signals. The degree of correlation for all pairs of stochastic signals s_i and s_j is given by the correlation $c_{\mathrm{s}\,ij}$. The whole PCB and the surrounding free-space region form a linear time-invariant (LTI) system, which can be described by an impulse response $Z\left(\boldsymbol{x}, t\right)$. The impulse response describes the propagation from each port exciting a transmission line on the PCB to all observation points, summarized in the vector $\boldsymbol{x}$, located on a virtual plane close to the surface of the PCB [120]. With a CAD model of the PCB available, one can calculate these impulse responses numerically. If multiple signal lines are excited with either correlated or uncorrelated signals, we can observe the field-field correlations for all pairs of observation points specified on a mesh grid on a virtual plane above the surface of the PCB. The elements of the field-field correlation matrix for the magnetic field are given by [16]

$$c_{\mathrm{H}_p\,mn}\left(\tau\right) = \lim_{T\to\infty} \frac{1}{2T} \int_{-T}^{T} H_p\left(\boldsymbol{x}_m, t\right) H_p\left(\boldsymbol{x}_n, t-\tau\right)\,\mathrm{d}t\,, \tag{5.114}$$

where $H_p\left(\boldsymbol{x}, t\right)$ is the magnetic field at position $\boldsymbol{x}$ with polarization $p \in \{x, y\}$. Also field cross-polarization correlations may be considered. We evaluate the spectral energy density for a grid of observation points, based on the computed impulse responses for arbitrary signal correlations. The magnetic field at each observation

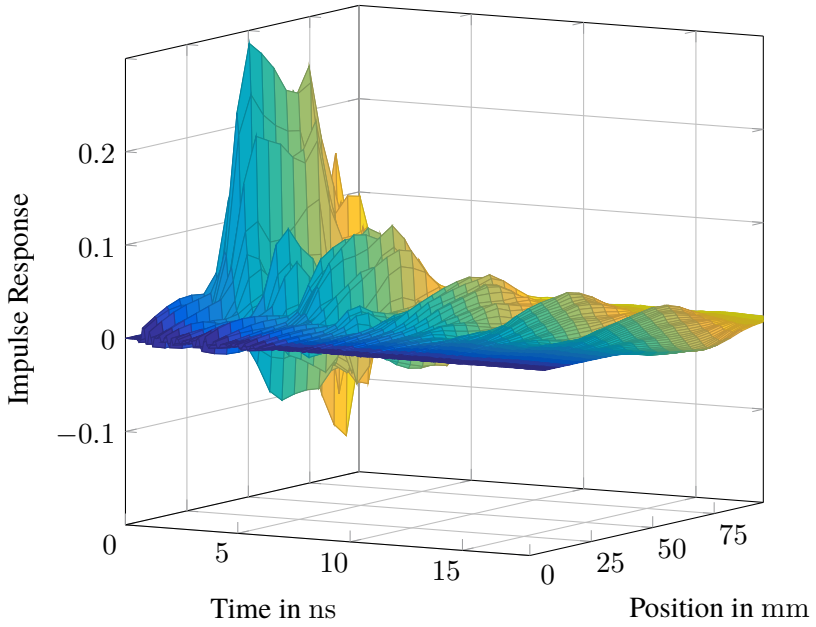

Figure 5.20 Impulse response over time, along $x = 35\,\mathrm{mm}$ for different y-positions. For these simulations, only port 1 has been excited.

point, excited by a superposition of N random signals propagating along transmission lines on the PCB, is given by the convolution [120]

$$H_p\left(\boldsymbol{x}, t\right) = \sum_{i=1}^{N} \int_{-\infty}^{\infty} s_i\left(\tau\right) Z_{\mathrm{H}_p\, i}\left(\boldsymbol{x}, t-\tau\right)\, \mathrm{d}\tau\,, \tag{5.115}$$

where $s_i\left(t\right)$ is the signal propagating along the i-th transmission line. The field-field correlations are given by

$$c_{\mathrm{H}_p\, mn}\left(\tau\right) = \lim_{T\to\infty} \frac{1}{2T} \sum_{i=1}^{N} \sum_{j=1}^{N} \int_{-T}^{T} \int_{-\infty}^{\infty} \int_{-\infty}^{\infty} Z_{\mathrm{H}_p\, i}\left(\boldsymbol{x}_m, t''\right) s_i\left(t\right) s_j\left(t'-t\right) Z_{\mathrm{H}_p\, j}\left(\boldsymbol{x}_n, \tau-t'-t''\right)\, \mathrm{d}t\, \mathrm{d}t'\, \mathrm{d}t''\,. \tag{5.116}$$

With the correlation information $c_{\mathrm{s}\, ij}$ of the i-th and the j-th signal from equation (5.113), we can simplify equation (5.116) and obtain

$$c_{\mathrm{H}_p\, mn}\left(\tau\right) = \sum_{i=1}^{N} \sum_{j=1}^{N} \int_{-\infty}^{\infty} \int_{-\infty}^{\infty} Z_{\mathrm{H}_p\, i}\left(\boldsymbol{x}_m, t''\right) c_{ij}^{s}\left(\tau-t'\right) Z_{\mathrm{H}_p\, j}\left(\boldsymbol{x}_n, t'-t''\right)\, \mathrm{d}t'\, \mathrm{d}t''\,. \tag{5.117}$$

This equation relates the auto-correlation and cross-correlation functions of the stochastic signals propagating along transmission lines on the PCB to the auto-correlations and cross-correlations of the magnetic fields at all pairs of observation points. The spectral energy density at each observation point x_m can be obtained by the Fourier transform of the auto-correlations $c_{\mathrm{H}_p\, mm}\left(\tau\right)$. It is given by

$$W_{\mathrm{mag}}\left(\omega\right) = \frac{\mu_0}{2} \int_{-\infty}^{\infty} c_{\mathrm{H}_p\, mm}\left(\tau\right) \mathrm{e}^{\mathrm{i}\omega\tau}\, \mathrm{d}\tau\,. \tag{5.118}$$

Let us now consider an example of an actual PCB, modeled in CST Microwave Studio. There are two high-speed signal lines close to each other on the PCB.

We are interested in the radiated EMI due to these two transmission lines, under consideration of the correlation between the stochastic data signals propagating along the lines. In Figure 5.19, the normalized spectral energy densities for a frequency of $2.44\,\mathrm{GHz}$ in a plane $5\,\mathrm{mm}$ above the PCB are shown, if the transmission lines are excited with either correlated or uncorrelated signals.

In order to model the correlation matrices at this plane, both transmission lines are excited with Gaussian pulses using discrete ports in CST Microwave Studio. The impulse responses of the magnetic fields are recorded on a rectangular 9×20 observation grid in a plane parallel to the PCB with $5\,\mathrm{mm}$ grid spacing in both directions. Figure 5.20 shows the impulse responses $Z_{\mathrm{H}_x\,1}\left(\boldsymbol{x}_m, t\right)$ for the x-polarized magnetic field at the observation points along the line $x = 35\,\mathrm{mm}$, which is closest to the excited transmission lines. These impulse responses were obtained for only the first transmission line excited.

By a superposition of the impulse responses of both individual transmission lines, one can reconstruct field-field correlations for arbitrary points in space, even in very complex environments. In this way, we have been able to give the spatial energy distribution in Figure 5.19, in terms of the diagonal elements of the propagated correlation matrices, using the impulse responses obtained from CST Microwave Studio. The propagated correlation matrix can be calculated for arbitrary source correlations by means of equation (5.117).

6 Near-Field Communication

6.1 Near-Field MIMO Communication

Stochastic random fields also play an important role in wireless communication scenarios. Ivrlač and Nossek stressed in [164], that we need a physics-based model in wireless communication in order to model noise correctly. Furthermore in [165], the same authors write "Information theory serves well as the mathematical theory of communication. However, it contains no provision that makes sure its theorems are consistent with the physical laws that govern any existing realization of a communication system.". They proposed a circuit theoretic noise model to overcome these limitations. The theoretical framework of stochastic electromagnetic fields can bridge this gap and provide a proper noise model, i.e. information about a random process received at an antenna if one assumes a certain stochastic noise source in free space. In wireless communication, the information-carrying signal needs to be modeled in terms of a stochastic process, as there is no a-priori knowledge of the data while the signals propagate along the communication paths. Thus, the concept of stochastic electromagnetic fields, as introduced in chapter 3, can be also applied in modeling modulated information-carrying signals in complex environments. In the remainder of this chapter, we want to give an outlook on an application of random field noise models to near-field MIMO communication. In this sense, we first establish a circuit model for the MIMO communication link. Let us consider a noiseless wireless communication scenario, as depicted in Figure 6.1. Two antenna arrays, a transmit antenna array, with N antenna elements, and a receive antenna array with M antenna elements are modeled by an impedance matrix $\underline{\boldsymbol{Z}} \in \mathbb{C}^{(N+M)\times(N+M)}$, such that

$$\begin{bmatrix} \underline{\boldsymbol{V}}_{\mathrm{T}} \\ \underline{\boldsymbol{V}}_{\mathrm{R}} \end{bmatrix} = \begin{bmatrix} \underline{\boldsymbol{Z}}_{\mathrm{T}} & \underline{\boldsymbol{Z}}_{\mathrm{TR}} \\ \underline{\boldsymbol{Z}}_{\mathrm{RT}} & \underline{\boldsymbol{Z}}_{\mathrm{R}} \end{bmatrix} \begin{bmatrix} \underline{\boldsymbol{I}}_{\mathrm{T}} \\ -\underline{\boldsymbol{I}}_{\mathrm{R}} \end{bmatrix}, \tag{6.1}$$

where $\underline{\boldsymbol{Z}}$ is partitioned in four block matrices, the transmit matrix $\underline{\boldsymbol{Z}}_{\mathrm{T}} \in \mathbb{C}^{N\times N}$, the receive matrix $\underline{\boldsymbol{Z}}_{\mathrm{R}} \in \mathbb{C}^{M\times M}$ and the two transimpedance matrices $\underline{\boldsymbol{Z}}_{\mathrm{TR}} \in \mathbb{C}^{N\times M}$ and $\underline{\boldsymbol{Z}}_{\mathrm{RT}} \in \mathbb{C}^{M\times N}$.

Suppose now that we have a vector signal generator, with inner impedance matrix $\underline{\boldsymbol{Z}}_{\mathrm{G}}$ directly connected to the N transmit antennas, and a load with impedance matrix $\underline{\boldsymbol{Z}}_{\mathrm{L}}$ connected to the M output antenna arrays. Our goal is to transfer maximum power from the generator to the load, through the given antenna multiport $\underline{\boldsymbol{Z}}$. The impedance the vector signal generator sees at its output is given by the antenna multiport connected to the load impedance. The load impedance M-port at the receive side can be described by the relation

$$\underline{\boldsymbol{V}}_{\mathrm{R}} = \underline{\boldsymbol{Z}}_{\mathrm{L}} \underline{\boldsymbol{I}}_{\mathrm{R}} \,. \tag{6.2}$$

Inserting this into (6.1) yields the description

$$\underline{\boldsymbol{V}}_{\mathrm{T}} = \underline{\boldsymbol{Z}}_{\mathrm{T}} \underline{\boldsymbol{I}}_{\mathrm{T}} - \underline{\boldsymbol{Z}}_{\mathrm{TR}} \underline{\boldsymbol{I}}_{\mathrm{R}} \,, \tag{6.3}$$

$$\underline{\boldsymbol{Z}}_{\mathrm{L}} \underline{\boldsymbol{I}}_{\mathrm{R}} = \underline{\boldsymbol{Z}}_{\mathrm{RT}} \underline{\boldsymbol{I}}_{\mathrm{T}} - \underline{\boldsymbol{Z}}_{\mathrm{R}} \underline{\boldsymbol{I}}_{\mathrm{R}} \,. \tag{6.4}$$

We express the received current $\underline{\boldsymbol{I}}_{\mathrm{R}}$ from equation (6.4) as

$$\underline{\boldsymbol{I}}_{\mathrm{R}} = \left(\underline{\boldsymbol{Z}}_{\mathrm{L}} + \underline{\boldsymbol{Z}}_{\mathrm{R}}\right)^{-1} \underline{\boldsymbol{Z}}_{\mathrm{RT}} \underline{\boldsymbol{I}}_{\mathrm{T}} \,, \tag{6.5}$$

and insert it into equation (6.3) and obtain

$$\underline{\boldsymbol{V}}_{\mathrm{T}} = \left[\underline{\boldsymbol{Z}}_{\mathrm{T}} - \underline{\boldsymbol{Z}}_{\mathrm{TR}} \left(\underline{\boldsymbol{Z}}_{\mathrm{L}} + \underline{\boldsymbol{Z}}_{\mathrm{R}}\right)^{-1} \underline{\boldsymbol{Z}}_{\mathrm{RT}}\right] \underline{\boldsymbol{I}}_{\mathrm{T}} \,. \tag{6.6}$$

So the total impedance, as seen by the generator is given by $\underline{\boldsymbol{Z}}_{\mathrm{T}} - \underline{\boldsymbol{Z}}_{\mathrm{TR}} \left(\underline{\boldsymbol{Z}}_{\mathrm{L}} + \underline{\boldsymbol{Z}}_{\mathrm{R}}\right)^{-1} \underline{\boldsymbol{Z}}_{\mathrm{RT}}$. In order to maximize the total power transmitted from the generator to the load, the generator impedance $\underline{\boldsymbol{Z}}_{\mathrm{G}}$ must be the complex conjugate transpose of the total impedance, seen by the generator [166]. Thus, we have

$$\underline{\boldsymbol{Z}}_{\mathrm{G}}^{\dagger} = \underline{\boldsymbol{Z}}_{\mathrm{T}} - \underline{\boldsymbol{Z}}_{\mathrm{TR}} \left(\underline{\boldsymbol{Z}}_{\mathrm{L}} + \underline{\boldsymbol{Z}}_{\mathrm{R}}\right)^{-1} \underline{\boldsymbol{Z}}_{\mathrm{RT}} \,. \tag{6.7}$$

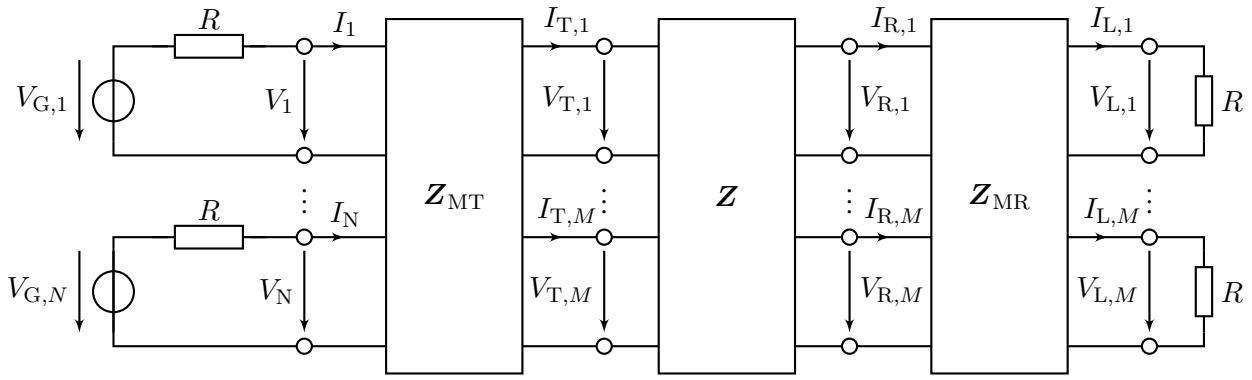

Figure 6.1 Multiport Model of a near-field MIMO communication link.

For the optimal load impedance, we can proceed similarly, by investigating the total impedance the load is connected to. This is given by the antenna multiport $\underline{\boldsymbol{Z}}$ connected to the generator impedance $\underline{\boldsymbol{Z}}_{\mathrm{G}}$. The generator impedance N-port can be described by the relation

$$\underline{\boldsymbol{V}}_{\mathrm{T}} = -\underline{\boldsymbol{Z}}_{\mathrm{G}}\underline{\boldsymbol{I}}_{\mathrm{T}}\,. \tag{6.8}$$

A description for the total impedance, the load is connected to can be calculated by inserting (6.8) into (6.1), and is given by

$$-\underline{\boldsymbol{Z}}_{\mathrm{G}}\underline{\boldsymbol{I}}_{\mathrm{T}} = \underline{\boldsymbol{Z}}_{\mathrm{T}}\underline{\boldsymbol{I}}_{\mathrm{T}} - \underline{\boldsymbol{Z}}_{\mathrm{TR}}\underline{\boldsymbol{I}}_{\mathrm{R}}\,, \tag{6.9}$$

$$\underline{\boldsymbol{V}}_{\mathrm{R}} = \underline{\boldsymbol{Z}}_{\mathrm{RT}}\underline{\boldsymbol{I}}_{\mathrm{T}} - \underline{\boldsymbol{Z}}_{\mathrm{R}}\underline{\boldsymbol{I}}_{\mathrm{R}}\,. \tag{6.10}$$

Now solving (6.9) for $\underline{\boldsymbol{I}}_{\mathrm{T}}$ and inserting the result into (6.10) yields

$$\underline{\boldsymbol{I}}_{\mathrm{T}} = \left(\underline{\boldsymbol{Z}}_{\mathrm{G}} + \underline{\boldsymbol{Z}}_{\mathrm{T}}\right)^{-1}\underline{\boldsymbol{Z}}_{\mathrm{TR}}\underline{\boldsymbol{I}}_{\mathrm{R}}\,, \tag{6.11}$$

and

$$\underline{\boldsymbol{V}}_{\mathrm{R}} = -\left[\underline{\boldsymbol{Z}}_{\mathrm{R}} - \underline{\boldsymbol{Z}}_{\mathrm{RT}}\left(\underline{\boldsymbol{Z}}_{\mathrm{G}} + \underline{\boldsymbol{Z}}_{\mathrm{T}}\right)^{-1}\underline{\boldsymbol{Z}}_{\mathrm{TR}}\right]\underline{\boldsymbol{I}}_{\mathrm{R}}\,. \tag{6.12}$$

Hence, for maximum power transfer from the generator to the load, a second condition given by

$$\underline{\boldsymbol{Z}}_{\mathrm{L}}^{\dagger} = \underline{\boldsymbol{Z}}_{\mathrm{R}} - \underline{\boldsymbol{Z}}_{\mathrm{RT}}\left(\underline{\boldsymbol{Z}}_{\mathrm{G}} + \underline{\boldsymbol{Z}}_{\mathrm{T}}\right)^{-1}\underline{\boldsymbol{Z}}_{\mathrm{TR}}\,, \tag{6.13}$$

in addition to (6.7) must hold. Equations (6.7) and (6.13) are transcendental equations that do not posses a formal algebraic solution. However, they can be solved numerically [167] by an iterative algorithm.

In a typical MIMO communication scenario, as depicted in Figure 6.1, there are N independent signal generators, i.e. digital-to-analog converters (DACs) with subsequent mixers and power amplifiers, that transmit the encoded messages through the channel to a number of M independent receivers, i.e. low-noise amplifiers with mixers and analog-to-digital converters (ADCs). Each transmit channel carries the respective generator signal, whereas all other signals superimposed on one particular channel are considered as noise, thus degrading signal quality. Typical transmitter and receiver topologies are designed for a characteristic inner impedance of $R = 50\,\Omega$. Thus, our goal is to design a decoupling and matching network for the transmit and for the receive side, such that power transfer from the transmitter to the receiver is maximized, and such that the respective transmit and receive channels are decoupled. For the transmit side, we want our system of N transmitters, modeled as voltage sources with inner impedance $R = 50\,\Omega$, to be matched to the antenna's input impedance, described by $\underline{\boldsymbol{Z}}_{\mathrm{G}}$. In the same way, we want the receive side, modeled by termination resistors of $R = 50\,\Omega$, to receive maximum power, so the loads should be matched to the output resistance $\underline{\boldsymbol{Z}}_{\mathrm{L}}$ of the antenna array.

We can describe the transmit matching network by a matrix $\underline{\boldsymbol{Z}}_{\mathrm{MT}} \in \mathbb{C}^{2N\times 2N}$ given by

$$\begin{bmatrix}\underline{\boldsymbol{V}}\\ \underline{\boldsymbol{V}}_{\mathrm{T}}\end{bmatrix} = \underline{\boldsymbol{Z}}_{\mathrm{MT}}\begin{bmatrix}\underline{\boldsymbol{I}}\\ -\underline{\boldsymbol{I}}_{\mathrm{T}}\end{bmatrix}\,. \tag{6.14}$$

The condition for power-matching is given by

$$\underline{\boldsymbol{V}}_{\mathrm{T}} = \underline{\boldsymbol{Z}}_{\mathrm{G}}^{\dagger} \underline{\boldsymbol{I}}_{\mathrm{T}} \,, \tag{6.15}$$

and the decoupling condition on the left-hand side of $\underline{\boldsymbol{Z}}_{\mathrm{MT}}$ in Figure 6.1 is given by

$$\underline{\boldsymbol{V}} = \underline{\boldsymbol{V}}_{\mathrm{G}} - R\mathbf{1}\underline{\boldsymbol{I}} \,, \tag{6.16}$$

with the $N \times N$ identity matrix $\mathbf{1}$. Substituting (6.15) and (6.16) with $\underline{\boldsymbol{V}}_{\mathrm{G}} = 0$ into (6.14) we obtain a system of equations, describing the elements of the DMN matrix $\underline{\boldsymbol{Z}}_{\mathrm{MT}}$

$$-R\mathbf{1}\underline{\boldsymbol{I}} = \underline{\boldsymbol{Z}}_{\mathrm{MT},11}\underline{\boldsymbol{I}} - \underline{\boldsymbol{Z}}_{\mathrm{MT},12}\underline{\boldsymbol{I}}_{\mathrm{T}} \,, \tag{6.17}$$

$$\underline{\boldsymbol{Z}}_{\mathrm{G}}^{\dagger}\underline{\boldsymbol{I}}_{\mathrm{T}} = \underline{\boldsymbol{Z}}_{\mathrm{MT},21}\underline{\boldsymbol{I}} - \underline{\boldsymbol{Z}}_{\mathrm{MT},22}\underline{\boldsymbol{I}}_{\mathrm{T}} \,. \tag{6.18}$$

Additional to equations (6.17) and (6.18), we require the decoupling and matching multiport $\underline{\boldsymbol{Z}}_{\mathrm{MT}}$ to be linear, lossless, and reciprocal. Linearity is accomplished by requiring the existence of a matrix $\underline{\boldsymbol{Z}}_{\mathrm{MT}}$, which is a linear mapping from the port currents to the port voltages. Being lossless, requires that the impedance matrix of the DMN is purely imaginary, i.e. $\mathrm{Re}\{\underline{\boldsymbol{Z}}_{\mathrm{MT}}\} = \mathbf{0}$. Reciprocity then requires that the describing impedance matrix is symmetric, i.e. $\underline{\boldsymbol{Z}}_{\mathrm{MT}} = \underline{\boldsymbol{Z}}_{\mathrm{MT}}^{\mathrm{T}}$. Thus, we can write for the block matrices $\underline{\boldsymbol{Z}}_{\mathrm{MT},11} \in \mathbb{C}^{N\times N}$, $\underline{\boldsymbol{Z}}_{\mathrm{MT},12} \in \mathbb{C}^{N\times N}$, $\underline{\boldsymbol{Z}}_{\mathrm{MT},21} \in \mathbb{C}^{N\times N}$, and $\underline{\boldsymbol{Z}}_{\mathrm{MT},22} \in \mathbb{C}^{N\times N}$

$$\underline{\boldsymbol{Z}}_{\mathrm{MT}} = \mathrm{i}\begin{bmatrix} \boldsymbol{X}_{\mathrm{MT},11} & \boldsymbol{X}_{\mathrm{MT},12} \\ \boldsymbol{X}_{\mathrm{MT},21} & \boldsymbol{X}_{\mathrm{MT},22} \end{bmatrix} \,, \tag{6.19}$$

with purely real sub-matrices $\boldsymbol{X}_{\mathrm{MT},11} \in \mathbb{R}^{N\times N}$, $\boldsymbol{X}_{\mathrm{MT},12} \in \mathbb{R}^{N\times N}$, $\boldsymbol{X}_{\mathrm{MT},21} \in \mathbb{R}^{N\times N}$, and $\boldsymbol{X}_{\mathrm{MT},22} \in \mathbb{R}^{N\times N}$. Inserting these additional conditions into equations (6.17) and (6.18) yields

$$-R\mathbf{1}\underline{\boldsymbol{I}} = \left[\mathrm{i}\boldsymbol{X}_{\mathrm{MT},11} + \boldsymbol{X}_{\mathrm{MT},12}\left(\underline{\boldsymbol{Z}}_{\mathrm{G}}^{\dagger} + \mathrm{i}\boldsymbol{X}_{\mathrm{MT},22}\right)^{-1}\boldsymbol{X}_{\mathrm{MT},21}\right]\underline{\boldsymbol{I}} \,, \tag{6.20}$$

and thus

$$-R\mathbf{1} = \mathrm{i}\boldsymbol{X}_{\mathrm{MT},11} + \boldsymbol{X}_{\mathrm{MT},12}\left(\mathrm{Re}\left\{\underline{\boldsymbol{Z}}_{\mathrm{G}}^{\dagger}\right\} + \mathrm{i}\,\mathrm{Im}\left\{\underline{\boldsymbol{Z}}_{\mathrm{G}}^{\dagger}\right\} + \mathrm{i}\boldsymbol{X}_{\mathrm{MT},22}\right)^{-1}\boldsymbol{X}_{\mathrm{MT},21} \,. \tag{6.21}$$

Equation (6.21) can only describe a reciprocal DMN, if $\underline{\boldsymbol{Z}}_{\mathrm{G}}^{\dagger} = \underline{\boldsymbol{Z}}_{\mathrm{G}}^{\dagger,\mathrm{T}} \Rightarrow \underline{\boldsymbol{Z}}_{\mathrm{G}}^{\dagger} = \underline{\boldsymbol{Z}}_{\mathrm{G}}^{*}$, i.e. the loaded transmit antenna represents a reciprocal multiport. A possible solution to equation (6.21) is given by [164], [167]

$$\underline{\boldsymbol{Z}}_{\mathrm{MT}} = \mathrm{i}\begin{bmatrix} \mathbf{0} & \sqrt{R}\left(\mathrm{Re}\left\{\underline{\boldsymbol{Z}}_{\mathrm{G}}^{\dagger}\right\}\right)^{\frac{1}{2}} \\ \sqrt{R}\left(\mathrm{Re}\left\{\underline{\boldsymbol{Z}}_{\mathrm{G}}^{\dagger}\right\}\right)^{\frac{1}{2}} & -\mathrm{Im}\left\{\underline{\boldsymbol{Z}}_{\mathrm{G}}^{\dagger}\right\} \end{bmatrix} \,. \tag{6.22}$$

The same can be done for the load side, where the DMN is described by an impedance matrix $\underline{\boldsymbol{Z}}_{\mathrm{MR}} \in \mathbb{C}^{2M\times 2M}$

$$\begin{bmatrix} \underline{\boldsymbol{V}}_{\mathrm{R}} \\ \underline{\boldsymbol{V}}_{\mathrm{L}} \end{bmatrix} = \underline{\boldsymbol{Z}}_{\mathrm{MR}}\begin{bmatrix} \underline{\boldsymbol{I}}_{\mathrm{R}} \\ -\underline{\boldsymbol{I}}_{\mathrm{L}} \end{bmatrix} \,. \tag{6.23}$$

In the case of load matching, the impedance seen by the receiver DMN is given by the Hermitian conjugate of the load impedance matrix $\underline{\boldsymbol{Z}}_{\mathrm{L}}^{\dagger}$. Hence, we have the matching condition

$$\underline{\boldsymbol{V}}_{\mathrm{R}} = -\underline{\boldsymbol{Z}}_{\mathrm{L}}^{\dagger}\underline{\boldsymbol{I}}_{\mathrm{R}} \,. \tag{6.24}$$

The load is finally given by M independent channels, each terminated by a load resistance of $R = 50\,\Omega$, modeling the input of a typical RF receiver. Thus, the independence of the load voltages can be described by the decoupling condition

$$\underline{\boldsymbol{V}}_{\mathrm{L}} = R\mathbf{1}\underline{\boldsymbol{I}}_{\mathrm{L}} \,. \tag{6.25}$$

Inserting the conditions (6.24) and (6.25) into (6.23) gives a system of equations, describing the elements of the impedance matrix $\underline{\boldsymbol{Z}}_{\mathrm{MR}}$ of the receiver DMN, which is given by

$$-\underline{\boldsymbol{Z}}_{\mathrm{L}}^{\dagger}\underline{\boldsymbol{I}}_{\mathrm{R}} = \underline{\boldsymbol{Z}}_{\mathrm{MR},11}\underline{\boldsymbol{I}}_{\mathrm{R}} - \underline{\boldsymbol{Z}}_{\mathrm{MR},12}\underline{\boldsymbol{I}}_{\mathrm{L}}\,, \tag{6.26}$$

$$R\mathbf{1}\underline{\boldsymbol{I}}_{\mathrm{L}} = \underline{\boldsymbol{Z}}_{\mathrm{MR},21}\underline{\boldsymbol{I}}_{\mathrm{R}} - \underline{\boldsymbol{Z}}_{\mathrm{MR},22}\underline{\boldsymbol{I}}_{\mathrm{L}}\,. \tag{6.27}$$

Similar to the transmit side, we additionally require the decoupling and matching multiport $\underline{\boldsymbol{Z}}_{\mathrm{MR}}$ to be linear, lossless, and reciprocal. Thus $\underline{\boldsymbol{Z}}_{\mathrm{MR}}$ needs to be purely imaginary, i.e. $\mathrm{Re}\{\underline{\boldsymbol{Z}}_{\mathrm{MR}}\} = \mathbf{0}$, and symmetric, i.e. $\underline{\boldsymbol{Z}}_{\mathrm{MR}} = \underline{\boldsymbol{Z}}_{\mathrm{MR}}^{\mathrm{T}}$. These conditions can be imposed by forcing the block matrix elements $\underline{\boldsymbol{Z}}_{\mathrm{MR},11} \in \mathbb{C}^{M\times M}$, $\underline{\boldsymbol{Z}}_{\mathrm{MR},12} \in \mathbb{C}^{M\times M}$, $\underline{\boldsymbol{Z}}_{\mathrm{MR},21} \in \mathbb{C}^{M\times M}$, and $\underline{\boldsymbol{Z}}_{\mathrm{MR},22} \in \mathbb{C}^{M\times M}$ to

$$\underline{\boldsymbol{Z}}_{\mathrm{MR}} = \mathrm{i}\begin{bmatrix} \boldsymbol{X}_{\mathrm{MR},11} & \boldsymbol{X}_{\mathrm{MR},12} \\ \boldsymbol{X}_{\mathrm{MR},21} & \boldsymbol{X}_{\mathrm{MR},22} \end{bmatrix}\,, \tag{6.28}$$

with purely real sub-matrices $\boldsymbol{X}_{\mathrm{MR},11} \in \mathbb{R}^{M\times M}$, $\boldsymbol{X}_{\mathrm{MR},12} \in \mathbb{R}^{M\times M}$, $\boldsymbol{X}_{\mathrm{MR},21} \in \mathbb{R}^{M\times M}$, and $\boldsymbol{X}_{\mathrm{MR},22} \in \mathbb{R}^{M\times M}$. Inserting the conditions for the impedance matrix to be reciprocal and lossless, given by equation (6.28) into the system of equations (6.26) and (6.27) yields

$$-R\mathbf{1}\underline{\boldsymbol{I}}_{\mathrm{L}} = \left[\mathrm{i}\boldsymbol{X}_{\mathrm{MR},22} + \boldsymbol{X}_{\mathrm{MR},21}\left(\underline{\boldsymbol{Z}}_{\mathrm{L}}^{\dagger} + \mathrm{i}\boldsymbol{X}_{\mathrm{MR},11}\right)^{-1}\boldsymbol{X}_{\mathrm{MR},12}\right]\underline{\boldsymbol{I}}_{\mathrm{L}}\,, \tag{6.29}$$

and thus

$$-R\mathbf{1} = \mathrm{i}\boldsymbol{X}_{\mathrm{MR},22} + \boldsymbol{X}_{\mathrm{MR},21}\left(\mathrm{Re}\left\{\underline{\boldsymbol{Z}}_{\mathrm{L}}^{\dagger}\right\} + \mathrm{i}\,\mathrm{Im}\left\{\underline{\boldsymbol{Z}}_{\mathrm{L}}^{\dagger}\right\} + \mathrm{i}\boldsymbol{X}_{\mathrm{MR},11}\right)^{-1}\boldsymbol{X}_{\mathrm{MR},12}\,. \tag{6.30}$$

Note that we also require here that the load impedance $\underline{\boldsymbol{Z}}_{\mathrm{L}}^{\dagger}$ is reciprocal, i.e. $\underline{\boldsymbol{Z}}_{\mathrm{L}}^{\dagger} = \underline{\boldsymbol{Z}}_{\mathrm{L}}^{\dagger,\mathrm{T}}$, and thus $\underline{\boldsymbol{Z}}_{\mathrm{L}}^{\dagger} = \underline{\boldsymbol{Z}}_{\mathrm{L}}^{*}$. Equation (6.30) has many solutions. One possible solution is given by [164], [167]

$$\underline{\boldsymbol{Z}}_{\mathrm{MR}} = \mathrm{i}\begin{bmatrix} -\mathrm{Im}\left\{\underline{\boldsymbol{Z}}_{\mathrm{L}}^{\dagger}\right\} & -\sqrt{R}\left(\mathrm{Re}\left\{\underline{\boldsymbol{Z}}_{\mathrm{L}}^{\dagger}\right\}\right)^{\frac{1}{2}} \\ -\sqrt{R}\left(\mathrm{Re}\left\{\underline{\boldsymbol{Z}}_{\mathrm{L}}^{\dagger}\right\}\right)^{\frac{1}{2}} & \mathbf{0} \end{bmatrix}\,. \tag{6.31}$$

Let us now investigate the whole MIMO communication link, with a given antenna array, described by the impedance matrix $\underline{\boldsymbol{Z}}$, together with transmit and receive DMN, described by impedance matrices $\underline{\boldsymbol{Z}}_{\mathrm{MT}}$ and $\underline{\boldsymbol{Z}}_{\mathrm{MR}}$, respectively. Using the power matching condition at the input, i.e. $\underline{\boldsymbol{I}} = \frac{1}{2}\frac{\underline{\boldsymbol{V}}_{\mathrm{G}}}{R}$, we can calculate the transmit currents through the transmit DMN from the generator voltages $\underline{\boldsymbol{V}}_{\mathrm{G}}$ by

$$\underline{\boldsymbol{I}}_{\mathrm{T}} = \mathrm{i}\frac{1}{2\sqrt{R}}\left(\mathrm{Re}\left\{\underline{\boldsymbol{Z}}_{\mathrm{G}}^{\dagger}\right\}\right)^{-\frac{1}{2}}\underline{\boldsymbol{V}}_{\mathrm{G}}\,. \tag{6.32}$$

With the impedance matrix of the antenna array, we can then evaluate the received current before the receiver DMN. The ratio between voltages and currents at the receive side is given by $\underline{\boldsymbol{V}}_{\mathrm{R}} = \underline{\boldsymbol{Z}}_{\mathrm{L}}\underline{\boldsymbol{I}}_{\mathrm{R}}$. Thus, we can replace $\underline{\boldsymbol{V}}_{\mathrm{R}}$ in (6.23), which then results in

$$\underline{\boldsymbol{I}}_{\mathrm{R}} = \mathrm{i}\frac{1}{2\sqrt{R}}\left(\underline{\boldsymbol{Z}}_{\mathrm{L}} + \underline{\boldsymbol{Z}}_{\mathrm{R}}\right)^{-1}\underline{\boldsymbol{Z}}_{\mathrm{RT}}\left(\mathrm{Re}\left\{\underline{\boldsymbol{Z}}_{\mathrm{G}}^{\dagger}\right\}\right)^{-\frac{1}{2}}\underline{\boldsymbol{V}}_{\mathrm{G}}\,. \tag{6.33}$$

Finally, we can interrelate the generator voltage vector $\underline{\boldsymbol{V}}_{\mathrm{G}}$ to the voltages $\underline{\boldsymbol{V}}_{\mathrm{L}}$ observed at the individual load impedances by

$$\underline{\boldsymbol{V}}_{\mathrm{L}} = \frac{1}{2}\left(\mathrm{Re}\left\{\underline{\boldsymbol{Z}}_{\mathrm{L}}^{\dagger}\right\}\right)^{\frac{1}{2}}\left(\underline{\boldsymbol{Z}}_{\mathrm{L}} + \underline{\boldsymbol{Z}}_{\mathrm{R}}\right)^{-1}\underline{\boldsymbol{Z}}_{\mathrm{RT}}\left(\mathrm{Re}\left\{\underline{\boldsymbol{Z}}_{\mathrm{G}}^{\dagger}\right\}\right)^{-\frac{1}{2}}\underline{\boldsymbol{V}}_{\mathrm{G}}\,. \tag{6.34}$$

We can summarize the MIMO communication link in a dimensionless transformation matrix $\underline{\boldsymbol{D}} \in \mathbb{C}^{M\times N}$, describing the linear relationship between the generator voltages $\underline{\boldsymbol{V}}_{\mathrm{G}}$ and the load voltages $\underline{\boldsymbol{V}}_{\mathrm{L}}$, such that

$$\underline{\boldsymbol{V}}_{\mathrm{L}} = \frac{1}{2}\underline{\boldsymbol{D}}\,\underline{\boldsymbol{V}}_{\mathrm{G}}\,, \tag{6.35}$$

with

$$\underline{\boldsymbol{D}} = \left(\mathrm{Re}\left\{\underline{\boldsymbol{Z}}_{\mathrm{L}}^{\dagger}\right\}\right)^{\frac{1}{2}} \left(\underline{\boldsymbol{Z}}_{\mathrm{L}} + \underline{\boldsymbol{Z}}_{\mathrm{R}}\right)^{-1} \underline{\boldsymbol{Z}}_{\mathrm{RT}} \left(\mathrm{Re}\left\{\underline{\boldsymbol{Z}}_{\mathrm{G}}^{\dagger}\right\}\right)^{-\frac{1}{2}} . \tag{6.36}$$

The total transmitted power, i.e. the power that is fed into the transmit DMN, which due to the losslessness of the DMN is equal to the power at the transmit ports of the antenna array, is given by

$$P_T = \frac{\boldsymbol{V}_{\mathrm{G}}^{\dagger}\boldsymbol{V}_{\mathrm{G}}}{4R} , \tag{6.37}$$

where we used the power matching condition $\underline{\boldsymbol{I}} = \frac{1}{2}\frac{\boldsymbol{V}_{\mathrm{G}}}{R}$ and $\underline{\boldsymbol{V}} = \frac{\boldsymbol{V}_{\mathrm{G}}}{2}$. The total power at the receive side is given by

$$P_{\mathrm{R}} = \frac{\boldsymbol{V}_{\mathrm{L}}^{\dagger}\boldsymbol{V}_{\mathrm{L}}}{R} = \frac{\underline{\boldsymbol{Z}}_{\mathrm{G}}^{\dagger}\underline{\boldsymbol{D}}^{\dagger}\underline{\boldsymbol{D}}\,\boldsymbol{V}_{\mathrm{G}}}{4R} , \tag{6.38}$$

where the transfer relation of the MIMO communication link (6.35) was inserted into the expression for the power in the load resistors R. The channel power gain G is defined as the maximal ratio of received power to transmit power, which is given by

$$G = \max \frac{P_{\mathrm{R}}}{P_{\mathrm{T}}} = \max_{\boldsymbol{V}_{\mathrm{G}}} \frac{\boldsymbol{V}_{\mathrm{G}}^{\dagger}\underline{\boldsymbol{D}}^{\dagger}\underline{\boldsymbol{D}}\,\boldsymbol{V}_{\mathrm{G}}}{\boldsymbol{V}_{\mathrm{G}}^{\dagger}\boldsymbol{V}_{\mathrm{G}}} = \mu_{\max}\left(\underline{\boldsymbol{D}}^{\dagger}\underline{\boldsymbol{D}}\right) , \tag{6.39}$$

where $\mu_{\max}(\ldots)$ denotes the maximum eigenvalue of its argument. As we are interested in multi-channel operation, we perform a singular value decomposition [164] of $\underline{\boldsymbol{D}}$,

$$\underline{\boldsymbol{D}} = \underline{\boldsymbol{R}}\,\mathrm{diag}\left[S_1, S_2, \ldots, S_L\right]\underline{\boldsymbol{Q}}^{\dagger} , \tag{6.40}$$

with the unitary matrices $\underline{\boldsymbol{R}} \in \mathbb{C}^{M\times M}$, $\underline{\boldsymbol{Q}}^{\dagger} \in \mathbb{C}^{N\times N}$ and the $M \times N$-dimensional diagonal real, non-negative matrix given by the $L = \mathrm{rank}\,(\underline{\boldsymbol{D}}) \leq \min(M, N)$ singular values of $\underline{\boldsymbol{D}}$, ordered such that $S_1 \geq S_2 \geq \ldots \geq S_L$. To this end, we define new channel inputs $\underline{\boldsymbol{X}}$ and new channel outputs $\underline{\boldsymbol{Y}}$ by [164], [167], [168]

$$\underline{\boldsymbol{X}} = \frac{1}{2\sqrt{R}}\underline{\boldsymbol{Q}}^{\dagger}\boldsymbol{V}_{\mathrm{G}} , \qquad \underline{\boldsymbol{Y}} = \frac{1}{\sqrt{R}}\underline{\boldsymbol{R}}^{\dagger}\boldsymbol{V}_{\mathrm{L}} . \tag{6.41}$$

Then it follows that

$$\begin{aligned}\underline{\boldsymbol{Y}} &= \frac{1}{\sqrt{R}}\underline{\boldsymbol{R}}^{\dagger}\boldsymbol{V}_{\mathrm{L}} = \frac{1}{2\sqrt{R}}\underline{\boldsymbol{R}}^{\dagger}\underline{\boldsymbol{D}}\,\boldsymbol{V}_{\mathrm{G}} = \frac{1}{2\sqrt{R}}\underline{\boldsymbol{R}}^{\dagger}\underline{\boldsymbol{R}}\,\mathrm{diag}\left[S_1, S_2, \ldots, S_L\right]\underline{\boldsymbol{Q}}^{\dagger}\boldsymbol{V}_{\mathrm{G}} \\ &= \frac{1}{2\sqrt{R}}\,\mathrm{diag}\left[S_1, S_2, \ldots, S_L\right]\underline{\boldsymbol{Q}}^{\dagger}\boldsymbol{V}_{\mathrm{G}} = \mathrm{diag}\left[S_1, S_2, \ldots, S_L\right]\underline{\boldsymbol{X}} ,\end{aligned} \tag{6.42}$$

and hence,

$$\underline{Y}_i = S_i \underline{X}_i . \tag{6.43}$$

The total transmit power in terms of the new channel input $\underline{\boldsymbol{X}}$ is given by

$$P_{\mathrm{T}} = \sum_{i=1}^{L} \left|\underline{X}_i\right|^2 . \tag{6.44}$$

Hence, the received power with respect to the new channel output $\underline{\boldsymbol{Y}}$ is equal to

$$P_{\mathrm{R}} = \sum_{i=1}^{L} \left|\underline{Y}_i\right|^2 = \sum_{i=1}^{L} S_i^2 \left|\underline{X}_i\right|^2 . \tag{6.45}$$

Overall, this means that by linear signal processing one can establish $L = \mathrm{rank}\,(\underline{\boldsymbol{D}}) \leq \min(M, N)$ independent channels in the information-theoretic sense. Now the question arises, how to distribute a given power budget at the transmitter to the L independent channels, such that the channel capacity can be achieved. The channel

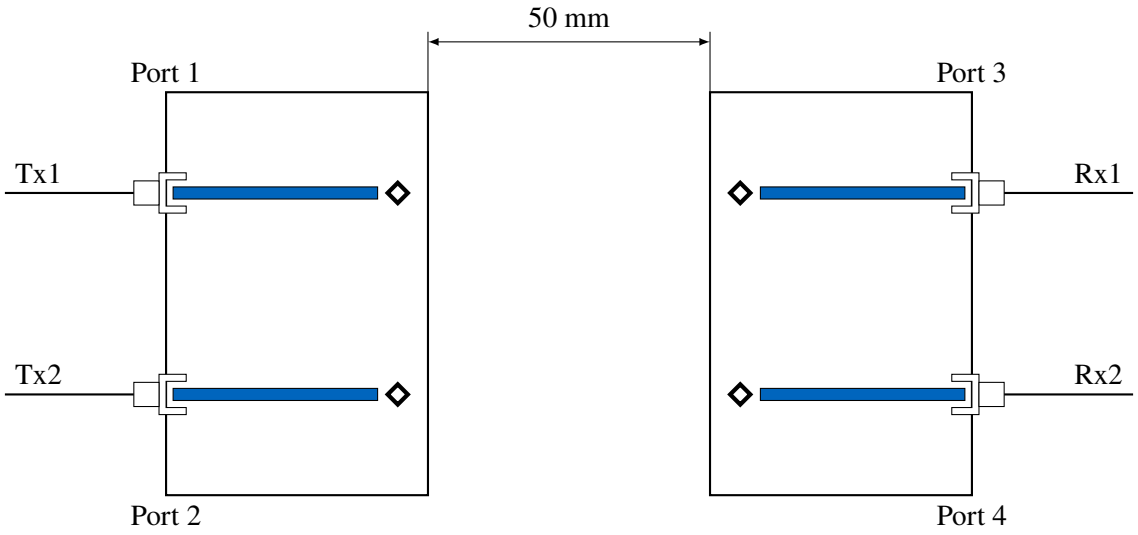

Figure 6.2 Antenna arrangement for MIMO transmission scenario.

capacity, and thus, the solution of this optimization problem depends on the noise model employed in the information-theoretic approach to the communication channel. Optimal solutions have been found for channels with additive white Gaussian noise and intersymbol interference in terms of the water filling algorithm [169]. It is desirable to have channels of equal strength, i.e.

$$S_1^2 \approx S_2^2 \approx \ldots \approx S_L^2 \,, \tag{6.46}$$

where S_i is ideally as large as possible. This opens the possibility for multichannel operation, i.e. where we can transmit information over L independent, equally strong channels. This scenario has been investigated numerically in [167], [168], [170] and experimentally in [155], without considering the design and realization of suitable DMNs.

6.2 Experimental Characterization

For an experimental study on the multistreaming capability of a given MIMO antenna arrangement, we study a transmission scenario as depicted in Figure 6.2. There are two antenna PCBs, each equipped with two Molex $2.4\,\mathrm{GHz}$ SMT On-ground MID Chip Antennas, together with passive Π-matching networks, connected to a $50\,\Omega$ transmission line and an SMA connector each.

The antenna PCBs are provided by NXP-Semiconductors. In this scenario, two antenna PCBs are arranged such that they are facing each other at a distance of $50\,\mathrm{mm}$. In order to determine the impedance matrix of the antenna multiport, we connected the four ports, depicted in Figure 6.2, to a vector network analyzer to obtain the scattering parameters. The reflection S-parameters for each of the four ports are given in Figure 6.3a. The antennas are designed for a resonance frequency of $f_\mathrm{r} = 2.4\,\mathrm{GHz}$. In Figure 6.3a one can see that port 1 has a slightly different resonance frequency, compared to the other ports. This can be explained by a defective antenna element, that needed to be replaced before measurement. The re-soldering of the antenna affected the matching for that port, such that there is this offset in resonance frequency.

The transmission S-parameters, i.e. the parameters measured with excitation at the transmit ports and observation at the receive ports are given in Figure 6.3b. From the measured S-Parameters, the impedance matrix of the antenna four-port can be determined by

$$\underline{\boldsymbol{Z}} = R\,(\mathbf{1} - \underline{\boldsymbol{S}})^{-1}\,(\mathbf{1} + \underline{\boldsymbol{S}}) \;. \tag{6.47}$$

for a fixed characteristic impedance $R = 50\,\Omega$. With the impedance matrix $\underline{\boldsymbol{Z}}$ of the antenna arrangement, we can calculate the respective generator and load impedances, $\underline{\boldsymbol{Z}}_\mathrm{G}$ and $\underline{\boldsymbol{Z}}_\mathrm{L}$. We then perform a singular

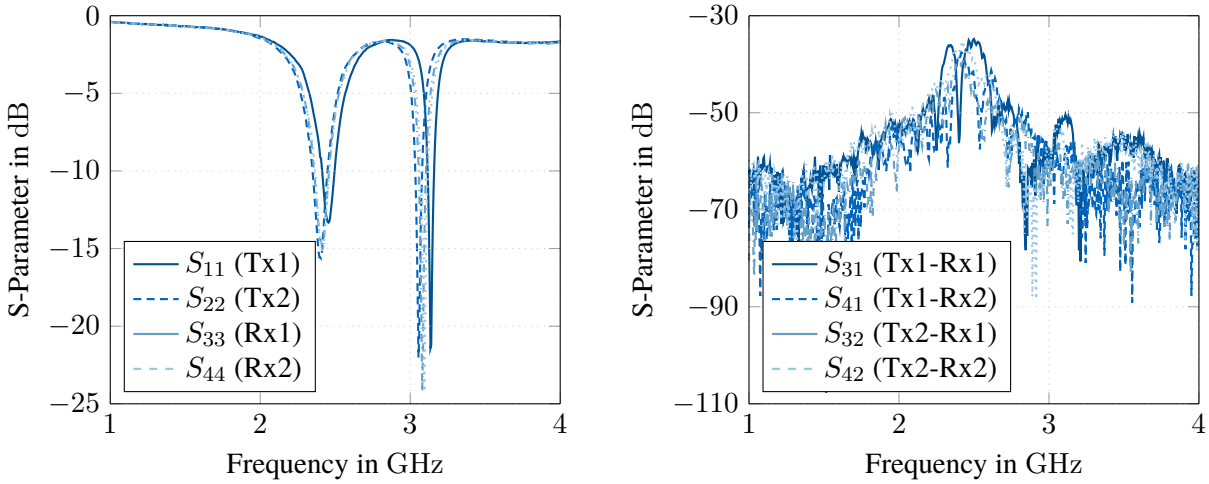

(a) Reflection S-Parameters for each of the four ports.

(b) Transmission S-Parameters for each of the four ports.

Figure 6.3 Transmission and reflection S-Parameters for the antenna multiport as depicted in Figure 6.2. The solid blue curve in the left figure (a) depicts S_{11}. The dashed blue curve represents S_{22}, while S_{33} and S_{44} are given by the solid and dashed light blue curvess, respectively. For figure (b), the blue curves represent S-parameters with excitation at port 1, while the light blue curves represent S-parameters with excitation at port 2.

value decomposition of the channel matrix $\boldsymbol{D}$ according to (6.40). The ratio of the second-largest singular value s_2^2 to the largest singular value s_1^2 is given in Figure 6.4. Here, one can see that for this scenario, the multistreaming capability is limited as the ratio of the channel strengths of the second strongest channel to the strongest channel is at most 0.3 in the usable frequency band from $2.25\,\mathrm{GHz}$ to $2.75\,\mathrm{GHz}$. It is expected that this MIMO performance can be drastically increased by designing and implementing decoupling and matching networks as suggested in section 6.1.

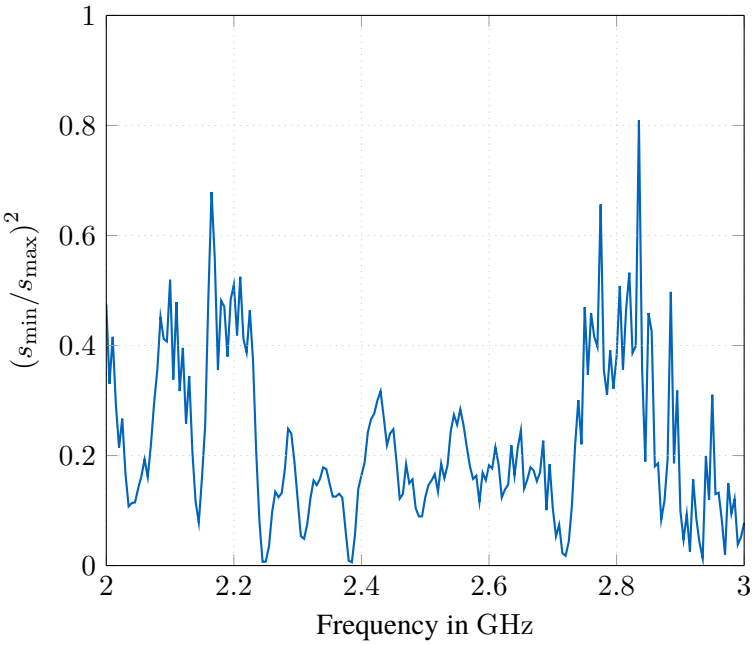

Figure 6.4 The ratio of second-largest squared singular value s_2^2 of the channel matrix $\boldsymbol{D}$ to the largest squared singular value s_1^2, as a measure for investigating multistreaming capability.

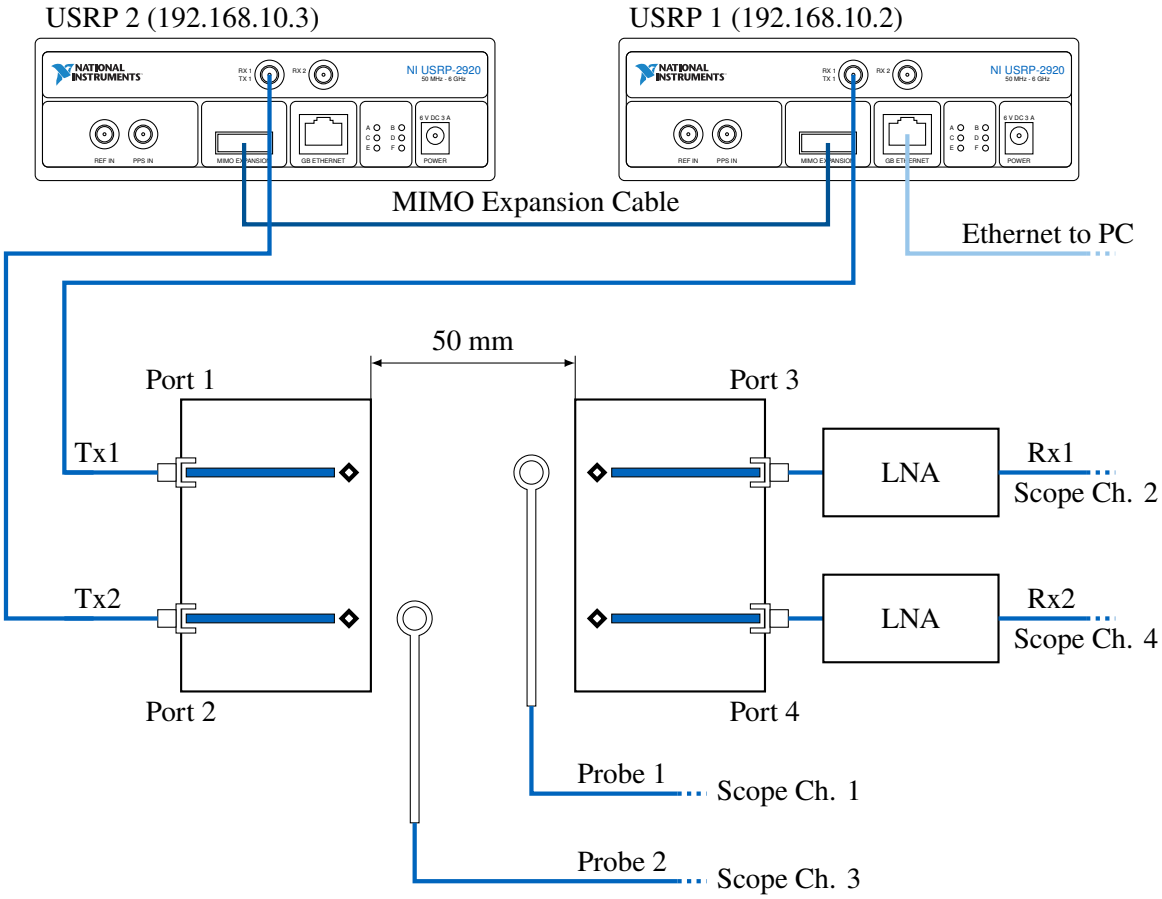

Figure 6.5 Measurement Setup for MIMO transmission scenario.

Furthermore, it was pointed out in [167], [168] that the multistreaming capability is sensitive to the distance of the antenna elements within transmit and receive groups, as well as between the respective transmit and receive elements and the respective frequency, where the wireless transmission takes place. Since in our setup, there was a fixed frequency of $2.4\,\mathrm{GHz}$, and the distances of the antennas within the transmit and receive groups were also fixed by the PCB, the only degree of freedom for optimizing MIMO capability would be tuning the distance between the two PCBs.

6.3 MIMO Communication Setup

In the following, we consider the same antenna arrangement as given in Figure 6.1, connected to two National Instruments USRP 2920 at the transmit side. The two USRPs are phase-synchronized using a dedicated MIMO expansion cable. The receive antennas are connected to two of the input ports of a Teledyne LeCroy SDA 813Zi-A digital oscilloscope with a bandwidth of $13\,\mathrm{GHz}$ and a sampling rate of $40\,\mathrm{GS\,s^{-1}}$. The other two input ports are connected to Langer EMV Technik RF-R 50-1 magnetic near-field probes, which are scanning the tangential magnetic field on a predefined grid above the antenna arrangement. A detailed description of the MIMO measurement setup is given in Figure 6.5. The goal of this setup is to create a model of an actual MIMO near-field communication scenario, with QPSK modulated data at a carrier frequency of $2.4\,\mathrm{GHz}$. In order to achieve this, the NI USRPs are connected to a computer that runs the control software for the MIMO communication scenario. A sketch of the structure of the control software is given in Figure 6.6. The data frames for the QPSK communication scenarios consist of a $26\,\mathrm{bit}$ header, followed by a block of $200\,\mathrm{bit}$ of scrambled payload data. For frame synchronization, a $13\,\mathrm{bit}$ Barker code is sent on both, the in-phase and the quadrature component of the complex baseband signal, accounting for a total of $26\,\mathrm{bit}$ header. The payload data section is scrambled using a linear feedback shift register in order to avoid a large number of consecutive zeros

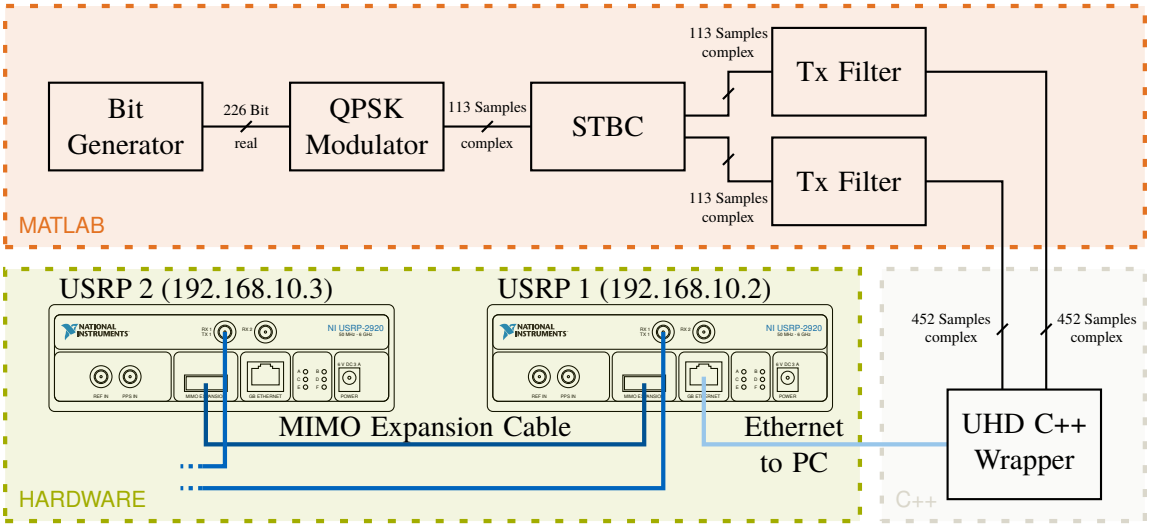

Figure 6.6 Software Setup for MIMO transmission scenario.

or ones. This is done in order to achieve an improved symbol timing recovery on the receive side. A $14\,\mathrm{bit}$ deterministic frame identifier, followed by a $186\,\mathrm{bit}$ pseudo-random bit sequence as payload, forms the input data fed into the scrambler. The real bit stream with a frame length of $226\,\mathrm{bit}$ is then modulated to I/Q symbols by a QPSK (quadrature phase-shift keying) modulation scheme. The resulting symbols are encoded for MIMO transmission in the space-time block coder, using the diversity scheme given in [171]. Note that we did not employ any other linear signal processing to this end, in order to make use of individual independent channels by preconditioning the transmit signal with the unitary matrix $\underline{\boldsymbol{Q}}^{\dagger}$ from the singular value decomposition of the channel matrix, as the multistreaming capability of our channel was estimated to be low, based on the measurements in the previous section.

In this chapter, we have demonstrated the design procedure for decoupling and matching multiports according to [164], [167]. Furthermore, we have presented measurements of a 2×2 near-field MIMO communication scenario using special $2.4\,\mathrm{GHz}$ helical PCB antennas. For the measurements, the antennas have only been matched to the $50\,\Omega$ line impedance of the feeding waveguides using simple Π-type matching networks. By investigating the ratio of the second-largest to the largest singular value, we can see that the multi-channel performance of this system is not optimal. It is believed that the MIMO capacity for the near-field communication link could be drastically improved by introducing decoupling and matching networks, as described in section 6.1. Finally, a measurement setup for near-field MIMO data transmission is presented. This setup can be used to investigate stochastic electromagnetic field propagation in near-field MIMO communication links, by applying the theoretical framework from chapter 3.

7 Data Reduction

Data reduction is important when considering scans of stochastic electromagnetic fields, as the data recorded can easily exceed the capabilities of current computer systems. Nevertheless, not all information recorded with near-field scanning, as described in chapter 4, is necessary in order to have a reasonably good description of a stationary Gaussian electromagnetic field, as we will demonstrate in the present chapter on data reduction. An in-depth treatment of data reduction for stochastic electromagnetic fields using principal component analysis was given in [38][1]. A similar approach for data reduction for stochastic fields was discussed in [172].

7.1 Principal Component Analysis

The amount of data for a field characterization by correlation information can be enormous. In frequency-domain, we need to store the frequency-domain auto-correlation and cross-correlation functions for each sampling point and for each pair of sampling points, respectively. The sampling of stochastic electromagnetic fields has been discussed in [173], as well as in chapter 4. Thereby, the number of correlation spectra over the considered frequency range is given by $N\left(2N-1\right)$ if both tangential polarizations are considered in each measurement point or $\frac{1}{2}N\left(N-1\right)$ considering only one polarization component, where N is the number of sampling points. The amount of data also depends linearly on the number of frequency bins considered for further analysis. To make further numerical treatment possible, e.g. for equivalent source localization in EMI scenarios [139] or for computationally propagating correlation spectra [16], we need to reduce the amount of data considerably, without loosing the relevant contained information. Principal component analysis (PCA) is well suited for this purpose [39], [173], [174]. In the following, we develop an algorithm based on PCA for reducing the dimensionality of a given set of correlation matrices, while retaining most of the information present in the original data. The algorithm will be flexible enough to allow for different qualities of the resulting approximations.

Principal component analysis can reduce the dimensionality of a given data set, consisting of a large number of interrelated variables while retaining nearly all of the contained variation. As a statistical method, Principal component analysis was developed independently by K. Pearson and H. Hotelling and had its major applications around the fields of psychology and education [175], [176]. Over the years, other disciplines started to use PCA and it became a standard procedure in multivariate statistics [177]. In the context of EMC investigations, it has been applied in [40], [41].

The principal components (PCs) are the projections of a given data set along the directions of largest variation. For further investigations let us introduce the first- and second-order statistics of a data set, represented by some multivariate random variable $\boldsymbol{X}$. The mean vector $\boldsymbol{\mu} \in \mathbb{C}^n$ and covariance matrix $\boldsymbol{C} \in \mathbb{C}^{n\times n}$ are given by

$$\boldsymbol{\mu} = \left\langle\!\left\langle \boldsymbol{X} \right\rangle\!\right\rangle, \tag{7.1}$$

$$\boldsymbol{C} = \left\langle\!\!\left\langle \left(\boldsymbol{X}-\boldsymbol{\mu}\right)\left(\boldsymbol{X}-\boldsymbol{\mu}\right)^{\dagger} \right\rangle\!\!\right\rangle. \tag{7.2}$$

The brackets $\left\langle\!\left\langle \cdot \right\rangle\!\right\rangle$ denote the forming of an ensemble average and $\cdot^{\dagger}$ indicates the Hermitian transpose. We now try to find a linear functional $\langle \boldsymbol{\alpha}_1, \cdot \rangle$, projecting the actual data $\boldsymbol{X}$ on that direction, such that the variance given by

$$\left\langle\!\!\left\langle \left(\boldsymbol{\alpha}_1^{\dagger}\boldsymbol{X}-\boldsymbol{\alpha}_1^{\dagger}\boldsymbol{\mu}\right)\left(\boldsymbol{\alpha}_1^{\dagger}\boldsymbol{X}-\boldsymbol{\alpha}_1^{\dagger}\boldsymbol{\mu}\right)^{\dagger} \right\rangle\!\!\right\rangle = \boldsymbol{\alpha}_1^{\dagger}\boldsymbol{C}\boldsymbol{\alpha}_1 \tag{7.3}$$

[1] The chapter on data reduction using principal component analysis was published under copyright of John Wiley and Sons in M. Haider and J. A. Russer, "Principal component analysis for efficient characterization of stochastic electromagnetic fields", *International Journal of Numerical Modelling: Electronic Networks, Devices and Fields*, vol. 31, no. 4, pp. 1–10, 2018. DOI: 10.1002/jnm.2246. The content (text and figures) is reproduced with permission of John Wiley and Sons.

is maximized. Furthermore, we introduce a constraint, such that $\boldsymbol{\alpha}_1$ assumes a finite value. Since we are only interested in the direction of maximum variance, we normalize the respective direction vector $\boldsymbol{\alpha}_1$ and thereby define a constraint for the optimization problem

$$\boldsymbol{\alpha}_1 = \underset{\|\boldsymbol{\alpha}_1\|^2=1}{\arg\max} \left(\boldsymbol{\alpha}_1^\dagger \boldsymbol{C} \boldsymbol{\alpha}_1 \right) , \tag{7.4}$$

where $\|\cdot\|$ denotes the Euclidean norm. A common approach for solving such optimization problems is the technique of Lagrange multipliers. We rewrite the problem with a Lagrange multiplier λ_1 which takes care of the constraint and we obtain

$$\mathcal{L}\left(\boldsymbol{\alpha}_1, \lambda_1\right) = \boldsymbol{\alpha}_1^\dagger \boldsymbol{C} \boldsymbol{\alpha}_1 - \lambda_1 \left(\boldsymbol{\alpha}_1^\dagger \boldsymbol{\alpha}_1 - 1 \right) , \tag{7.5}$$

to be maximized. Differentiation with respect to $\boldsymbol{\alpha}_1$, and forcing the result to be zero yields

$$\left(\boldsymbol{C} - \lambda_1 \mathbf{1}\right) \boldsymbol{\alpha}_1 = 0 , \tag{7.6}$$

with the identity matrix $\mathbf{1}$. Equation (7.6) is an eigenvalue problem for the covariance matrix $\boldsymbol{C}$. The Lagrange multiplier λ_1 turns out to be an eigenvalue and $\boldsymbol{\alpha}_1$ turns out to be an eigenvector. Recall that the quantity we wanted to maximize was $\boldsymbol{\alpha}_1^\dagger \boldsymbol{C} \boldsymbol{\alpha}_1$. This can be reformulated in terms of eigenvalues as

$$\boldsymbol{\alpha}_1^\dagger \boldsymbol{C} \boldsymbol{\alpha}_1 = \boldsymbol{\alpha}_1^\dagger \lambda_1 \boldsymbol{\alpha}_1 = \lambda_1 \boldsymbol{\alpha}_1^\dagger \boldsymbol{\alpha}_1 = \lambda_1 , \tag{7.7}$$

because we restricted $\boldsymbol{\alpha}_1$ to have unit norm. Therefore, the largest eigenvalue λ_1 of $\boldsymbol{C}$ gives the factor for the first principal component, which is itself given by the corresponding eigenvector.

The second PC $\boldsymbol{\alpha}_2$ is then given by the eigenvector corresponding to the second largest eigenvalue λ_2. In general, the n-th PC is given by the direction of the eigenvector corresponding to the n-th largest eigenvalue. The total number of principal components of a given covariance matrix $\boldsymbol{C}$ is determined by the rank of $\boldsymbol{C}$.

Since the PCs $\{\boldsymbol{\alpha}_n\}_{n=1}^N$ form an orthonormal eigenvector basis, we can express $\boldsymbol{C}$ by

$$\boldsymbol{C} = \sum_{n=1}^{N} \lambda_n \boldsymbol{\alpha}_n \boldsymbol{\alpha}_n^\dagger . \tag{7.8}$$

Covariance matrices are Hermitian and therefore yield orthogonal eigenvectors, which is shown by the following lemma.

Lemma 7.1. *Let $\boldsymbol{C} \in \mathbb{C}^{n \times n}$ be a Hermitian matrix with eigenvectors $\boldsymbol{\alpha}_1, \ldots, \boldsymbol{\alpha}_n$. Then the eigenvectors of $\boldsymbol{C}$ are orthogonal pairwise, i.e.*

$$\boldsymbol{\alpha}_i^\dagger \boldsymbol{\alpha}_j = 0 ,$$

for $i \neq j$.

Proof. Let λ_1 and λ_2 be two different eigenvalues of $\boldsymbol{C}$ with the corresponding eigenvectors $\boldsymbol{\alpha}_1$ and $\boldsymbol{\alpha}_2$. Then it holds that

$$\boldsymbol{\alpha}_1^\dagger \boldsymbol{C} \boldsymbol{\alpha}_2 = \boldsymbol{\alpha}_1^\dagger \left(\lambda_2 \boldsymbol{\alpha}_2\right) = \lambda_2 \boldsymbol{\alpha}_1^\dagger \boldsymbol{\alpha}_2 . \tag{7.9}$$

It also holds that

$$\boldsymbol{\alpha}_1^\dagger \boldsymbol{C}^\dagger \boldsymbol{\alpha}_2 = \left(\boldsymbol{C} \boldsymbol{\alpha}_1\right)^\dagger \boldsymbol{\alpha}_2 = \left(\lambda_1 \boldsymbol{\alpha}_1\right)^\dagger \alpha_2 = \lambda_1 \boldsymbol{\alpha}_1^\dagger \boldsymbol{\alpha}_2 . \tag{7.10}$$

For the last step, recall that a Hermitian matrix has real eigenvalues. From (7.9) and (7.10), we obtain that

$$\lambda_1 \boldsymbol{\alpha}_1^\dagger \boldsymbol{\alpha}_2 = \lambda_2 \boldsymbol{\alpha}_1^\dagger \boldsymbol{\alpha}_2 . \tag{7.11}$$

Since we required $\lambda_1 \neq \lambda_2$, this completes the proof because equation (7.11) can only hold if $\boldsymbol{\alpha}_1^\dagger \boldsymbol{\alpha}_2 = 0$. Thus the eigenvectors of a Hermitian matrix have to be orthogonal. □

In matrix-vector notation, we can rewrite equation (7.8) as

$$\boldsymbol{C} = \boldsymbol{A}\boldsymbol{\Lambda}\boldsymbol{A}^{\dagger}\,, \tag{7.12}$$

where the columns of the matrix $\boldsymbol{A}$ are formed by the PCs $\{\boldsymbol{\alpha}_n\}_{n=1}^{N}$, while the matrix $\boldsymbol{\Lambda}$ is a diagonal matrix with the respective eigenvalues on the main diagonal. Since we have normalized the eigenvectors to have unit length, the matrix $\boldsymbol{A}$ is unitary, i.e. $\boldsymbol{A}^{\dagger} = \boldsymbol{A}^{-1}$.

Now, when it comes to reducing complexity by applying PCA, the question arises, how many PCs are required to represent a given data set accurately. For this purpose, we can consider the cumulative percentage of total variance (CPTV). Usually, most of the variance is preserved by considering only the first few PCs. The CPTV provides a guideline for the number of PCs to retain, to preserve a predefined percentage of the total variance. Let us first define the term total variance.

Definition 7.1 (Total Variance)**.** *Let $\boldsymbol{C}$ be a covariance matrix of a given multivariate data set, represented by a random variable $\boldsymbol{X}$. We define the total variance contained in the data set by*

$$c_{\text{total}} = \operatorname{Tr}(\boldsymbol{C})\,.$$

The trace of a matrix $\boldsymbol{C} \in \mathbb{C}^{n\times n}$ is given by the sum of the diagonal elements of $\boldsymbol{C}$. It is also equal to the sum of the eigenvalues of $\boldsymbol{C}$, which is shown by the following lemma.

Lemma 7.2. *Let $\boldsymbol{C} \in \mathbb{C}^{n\times n}$ be a matrix with eigenvalues $\{\lambda_n\}_{n=1}^{N}$ and corresponding eigenvectors $\{\boldsymbol{\alpha}_n\}_{n=1}^{N}$. Then the trace of $\boldsymbol{C}$ is equal to the sum of eigenvalues,*

$$\operatorname{Tr}(\boldsymbol{C}) = \sum_{i=1}^{n} c_{ii} = \sum_{i=1}^{n} \lambda_i\,.$$

Proof. We know that we can express the matrix $\boldsymbol{C}$ in terms of

$$\boldsymbol{C} = \boldsymbol{A}\boldsymbol{\Lambda}\boldsymbol{A}^{\dagger}\,,$$

by equation (7.12). Thus, we can write

$$\operatorname{Tr}(\boldsymbol{C}) = \operatorname{Tr}\left(\boldsymbol{A}\boldsymbol{\Lambda}\boldsymbol{A}^{\dagger}\right) = \operatorname{Tr}\left(\boldsymbol{A}^{\dagger}\boldsymbol{A}\boldsymbol{\Lambda}\right) = \operatorname{Tr}(\boldsymbol{\Lambda})\,.$$

This holds since the trace is invariant under cyclic permutations [149], which will not be proven here, and since the matrix $\boldsymbol{A}$ is unitary. This completes the proof, since $\boldsymbol{\Lambda}$ is a diagonal matrix consisting of the respective eigenvalues of $\boldsymbol{C}$, i.e.

$$\operatorname{Tr}(\boldsymbol{C}) = \operatorname{Tr}(\boldsymbol{\Lambda}) = \sum_{i=1}^{n} \lambda_i\,.$$

□

Let us now consider a matrix $\boldsymbol{C}'$, which is formed by equation (7.12) but with considering a reduced set of the m largest PCs. We define the CPTV p_m by

$$p_m = 100\,\% \cdot \frac{\operatorname{Tr}(\boldsymbol{C}')}{\operatorname{Tr}(\boldsymbol{C})} = 100\,\% \cdot \frac{\sum_{i=1}^{m} \lambda_i}{\sum_{i=1}^{n} \lambda_i}\,. \tag{7.13}$$

By specifying the desired value for p_m, one can obtain the number of PCs necessary, in order to achieve this value. Based on this method, an algorithm was implemented in MATLAB for reducing the complexity of correlation spectra, describing stochastic EM fields.

7.2 Power Iteration

As discussed in section 7.1, PCA is about estimating the direction of largest variation, which is given by the eigenvector corresponding to the largest eigenvalue. An efficient iterative method for calculating the dominant eigenvector of a matrix is known by means of the power iteration algorithm [149]. This method is particularly fast, if the largest and second-largest eigenvalues are well separated, as we shall see in the following. The method is called power iteration since it involves matrix powers. The procedure is given by

$$\boldsymbol{x}^{(k)} = \frac{\boldsymbol{A}^k \boldsymbol{x}^{(0)}}{\left\| \boldsymbol{A}^k \boldsymbol{x}^{(0)} \right\|}, \tag{7.14}$$

with the known square-matrix $\boldsymbol{A} \in \mathbb{C}^{N \times N}$ whose dominant eigenvector is to be determined and a random initial vector $\boldsymbol{x}^{(0)} \in \mathbb{C}^N$. The initial random vector $\boldsymbol{x}^{(0)}$ can be expanded into a series of eigenvectors of the matrix $\boldsymbol{A}$,

$$\boldsymbol{x}^{(0)} = \sum_{i=1}^{N} \alpha_i \boldsymbol{v}_i \,. \tag{7.15}$$

Inserting this expansion into the iteration process (7.14) yields

$$\boldsymbol{x}^{(k)} = \frac{\boldsymbol{A}^k \left(\sum\limits_{i=1}^{N} \alpha_i \boldsymbol{v}_i \right)}{\left\| \boldsymbol{A}^k \boldsymbol{x}^{(0)} \right\|} = \frac{\sum\limits_{i=1}^{N} \alpha_i \lambda_i^k \boldsymbol{v}_i}{\left\| \boldsymbol{A}^k \boldsymbol{x}^{(0)} \right\|} \,. \tag{7.16}$$

We now label the eigenvalues of $\boldsymbol{A}$ in descending order, i.e. $\lambda_1 \geq \lambda_2 \geq \ldots \geq \lambda_n$. Since we are only interested in the largest eigenvalue-eigenvector pair, we bring λ_1 in front

$$\boldsymbol{x}^{(k)} = \frac{\lambda_1^k \left[\alpha_1 \boldsymbol{v}_1 + \sum\limits_{i=2}^{N} \alpha_i \left(\frac{\lambda_i}{\lambda_1} \right)^k \boldsymbol{v}_i \right]}{\left\| \boldsymbol{A}^k \boldsymbol{x}^{(0)} \right\|} = \frac{\alpha_1 \boldsymbol{v}_1 + \boldsymbol{e}^{(k)}}{\left\| \alpha_1 \boldsymbol{v}_1 + \boldsymbol{e}^{(k)} \right\|} \,. \tag{7.17}$$

Here, we introduced the residual or error vector $\boldsymbol{e}_k$ as

$$\boldsymbol{e}^{(k)} = \sum_{i=2}^{N} \alpha_i \left(\frac{\lambda_i}{\lambda_1} \right)^k \boldsymbol{v}_i \,, \tag{7.18}$$

where $\left(\frac{\lambda_i}{\lambda_1} \right) \leq 1$, since $\lambda_1 \geq \lambda_i$ for $i = \{2, \ldots, N\}$. Hence, for the limit $k \to \infty$ the error term vanishes, i.e.

$$\lim_{k \to \infty} \left\| \boldsymbol{e}^{(k)} \right\| = 0 \,. \tag{7.19}$$

The iterative method then converges to the first, i.e. the dominant eigenvector $\boldsymbol{v}_1$, which is determined by

$$\lim_{k \to \infty} \boldsymbol{x}^{(k)} = \frac{\alpha_1 \boldsymbol{v}_1}{\left\| \alpha_1 \boldsymbol{v}_1 \right\|} = \frac{\alpha_1 \boldsymbol{v}_1}{|\alpha_1| \left\| \boldsymbol{v}_1 \right\|} = \boldsymbol{v}_1 \,, \tag{7.20}$$

with $|\cdot|$ denoting the absolute value of the complex coefficient α_1. The procedure can be rewritten in an iterative form for obtaining the eigenvector $\boldsymbol{v}_1$,

$$\boldsymbol{v}_1^{(k+1)} = \frac{\boldsymbol{A} \boldsymbol{v}_1^{(k)}}{\left\| \boldsymbol{A} \boldsymbol{v}_1^{(k)} \right\|} \,. \tag{7.21}$$

Now, the calculation of the corresponding eigenvalue remains to be done. If λ_1 is the eigenvalue of a matrix $\boldsymbol{A}$, and $\boldsymbol{v}_1$ is the corresponding eigenvector, it holds that

$$\boldsymbol{A} \boldsymbol{v}_1 = \lambda_1 \boldsymbol{v}_1 \,. \tag{7.22}$$

An eigenvector $\boldsymbol{v}_1$ of a matrix $\boldsymbol{A}$ is not rotated by the action of $\boldsymbol{A}$. It is only scaled by a constant λ_1 which is then called the eigenvalue. Consequently, we can obtain the scaling constant by projecting our system onto the direction of $\boldsymbol{v}_1$, using the inner product

$$\langle \boldsymbol{v}_1, \boldsymbol{A}\boldsymbol{v}_1 \rangle = \boldsymbol{v}_1^\dagger \boldsymbol{A}\boldsymbol{v}_1 = \lambda_1 \boldsymbol{v}_1^\dagger \boldsymbol{v}_1 \,. \tag{7.23}$$

Solving equation (7.23) for λ_1 then finally provides us with a rule for calculating the corresponding eigenvalue,

$$\lambda_1 = \frac{\boldsymbol{v}_1^\dagger \boldsymbol{A}\boldsymbol{v}_1}{\boldsymbol{v}_1^\dagger \boldsymbol{v}_1} = \frac{\boldsymbol{v}_1^\dagger \boldsymbol{A}\boldsymbol{v}_1}{\|\boldsymbol{v}_1\|^2} \,. \tag{7.24}$$

The iterative estimation for the largest eigenvalue in each round is therefore given by the Rayleigh quotient,

$$\lambda_1^{(k)} = \frac{\boldsymbol{v}_1^{(k)\dagger} \boldsymbol{A}\boldsymbol{v}_1^{(k)}}{\boldsymbol{v}_1^{(k)\dagger} \boldsymbol{v}_1^{(k)}} = \frac{\boldsymbol{v}_1^{(k)\dagger} \boldsymbol{A}\boldsymbol{v}_1^{(k)}}{\left\|\boldsymbol{v}_1^{(k)}\right\|^2} \,. \tag{7.25}$$

On the basis of these two iterations, for $\boldsymbol{v}_1$ and λ_1, we can formulate an algorithm for sequential efficient calculation of PCs.

7.3 Efficient Approximation of Correlation Matrices

For an efficient approximation of correlation matrices, describing the sources of stochastic electromagnetic fields, we consider a reduced set of principal components as discussed at the end of Section 7.1. The size of the reduced set is determined by a chosen cumulative percentage of total variance p^*. This p^* also determines the quality of the approximation by m PCs. The algorithm for generating a reduced set of PCs which later approximates the given correlation matrix $\boldsymbol{C}$ is outlined as follows:

- Calculate the largest eigenvalue and corresponding eigenvector using power iteration (according to section 7.2), which is the first principal component.
- Check whether the first PC already accounts for the desired cumulative percentage of total variance (CPTV).
- If the first PC already accounts for the desired CPTV, terminate the algorithm, if not, calculate the second-largest PC and check if the sum of first and second-largest PCs account for the desired CPTV.
- Proceed with calculating PCs until the sum of calculated PCs accounts for the desired CPTV.

To determine whether or not the sum of k PCs accounts for a previously specified CPTV, we investigate the residual

$$R_n^{(k)} = \left| \mathrm{Tr}\,(\boldsymbol{C}) - \sum_{i=1}^{k} \lambda_i \right| = \left| \sum_{i=1}^{n} \lambda_i - \sum_{i=1}^{k} \lambda_i \right| = \left| \sum_{i=k}^{n} \lambda_i \right| \,. \tag{7.26}$$

This is the absolute value of the difference between the total variance of $\boldsymbol{C}$ and the variance accounted for by the sum of up to k PCs. The residual converges to zero as

$$\lim_{k\to n} R_n^{(k)} = \lim_{k\to n} \left| \sum_{i=1}^{n} \lambda_i - \sum_{i=1}^{k} \lambda_i \right| = \left| \sum_{i=1}^{n} \lambda_i - \sum_{i=1}^{n} \lambda_i \right| = 0 \,. \tag{7.27}$$

For a previously specified CPTV $p^* \in [0, 1]$, we formulate the termination criterion for our algorithm by

$$\frac{\left| \mathrm{Tr}\,(\boldsymbol{C}) - \sum\limits_{i=1}^{k} \lambda_i \right|}{|\mathrm{Tr}\,(\boldsymbol{C})|} < 1 - p^* \,. \tag{7.28}$$

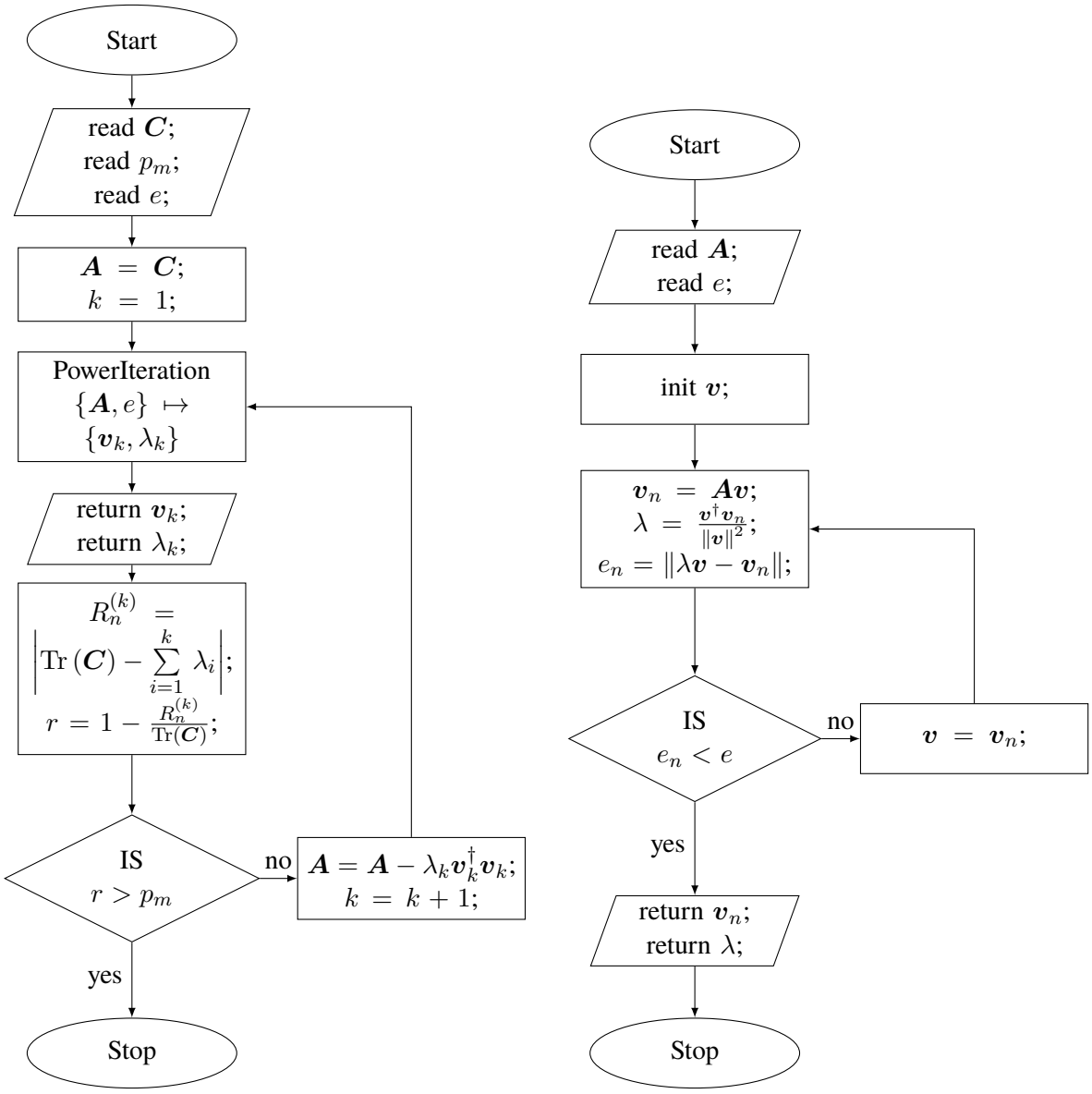

(a) Efficient PCA Algorithm. **(b)** Power Iteration Algorithm.

Figure 7.1 Flowcharts of the Efficient PCA and Power Iteration Algorithms (from [38]).

Figure 7.1 gives the algorithmic flowcharts for the efficient PCA calculation as well as for the power iteration method discussed in section 7.2. Calculating eigenvectors and corresponding eigenvalues using power iteration is a rather costly computational task, which has a cost per step of $\mathcal{O}\left(n^2\right)$. In the worst case, n eigenvalues have to be calculated for a $n \times n$ covariance matrix, which results in a worst-case complexity of $\mathcal{O}\left(n^3\right)$. Fortunately, the number of independent sources, i.e. the number of dominant PCs, for practical stochastic EM field problems is typically low compared to the number of sampling points, which results in an overall lower average complexity.

The algorithm presented above can significantly save computational cost for determining the PCs in cases, where we have several dominant PCs. While the size of the correlation matrix is determined by the number of measurement points, the number of dominant PCs is governed by the number of stochastically independent sources. For testing the speed up in computation time, a 5000×5000 matrix with three dominant eigenvalues has been generated and has been superimposed with white noise. Due to the added noise, the matrix has full rank, which is a typical scenario for an actual measurement. The presented efficient PCA algorithm has been compared to a PCA based on singular value decomposition, both implemented in MATLAB on a computer with an Intel Core i7 3930K, 3.2 GHz CPU. A script, running the algorithms sequentially evaluates the run-time

Table 7.1 Configuration of run-time evaluation script

Parameter	Value
Size of the matrix	5000×5000
Number of dominant eigenvalues	3
Weights of the eigenvalues	$[10, 5, 2.5]^{\mathrm{T}}$
Weight of noise	0.1
Cumulative percentage of total variance	0.99
Accuracy for power iteration	$1 \cdot 10^{-6}$

Table 7.2 Average run-times after ten rounds

Method	Run-Time
PCA based on SVD	31.5978 s
Proposed efficient PCA	0.7202 s

for each method. Each method is performed multiple times, while the run-times are recorded. In the end, the average of the run-times for each method is calculated. The configuration of the script, used for evaluating the run-times is shown in Table 7.1, and average results for the run-times are listed in Table 7.2. In this specific configuration, a speed-up in run-time by a factor of 40 could be achieved using the presented efficient PCA algorithm over a PCA based on singular value decomposition. A measurement example demonstrating the data reduction possible is shown in the following section.

7.4 Measurement Example

Measurements were performed with a two probe scanning system on a rectangular grid of measurement points. The grid of size 6×6 requires measurement of 1260 point pairs, considering a single polarization only, yielding a 36×36 correlation matrix.

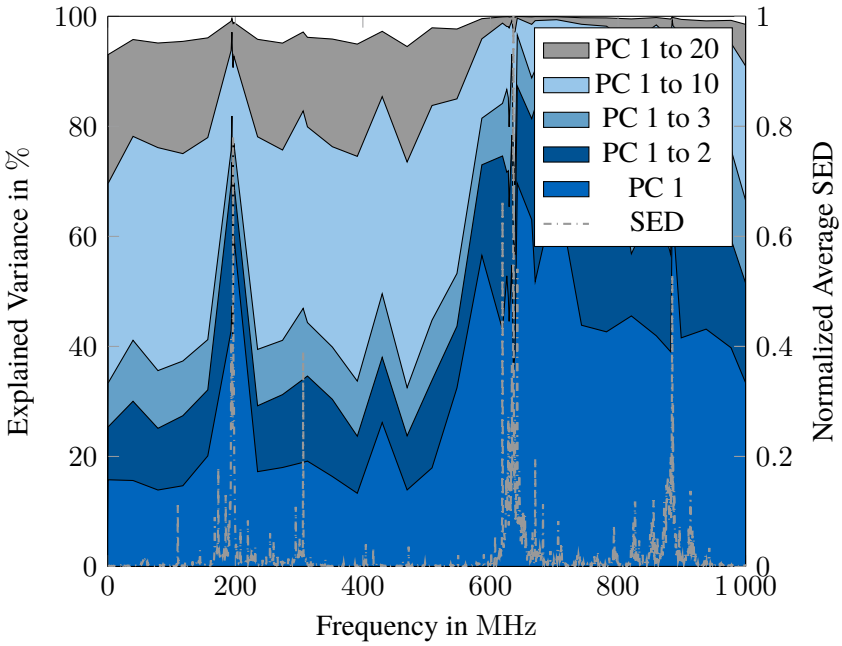

Figure 7.2 Number of PCs over Frequency (from [38]).

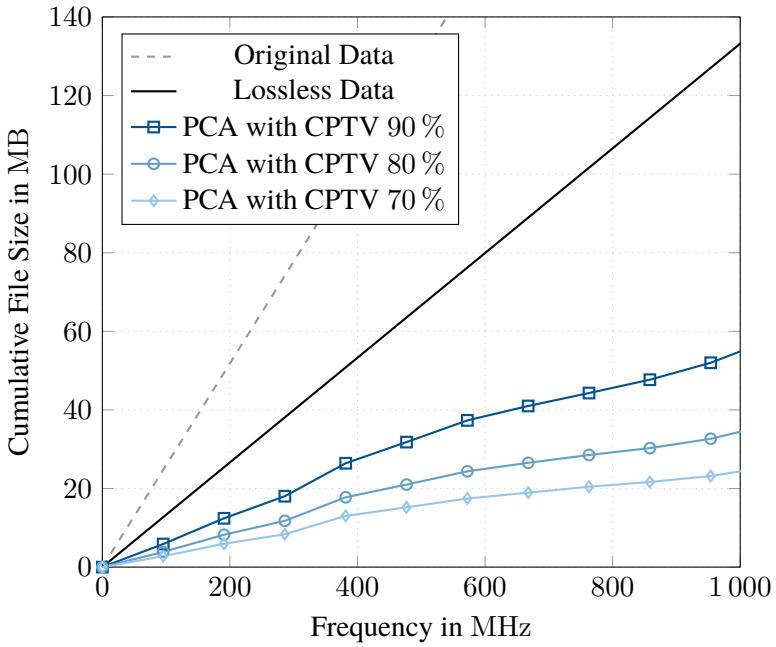

Figure 7.3 Cumulative File Size over Frequency (from [38]).

The measurement points were arranged in a uniform grid with 10 mm spacing just above a printed circuit board (PCB) containing a test structure of two coupled microstrip lines. One microstrip line is fed with a signal from a pseudo-random noise source, generating a pseudo-random bit sequence with a fundamental clock rate at 180 MHz. Correlation data has been obtained in the time-domain. Correlation spectra are obtained by Fourier transformation and cover a frequency range from DC to 1.2 GHz, resolved in about 32,000 frequency bins. Figure 7.2 shows how much of the variance of the correlation matrix can be accounted for by the first few dominant PCs. The plot shows the explained variance vs. frequency for the first dominant PC and the first few dominant PCs jointly. Also the normalized spectral energy density (SED) vs. frequency is plotted. The number of PCs required to explain a certain percentage of the variance varies over frequency. The first 10 most significant PCs account here for 70 % to almost 100 % of the variance. Over all frequencies, on average 7 PCs are required to account for more than 90 % of the variance. The amount of memory required for storing the correlation matrix over all frequencies is shown in Figure 7.3. The graph shows the cumulative file size from DC to the respective frequency. The original correlation matrix is a Hermitian matrix, and we can reduce the data without any loss by storing only the upper or lower triangular matrix. The graph shows the file size for retaining the dominant PCs accounting for 70 %, 80 %, and 90 % of the cumulative percentage of total variance, respectively. In agreement with Figure 7.2, the cumulative file size increases slower at frequencies between 600 MHz to 700 MHz, where fewer dominant PCs are required to account for the same percentage of explained total variance, than at lower frequencies. In this specific example, memory requirements for storing the correlation information up to 1 GHz can be reduced by PCA to around 55 MB, retaining 90 % of the variance, compared to around 130 MB required for storing all data lossless. Considering this setup, however, with the number of measurement points increased to 20×20 yields already 16 GB of data for the lossless storage without PCA. Hence, the benefit of memory savings by applying PCA becomes significant as data size increases. Furthermore, the savings become more significant, also in percentage, as the matrix size increases due to more measuring points, while the number of dominant PCs, governed by the number of stochastically independent sources, remains at a much lower level. Figure 7.4a shows a graphic visualization of the absolute values of the correlation matrix at a frequency of 636 MHz with maximum SED. A graphic representation of the reconstructed correlation matrix at this frequency obtained from the three dominant PCs is shown in Figure 7.4b. Good agreement is found between the original and reconstructed correlation matrix, which accounts for 90 % of the variance of the original correlation matrix.

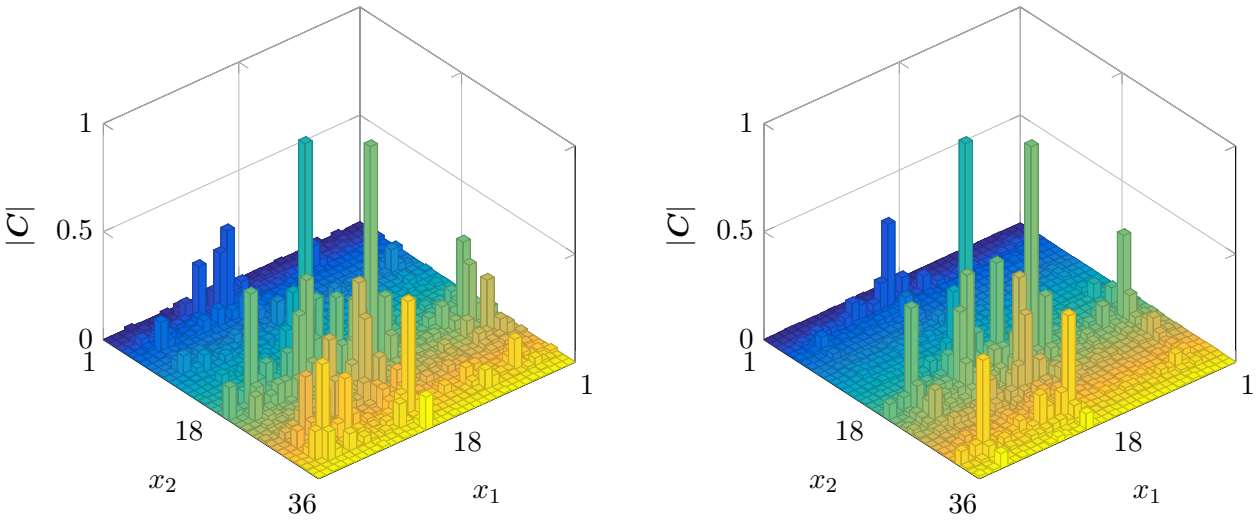

(a) Original correlation matrix at 635.99 MHz.

(b) Reconstructed correlation matrix at 635.99 MHz.

Figure 7.4 Visualized Original (a) and Reconstructed (b) Correlation Matrix at 635.99 MHz (from [38]).

The source correlation information may also be reconstructed from a single PC only, allowing for a separation of the stochastically independent sources and an individual consideration of each source distribution for further numerical processing. In this case, each source distribution represents the fully correlated case.

In summary, we have applied principal component analysis for the correlation matrices characterizing stochastic electromagnetic fields. We have shown that a substantial reduction of the required memory for storing the frequency depended correlation matrices can be achieved while retaining the most relevant information. The dimension of correlation matrices scales with the square of the number of measurement points, whereas the number of dominant PCs is fixed by the number of stochastically independent sources. Thus, memory savings become most significant for large numbers of measurement points. A reconstruction of correlation matrices from the most significant PCs showed a good agreement with the original correlation matrix. Furthermore, we have shown an efficient implementation of the PCA using a power iteration algorithm. This algorithm is very suitable for the typical scenario where an eigenvalue decomposition of the correlation matrix will reveal a full rank matrix, however, only relatively few PCs will have a significant contribution to the variance.

8 Conclusion and Outlook

In the first chapter of this thesis, we have revisited mathematical fundamentals of linear algebra, functional analysis, probability theory, and vector calculus, relevant to this work. Based on this, we developed a mathematical framework for describing stochastic electromagnetic fields. It was shown that this framework, where the general description of a random field is based on characteristic functionals, can properly describe the propagation of stochastic electromagnetic fields under linear transformations. It was also shown that the existing theory for stationary ergodic Gaussian fields is a special case of the new theoretical framework, which is a very important result, as it justifies several assumptions that have been made in the past.

We also discussed the characterization of the stationary Gaussian electromagnetic field, radiated from sources in a closed environment based on the data obtained by sampling the tangential field components on a surface, enclosing the device under test. By simultaneously sampling the field at pairs of points on the scan plane, one is able to calculate auto-correlation and cross-correlation functions of the sampled field amplitudes in a further post-processing step. The advantages of time-domain measurements over frequency-domain measurements, especially for broad-band unintentionally radiated emissions have been worked out. A fully capable two-probe near-field scanning system has been realized which was constantly improved during the course of this thesis. For obtaining accurate quantitative measurement results it is inevitable to discuss the de-embedding of the field probes used for sampling the stochastic electromagnetic field. We also presented a procedure for equivalent source reconstruction, based on correlation information. In that algorithm, the obtained correlation matrix at a certain frequency is projected to a finely resolved grid on the source plane, with an estimated inverse propagator, which is the best fit in the least-squares sense.

The propagation of stochastic electromagnetic fields, or more precisely, the numerical propagation of correlation dyadics, describing Gaussian random fields was extensively discussed. Different numerical propagation methods, operating in both, in the frequency-domain and in the time-domain, have been introduced and revisited carefully. We have compared measured and numerically propagated data in the near-field, using a method of moments based scheme and a Wigner-function based numerical propagator. Both propagated results are evaluated with respect to experimental data, obtained in the observation plane. Good agreement with experiment could be obtained for both results, where the exact method of moments based propagator slightly outperforms the simpler but faster Wigner-propagator in terms of accuracy. For free-space propagation, both methods are applicable, but for propagation in complex environments, the method of moments scheme can be adapted to a newly computed numerical Green's function of the complex structure, whereas the Wigner propagator is only suitable as an approximation for free space. The integration of the stochastic field propagation mechanisms with existing full-wave numerical field solver tools was also discussed. We have presented simulation results for the spectral energy density above a real PCB, where we have simulated the propagation of correlation information for different degrees of source correlations.

One key application for the theory of stochastic electromagnetic fields has been identified to be wireless chip-to-chip communication [178]. Stochastic electromagnetic fields can be used to accurately model the near-field noise contributions in a densely packed integrated environment. We have described the conditions for constructing decoupling and matching networks and we presented an experimental setup for multiple-input multiple-output communication in the near-field. In this setup, we neglected the decoupling of the different antennas in the system, which led to a reduced MIMO gain. Nevertheless, we recorded field correlation functions above the measurement setup experimentally, which can provide insight into the noise levels, one has to deal with in such scenarios, after further investigations.

Data management for measured and simulated results for broad-band stochastic electromagnetic fields is key, as the amounts of data, as well as simulation and measurement times, are in general very high if a suitable spatial resolution is desired. We have developed an algorithm based on principal component analysis, which is capable of effectively reducing the amount of data by only retaining those samples, which provide the largest

share in total variance, i.e. energy of the data. As the number of independent random sources is typically much lower than the number of spatial scanning points, it was shown that this procedure provides a good trade-off between retaining the relevant information and data reduction.

For the industrial application of the characterization techniques developed in this thesis, e.g. in computer-aided fabrication of electronic systems, it remains to improve the measurement and simulation runtimes, as well as the amount of data that is captured. We suggest a study on the impact of sparse sampling, i.e. how can we predict the field correlations on a measurement grid if only a subset of the spatially distributed point-pairs is actually determined experimentally. There is interesting preliminary work on sparse sampling [179], [180], which could possibly help in reconstructing the full correlation information from a reduced measurement subset, where the measurement pairs are chosen randomly. This would be a huge advantage, as the data reduction mechanism from [38] introduced in this thesis still requires knowledge of all correlation pairs, prior to data reduction. Another important point is the construction of an improved measurement device, which should be capable of recording field samples at multiple points simultaneously, as suggested in [125]. Using such an advanced device, correlation functions can be calculated for multiple point pairs with one single measurement, which would also drastically reduce the measurement time. Another option here would be to reduce the number of reference points, i.e. not calculating every possible combination of point pairs. This means that one probe still scans all grid points on a measurement grid above the device under test, while the second probe only scans at points on a reduced grid. The loss in information, especially for the propagation of the resulting correlation dyadics needs to be studied both, theoretically and experimentally in order to decide if such a procedure is feasible in the future. Furthermore, there is a need for implementing a universal strategy for the case of cyclostationary random fields. Altogether, there remain challenging and interesting problems to be solved, which makes studying stochastic electromagnetic fields more interesting than ever for future researchers, working on that topic.

Own Publications

Journal Articles

- M. Haider, B. P. Stošić, M. H. Baharuddin, N. S. Dončov, D. W. P. Thomas, P. Russer, and J. A. Russer, "Modeling of aperture fields for cavities excited by stochastic current sources", *Microwave Review*, vol. 22, no. 2, pp. 21–26, Dec. 2016.
- M. Haider and J. A. Russer, "Principal component analysis for efficient characterization of stochastic electromagnetic fields", *International Journal of Numerical Modelling: Electronic Networks, Devices and Fields*, pp. 1–10, Jul. 2018, jnm.2246. DOI: 10.1002/jnm.2246.
- W. Kaiser, M. Haider, J. A. Russer, P. Russer, and C. Jirauschek, "Quantum theory of the dissipative Josephson parametric amplifier", *International Journal of Circuit Theory and Applications*, vol. 45, no. 7, pp. 864–881, Jul. 2017, cta.2354. DOI: 10.1002/cta.2354.
- M. Haider and J. A. Russer, "Differential form representation of stochastic electromagnetic fields", *Advances in Radio Science*, vol. 15, pp. 21–28, 2017. DOI: 10.5194/ars-15-21-2017.
- W. Kaiser, M. Haider, J. A. Russer, P. Russer, and C. Jirauschek, "Markovian dynamics of Josephson parametric amplification", *Advances in Radio Science*, vol. 15, pp. 131–140, 2017. DOI: 10.5194/ars-15-131-2017.
- M. Haider and J. A. Russer, "A learning app for RF nanotechnology: The Josephson parametric microwave amplifier", *IEEE Microwave Magazine*, vol. 19, no. 4, pp. 101–107, Jun. 2018. DOI: 10.1109/MMM.2018.2813859.
- M. Bobinger, M. Haider, Y. Goliya, A. Albrecht, M. Becherer, P. Lugli, A. Rivadeneyra, and J. Russer, "On the sintering of solution-based silver nanoparticle thin-films for sprayed and flexible antennas", *Nanotechnology*, vol. 29, no. 48, p. 485 701, 2018. DOI: 10.1088/1361-6528/aae0e0.
- G. Gradoni, J. A. Russer, M. H. Baharuddin, M. Haider, P. Russer, C. Smartt, S. C. Creagh, G. Tanner, and D. W. P. Thomas, "Stochastic electromagnetic field propagation— measurement and modelling", *Philosophical Transactions of the Royal Society of London A: Mathematical, Physical and Engineering Sciences*, vol. 376, no. 2134, 2018. DOI: 10.1098/rsta.2017.0455.
- J. A. Russer, M. Haider, and P. Russer, "Time-domain modeling of noisy electromagnetic field propagation", *IEEE Transactions on Microwave Theory and Techniques*, vol. 66, no. 12, pp. 5415–5428, Dec. 2018. DOI: 10.1109/TMTT.2018.2874985.
- Y. Goliya, A. Rivadeneyra, J. F. Salmeron, A. Albrecht, J. Mock, M. Haider, J. A. Russer, B. Cruz, P. Eschlwech, E. Biebl, M. Becherer, and M. R. Bobinger, "Next generation antennas based on screen-printed and transparent silver nanowire films", *Advanced Optical Materials*, vol. 7, no. 21, p. 1 900 995, Aug. 2019. DOI: 10.1002/adom.201900995.

Conference Proceedings

- J. A. Russer, M. Haider, M. H. Baharuddin, C. Smartt, S. Wane, D. Bajon, A. Baev, Y. Kuznetsov, D. W. P. Thomas, and P. Russer, "Near-field correlation measurement and evaluation of stationary and cyclostationary stochastic electromagnetic fields", in *46th European Microwave Conference (EuMC 2016)*, Oct. 2016, pp. 481–484. DOI: 10.1109/EuMC.2016.7824384.

- J. A. Russer, M. Haider, M. H. Baharuddin, C. Smartt, A. Baev, S. Wane, D. Bajon, Y. Kuznetsov, D. W. P. Thomas, and P. Russer, "Correlation measurement and evaluation of stochastic electromagnetic fields", in *International Symposium on Electromagnetic Compatibility (EMC Europe 2016)*, Sep. 2016, pp. 12–16. DOI: 10.1109/EMCEurope.2016.7739292.
- Q. Hirmer, A. Albrecht, M. Bobinger, M. Loch, M. Haider, J. A. Russer, M. Becherer, and P. Lugli, "Inkjet-printed patch antennas for wireless chip-to-chip communication on flexible substrates", in *13th Conference on Ph.D. Research in Microelectronics and Electronics (PRIME 2017)*, Jun. 2017, pp. 141–144. DOI: 10.1109/PRIME.2017.7974127.
- M. Bobinger, V. Dergianlis, A. Albrecht, M. Haider, Q. Hirmer, M. Becherer, and P. Lugli, "Solution processing of silver nanowires for transparent heaters and flexible electronics", in *13th Conference on Ph.D. Research in Microelectronics and Electronics (PRIME 2017)*, Jun. 2017, pp. 9–12. DOI: 10.1109/PRIME.2017.7974094.
- Y. Kuznetsov, A. Baev, A. Gorbunova, M. Konovalyuk, J. A. Russer, M. Haider, and P. Russer, "Cross-correlation analysis of the cyclostationary near-field unintentional radiations from the PCB", in *International Symposium on Electromagnetic Compatibility (EMC Europe 2017)*, Sep. 2017, pp. 1–6. DOI: 10.1109/EMCEurope.2017.8094730.
- D. W. P. Thomas, M. H. Baharuddin, C. Smartt, G. Gradoni, G. Tanner, S. Creagh, N. Dončov, M. Haider, and J. A. Russer, "Near-field scanning of stochastic fields considering reduction of complexity", in *International Symposium on Electromagnetic Compatibility (EMC Europe 2017)*, Sep. 2017, pp. 1–6. DOI: 10.1109/EMCEurope.2017.8094766.
- M. Haider, J. A. Russer, A. Baev, Y. Kuznetsov, and P. Russer, "Principal component analysis applied in modeling of stochastic electromagnetic field propagation", in *47th European Microwave Conference (EuMC 2017)*, Oct. 2017, pp. 1–4.
- J. A. Russer, M. Ivrlač, M. Haider, S. Wane, D. Bajon, P. Russer, and J. A. Nossek, "Multiport model of Hertzian dipoles coupled in the near-field", in *47th European Microwave Conference (EuMC 2017)*, Oct. 2017, pp. 1–4. DOI: 10.23919/EuMC.2017.8231088.
- A. Baev, Y. Kuznetsov, M. Haider, J. A. Russer, and P. Russer, "Time-domain characterization of probes for two-point measurements of stochastic EM fields", in *International Conference on Electromagnetics in Advanced Applications (ICEAA 2017)*, Sep. 2017, pp. 1521–1524. DOI: 10.1109/ICEAA.2017.8065572.
- Y. Kuznetsov, A. Baev, M. Haider, J. A. Russer, and P. Russer, "Time-domain far-field measurements for cross-correlation analysis", in *International Conference on Electromagnetics in Advanced Applications (ICEAA 2017)*, Sep. 2017, pp. 1517–1520. DOI: 10.1109/ICEAA.2017.8065571.
- J. A. Russer, M. Haider, and P. Russer, "Network methods for full-wave modeling of stochastic electromagnetic fields", in *International Conference on Electromagnetics in Advanced Applications (ICEAA 2017)*, Sep. 2017, pp. 1494–1497. DOI: 10.1109/ICEAA.2017.8065565.
- M. Haider and J. A. Russer, "Field modeling of dynamic inductive power supply of electric vehicles on the road", in *International Conference on Electromagnetics in Advanced Applications (ICEAA 2017)*, Sep. 2017, pp. 1490–1493. DOI: 10.1109/ICEAA.2017.8065564.
- ——, "Equivalent source localization for stochastic electromagnetic fields", in *International Conference on Electromagnetics in Advanced Applications (ICEAA 2017)*, Sep. 2017, pp. 1486–1489. DOI: 10.1109/ICEAA.2017.8065563.
- ——, "The correlation transmission line matrix (CTLM) method", in *International Conference on Electromagnetics in Advanced Applications (ICEAA 2017)*, Sep. 2017, pp. 1509–1512. DOI: 10.1109/ICEAA.2017.8065569.

- N. Dončov, B. Stošić, Z. Stanković, J. A. Russer, M. Haider, M. H. Baharuddin, and D. W. P. Thomas, "Characterization of EM field above a single aperture or air-vents of an enclosure for a variable degree of correlation between stochastic sources inside", in *International Conference on Electromagnetics in Advanced Applications (ICEAA 2017)*, Sep. 2017, pp. 1399–1402. DOI: 10.1109/ICEAA.2017.8065539.
- W. Kaiser, M. Haider, J. A. Russer, P. Russer, and C. Jirauschek, "Generalized Langevin theory for Josephson parametric amplification", in *IEEE MTT-S International Microwave Symposium (IMS 2017)*, Jun. 2017, pp. 1181–1184. DOI: 10.1109/MWSYM.2017.8058812.
- J. A. Russer, M. Haider, D. Bajon, S. Wane, and P. Russer, "An extension of the transverse wave formulation to model stochastic electromagnetic fields", in *IEEE MTT-S International Microwave Symposium (IMS 2017)*, Jun. 2017, pp. 700–703. DOI: 10.1109/MWSYM.2017.8058668.
- J. A. Russer, M. Haider, M. Weigelt, M. Becherer, S. Kahlert, C. Merz, M. Hoja, J. Franke, and P. Russer, "A system for wireless inductive power supply of electric vehicles while driving along the route", in *7th International Electric Drives Production Conference (EDPC 2017)*, Wuerzburg, Germany, Dec. 2017, pp. 1–6. DOI: 10.1109/EDPC.2017.8328158.
- J. A. Russer, M. T. Ivrlač, M. Haider, S. Wane, D. Bajon, and J. A. Nossek, "A compact Hertzian dipoles multiport model for near-field MIMO system assessment", in *IEEE Radio and Wireless Symposium (RWS 2018)*, Anaheim, CA, Jan. 2018, pp. 31–34. DOI: 10.1109/RWS.2018.8304938.
- M. Haider and J. A. Russer, "Computer aided analysis of EMI radiated from printed circuit boards", in *2nd URSI Atlantic Radio Science Conference (AT-RASC 2018)*, Gran Canaria, Spain, May 2018, pp. 1–3. DOI: 10.23919/URSI-AT-RASC.2018.8471650.
- Y. Kuznetsov, A. Baev, M. Haider, A. Gorbunova, M. Konovaluk, and J. A. Russer, "Cyclostationary source separation in the near-field of electronic devices", in *2nd URSI Atlantic Radio Science Conference (AT-RASC 2018)*, Gran Canaria, Spain, May 2018, pp. 1–4. DOI: 10.23919/URSI-AT-RASC.2018.8471349.
- M. Haider, P. Corrales, D. Bajon, S. Wane, and J. A. Russer, "Near-field MIMO system assessment", in *2nd URSI Atlantic Radio Science Conference (AT-RASC 2018)*, Gran Canaria, Spain, May 2018, pp. 1–3. DOI: 10.23919/URSI-AT-RASC.2018.8471642.
- M. Haider, A. Baev, Y. Kuznetsov, and J. A. Russer, "Near-field to far-field propagation of correlation information for noisy electromagnetic fields", in *48th European Microwave Conference (EuMC 2018)*, Madrid, Spain, 2018, pp. 1190–1193. DOI: 10.23919/EuMC.2018.8541636.
- J. A. Russer and M. Haider, "Time-domain modeling of noisy electromagnetic field propagation", in *IEEE MTT-S International Microwave Symposium (IMS 2018)*, Philadelphia, PA, Jun. 2018, pp. 1013–1016. DOI: 10.1109/MWSYM.2018.8439151.
- A. Gorbunova, Y. Kuznetsov, A. Baev, M. Konovalyuk, J. A. Russer, and M. Haider, "Time-domain stochastic electromagnetic field propagator based on Jefimenko's equations", in *Baltic URSI Symposium*, Poznan, Poland, May 2018, pp. 188–191. DOI: 10.23919/URSI.2018.8406708.
- A. Rivadeneyra, M. Haider, V. Bhatt, A. Albrecht, J. F. Salmeron, and M. Becherer, "Modular platform for sensor networks", in *8. MSE Kolloquium 2018 Advances in Energy Transition*, Munich School of Engineering (TUM MSE), Jul. 2018.
- Y. Kuznetsov, A. Baev, M. Konovalyuk, A. Gorbunova, M. Haider, J. A. Russer, and P. Russer, "Characterization of the cyclostationary emissions in the near-field of electronic device", in *International Symposium on Electromagnetic Compatibility (EMC Europe 2018)*, Aug. 2018, pp. 573–578. DOI: 10.1109/EMCEurope.2018.8485054.

- M. Haider, J. A. Russer, J. Abundis Patino, C. Jirauschek, and P. Russer, "A Josephson traveling wave parametric amplifier for quantum coherent signal processing", in *IEEE MTT-S International Microwave Symposium (IMS 2019)*, Jun. 2019, pp. 956–958. DOI: 10.1109/MWSYM.2019.8700875.
- J. A. Russer, M. Haider, C. Jirauschek, and P. Russer, "On the possibility of quantum simulation of electromagnetic structures", in *IEEE MTT-S International Microwave Symposium (IMS 2019)*, Jun. 2019, pp. 267–270. DOI: 10.1109/MWSYM.2019.8700886.
- M. Haider, Y. Yuan, J. Abundis Patino, J. A. Russer, P. Russer, and C. Jirauschek, "Circuit quantum electrodynamic model of a resonantly phase-matched Josephson traveling wave parametric amplifier", in *Conference on Lasers and Electro-Optics Europe / European Quantum Electronics Conference (CLEO/Europe-EQEC 2019)*, Jun. 2019, p. 1. DOI: 10.1109/CLEOE-EQEC.2019.8871821.
- S. Wane, P. Corrales, T. V. Dinh, M. Haider, J. A. Russer, Q.-H. Tran, C.-J. Lin, S.-W. Chang, W.-T. Tsai, R. Giacometti, V. Huard, and N. Gross, "Millimeter-wave beamformer chips with smart-antennas for 5G: Toward holistic RFSOI technology solutions including RF-ADCs", in *IEEE Texas Symposium on Wireless and Microwave Circuits and Systems (WMCS)*, Mar. 2019, pp. 1–4. DOI: 10.1109/WMCaS.2019.8732565.
- Y. Kuznetsov, A. Baev, A. Gorbunova, M. Konovalyuk, J. A. Russer, M. Haider, and P. Russer, "Cyclostationary characterization of the interference induced by crosstalk between transmission lines", in *International Symposium on Electromagnetic Compatibility (EMC Europe 2019)*, Sep. 2019, pp. 574–579. DOI: 10.1109/EMCEurope.2019.8871986.
- Y. Kuznetsov, A. Baev, M. Konovalyuk, A. Gorbunova, J. A. Russer, M. Haider, and P. Russer, "Far-field cyclostationary characterization of emissions from DUT based on the Jefimenko's equations", in *International Symposium on Electromagnetic Compatibility (EMC Europe 2019)*, Sep. 2019, pp. 586–591. DOI: 10.1109/EMCEurope.2019.8872014.
- M. Haider, P. Corrales, N. Gross, C.-J. Lin, S.-W. Chang, W.-T. Tsai, S. Wane, D. Bajon, and J. A. Russer, "Characterization of 5G phased arrays at 28 GHz by time-domain near-field scanning", in *49th European Microwave Conference (EuMC 2019)*, Oct. 2019, pp. 416–419. DOI: 10.23919/EuMC.2019.8910912.
- S. Wane, D. Bajon, P. Corrales, M. Haider, J. A. Russer, Q.-H. Tran, C.-J. Lin, S.-W. Chang, W.-T. Tsai, R. Giacometti, and N. Gross, "Cognitive beamformer chips with smart-antennas for 5G and beyond: Holistic RFSOI technology solutions including ASIC correlators", in *49th European Microwave Conference (EuMC 2019)*, Oct. 2019, pp. 1088–1091. DOI: 10.23919/EuMC.2019.8910898.
- M. Haider and J. A. Russer, "A generalized mathematical framework for modeling stochastic electromagnetic fields", in *International Conference on Electromagnetics in Advanced Applications (ICEAA 2019)*, Sep. 2019, pp. 1013–1017. DOI: 10.1109/ICEAA.2019.8879319.
- J. A. Russer, M. Haider, A. Baev, Y. Kuznetsov, and P. Russer, "Time-domain analysis of stochastic electromagnetic fields based on Jefimenko's equation", in *International Conference on Electromagnetics in Advanced Applications (ICEAA 2019)*, Sep. 2019, pp. 1241–1245. DOI: 10.1109/ICEAA.2019.8879022.
- Y. Kuznetsov, A. Baev, M. Konovalyuk, A. Gorbunova, M. Haider, and J. A. Russer, "Cyclostationary source separation based on electromagnetic measurements in the near-field of PCB", in *Photonics and Electromagnetics Research Symposium (PIERS 2019)*, Rome, Italy, Jun. 2019.

Conference Talks

- M. Haider and J. A. Russer, "Differential form representation of stochastic electromagnetic fields", in *Kleinheubacher Tagung 2016, Talk KH2016-B-13, 2016-09*, U.R.S.I. Germany, Sep. 2016.
- W. Kaiser, M. Haider, J. A. Russer, P. Russer, and C. Jirauschek, "Modeling of the lossy Josephson parametric amplifier", in *Kleinheubacher Tagung 2016, Talk KH2016-D-10, 2016-09*, Sep. 2016.

- Y. Kuznetsov, A. Baev, M. Haider, J. A. Russer, and P. Russer, "Cyclostationary characterization of electromagnetic interference with spread spectrum clocking", in *Kleinheubacher Tagung 2016, Talk KH2016-E-07, 2016-09*, U.R.S.I. Germany, Sep. 2016.
- J. A. Russer, M. Haider, A. Baev, S. Wane, D. Bajon, Y. Kuznetsov, and P. Russer, "Measurement of radiated cyclostationary EMI", in *Kleinheubacher Tagung 2016, Talk KH2016-B-15, 2016-09*, Sep. 2016.
- J. A. Russer, M. Haider, J.-B. Gros, D. Bajon, S. Wane, and P. Russer, "Correlation transverse wave formulation (CTWF) for modeling of stochastic electromagnetic fields", in *Kleinheubacher Tagung 2016, Talk KH2016-B-14, 2016-09*, Sep. 2016.
- M. Haider, J. A. Russer, and P. Russer, "Localizing equivalent dipole sources for radiated stochastic interference", in *Kleinheubacher Tagung 2017, Talk KH2017-Di-S2-03, 2017-09*, U.R.S.I. Germany, Sep. 2017.
- B. Stošić, M. Haider, J. A. Russer, N. Dončov, and P. Russer, "Modeling of propagation of correlation information of stochastic signals in multiport devices by using wave digital network", in *Kleinheubacher Tagung 2017, Talk KH2017-Di-S2-02, 2017-09*, U.R.S.I. Germany, Sep. 2017.
- M. Haider and J. A. Russer, "Numerical modelling of stochastic electromagnetic fields using CST Microwave Studio", in *Symposium: New Trends in EMI Characterization, Munich*, Arbeitskreis für Mikrowellen- und Kommunikationstechnik e. V., May 2017.
- M. Bobinger, M. Haider, A. Albrecht, Y. Goliya, J. Russer, M. Becherer, and P. Lugli, "Highly conductive thin-films based on solution-processed silver nanoparticles for spray-on antennas", in *DPG-Verhandlungen DS: Fachverband Dünne Schichten DS 17: Poster Session I DS 17.57: Poster B*, Deutsche Physikalische Gesellschaft DPG, Mar. 2018.
- M. Haider and J. A. Russer, "Stationary and cyclostationary analysis in EMI and MIMO system characterization", in *Nice-Nottingham Days of Waves in Complex Media (NND 2018)*, Nice, France, Jul. 2018.
- M. Franckie, J. Popp, M. Haider, C. Jirauschek, and J. Faist, "Numerical optimization of mid-IR QCL frequency combs", in *Infrared Terahertz Quantum Workshop (ITQW 2019)*, Sep. 2019.
- M. V. Koleva, O. Maier, M. Haider, C. Jirauschek, K. Müller, and G. Slavcheva, "Optical polarisation rotation through spin-photon entanglement in a charged quantum dot-micropillar system: Intermediate and strong light-matter coupling case studies", in *Quantum Light for Investigating Complex Molecules and Materials*, Sep. 2019. DOI: 10.13140/RG.2.2.14095.74402.

Bibliography

[1] J. C. Maxwell, *A Treatise on Electricity and Magnetism*. Oxford Clarendon Press, 1873, vol. 2.

[2] C. E. Shannon, "A mathematical theory of communication", *Bell System Technical Journal*, vol. 27, no. 3, pp. 379–423, 1948. DOI: 10.1002/j.1538-7305.1948.tb01338.x.

[3] C. Christopoulos, *Principles and Techniques of Electromagnetic Compatibility*, 2nd ed. Taylor & Francis, 2007.

[4] T. Wu, F. Buesink, and F. Canavero, "Overview of signal integrity and EMC design technologies on PCB: Fundamentals and latest progress", *IEEE Transactions on Electromagnetic Compatibility*, vol. 55, no. 4, pp. 624–638, Aug. 2013. DOI: 10.1109/TEMC.2013.2257796.

[5] H. Boss, "Demystifying signal and power integrity [from the Guest Editor's Desk]", *IEEE Microwave Magazine*, vol. 12, no. 5, pp. 6–10, Aug. 2011. DOI: 10.1109/MMM.2011.941406.

[6] S. Wane, O. Doussin, D. Bajon, J. Russer, and P. Russer, "Stochastic approach for power integrity, signal integrity, EMC and EMI analysis of moving objects", in *International Conference on Electromagnetics in Advanced Applications*, Sep. 2015, pp. 1554–1557. DOI: 10.1109/ICEAA.2015.7297386.

[7] J. A. Russer, M. Haider, and P. Russer, "Time-domain modeling of noisy electromagnetic field propagation", *IEEE Transactions on Microwave Theory and Techniques*, vol. 66, no. 12, pp. 5415–5428, Dec. 2018. DOI: 10.1109/TMTT.2018.2874985.

[8] E. Li, X. Wei, A. C. Cangellaris, E. Liu, Y. Zhang, M. D'Amore, J. Kim, and T. Sudo, "Progress review of electromagnetic compatibility analysis technologies for packages, printed circuit boards, and novel interconnects", *IEEE Transactions on Electromagnetic Compatibility*, vol. 52, no. 2, pp. 248–265, May 2010. DOI: 10.1109/TEMC.2010.2048755.

[9] H. Hillbrand and P. Russer, "An efficient method for computer aided noise analysis of linear amplifier networks", *IEEE Transactions on Circuits and Systems*, vol. 23, no. 4, pp. 235–238, Apr. 1976. DOI: 10.1109/TCS.1976.1084200.

[10] H. A. Haus and R. B. Adler, *Circuit Theory of Linear Noisy Networks*. John Wiley & Sons, 1957.

[11] P. Russer and S. Müller, "Noise analysis of linear microwave circuits", *International Journal of Numerical Modelling: Electronic Networks, Devices and Fields*, vol. 3, no. 4, pp. 287–315, Dec. 1990. DOI: 10.1002/jnm.1660030408.

[12] P. Russer, "Noise analysis of linear microwave circuits with general topology", *Review of Radio Science 1993-1996*, pp. 361–393, 1996.

[13] P. Russer and S. Müller, "Noise analysis of microwave circuits with general topology", in *IEEE MTT-S International Microwave Symposium Digest*, vol. 3, 1992, pp. 1481–1484. DOI: 10.1109/MWSYM.1992.188039.

[14] ——, "Noise analysis of circuits with general topology and arbitrary representation", in *Asia-Pacific Microwave Conference (APMC 1992)*, vol. 2, 1992, pp. 819–822. DOI: 10.1109/ULTSYM.1992.275940.

[15] J. A. Russer and P. Russer, "Stochastic electromagnetic fields", in *German Microwave Conference*, Mar. 2011, pp. 1–4.

[16] ——, "Modeling of noisy EM field propagation using correlation information", *IEEE Transactions on Microwave Theory and Techniques*, vol. 63, no. 1, pp. 76–89, Jan. 2015. DOI: 10.1109/TMTT.2014.2376962.

[17] G. Gradoni, S. C. Creagh, G. Tanner, C. Smartt, and D. W. P. Thomas, "A phase-space approach for propagating field–field correlation functions", *New Journal of Physics*, vol. 17, no. 9, p. 093 027, Sep. 2015. DOI: 10.1088/1367-2630/17/9/093027.

[18] B. Fourestié, Z. Altman, J.-C. Bolomey, J. Wiart, and F. Brouaye, "Statistical modal analysis applied to near-field measurements of random emissions", *IEEE Transactions on Antennas and Propagation*, vol. 50, no. 12, pp. 1803–1812, Dec. 2002. DOI: 10.1109/TAP.2002.807495.

[19] L. R. Arnaut and C. S. Obiekezie, "Stochastic analysis of wideband near-field emissions from dipole antennas and integrated circuits", *IEEE Transactions on Electromagnetic Compatibility*, vol. 56, no. 1, pp. 93–101, Feb. 2014. DOI: 10.1109/TEMC.2013.2273737.

[20] D. Middleton, *An Introduction to Statistical Communication Theory*. John Wiley & Sons, IEEE-Press, 1996.

[21] J. A. Russer, A. Cangellaris, and P. Russer, "Correlation transmission line matrix (CTLM) modeling of stochastic electromagnetic fields", in *IEEE MTT-S International Microwave Symposium (IMS)*, May 2016, pp. 1–4. DOI: 10.1109/MWSYM.2016.7540091.

[22] M. Haider and J. A. Russer, "The correlation transmission line matrix (CTLM) method", in *International Conference on Electromagnetics in Advanced Applications (ICEAA)*, Sep. 2017, pp. 1509–1512. DOI: 10.1109/ICEAA.2017.8065569.

[23] G. Gradoni, J. A. Russer, M. H. Baharuddin, M. Haider, P. Russer, C. Smartt, S. C. Creagh, G. Tanner, and D. W. P. Thomas, "Stochastic electromagnetic field propagation— measurement and modelling", *Philosophical Transactions of the Royal Society of London A: Mathematical, Physical and Engineering Sciences*, vol. 376, no. 2134, Oct. 2018. DOI: 10.1098/rsta.2017.0455.

[24] J. A. Russer, M. Haider, D. Bajon, S. Wane, and P. Russer, "An extension of the transverse wave formulation to model stochastic electromagnetic fields", in *IEEE MTT-S International Microwave Symposium*, Jun. 2017, pp. 700–703. DOI: 10.1109/MWSYM.2017.8058668.

[25] P. Abrahamsen, *A review of Gaussian random fields and correlation functions*, 1997.

[26] S. M. Smith and C. Furse, "Stochastic FDTD for analysis of statistical variation in electromagnetic fields", *IEEE Transactions on Antennas and Propagation*, vol. 60, no. 7, pp. 3343–3350, Jul. 2012. DOI: 10.1109/TAP.2012.2196962.

[27] A. C. Yücel, H. Bağci, and E. Michielssen, "An adaptive multi-element probabilistic collocation method for statistical EMC/EMI characterization", *IEEE Transactions on Electromagnetic Compatibility*, vol. 55, no. 6, pp. 1154–1168, Dec. 2013. DOI: 10.1109/TEMC.2013.2265047.

[28] P. Li and L. J. Jiang, "Uncertainty quantification for electromagnetic systems using ASGC and DGTD method", *IEEE Transactions on Electromagnetic Compatibility*, vol. 57, no. 4, pp. 754–763, Aug. 2015. DOI: 10.1109/TEMC.2015.2403304.

[29] Z. Peng and S. Lin, "EM-CAD for complex electronics systems: A journey from order to chaos", in *IEEE MTT-S International Conference on Numerical Electromagnetic and Multiphysics Modeling and Optimization for RF, Microwave, and Terahertz Applications (NEMO)*, May 2017, pp. 61–63. DOI: 10.1109/NEMO.2017.7964187.

[30] A. Gorbunova, A. Baev, M. Konovalyuk, and Y. Kuznetsov, "Localization of cyclostationary EMI sources based on near-field measurements", in *IEEE International Symposium on Electromagnetic Compatibility (EMC)*, Aug. 2015, pp. 450–455. DOI: 10.1109/ISEMC.2015.7256204.

[31] J. A. Russer, P. Russer, M. Konovalyuk, A. Gorbunova, A. Baev, and Y. Kuznetsov, "Near-field propagation of cyclostationary stochastic electromagnetic fields", in *International Conference on Electromagnetics in Advanced Applications (ICEAA)*, Sep. 2015, pp. 1456–1459. DOI: 10.1109/ICEAA.2015.7297360.

[32] ——, "Analysis of cyclostationary stochastic electromagnetic fields", in *International Conference on Electromagnetics in Advanced Applications (ICEAA)*, Sep. 2015, pp. 1452–1455. DOI: 10.1109/ICEAA.2015.7297359.

[33] Y. Kuznetsov, A. Baev, M. Konovalyuk, A. Gorbunova, M. Haider, J. A. Russer, and P. Russer, "Characterization of the cyclostationary emissions in the near-field of electronic device", in *International Symposium on Electromagnetic Compatibility (EMC Europe)*, Aug. 2018, pp. 573–578. DOI: 10.1109/EMCEurope.2018.8485054.

[34] Y. Kuznetsov, A. Baev, A. Gorbunova, M. Konovalyuk, J. A. Russer, M. Haider, and P. Russer, "Cross-correlation analysis of the cyclostationary near-field unintentional radiations from the PCB", in *International Symposium on Electromagnetic Compatibility (EMC Europe)*, Sep. 2017, pp. 1–6. DOI: 10.1109/EMCEurope.2017.8094730.

[35] Y. Kuznetsov, A. Baev, M. Haider, A. Gorbunova, M. Konovaluk, and J. A. Russer, "Cyclostationary source separation in the near-field of electronic devices", in *2nd URSI Atlantic Radio Science Conference (AT-RASC)*, May 2018, pp. 1–4. DOI: 10.23919/URSI-AT-RASC.2018.8471349.

[36] J. A. Russer, M. Haider, M. H. Baharuddin, C. Smartt, S. Wane, D. Bajon, A. Baev, Y. Kuznetsov, D. W. P. Thomas, and P. Russer, "Near-field correlation measurement and evaluation of stationary and cyclostationary stochastic electromagnetic fields", in *46th European Microwave Conference (EuMC)*, Oct. 2016, pp. 481–484. DOI: 10.1109/EuMC.2016.7824384.

[37] W. A. Gardner, A. Napolitano, and L. Paura, "Cyclostationarity: Half a century of research", *Signal Processing*, vol. 86, no. 4, pp. 639–697, 2006. DOI: 10.1016/j.sigpro.2005.06.016.

[38] M. Haider and J. A. Russer, "Principal component analysis for efficient characterization of stochastic electromagnetic fields", *International Journal of Numerical Modelling: Electronic Networks, Devices and Fields*, vol. 31, no. 4, pp. 1–10, 2018. DOI: 10.1002/jnm.2246.

[39] J. A. Russer, T. Asenov, and P. Russer, "Modeling of noisy electromagnetic fields using principal component analysis", in *44th European Microwave Conference (EuMC)*, Oct. 2014, pp. 1099–1102. DOI: 10.1109/EuMC.2014.6986631.

[40] L. R. Arnaut, C. S. Obiekezie, and D. W. P. Thomas, "Empirical emission eigenmodes of printed circuit boards", *IEEE Transactions on Electromagnetic Compatibility*, vol. 56, no. 3, pp. 715–725, Jun. 2014. DOI: 10.1109/TEMC.2013.2292548.

[41] L. R. Arnaut and C. S. Obiekezie, "Comparison of complex principal and independent components for quasi-Gaussian radiated emissions from printed circuit boards", *IEEE Transactions on Electromagnetic Compatibility*, vol. 56, no. 6, pp. 1598–1603, Dec. 2014. DOI: 10.1109/TEMC.2014.2343912.

[42] E. Zermelo, *Collected Works*, H.-D. Ebbinghaus, C. G. Fraser, and A. Kanamori, Eds. Springer-Verlag, 2010, vol. 1. DOI: 10.1007/978-3-540-79384-7.

[43] S. Lang, *Real and Functional Analysis*, 3rd ed. Springer-Verlag, 1993.

[44] ——, *Undergraduate Algebra*, 3rd ed. Springer-Verlag, 2005.

[45] D. G. Dudley, *Mathematical Foundations for Electromagnetic Theory*, ser. IEEE Press Series on Electromagnetic Waves. John Wiley & Sons, IEEE-Press, 1994.

[46] R. D. Richtmyer, *Principles of Advanced Mathematical Physics*, ser. Texts and Monographs in Physics. Springer-Verlag, 1978, vol. 1. DOI: 10.1007/978-3-642-46378-5.

[47] P. R. Halmos, *Introduction to Hilbert Space and the Theory of Spectral Multiplicity*. New York: Chelsea Publishing Company, 1951.

[48] W. B. Davenport and W. L. Root, *An Introduction to the Theory of Random Signals and Noise*. John Wiley & Sons, IEEE-Press, 1987.

[49] N. Schmitz, *Vorlesungen über Wahrscheinlichkeitstheorie*. Stuttgart: Teubner, 1996. DOI: 10.1007/978-3-322-89225-6.

[50] A. N. Kolmogorov, *Foundations of the Theory of Probability*, 2nd ed. Chelsea Publishing Company, 1956.

[51] A. Kolmogoroff, *Grundbegriffe der Wahrscheinlichkeitsrechnung*. Springer-Verlag, 1933.

[52] P. Billingsley, *Probability and Measure*, 3rd ed., ser. Wiley Series in Probability and Mathematical Statistics. John Wiley & Sons, 1995.

[53] O. Kallenberg, *Foundations of Modern Probability*. Springer-Verlag, 1997.

[54] I. I. Gikhman and A. V. Skorokhod, *The Theory of Stochastic Processes I*. Springer-Verlag, 2004.

[55] M. Loéve, *Probability Theory I*, 4th ed., ser. Graduate Texts in Mathematics. Springer-Verlag, 1977, vol. 45.

[56] P. Schuster, *Stochasticity in Processes: Fundamentals and Applications to Chemistry and Biology*, ser. Springer Series in Synergetics. Springer-Verlag, 2016. DOI: 10.1007/978-3-319-39502-9.

[57] H. Cramér, *Mathematical Methods of Statistics*, ser. Princeton Mathematical Series. Princeton University Press, 1946, vol. 9.

[58] K. Itô, *Essentials of Stochastic Processes*. American Mathematical Society, 2006, vol. 231.

[59] J. L. Doob, *Stochastic Processes*. John Wiley & Sons, 1953.

[60] J. M. Howie, *Complex Analysis*, ser. Springer Undergraduate Mathematics Series. Springer-Verlag, 2003. DOI: 10.1007/978-1-4471-0027-0.

[61] A. Klenke, *Probability Theory: A Comprehensive Course*. Springer-Verlag, 2008. DOI: 10.1007/978-1-84800-048-3.

[62] R. B. Ash and M. F. Gardner, *Topics in Stochastic Processes*. 111 Fifth Avenue, New York, USA: Academic Press, Inc., 1975.

[63] J. Lamperti, *Stochastic Processes: A Survey of The Mathematical Theory*, ser. Applied Mathematical Sciences. Springer-Verlag, 1977, vol. 23.

[64] Y. Mishura and G. Shevchenko, *Theory and Statistical Applications of Stochastic Processes*. ISTE, John Wiley & Sons, 2017.

[65] J. L. Doob, "Probability in function space", *Bulletin of the American Mathematical Society*, vol. 53, no. 1, pp. 15–30, 1947.

[66] K. Itô, "The canonical modification of stochastic processes", *Journal of the Mathematical Society of Japan*, vol. 20, no. 1-2, pp. 130–150, 1968.

[67] M. A. Pons, *Real Analysis for the Undergraduate*. Springer-Verlag, 2014. DOI: 10.1007/978-1-4614-9638-0.

[68] Z. Kotulski, "Equations for the characteristic functional and moments of the stochastic evolutions with an application", *SIAM Journal on Applied Mathematics*, vol. 49, no. 1, pp. 296–313, 1989. DOI: 10.1137/0149018.

[69] H. L. Hurd and A. Miamee, *Periodically Correlated Random Sequences: Spectral Theory and Practice*. John Wiley & Sons, 2007.

[70] W. A. Gardner, "Representation and estimation of cyclostationary processes", PhD thesis, Department of Electrical and Computer Engineering, University of Massachusetts, 1972.

[71] G. D. Birkhoff, "Proof of the ergodic theorem", *Proceedings of the National Academy of Sciences*, vol. 17, no. 12, pp. 656–660, 1931. DOI: 10.1073/pnas.17.2.656.

[72] P. Russer, "Electromagnetics in a complex world", in, ser. Springer Proceedings in Physics. Springer-Verlag, 2004, ch. Exterior differential forms in teaching electromagnetics, pp. 9–24. DOI: 10.1007/978-3-642-18596-0.

[73] P. R. Girard, *Quaternions, Clifford Algebras and Relativistic Physics*. Birkhäuser Verlag, 2007.

[74] T. Rozzi, M. Mongiardo, F. Mastri, D. Mencarelli, G. Monti, and G. Venanzoni, "Electromagnetic field modeling through the use of Dirac matrices and geometric algebra", in *International Conference on Electromagnetics in Advanced Applications (ICEAA)*, Sep. 2017, pp. 757–760. DOI: 10.1109/ICEAA.2017.8065359.

[75] F. Gronwald, F. W. Hehl, and J. Nitsch, "Axiomatics of classical electrodynamics and its relation to gauge field theory", *arXiv preprint physics/0506219*, 2005.

[76] M. Haider and J. A. Russer, "Differential form representation of stochastic electromagnetic fields", *Advances in Radio Science*, vol. 15, pp. 21–28, 2017. DOI: 10.5194/ars-15-21-2017.

[77] E. B. Wilson and J. W. Gibbs, *Vector Analysis*, 2nd ed. Yale University Press, 1929.

[78] O. Heaviside, *Electromagnetic Theory*. London, UK: The Electrician Printing and Publishing Company, 1893, vol. 1.

[79] O. Forster, *Analysis 3*. Springer-Verlag, 1981. DOI: 10.1007/978-3-663-14081-8.

[80] S. Lang, *Fundamentals of Differential Geometry*, ser. Graduate Texts in Mathematics. Springer-Verlag, 1999, vol. 191.

[81] I. V. Lindell, *Differential Forms in Electromagnetics*. IEEE Press, New York, 2004.

[82] P. C. Matthews, *Vector Calculus*, ser. Springer Undergraduate Mathematics Series. Springer-Verlag, 1998.

[83] P. Russer, *Electromagnetics, Microwave Circuit and Antenna Design for Communications Engineering*, 2nd ed. Artech House, 2006.

[84] J. P. D'Angelo, *Hermitian Analysis*. Springer-Verlag, 2013. DOI: 10.1007/978-1-4614-8526-1.

[85] T. Olson, *Applied Fourier Analysis*. Birkhäuser Verlag, 2017. DOI: 10.1007/978-1-4939-7393-4.

[86] G. Gradoni, J. Yeh, T. M. Antonsen, S. Anlage, and E. Ott, "Wave chaotic analysis of weakly coupled reverberation chambers", in *2011 IEEE International Symposium on Electromagnetic Compatibility*, Aug. 2011, pp. 202–207. DOI: 10.1109/ISEMC.2011.6038310.

[87] M. L. Mheta, *Random Matrices*, 3rd ed., ser. Pure and Applied Mathematics. Elsevier, 2004, vol. 142.

[88] P. Manfredi, M. Fontana, I. S. Stievano, and F. G. Canavero, "Comparison of stochastic methods for the variability assessment of technology parameters", *Radio Science*, vol. 47, no. 06, pp. 1–8, Dec. 2012. DOI: 10.1029/2011RS004881.

[89] P. Sumant, H. Wu, A. Cangellaris, and N. Aluru, "Reduced-order models of finite element approximations of electromagnetic devices exhibiting statistical variability", *IEEE Transactions on Antennas and Propagation*, vol. 60, no. 1, pp. 301–309, Jan. 2012. DOI: 10.1109/TAP.2011.2167935.

[90] R. G. Ghanem and P. D. Spanos, *Stochastic Finite Elements: A Spectral Approach*. Springer-Verlag, 1991. DOI: 10.107/978-1-4612-3094-6.

[91] L. Weiss and W. Mathis, "Generalized telegraphist's equations for deformed waveguides", *Electromagnetics*, vol. 18, no. 4, pp. 353–365, 1998. DOI: 10.1080/02726349808908594.

[92] P. J. Schreier and L. L. Scharf, *Statistical Signal Processing of Complex-Valued Data*. Cambridge University Press, 2010.

[93] R. P. Feynman, R. B. Leighton, and M. Sands, *The Feynman Lectures on Physics*. Addison-Wesley Publishing Company, 1964, vol. 2.

[94] L. B. Felsen and N. Marcuvitz, *Radiation and Scattering of Waves*, ser. IEEE Press Series on Electromagnetic Waves. John Wiley & Sons, IEEE-Press, 1994.

[95] Y. Kuznetsov, A. Baev, M. Konovalyuk, A. Gorbunova, J. A. Russer, and M. Haider, "Time-domain stochastic electromagnetic field propagator based on Jefimenko's equations", in *Baltic URSI Symposium (URSI)*, May 2018, pp. 188–191. DOI: 10.23919/URSI.2018.8406708.

[96] O. D. Jefimenko, *Electricity and Magnetism: An Introduction to the Theory of Electric and Magnetic Fields*, 2nd ed. Electret Scientific Company, 1989.

[97] D. J. Griffiths, *Introduction to Electrodynamics*, 4th ed. Pearson Education, 2013.

[98] R. Nevels and J. Jeong, "The time domain Green's function and propagator for Maxwell's equations", *IEEE Transactions on Antennas and Propagation*, vol. 52, no. 11, pp. 3012–3018, Nov. 2004. DOI: 10.1109/TAP.2004.835123.

[99] J. A. Stratton, *Electromagnetic Theory*, ser. International Series in Pure and Applied Physics. McGraw-Hill, 1941.

[100] J. J. H. Wang, *Generalized Moment Methods in Electromagnetics*. John Wiley & Sons, 1991.

[101] R. F. Harrington, *Time-Harmonic Electromagnetic Fields*, ser. IEEE Press Series on Electromagnetic Wave Theory. John Wiley & Sons, IEEE-Press, 2001.

[102] C. A. Balanis, *Advanced Engineering Electromagnetics*, 2nd ed. John Wiley & Sons, 2012.

[103] I. V. Lindell, "Huygens' principle in electromagnetics", *IEE Proceedings - Science, Measurement and Technology*, vol. 143, no. 2, pp. 103–105, Mar. 1996. DOI: 10.1049/ip-smt:19960218.

[104] S. A. Schelkunoff, "Some equivalence theorems of electromagnetics and their application to radiation problems", *The Bell System Technical Journal*, vol. 15, no. 1, pp. 92–112, Jan. 1936. DOI: 10.1002/j.1538-7305.1936.tb00720.x.

[105] I. Gohberg and S. Goldberg, *Basic Operator Theory*. Birkhäuser Verlag, 1981. DOI: 10.1007/978-1-4612-5985-5.

[106] G. Barton, *Elements of Green's Functions and Propagation*. Clarendon Press, 1989.

[107] P. Russer, "EMC measurements in the time-domain", in *XXXth URSI General Assembly and Scientific Symposium*, Aug. 2011, pp. 1–35. DOI: 10.1109/URSIGASS.2011.6050792.

[108] J. A. Russer and M. Haider, "Time-domain modeling of noisy electromagnetic field propagation", in *IEEE MTT-S International Microwave Symposium (IMS)*, Jun. 2018, pp. 1013–1016. DOI: 10.1109/MWSYM.2018.8439151.

[109] S. Gregson, J. McCormick, and C. Parini, *Principles of Planar Near-Field Antenna Measurements*, ser. IET Electromagnetic Waves Series. The Institution of Engineering and Technology, 2007, vol. 53.

[110] A. Yaghjian, "An overview of near-field antenna measurements", *IEEE Transactions on Antennas and Propagation*, vol. 34, no. 1, pp. 30–45, Jan. 1986. DOI: 10.1109/TAP.1986.1143727.

[111] "Integrated circuits - measurement of electromagnetic emissions - part 3: Measurement of radiated emissions - surface scan method", International Electrotechnical Commission, Geneva, Switzerland, Standard, Aug. 2014.

[112] F. Krug and P. Russer, "Quasi-peak detector model for a time-domain measurement system", *IEEE Transactions on Electromagnetic Compatibility*, vol. 47, no. 2, pp. 320–326, May 2005. DOI: 10.1109/TEMC.2005.847410.

[113] ——, "The time-domain electromagnetic interference measurement system", *IEEE Transactions on Electromagnetic Compatibility*, vol. 45, no. 2, pp. 330–338, May 2003. DOI: 10.1109/TEMC.2003.811303.

[114] ——, "Time-domain broad-band EMI measurement techniques", in *32nd European Microwave Conference*, Sep. 2002, pp. 1–4. DOI: 10.1109/EUMA.2002.339366.

[115] ——, "Ultra-fast broadband EMI measurement in time-domain using FFT and periodogram", in *IEEE International Symposium on Electromagnetic Compatibility*, vol. 2, Aug. 2002, pp. 577–582. DOI: 10.1109/ISEMC.2002.1032655.

[116] S. Braun, A. Frech, and P. Russer, "A low-noise realtime time-domain EMI measurement system", in *18th International Zurich Symposium on Electromagnetic Compatibility*, Sep. 2007, pp. 381–384. DOI: 10.1109/EMCZUR.2007.4388275.

[117] S. Braun, M. Aidam, and P. Russer, "Development and evaluation of a realtime time-domain EMI measurement system for automotive testing", in *IEEE International Symposium on Electromagnetic Compatibility*, Jul. 2007, pp. 1–4. DOI: 10.1109/ISEMC.2007.169.

[118] J. A. Russer, N. Uddin, A. S. Awny, A. Thiede, and P. Russer, "Near-field measurement of stochastic electromagnetic fields", *IEEE Electromagnetic Compatibility Magazine*, vol. 4, no. 3, pp. 79–85, Nov. 2015. DOI: 10.1109/MEMC.2015.7336761.

[119] J. A. Russer, S. Braun, A. Frech, and P. Russer, "Time-domain measurement of spectra of stochastic electromagnetic fields", in *International Conference on Electromagnetics in Advanced Applications (ICEAA)*, Sep. 2013, pp. 1123–1126. DOI: 10.1109/ICEAA.2013.6632417.

[120] A. V. Oppenheim and R. W. Schafer, *Discrete-time Signal Processing*, 2nd ed. Prentice Hall, 1998.

[121] C. E. Shannon, "Communication in the presence of noise", *Proceedings of the IRE*, vol. 37, no. 1, pp. 10–21, Jan. 1949. DOI: 10.1109/JRPROC.1949.232969.

[122] X. Ren, P. Maheshwari, Y. Zhang, V. Khilkevich, J. Fan, Y. Zhou, Y. Bai, and X. Yu, "The impact of near-field scanning size on the accuracy of far-field estimation", in *IEEE International Symposium on Electromagnetic Compatibility (EMC)*, Aug. 2014, pp. 582–587. DOI: 10.1109/ISEMC.2014.6899038.

[123] D. W. P. Thomas, C. Smartt, H. Nasser, M. Baharuddin, S. Greedy, G. Gradoni, S. C. Creagh, and G. Tanner, "Time domain measurement of near field emissions from complex PCBs", in *46th European Microwave Conference (EuMC)*, Oct. 2016, pp. 707–710. DOI: 10.1109/EuMC.2016.7824441.

[124] J. A. Russer, G. Scarpa, P. Lugli, and P. Russer, "On the modeling of radiated EMI on the basis of near-field correlation measurements", in *41st European Microwave Conference (EuMC)*, Oct. 2011, pp. 9–12. DOI: 10.23919/EuMC.2011.6101973.

[125] P. Russer, "Verfahren und Anordnung zur Nahfeldmessung von elektromagnetischen Emissionen im Zeitbereich", Patent DE10 2009 035 421 A1, Anm. Dat. 31.07.2009, Off. Dat. 03.02.2011, 2011.

[126] S. Gottschalk, M. C. Lin, and D. Manocha, "OBBTree: A hierarchical structure for rapid interference detection", in *Proceedings of the 23rd Annual Conference on Computer Graphics and Interactive Techniques*, 1996, pp. 171–180. DOI: 10.1145/237170.237244.

[127] T. Möller, "A fast triangle-triangle intersection test", *Journal of Graphics Tools*, vol. 2, no. 2, pp. 25–30, Nov. 1997. DOI: 10.1080/10867651.1997.10487472.

[128] R. D. Pollard and R. Q. Lane, "The calibration of a universal test fixture", in *IEEE MTT-S International Microwave Symposium Digest*, May 1983, pp. 498–500. DOI: 10.1109/MWSYM.1983.1130960.

[129] A. Baev, Y. Kuznetsov, M. Haider, J. A. Russer, and P. Russer, "Time-domain characterization of probes for two-point measurements of stochastic EM fields", in *International Conference on Electromagnetics in Advanced Applications (ICEAA)*, Sep. 2017, pp. 1521–1524. DOI: 10.1109/ICEAA.2017.8065572.

[130] G. Müller, A. Bergmann, W. Ruile, R. Weigel, and P. Russer, "Experimental determination of the complete scattering matrix of SAW reflectors by a new deembedding method", in *Proceedings of IEEE Ultrasonics Symposium*, vol. 1, Oct. 1994, pp. 151–154. DOI: 10.1109/ULTSYM.1994.401570.

[131] W. Dressel, T. Mangold, L. Vietzorreck, and P. Russer, "Time domain characterization of multichip module elements", in *IEEE MTT-S International Microwave Sympsoium Digest*, vol. 2, May 2001, pp. 1033–1036. DOI: 10.1109/MWSYM.2001.967068.

[132] "Integrated circuits - measurement of electromagnetic emissions - part 6: Measurement of conducted emissions - magnetic probe method", International Electrotechnical Commission, Geneva, Switzerland, Standard, May 2008.

[133] Langer EMV-Technik. (Mar. 2015). RF probe correction datasheet, [Online]. Available: https://www.langer-emv.de/.

[134] A. Baev, A. Gorbunova, M. Konovalyuk, Y. Kuznetsov, and J. A. Russer, "Stochastic EMI sources localization based on ultra wide band near-field measurements", in *43rd European Microwave Conference (EuMC)*, Oct. 2013, pp. 1131–1134. DOI: 10.23919/EuMC.2013.6686861.

[135] M. Haider, J. A. Russer, A. Baev, Y. Kuznetsov, and P. Russer, "Principal component analysis applied in modeling of stochastic electromagnetic field propagation", in *47th European Microwave Conference (EuMC)*, Oct. 2017, pp. 1–4.

[136] J. A. Russer and P. Russer, "Network methods applied to the computation of stochastic electromagnetic fields", in *International Conference on Electromagnetics in Advanced Applications (ICEAA)*, Sep. 2011, pp. 1152–1155. DOI: 10.1109/ICEAA.2011.6046513.

[137] R. F. Harrington, *Field Computation by Moment Methods*, ser. IEEE Press Series on Electromagnetic Waves. John Wiley & Sons, IEEE-Press, 1993.

[138] J. E. Jackson, *A User's Guide to Principal Components*, 1st ed. John Wiley & Sons, 1991.

[139] M. Haider and J. A. Russer, "Equivalent source localization for stochastic electromagnetic fields", in *International Conference on Electromagnetics in Advanced Applications (ICEAA)*, Sep. 2017, pp. 1486–1489. DOI: 10.1109/ICEAA.2017.8065563.

[140] A. Gorbunova, A. Baev, M. Konovalyuk, Y. Kuznetsov, and J. A. Russer, "Stochastic EMI sources localization algorithm based on time domain planar near-field scanning", in *International Symposium on Electromagnetic Compatibility*, Sep. 2013, pp. 972–976.

[141] A. L. Swindlehurst and T. Kailath, "A performance analysis of subspace-based methods in the presence of model errors. I. The MUSIC algorithm", *IEEE Transactions on Signal Processing*, vol. 40, no. 7, pp. 1758–1774, Jul. 1992. DOI: 10.1109/78.143447.

[142] B. Ottersten and T. Kailath, "Direction-of-arrival estimation for wide-band signals using the ESPRIT algorithm", *IEEE Transactions on Acoustics, Speech, and Signal Processing*, vol. 38, no. 2, pp. 317–327, Feb. 1990. DOI: 10.1109/29.103067.

[143] Z. Stanković, N. Dončov, J. A. Russer, T. Asenov, and B. Milovanović, "Efficient DOA estimation of impinging stochastic EM signal using neural networks", in *International Conference on Electromagnetics in Advanced Applications (ICEAA)*, Sep. 2013, pp. 575–578. DOI: 10.1109/ICEAA.2013.6632306.

[144] D. Schaefer, A. Lauer, and R. Baggen, "Characterization of noisy EM fields by cross spectral density eigenvalue analysis", in *International Conference on Electromagnetics in Advanced Applications (ICEAA)*, Sep. 2017, pp. 902–905. DOI: 10.1109/ICEAA.2017.8065400.

[145] Y. Kuznetsov, A. Baev, A. Gorbunova, M. Konovalyuk, D. Thomas, C. Smartt, M. H. Baharuddin, J. A. Russer, and P. Russer, "Localization of the equivalent sources on the PCB surface by using ultra-wideband time domain near-field measurements", in *International Symposium on Electromagnetic Compatibility (EMC Europe)*, Sep. 2016, pp. 1–6. DOI: 10.1109/EMCEurope.2016.7739184.

[146] M. Konovalyuk, A. Gorbunova, A. Baev, and Y. Kuznetsov, "Parametric identification of stochastic EMI sources based on near-field measurements", in *44th European Microwave Conference (EuMC)*, Oct. 2014, pp. 1087–1090. DOI: 10.1109/EuMC.2014.6986628.

[147] A. Gorbunova, A. Baev, M. Konovalyuk, and Y. Kuznetsov, "Parametric reconstruction of stochastic EMI sources based on two-point planar near-field scanning", in *International Symposium on Electromagnetic Compatibility*, Sep. 2014, pp. 102–107. DOI: 10.1109/EMCEurope.2014.6930885.

[148] A. Baev, A. Gorbunova, M. Konovalyuk, Y. Kuznetsov, and J. A. Russer, "Planar stochastic sources localization algorithm in EMC problems", in *International Conference on Electromagnetics in Advanced Applications (ICEAA)*, Sep. 2013, pp. 440–443. DOI: 10.1109/ICEAA.2013.6632275.

[149] G. H. Golub and C. F. Van Loan, *Matrix Computations*, 4th ed. Baltimore, MD, USA: John Hopkins University Press, 2013.

[150] Z. Chen and S. Luo, "Generalization of the finite-difference-based time-domain methods using the method of moments", *IEEE Transactions on Antennas and Propagation*, vol. 54, no. 9, pp. 2515–2524, Sep. 2006. DOI: 10.1109/TAP.2006.880733.

[151] M. Krumpholz and P. Russer, "A field theoretical derivation of TLM", *IEEE Transactions on Microwave Theory and Techniques*, vol. 42, no. 9, pp. 1660–1668, Sep. 1994. DOI: 10.1109/22.310559.

[152] M. Haider, A. Baev, Y. Kuznetsov, and J. A. Russer, "Near-field to far-field propagation of correlation information for noisy electromagnetic fields", in *48th European Microwave Conference (EuMC)*, Sep. 2018, pp. 1190–1193. DOI: 10.23919/EuMC.2018.8541636.

[153] Y. Kuznetsov, A. Baev, M. Haider, J. A. Russer, and P. Russer, "Time-domain far-field measurements for cross-correlation analysis", in *International Conference on Electromagnetics in Advanced Applications (ICEAA)*, Sep. 2017, pp. 1517–1520. DOI: 10.1109/ICEAA.2017.8065571.

[154] J. A. Russer, G. Scarpa, P. Lugli, and P. Russer, "Sensing of stochastic waves with circular antenna arrays", in *42nd European Microwave Conference (EuMC)*, Oct. 2012, pp. 971–974. DOI: 10.23919/EuMC.2012.6459361.

[155] M. Haider, P. Corrales, D. Bajon, S. Wane, and J. A. Russer, "Near-field MIMO system assessment", in *2nd URSI Atlantic Radio Science Meeting (AT-RASC)*, May 2018, pp. 1–3. DOI: 10.23919/URSI-AT-RASC.2018.8471642.

[156] W. J. R. Hoefer, "The transmission-line matrix method - theory and applications", *IEEE Transactions on Microwave Theory and Techniques*, vol. 33, no. 10, pp. 882–893, Oct. 1985. DOI: 10.1109/TMTT.1985.1133146.

[157] G. Kron, "Equivalent circuit of the field equations of Maxwell-I", *Proceedings of the IRE*, vol. 32, no. 5, pp. 289–299, May 1944. DOI: 10.1109/JRPROC.1944.231021.

[158] P. B. Johns and R. L. Beurle, "Numerical solution of 2-dimensional scattering problems using a transmission-line matrix", *Proceedings of the Institution of Electrical Engineers*, vol. 118, no. 9, pp. 1203–1208, Sep. 1971. DOI: 10.1049/piee.1971.0217.

[159] P. Russer and M. Krumpholz, "The Hilbert space formulation of the TLM method", *International Journal of Numerical Modelling: Electronic Networks, Devices and Fields*, vol. 6, no. 1, pp. 29–45, 1993. DOI: 10.1002/jnm.1660060105.

[160] M. Krumpholz, B. Bader, and P. Russer, "On the theory of discrete TLM Green's functions in three-dimensional TLM", *IEEE Transactions on Microwave Theory and Techniques*, vol. 43, no. 7, pp. 1472–1483, Jul. 1995. DOI: 10.1109/22.392904.

[161] G. Gradoni, L. R. Arnaut, S. C. Creagh, G. Tanner, M. H. Baharuddin, C. Smartt, and D. W. P. Thomas, "Wigner-function-based propagation of stochastic field emissions from planar electromagnetic sources", *IEEE Transactions on Electromagnetic Compatibility*, vol. 60, no. 3, pp. 580–588, Jun. 2018. DOI: 10.1109/TEMC.2017.2738329.

[162] M. H. Baharuddin, H. Nasser, C. Smartt, D. W. P. Thomas, G. Gradoni, S. C. Creagh, and G. Tanner, "Measurement and wigner function analysis of field-field correlation for complex PCBs in near field", in *International Symposium on Electromagnetic Compatibility (EMC Europe)*, Sep. 2016, pp. 7–11. DOI: 10.1109/EMCEurope.2016.7739237.

[163] E. Wigner, "On the quantum correction for thermodynamic equilibrium", *Physical Review*, vol. 40, pp. 749–759, 5 Jun. 1932. DOI: 10.1103/PhysRev.40.749.

[164] M. T. Ivrlač and J. A. Nossek, "Toward a circuit theory of communication", *IEEE Transactions on Circuits and Systems*, vol. 57, no. 7, pp. 1663–1683, Jul. 2010. DOI: 10.1109/TCSI.2010.2043994.

[165] ——, "The multiport communication theory", *IEEE Circuits and Systems Magazine*, vol. 14, no. 3, pp. 27–44, 2014. DOI: 10.1109/MCAS.2014.2333618.

[166] S. J. Orfanidis, *Electromagnetic Waves and Antennas*. Rutgers University, 2016.

[167] S. Phang, M. T. Ivrlač, G. Gradoni, S. C. Creagh, G. Tanner, and J. A. Nossek, "Near-field MIMO communication links", *IEEE Transactions on Circuits and Systems*, vol. 65, no. 9, pp. 3027–3036, Sep. 2018. DOI: 10.1109/TCSI.2018.2796305.

[168] J. A. Russer, M. T. Ivrlač, M. Haider, S. Wane, D. Bajon, and J. A. Nossek, "A compact Hertzian dipoles multiport model for near-field MIMO system assessment", in *IEEE Radio and Wireless Symposium (RWS)*, Jan. 2018, pp. 31–34. DOI: 10.1109/RWS.2018.8304938.

[169] W. Yu, W. Rhee, S. Boyd, and J. M. Cioffi, "Iterative water-filling for Gaussian vector multiple-access channels", *IEEE Transactions on Information Theory*, vol. 50, no. 1, pp. 145–152, Jan. 2004. DOI: 10.1109/TIT.2003.821988.

[170] J. A. Russer, M. T. Ivrlač, M. Haider, S. Wane, D. Bajon, P. Russer, and J. A. Nossek, "Multiport model of Hertzian dipoles coupled in the near-field", in *47th European Microwave Conference (EuMC)*, Oct. 2017, pp. 1293–1296. DOI: 10.23919/EuMC.2017.8231088.

[171] S. M. Alamouti, "A simple transmit diversity technique for wireless communications", *IEEE Journal on Selected Areas in Communications*, vol. 16, no. 8, pp. 1451–1458, Oct. 1998. DOI: 10.1109/49.730453.

[172] D. W. P. Thomas, M. H. Baharuddin, C. Smartt, G. Gradoni, G. Tanner, S. Creagh, N. Dončov, M. Haider, and J. A. Russer, "Near-field scanning of stochastic fields considering reduction of complexity", in *International Symposium on Electromagnetic Compatibility (EMC Europe)*, Sep. 2017, pp. 1–6. DOI: 10.1109/EMCEurope.2017.8094766.

[173] J. A. Russer, T. Asenov, and P. Russer, "Sampling of stochastic electromagnetic fields", in *IEEE MTT-S International Microwave Symposium Digest*, Jun. 2012, pp. 1–3. DOI: 10.1109/MWSYM.2012.6259785.

[174] J. A. Russer, M. Haider, M. H. Baharuddin, C. Smartt, A. Baev, S. Wane, D. Bajon, Y. Kuznetsov, D. Thomas, and P. Russer, "Correlation measurement and evaluation of stochastic electromagnetic fields", in *International Symposium on Electromagnetic Compatibility (EMC Europe)*, Sep. 2016, pp. 12–16. DOI: 10.1109/EMCEurope.2016.7739292.

[175] H. Hotelling, "Analysis of a complex of statistical variables into principal components", *Journal of Educational Psychology*, vol. 24, pp. 417–441, Sep. 1933. DOI: 10.1037/h0071325.

[176] K. Pearson, "On lines and planes of closest fit to systems of points in space", *Philosophical Magazine*, vol. 2, pp. 559–572, 6 1901.

[177] I. T. Jolliffe, *Principal Component Analysis*, 2nd ed., ser. Springer Series in Statistics. Springer-Verlag, 2002. DOI: 10.1007/b98835.

[178] NEMF21 Project Consortium, "Noisy electromagnetic fields: A technological platform for chip-to-chip communication in the 21st century", Horizon 2020, European Commission, Final Report, Mar. 2019.

[179] E. Candes and T. Tao, "Near optimal signal recovery from random projections: Universal encoding strategies?", *arXiv preprint math/0410542*, 2004.

[180] E. Candes, J. Romberg, and T. Tao, "Robust uncertainty principles: Exact signal reconstruction from highly incomplete frequency information", *arXiv preprint math/0409186*, 2004.

Acknowledgments

On these final pages, I want to express my deepest gratitude to all the people who helped me on my way towards my Ph.D. Without your constant help and encouragement, I would not be where I am now.

First of all, I want to thank my supervisor PD Dr. habil. Johannes A. Russer for giving me the opportunity to work with him on the highly interesting and demanding topic of stochastic electromagnetic fields. He raised my interest in the topic already in 2014 when I was working on my Bachelor's thesis. One and a half years later, I started my master's thesis on near-field scanning of stochastic electromagnetic fields, and I was deeply honored when he offered me a position within the NEMF21 project, for working towards my Ph.D. During the three years, he has been the most brilliant supervisor one can think of. His way of asking the right questions at the right time and his constant encouragement led to a working atmosphere that kept me constantly motivated. There has been the one or other night-shift ahead of a conference deadline, which I will never forget. Also, the possibility to travel to several renowned conferences, even if they are far abroad is something I am highly grateful for. I also want to thank Prof. Peter Russer for all the inspirational discussions and his brilliant ideas, that deeply influenced a good share of the content presented here. He also brought the quantum mechanical modeling of superconducting devices to my attention, which developed into a fruitful side project. In general, I am very grateful that I have been integrated into a highly skilled and enormously productive research group around Peter and Johannes Russer. It was also the variety of topics, collaborations, and possibilities that stunned me. Besides my work on stochastic electromagnetic fields I was encouraged to get involved in ongoing work towards field modeling for a moving field inductive power transfer system, an innovative solution for future electric mobility concepts, and also in the quantum mechanical modeling of Josephson devices. These diversified research activities made my working days so enjoyable, as I was given the possibility to contribute to a whole variety of different projects. Because of all this, I am also very happy that the efforts of Dr. Russer as my doctoral supervisor got recognized by the TUM Department of Electrical and Computer Engineering for he was awarded as one of the three best supervisors in the department. Great thanks also go to Prof. Paolo Lugli who housed us at his Chair of Nanoelectronics. When Prof. Lugli left to become the head of the Free University of Bozen/Bolzano, one cannot imagine a better substitute than Prof. Markus Becherer, both scientifically and personally. He kept the institute running and he was always planning ahead. His leadership skills and his contagious cheerfulness are remarkable. Starting with the end of my master's thesis Prof. Becherer and I somehow inherited the responsibility for the IT infrastructure of our institute. Together, we created a good package of IT services we offer at our institute, which is apparently good enough such that he brought up the idea of copying it for the newly created ZEITlab. ZEITlab is the new joint clean-room and semiconductor technology laboratory of the electrical engineering department of TUM, which Prof. Becherer orchestrated. For all his efforts, the whole institute owes him deepest gratitude and he has our highest admiration. My mentor during this thesis was Prof. Christian Jirauschek, whom I owe special thanks, first of all for the fruitful collaborations we had during my Ph.D. and also the constant personal support and trustful relationship. I am also very happy and thankful that Prof. Jirauschek offered me a Post-Doc position in his Computational Photonics group, where I am looking forward to all the interesting projects that are about to come.

The wide network of renowned international researchers, my supervisor Dr. Russer brought me in contact to, opened a lot of interesting collaborations. Some of those I want to mention here, as they had a great impact on my work. Dr. HDR Sidina Wane, the president and CEO of eV-Technologies changed my mind from approaching stochastic electromagnetic fields from a pure research-oriented view towards entrepreneurial thinking, as he always pointed out the industrial applications of the theories and methods we developed together. Together with Prof. Damienne Bajon from ISAE SUPAERO in Toulouse, we had several different and highly interesting collaborations on developing new methods for the propagation of stochastic electromagnetic fields, and we also worked together on measurements for near-field MIMO communication and FMCW radars. Pablo Corrales, who is now also with eV-Technologies conducted several measurements together with Dr. Wane and Prof. Bajon

here at TUM. I have never met anybody who is more professional in organizing complex measurement setups than Pablo. Thank you for the great work we did together. Another longstanding collaboration of Peter and Johannes Russer that had a lot of influence on my work here is the one with Prof. Yury Kuznetsov and Dr. Andrey Baev from the Moscow Aviation Institute. Their way of planing experiments ahead is encouraging and their input on cyclostationary random fields is highly appreciated. Through a DAAD-funded exchange program I had the opportunity to visit Prof. Nebojša Dončov and Dr. Biljana Stošić from the University of Niš, Serbia. We had a great time there, and I really enjoyed the stimulating scientific discussions.

The Chair for Nanoelectronics used to be a large institute, and I am very glad to have the best colleagues ever. People worked at widely different topics, but still, we managed to also find some collaborations internally. Some of those, I want to explicitly mention here, which are the work with Dr. Marco Bobinger on sprayed silver nanoparticle and nanowire antennas, a project with Dr. Andreas Albrecht on ink-jet printing techniques and rapid prototyping of flexible radiating structures, and finally, the modeling of quantum effects in Josephson parametric amplifiers with Waldemar Kaiser and Jesus Abundis Patino.

I also want to thank the other members of the NEMF21 Horizon 2020 project and the members of the COST IC 1407 ACCREDIT project for their inputs and for the stimulating discussions.

Our institute would not be such a pleasant place to work without those people who keep it all together. Those are especially our secretaries Lucia Weik, Kathrin Blahetek, and Susanne Maier, who absorbed most of the administrative overhead, one is confronted with as a researcher at a large university. Special thanks also go to Rosemarie Mittermeier, who keeps our labs running with everlasting patience and endurance.

A lot of things that have been achieved during this thesis, especially within the side projects, would not have been possible without the excellent work of my outstanding Bachelor and Master students. It was an honor to be your supervisor and I hope you all had a great time at our institute. As I cannot express the contributions of my students in a form that is short enough for the format here, I have decided to list their names along with the titles of their theses.

- Waldemar Kaiser - Quantum Mechanical Modeling of the Dissipative Josephson Parametric Amplifier (Master's Thesis)
- Quirin Hirmer - Antenna Prototyping and Antenna Designs for Chip-to-Chip Communication (Master's Thesis)
- Canbey Oguz - Modeling and Realization of a Moving Field Inductive Power Transfer System (Bachelor's Thesis)
- Mirco Metz - Simulation of a Moving Field Inductive Power Transfer (MFIPT) Control System (Bachelor's Thesis)
- Yongjie Yuan - A Quantum Model of a Resonantly Phase-Matched Josephson Traveling Wave Parametric Amplifier (Master's Thesis)

As already said before, I am glad that I can cheerfully claim to have the best colleagues ever. From all my coworkers, I want to thank especially those, I have shared my office with. These are Marius Loch, Tobias Haeberle, Robin Nagel, Andreas Albrecht, Marco Bobinger, Simon Mendisch, and Martina Kiechle. Thank you for the great time we spent together and for the welcome distractions. Furthermore, I want to thank the technical program committee and all participants of the International Conference on Mostly Scientific Topics (ICMST).

The constant encouragement and selfless support received from our best friends, Bernhard Wörndl-Aichriedler and Nicole Miletic is also highly appreciated.

Last but not least, I just want to say thank you to my Family, Hans Michael, Manuela, Markus, Daniela, and of course my little nieces Lena Sophie and Isabella Marie Haider. Thank you for all the love and support I have received from you during the last years and throughout my whole life. Finally, I am particularly honored to dedicate this work as a whole to my beloved wife Elisabeth Haider, whom I married on March 29, 2019, just a few weeks before submitting this thesis.